Terms and Conditions of Use of Digitised Theses from Trinity College Library Dublin

Copyright statement

All material supplied by Trinity College Library is protected by copyright (under the Copyright and Related Rights Act, 2000 as amended) and other relevant Intellectual Property Rights. By accessing and using a Digitised Thesis from Trinity College Library you acknowledge that all Intellectual Property Rights in any Works supplied are the sole and exclusive property of the copyright and/or other IPR holder. Specific copyright holders may not be explicitly identified. Use of materials from other sources within a thesis should not be construed as a claim over them.

A non-exclusive, non-transferable licence is hereby granted to those using or reproducing, in whole or in part, the material for valid purposes, providing the copyright owners are acknowledged using the normal conventions. Where specific permission to use material is required, this is identified and such permission must be sought from the copyright holder or agency cited.

Liability statement

By using a Digitised Thesis, I accept that Trinity College Dublin bears no legal responsibility for the accuracy, legality or comprehensiveness of materials contained within the thesis, and that Trinity College Dublin accepts no liability for indirect, consequential, or incidental, damages or losses arising from use of the thesis for whatever reason. Information located in a thesis may be subject to specific use constraints, details of which may not be explicitly described. It is the responsibility of potential and actual users to be aware of such constraints and to abide by them. By making use of material from a digitised thesis, you accept these copyright and disclaimer provisions. Where it is brought to the attention of Trinity College Library that there may be a breach of copyright or other restraint, it is the policy to withdraw or take down access to a thesis while the issue is being resolved.

Access Agreement

By using a Digitised Thesis from Trinity College Library you are bound by the following Terms & Conditions. Please read them carefully.

I have read and I understand the following statement: All material supplied via a Digitised Thesis from Trinity College Library is protected by copyright and other intellectual property rights, and duplication or sale of all or part of any of a thesis is not permitted, except that material may be duplicated by you for your research use or for educational purposes in electronic or print form providing the copyright owners are acknowledged using the normal conventions. You must obtain permission for any other use. Electronic or print copies may not be offered, whether for sale or otherwise to anyone. This copy has been supplied on the understanding that it is copyright material and that no quotation from the thesis may be published without proper acknowledgement.

Accurate Modelling and Synthesis of the Lead II ECG Signal

Gavin P. Shorten

A Thesis Submitted for the Degree of

Doctor of Philosophy

April 2012

Department of Electronic and Electrical Engineering

University of Dublin, Trinity College

Declaration

1. I declare that this thesis has not been submitted as an exercise for a degree at this or any other university and it is entirely my own work.

2. I agree to deposit this thesis in the University's open access institutional repository or allow the library to do so on my behalf, subject to Irish Copyright Legislation and Trinity College Library conditions of use and acknowledgement.

"Research is to see what everybody else has seen, and to think what nobody else has thought."

Albert von Szent-Gyrgyi de Nagyrpolt (1893-1986)

Dedication

Dedicated to my parents and my fiancé Trish, thank you for everything.

Summary

This thesis is a study of Lead II ECG signal synthesis. The principal problem of ECG signal synthesis is two fold, the first concerns the accuracy of the instrument used to deliver the synthesised signal and the second concerns the correlation between the synthesised signal and the characteristics of *in vivo* ECG. This research addresses both problems with the design of an accurate ECG signal generator and the characterisation of the timing of the ECG Lead II signal.

In ECG synthesis for test purposes, the ability to supply a modelled and synthesised ECG as an output analogue signal is based firmly on the instrument used to generate the test signal itself. Significant limitations in terms of bit resolution, noise performance, temperature characteristics, amplitude level, timing variability and the overall suitability of the ECG signal generators found in the literature are highlighted. Therefore, attention has been given to overcoming these limitations and providing a modern ECG signal generator which provides fully defined and stringently tested levels of accuracy.

The ECG signal is typically analysed in the time domain and clinical diagnoses and treatments based on observations of the amplitude and duration of the constituent components within the ECG. Synthesised signals should reflect these characteristics as observed *in vivo* and hence modelling of such attributes are investigated. Inaccuracies in the characterisation of the timing variations of the ECG signal with respect to heart rate using the time-frequency based wavelet analysis technique carried out in the past are discussed. By careful review dynamic time warping is identified as a more suitable means of characterising the timing of the ECG signal. Improvements to the dynamic time warping algorithm, both in terms of pre-processing and classification of results, are made in order to asses the timing of the ECG signals more accurately. The suitability and accuracy of the improved algorithm are verified by extensive testing.

Using the improved algorithm seven equations which characterise the variation of

the ECG signal constituent components with respect to heart rate are derived from a database of exercise ECG recordings. The equations are compared to large scale clinical investigations of the same phenomena and are shown to reflect clinical metrics for the behaviour of the ECG with respect to heart rate. The hardware and timing model can be combined to provide a realistic, accurate and variable synthesised ECG signal.

Acknowledgements

Firstly I would like to thank my supervisor, Martin J. Burke for giving me the opportunity to undertake a PhD with his supervision.

I would like to thank the Irish Research Council for Science, Engineering and Technology for funding this work for the first three years.

A big note of thanks to the technical staff of the department, Conor Nolan, Shane Hunt, Sean O'Callaghan and most notably the late Ms. Bernadette Clerkin, who have helped me throughout my studies.

Thanks is also due to my colleagues John Squires, Darren Kavanagh, Roberta Dozio, Cedric Assambo, Colin Couper and Liam Cleary who have always been very helpful with regards to my work but more importantly have created a friendly working environment in the Printing House.

Last but by no means least, I want to thank my parents Colm and Geraldine, my brothers Graham and Sam and my fiancé Trish for their support, seemingly endless patience and inspiration during the course of my life.

Gavin Shorten

Dublin, April 2012

Contents

List of Figures

List of Tables

Chapter 1

Introduction

1.1 The Importance of the Electrocardiogram

The Electrocardiogram, or ECG, has been an integral part of cardiovascular medicine since its first successful recording by Einthoven in 1904 [1]. The observation of electrical activity on the surface of the body, resulting from the depolarisation and repolarisation of the heart muscles can be used to gain insight into the condition of a subjects heart. Despite the introduction of modern cardio-diagnostic tools such as angiography, the ECG is as prevalent and vital today as a front-line tool in coronary care as it has ever been.

With the ubiquitous spread of electronic instrumentation, increased awareness of the importance of cardiovascular health and the development of the portable Holter monitor, ECG recording machines can now be found in the GP's surgery, sports clubs, ambulatory clinical measurements and even the home. Development of the modern ECG machine has made it easy to use, portable and relatively inexpensive. Initial diagnosis of cardiovascular illness is often made based on rudimentary amplitude and timing variations observed in the ECG recording. Since the usefulness of the ECG machine depends heavily on its accuracy in displaying the electrical activity on the surface of the body, the instrument's ability to preserve the morphology of the ECG signal is of paramount importance.

1.2 The ECG Lead II Signal

The ECG signal is recorded using up to ten electrodes and observation of up to twelve lead configurations or observation angles from which the electrical activity on the body can be observed. Each lead provides different insight into the functioning of the heart but the one most commonly used is the Lead II configuration because it typically provides the cleanest and most readily observed recording. A typical ECG Lead II signal and its constituent waves are shown below in Figure 1.1.

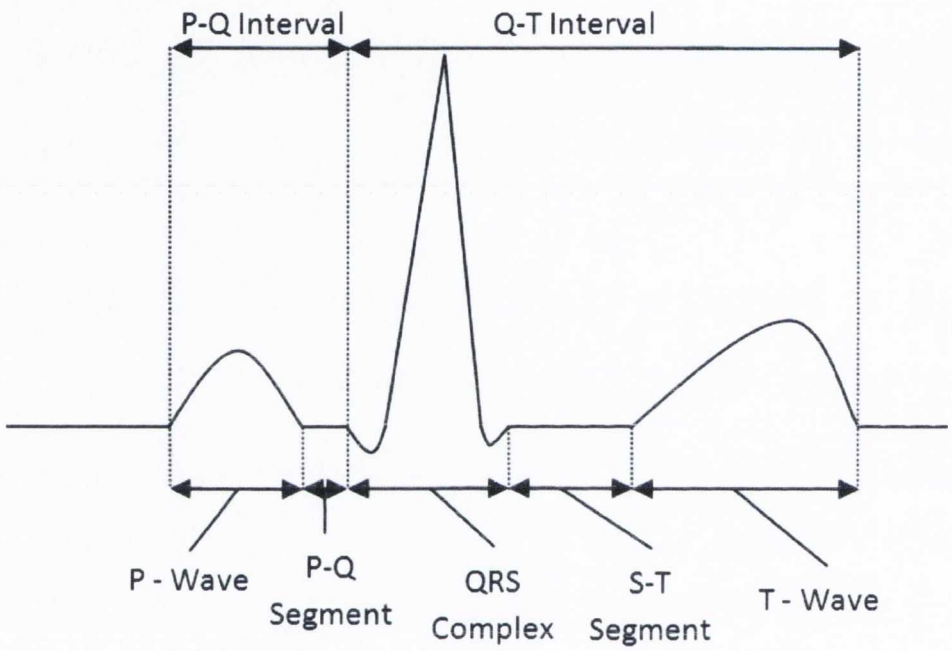

Figure 1.1: The ECG Lead II Signal and its constituent components

The P Wave: The contraction of the relatively small muscle mass of the atria results in the P-wave or first deflection from the isoelectric level. The electrical discharge which started in the sinoatrial (SA) node spreads through the atrial muscle fibres towards the atrioventricular (AV) node.

The QRS Wave: After the excitation reaches the ventricles via the AV node and the left and right bundle branches the resulting contraction of the ventricles causes a large deflection known as the QRS complex. The QRS complex shown in Figure 1.1 shows the R wave preceded by a Q wave and followed by a S wave although even in healthy ECG recordings it is possible that neither of these waves are visible in the recording.

The T Wave: After the contraction of the ventricles the return to the resting electrical state or repolarisation of the ventricles results in the longest duration deflection

known as the T-wave.

The T wave can be followed by a short duration very low amplitude wave known as a U wave. The genesis of this wave is speculated in the literature, often being attributed to repolarisation of the papillary muscles [2] of the heart (see Figure 2.1). However, it is known to be present and absent in normal healthy subjects [3] and is rarely given any diagnostic significance. As such is not considered further in this research.

The amplitude and duration of each of the three waves, the segments between waves (PQ and ST) and the associated division of the complete signal into intervals (PQ and QT) are used to draw conclusions regarding the state of the various muscles and fibres engaged in the heart beat process [2]. Any test signal used to calibrate an ECG recording machine should provide fully controlled timing and amplitude characteristics based on those found during in *in-vivo* ECG recordings. A universal test signal or instrument that can provide widely varying characteristics would be invaluable but must be based on observation of real-life ECG recordings and indeed their classification by expert cardiologists. The duration of each component shall be defined more comprehensively in Chapter 8.

1.3 ECG Signal Synthesis

The testing, calibration and commissioning of ECG recording machines fundamentally relies on the delivery of a synthesised test signal that is accurate and has the amplitude and timing characteristics typical of actual ECG signals. Test signals resulting from models which are synthesized only by a software package are not reliable as a representation of an *in-vivo* signal and are limited by the often synthetic nature of mathematically generated waveforms which are not derived from observed or measured signals. The advantages of having an actual ECG signal generator to provide test signals which are fully controllable in terms of output heart rate and resulting component durations, offset voltage and amplitude variation are many and shall be discussed throughout this thesis.

The modernisation of biomedical instrumentation and the field of medicine as a whole in recent decades has seen a radical merging of computer technology, information and medical science and the creation of a discipline known as Health Informatics. Health Informatics is concerned with the acquisition, storage and communication of information within the field of medicine. ECG recording technology has reflected this

modernization but this has not been accompanied by an increase in the accuracy and reliability of ECG signal generators and calibration instruments. Examination of the ECG signal generators reported in the literature shows a lack of sophistication and accessibility required in the current era of biomedical instrumentation.

It is accepted that a fully operational ECG signal generator should be capable of providing QRS complex amplitudes of 100 μV to 10 mV [4]. Many instruments reported in the literature claim to offer a 16-bit digital-to-analogue reconstructed test signal with 100 μV minimum output voltage. However, close examination of the literature and the components used in the designs shows that at 100 μV the instruments yield as little as 1-bit resolution [5]. Furthermore, the ECG signals are output directly using devices such as digital-to-analogue converters (DAC), the performance of which are not defined at these low voltage levels. At such low voltage levels effects such as voltage offset, temperature variations and semiconductor noise are also very significant but are not considered in the analysis of the instruments' performance nor are any test results presented.

1.4 ECG Modelling

Modelling of the ECG signal has been the subject of research for a number of decades [6]-[7]. Like so many aspects of biomedical research, the approach taken to modelling the signal and any measurement of the degree of success of the model is dependent on the intended application of the model and objective of the research. There is no "universal" model for the behaviour of the heart muscles, the resulting electrical discharges or the different phenomena observed during ECG recording due to the high variability between individuals, nor is there ever likely to be one due to its very nature. Some models attempt to characterise the effects of various phenomena and the resulting "artefacts" introduced into the ECG recording because of them, while others attempt to characterise and model a healthy ECG signal. The attempts at modelling the ECG signal can be classified loosely into two forms.

Firstly, attempts have been made to model the effects of other phenomena such as respiratory sinus arrhythmia and the presence of Mayer waves on the ECG [8] by creating a three dimensional statespace to simulate the effects of these phenomena on the shape of the resulting ECG signal and the resulting effect on the associated heart rate, known as heart rate variability (HRV). However, these numerical models

are more suited to analysis of the effects of these phenomena on the ECG rather than the characterisation of the ECG signal itself. Timing parameters of the actual constituent P, QRS and T waves are characterised only by manual observation of a normal ECG recording [9]. The author therefore believes these models to be less suitable to calibration and testing of ECG equipment.

Other approaches take well sampled ECG recordings classified as healthy and free from any significant artefact and model the timing of the constituent waves and intervals with respect to heart rate [10]. The resulting characterisation provides a timing model typical of the variation of the constituent waves of a healthy ECG signal. One criticism of the time characterisations found in the literature is that the onset and termination of the P, QRS and T-waves are typically defined by association with fiducial points in a synthetic signal rather than the onset and terminations as defined in a clinical setting by cardiologists [11]. The shapes of the constituent waves have also been modelled using known functions such as Gaussian pulses to characterise the slopes of the signal.

1.5 Aims of the Research Project

No model or hardware platform can claim to provide a test signal with universal characterisation of the ECG signal. The fact that no two heart muscles are identical aside, there are essentially an infinite number of variables that can affect the recorded ECG signal as it appears on the surface of the body. These variables encompass biological effects such as random muscle noise, a non-linear non-stationary respiratory system and the impedance of the skin and its effect on the electrode contact, to name but a few. The heart itself and the variation within its cycle has been proven to be subject to the circadian cycle and even seasonal variation. However, for test purposes a model and test signal based closely on *in-vivo* healthy ECG recordings and their interpretation by expert cardiologists is desirable.

The purpose of this project is to provide firstly a hardware platform which fulfils all of the technical requirements necessary to guarantee an accurate, fully programmable synthesized ECG signal in a modern and accessible instrument. Rather than being merely a design exercise the final instrument shall use leading edge components in a novel arrangement to overcome the current technical limitations of ECG signal generator technology with the portability and interface-ability expected of modern biomedical

instruments. A careful review process will identify the specific technical limitations of current ECG signal generator technology. The system will overcome each of these limitations and the instrument's performance will be tested exhaustively. Rather than an instrument suitable only for the test bench the system shall be portable and have the ability to be employed in multiple environments with consistent results.

With the hardware in place, an ECG model that has been derived from observation of the timing characteristics of *in-vivo* ECG recordings shall be developed. The timing characterisation shall be performed using the location of key fiducial points in reference signals as defined by expert cardiologists rather than a synthetic signal to identify the timing components of the constituent waves. The necessity for a new mathematical characterisation shall be demonstrated and the duration equations compared with the most comprehensive investigation to date and also put in the context of larger clinical studies of the component durations.

Chapter 2

The Human Heart and the Electrocardiogram

2.1 Introduction

In this chapter a brief introduction to the functionality of the heart and the process known as electrocardiography is presented. The human heart is one of the major organs within the body and it belongs to a system known as the cardiovascular system [12]. The cardiovascular system is the first to form in a human embryo and hence the heart is the primary functional organ. This is necessary because a growing embryo requires a means of obtaining oxygen, nutrients and of disposal of wastes during embryonic development [12]. Clinically, the heart is regarded as one of the most important organs in the human body.

The excitation of the heart due to active bio-potentials within its tissues and fibres causes the heart to beat and cyclically pump oxygenated blood around the body. This electrical excitation produces an electric field which can be observed on the surface of the human body. Detection and recording of electric signals on the surface of the body was first performed successfully by Einthoven [1] in 1904 by connecting electrodes to the limbs. This process became known as electrocardiography or ECG measurement. Observation of the electrical signals allows the user to gain an insight into the state of the heart.

Due to its non-invasive nature the use of the ECG has been the subject of biomedical research since its inception and first successful recording by Einthoven. Using the ECG observations regarding the rhythmic pattern of the ECG signal and the shape

and duration of the constituent waves as defined in Figure 1.1, cardiologists can form diagnoses regarding the underlying heart and cardiovascular system. The identification of normal and abnormal characteristics of the ECG is also discussed in this chapter.

2.2 The Heart and Cardiovascular System

The investigation of the heart and the associated cardiovascular system has been the focus of research for centuries. In approximately 1628 William Harvey discovered that blood flowed in only one direction through blood vessels and hence discovered that blood circulates around the body i.e. there exists a cardiovascular system [13]. Harvey's discovery was based on anatomical dissection and deductive reasoning due to the absence of modern instruments such as the microscope. However, in the 17^{th} century Marcello Malpighi observed the presence of capillaries and the link between arteries carrying blood away from the heart and veins carrying blood toward the heart [13]. The research and growth in understanding of the system has continued to this day and medical research has gained a detailed knowledge of how the cardiovascular system operates. A cross sectional view of the heart is shown in Figure 2.1.

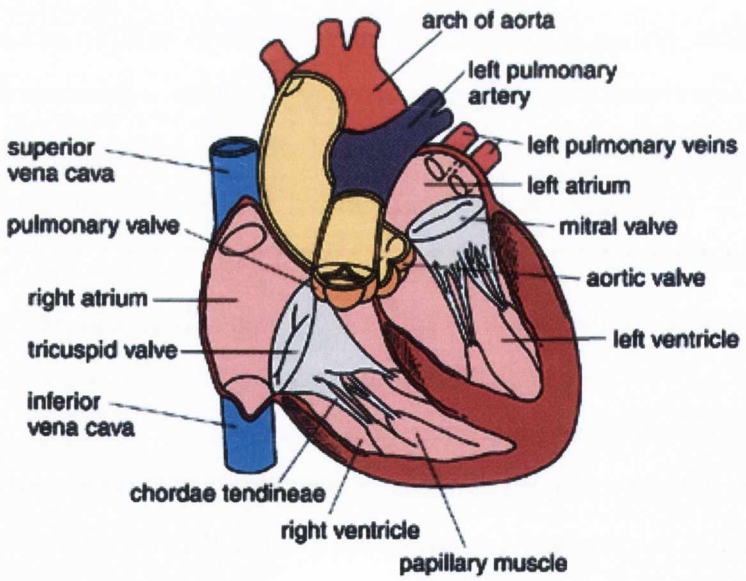

Figure 2.1: A cross section of the human heart [14]

The heart actually operates as two separate pumps [15] and hence there are two basic routes that carry blood throughout the body. The "right heart" (atrium, ventricle etc) pumps blood through the lungs, where carbon dioxide is released and oxygen is absorbed. From the lungs the oxygenated blood travels back to the heart and into

the left atrium. This loop is called pulmonary circulation. Secondly, the "left heart" pumps the freshly oxygenated blood to all other organs, limbs and tissues of the body. Oxygen and nutrients are distributed via the blood to nourish the cells around the body whilst carbon dioxide and wastes are collected and carried to the lungs and kidneys to be excreted. This loop is known as the systemic circulation loop [13].

The continuous rhythmic pumping of the organ is caused by contractions of the muscles within the heart which pump blood from chamber to chamber and then throughout the circulatory system. These cardiac rhythms are controlled by special mechanisms within in the heart that transmit action potentials or electrical pulses to excite the muscles within. For the purposes of this thesis it is the observation of these action potentials or electrical signals and their transmission within the heart that are of most importance.

2.3 Bioelectricity and its Conduction Within the Heart

The heart serves as a pump due to muscle contraction under electrical stimulus. When an electrical trigger signal is received by a muscle the heart will begin to contract. The process starts in the atria which undergo a ripple like contraction [16]. Following this the ventricles contract from the bottom of the muscle upwards. The ventricular contraction and relaxation are known as systole and diastole [ibid]. To understand the presence of electrical fields and potentials in the heart and surrounding tissues a brief introduction to bioelectricity is required.

2.3.1 Bioelectricity

Ionic potentials are present in some cells of the body due to differences in chemical content such as Sodium (Na^+), Chloride (Cl^-) and Potassium (K^+) ions. A cell wall is semi-permeable in that it will allow some ions to pass through its walls quite freely whilst inhibiting others. This may be dependent on the atomic size and charge of the ions in question. In humans, cell membranes are usually more permeable to Chloride and Potassium than Sodium. The result is that the number of positive ions inside the cell is less than the number outside the cell. The phenomenon which keeps the Sodium outside and Potassium inside is known as the Sodium-Potassium pump [ibid].

The pumping out of the Sodium and in of the Potassium is not equal and the result is that the inside of the cell is less positive than the outside of the cell. Consequently the cell is said to be polarized and the difference between the charge inside and outside of the cell is known as a resting potential and is typically quoted as being between 70 to 90 mV [ibid]. The polarisation conditions of a cell at rest are shown in Figure 2.2.

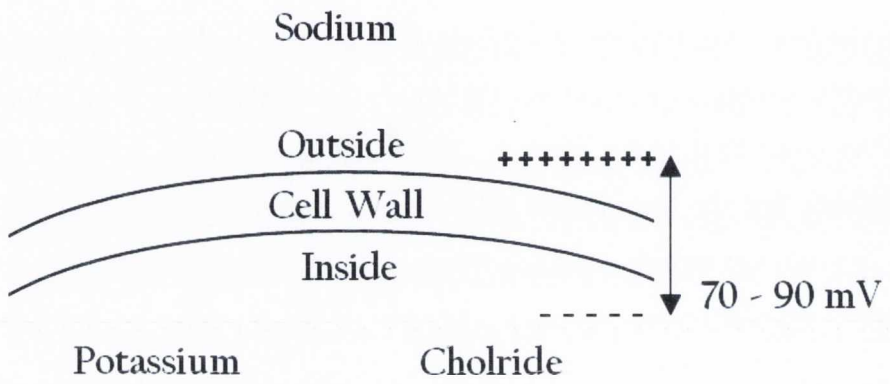

Figure 2.2: Cell polarisation at rest with a resting potential of 70 to 90 mV

When a cell is stimulated by an electric charge, the cell membrane changes dramatically such that the Sodium ions rush into the cell and the Potassium ions inside the cell rush outwards. The resulting movement of charge and change in the cell potential is called an action potential. The cell has been depolarised by the application of the electrical charge. Each type of cardiac cell found in the various parts of the heart e.g. the atria, ventricles etc has its own distinct action potential [ibid].

2.3.2 Electroconduction in the Heart

The heart can hence be thought of as a circuit which transmits pulses via fibres around the muscle to excite the muscle and pump blood around the pulmonary and systemic loops. To understand the conduction process the heart is often represented as a wiring diagram [17]. Figure 2.3 contains the main elements of the cardiovascular electroconduction system.

The sinoatrial (SA) node provides the trigger electrical stimulus to start the heart beat. A small bundle of cells located in the upper right atrium the SA node emits a bioelectric pulse as discussed in Section 2.3.1. The SA node is essentially the pacemaker which controls the rhythm of the heart beat and is capable of self firing although it is also controlled by the body's central nervous system to increase or decrease the

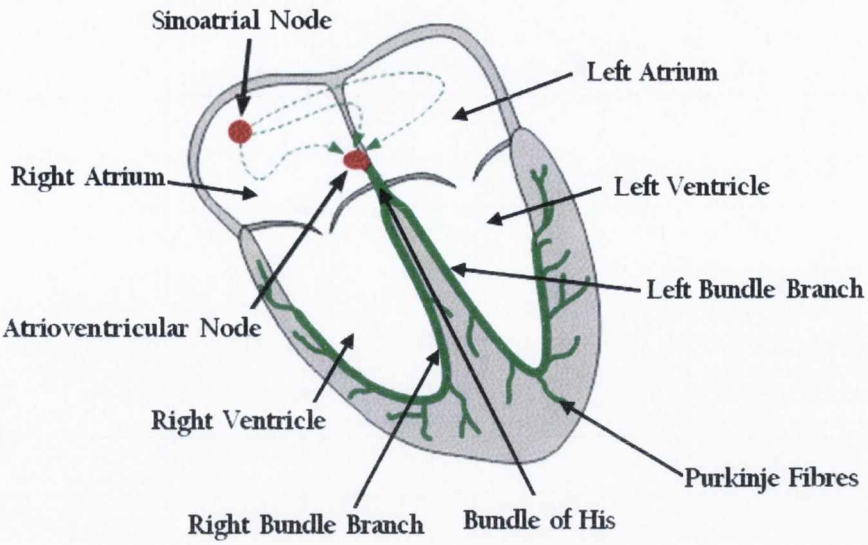

Figure 2.3: The electroconduction system of the heart, modified from [18]

frequency of heart beat. When the SA node fires, the resulting electrical current spreads across the right and left atria causing them to contract. Blood is forced out of the atria and into the lower ventricles on both sides of the heart. The electrical signal moves quickly from the SA node towards the atrioventricular (AV) node in approximately 30 to 50 ms [3].

To allow the ventricles to empty their contents before contracting due to the approaching action potential the AV node operates as a delay unit slowing the action potential by a further 110 ms before the pulse is passed on by the AV node. The pulse is then passed from the AV node and sent towards the ventricle via a branch of fibres known as the Bundle of His that subsequently spits into left and right bundle branches as seen in Figure 2.3.

Once the pulse reaches the left and right bundle branches it travels very quickly via the Purkinje fibres which excite the ventricle muscles of the heart from the bottom up. The pulse can reach the furthest fibres just 60 ms after leaving the AV node. The action potential now causes ventricular contraction which forces the blood from the ventricles out into the pulmonary and systemic loops. The contraction of such a large number of cells at the same time creates a significant electrical signal and a resulting electric field to be emitted. These electric signals can be detected using electrodes placed on the surface of the body i.e. on the subject's chest or limbs. The detection of these signals is what is known today as the electrocardiogram or ECG signal. The different parts of the ECG waveform as shown in Figure 1.1 correspond to different

stages in the cardiac cycle. The P wave indicates atrial contraction, ventricular systole occurs after the QRS complex and the re-polarisation of the ventricles after excitation is indicated by the T wave. The duration, shape and rhythm of these signals can hence provide an insight into the state of the heart and the cardiovascular system.

2.4 The Electrocardiogram

The accurate detection of the resulting electric signals the beating of the heart on the surface of the body is still the subject of countless research projects including [19, 20]. The heart can be treated as a potential source that spreads electrical currents through out the body. Recording of the waveforms produced by this potential source can be performed in a number of ways.

2.4.1 The Einthoven Triangle

The earliest record of a functional ECG recording was presented by Willem Einthoven circa 1904 [1]. Einthoven originally used four electrodes connected to the limbs of a subject for the recording process, although it was later found that the electrodes could be moved to locations on the thorax without loss of signal strength. Einthoven developed the Leads known as the Einthoven triangle as shown in Figure 2.4.

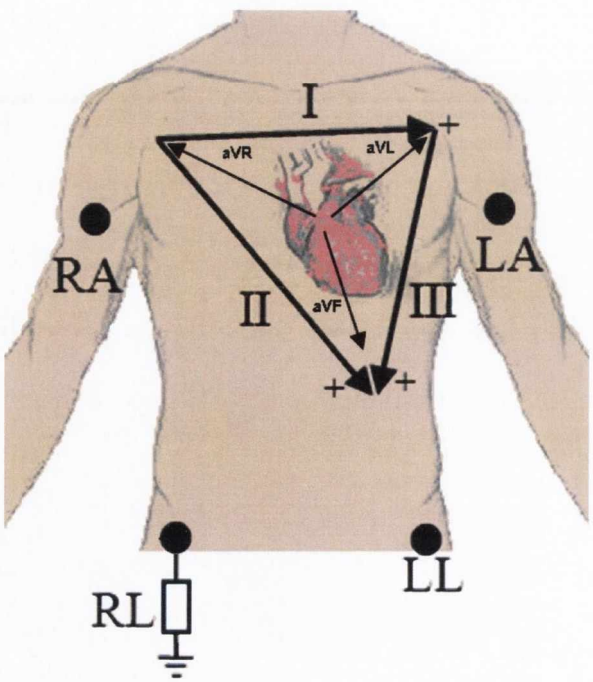

Figure 2.4: The Einthoven triangle and the augmented leads, modified from [20]

The Leads shown by the arrows in Figure 2.4 represent different pairings of the electrodes and each offers a different view of the electrical activity in the heart. A cardiologist can view these different Leads and correlate anomalies in the recorded signal with observations in diseased subjects in the past. The Leads I, II and III are known as the bipolar limb leads and are connected to an ECG recorder's differential amplifier as follows [3]:

- Lead I: LA is connected to the amplifier's non-inverting input, while RA is connected to the inverting input.
- Lead II: LL electrode is connected to the amplifier's non-inverting input and RA to the inverting input. LA and RL are shorted to each other. One can see from Figure 2.4 that the Lead II follows the direction of the initial SA node excitations through to the lower ventricles i.e. the primary cardiac electroconduction vector. For this reason the QRS complex and P waves are often larger in amplitude and easier to observe in Lead II than in other leads, making it the most suitable for single lead monitoring.
- Lead III: The LL is connected to the non-inverting amplifier input and LA the inverting input, while the other two electrodes are shorted together.

These three standard leads allow a view of the heart along the vectors shown in Figure 2.4. The three leads can also be used to examine the composite potential from all three standard leads to give three more leads known as the unipolar or augmented leads aVR, aVL and aVf. These leads are created by connecting one of the electrodes to the non-inverting input, e.g. RA for aVR and averaging the other two via a resistive network, LA and LL at the inverting input of the differential amplifier.

2.4.2 The 12-Lead ECG

The standard three Lead ECG can be extended to provide a total of six Leads using the augmented setup. However, another six leads known as the unipolar chest leads or "V" leads can also be used. In this arrangement the signals from RA, LA and LL are summed in a resistor network at the inverting input of the ECG recorder differential amplifier. Each of the V leads V_1-V_6 can be connected to the non-inverting input of the differential amplifier to provide the additional six signals. The approximate placement

of the ten electrodes required for a 12-Lead ECG recording is shown in Figure 2.5. Other types of ECG recording include inter-digital, oesophageal and fetal ECG. Due to the practical difficulties of 12-lead ECG attempts have been made to synthesise 12-lead ECG based on the 3-lead set-up [21, 22], although 12-Lead ECG is still considered the ideal.

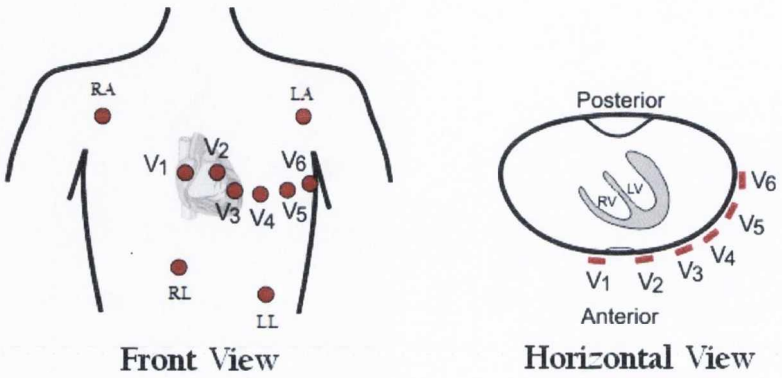

Figure 2.5: The unipolar chest lead placement, modified from [23]

2.5 Sources of Contamination of the ECG

The clarity of detected ECG signals is subject to a number of sources of contamination, some of which are briefly discussed here.

2.5.1 Power Line and Local Equipment Interference

The ECG signal is comparatively low in amplitude when put in the context of industrial, household and other medical equipment. Therefore, surrounding equipment can cause interference in the recording of potentials measured on the surface of the body. Another significant in band source of contamination is caused by the mains power supply [20, 23–25]. Attempts have been made to remove this interference using in-band notch filters [26]. However, such filtering is not allowable under the constraints which govern diagnostic quality ECG recording [27, 28]. Removal of the mains supply is typically reliant on the common mode rejection ratio (CMRR) of the ECG amplifier.

2.5.2 Motion Artefacts

Motion artefacts are transient variations in the ECG baseline typically referred to as baseline wander [29]. They are typically caused by changes in the skin-electrode impedance associated with exercise movement and are a significant obstacle in the

development of dry electrode recording. The removal of baseline wander is discussed in Chapter 6.

2.5.3 Electrode Contact Noise

Loss of good contact at the skin-electrode interface can cause a degradation of the resulting recorded signal. It is similar to baseline wander in appearance but if the contact is normally good the artefact should be minimal or short in duration.

2.5.4 Muscle Contraction Noise

As discussed in Section 2.3.2, the ECG is a detection of the summation of bioelectricity emitted by the cells during excitation. However, other muscles also contract during ECG recording and can generate large amplitudes during stress testing. Muscle contraction noise is usually higher in frequency than the ECG and can be removed by low pass filtering as shall be seen in Chapter 6.

2.5.5 The ECG Recording Machine

Like any other biomedical instrument the device has its own inherent sources of error such as component temperature coefficients and noise associated with semiconductor devices. If the instrument is not working correctly it could introduce noise and artefact into the signal that could be misconstrued by the user as diagnostically significant. Although not necessarily an artefact associated with ECG recording the necessity to guarantee the accuracy of the ECG machine itself is paramount. The issue is that the ECG machine cannot be tested by connecting it to a subject since the recorded signal is essentially unknown and hence noise or artefact introduced by the ECG machine itself is indistinguishable. Therefore, it is the elimination of any possible distortion of the signal by the ECG recorder that is the motivation for providing a clean, stable and controllable test signal.

2.6 Heart Rate Determination using the ECG

The characteristic most frequently measured during ECG is the subjects heart-rate. The heart-rate is typically expressed as the number of beats per minute. In theory it could be measured from the onset of the P wave in an ECG beat to the P wave onset

of the following beat. In practice, however, the heart-rate is usually determined by measuring the time between successive R-peaks since the R-peak is the most readily identifiable component in an ECG recording. The equation for heart rate (HR) is given by:

$$HR = \frac{60}{T_{RR}} \tag{2.1}$$

where T_{RR} is the cardiac cycle time in seconds measured between successive R peaks as shown in Figure 2.6.

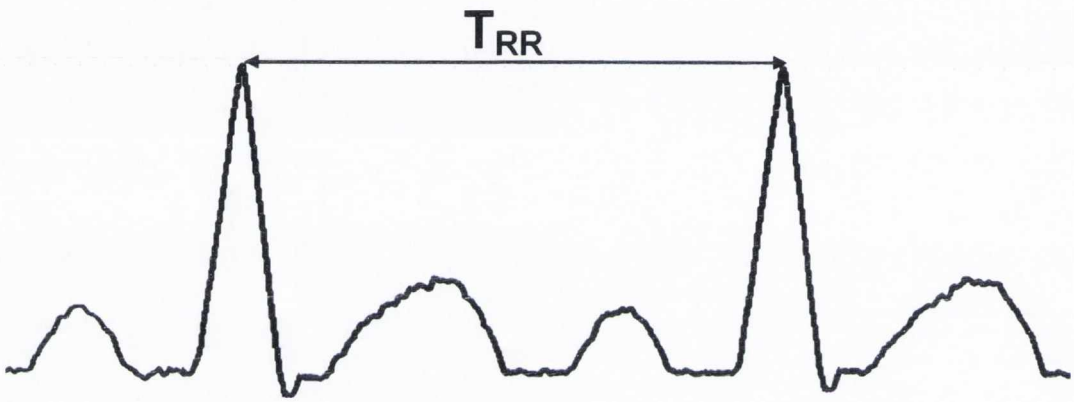

Figure 2.6: The cardiac cycle time T_{RR} is measured between successive R peaks

The variation of the RR interval, and subsequent heart rate variability (HRV) within a subjects ECG can provide information on how the autonomic nervous system acts on the cardiovascular system and to diagnose heart abnormalities [30].

2.7 Diagnosis via Abnormalities in the ECG

Observation of the timing and shape of the ECG signals in each of the leads can be used by a cardiologist to form a rapid diagnosis of a subject's clinical status. There are a variety of abnormalities that can be correlated with illnesses using the ECG. To illustrate the importance of each constituent wave in the ECG when used as a clinical tool a number of examples of subject abnormalities detectable via ECG are described in this section:

2.7.1 Ventricular Fibrillation

If the ventricles are not contracting correctly then blood is not being pumped to the pulmonary and systemic loops adequately. The ECG signal becomes completely disorganised and no QRS complex is decipherable in the resulting low amplitude signal [17]. Ventricular arrhythmia will cause the patient to loose consciousness rapidly and can prove fatal within just a few minutes if not corrected [3].

2.7.2 Atrial Fibrillation

In this type of fibrillation the atria quiver rather than contracting regularly. It is often caused by the presence of multiple pace making sites in the right atrium instead of a single cluster of cells which form a healthy SA node [3]. This is usually discovered by the absence of a clear P wave in the ECG recording. The QRS complex becomes irregular but is still present and hence it is less serious than ventricular fibrillation because the ventricles continue to beat.

2.7.3 Blockage of the AV node and Bundle Branches

A blockage in the left and right bundle branches can be observed by a widening in the QRS complex i.e. increased duration [2]. If complete left and right bundle branch block occurs the action potential can not depolarise the ventricles and the heart will cease to pump adequately. Complete AV node blockage can have similar consequences and can be identified by a long QT interval duration.

2.7.4 Hypercalcemia and Myocardial Infarction

Hypercalcemia is an excess of calcium in the blood and can be a symptom of serious underlying conditions such as kidney failure, cancerous tumours and adrenal gland failure. It can be diagnosed via the ECG by observation of a shorter than normal QT interval. Myocardial infarction or heart attack is the interruption of blood supply to part of the heart. It can be caused by blockages in the arteries feeding the heart and if left untreated can lead to death. Myocardial infarction can often go unnoticed i.e. no chest pain but is detectable by an excessively long QT interval duration [2].

2.8 Conclusion

The complexities of the human heart have been introduced in this chapter. The pumping of the heart relies on the excitation of the muscles of the atria and ventricles by low amplitude electrical signals transmitted throughout the heart by fibres. The summation of these electrical signals emitted during the heart beat can be viewed on the surface of the body as the ECG signal.

The signals are low in amplitude and subject to many corruptive sources of contamination and distortion. However, when recorded accurately it has been demonstrated that the signals can be used to diagnose a variety of clinical conditions not only directly associated with the cardiovascular system but also chemical imbalances within the body. Electrocardiography is rapidly applicable and non-invasive.

Chapter 3

A Review of ECG Signal Generator Technology

The use of ECG recordings as a diagnostic tool relies heavily on the fidelity of the recorded signal. A number of signal generators have been previously presented in the literature. However, the platforms they have been developed on have become dated and more importantly their architectures do not provide the necessary accuracy. The shortcomings of previous instruments are reviewed here and issues regarding amplitude range, voltage offset correction and temperature stability are highlighted. The devices can be grouped into three types software based simulators, PC based signal generators and standalone microprocessor instruments.

The accuracy of an ECG signal generator cannot be determined by comparison to a single testing protocol [31] since no record of one has been reported in the literature [32]. As a result testing must be performed using due diligence and by analysis of the instrument in light of its intended application. It is demonstrated in this chapter how claims of accuracy are frequently made without the necessary testing to verify these claims. Hence, this review also contributes to the testing strategy used in Chapter 4.

3.1 Software Based ECG Signal Simulators

There have been a number of purely software based ECG signal simulators proposed in the literature some of which shall be discussed here. The obvious limitations of these designs are that they are merely software based and can only be used to test ECG signal processing algorithms. ECG computer based simulation has been a topic

of research for decades and an awareness of the approaches taken to purely "soft" ECG simulation is useful.

3.1.1 Classical Software Simulations

The rapid introduction of the PC into research during the late 1980's sparked an increase in ECG synthetic signal simulation for testing. The necessity for realistic looking ECG's can be found in early simulation designs such as that of Shuqian *et al.* [33]. The necessity for simulated signals to reflect *in-vivo* ECG recordings was satisfied by using a set of parameters known as The Minnesota codes [34], to define simulated signal features such as amplitude and duration. The simulation was useful for generating up to 100 different types of ECG arrhythmia. However, how the signal features can vary with heart rate e.t.c. were not considered. The output signals are fixed to the code, or feature parameters as defined by the original Minnesota codes.

The author does state that the signals could be generated as actual analogue test signals using a digital to analogue D/A card with the PC. However, the assumption that the test signals can be delivered adequately in this fashion is at best idealistic as shall become apparent through out this and the following chapter. In an attempt to overcome the somewhat restricted nature of the output signal, a later design by Sadighi *et al.* [35] takes ten ECG recordings and allows the randomised selection of the waveforms to be output in sequence to reflect variation in the ECG signal. The heart rate of successive beats is also varied randomly to reflect the variability of the heart rate. Although crude in that the resulting ECG output is the result of a numerical, essentially random process, it does provide signals which at least vary, even if not in any way reflective of true ECG variations. Again, no details are provided for generating the signal as anything other than a teaching tool or software test signal.

3.1.2 Modern Software Simulation

Naturally the sophistication of ECG simulation packages has increased since the earliest found in the literature. A modern ECG simulation method proposed by Josko *et al.* [36] has been developed in the Matlab simulation environment. Implemented and tested in SIMULINK, Matlab's simulation tool, the simulated signals are generated using pulse generators, the amplitude, period and phase of which can be altered to change the features of the resulting signal. After filtering and summing the constituent pulses

together to form a complete ECG beat, noise and power-line interference can be added to the signal.

The method of adding noise and altering the heart rate and the constituent component durations is somewhat adhoc in that no basis is provided for simulating the signal in a manner reflective of actual ECG recordings i.e. amplitude levels. The artefact or noise is added to reflect real-life measurements but without being correlated to real-life situations in any fashion. The simulated signals could be useful for testing software processing algorithms, an example of which - a QRS peak detector, is given although this could probably be performed using actual ECG signals, hence questioning the necessity of a synthetic signal in this application. The usefulness of the "Virtual Instrument" is claimed to be that it provides a complete testing platform for ECG acquisition (among other advantages). However, the resulting simulated test signals are not actual analogue signals. Its ability to test ECG acquisition machines i.e. ECG recording machines is therefore uncertain.

3.2 PC Based Hardware ECG Signal Generators

An alternative approach is to simulate the signal in software, be it on a PC or other processor, and output the signal via an analogue conditioning stage. In doing so, the ECG signal generator can be used to test the front end recording unit of ECG machines and if the test signal is properly defined before simulation it can also be used to test the back end signal processing algorithms such as peak detectors and automatic annotation algorithms also. As a result, the majority of ECG simulator or signal generators found in the literature include an actual output hardware stage to provide an analogue ECG signal. For the purposes of this review the designs shall be grouped into PC dependent designs and standalone designs which can operate independently of a PC. The PC based designs created over the last twenty years have varying degrees of complexity, and a cross section of different approaches to a PC based design are reviewed.

3.2.1 A PC-based Generator by Franchi *et al.*

A PC-based generator was devised by Franchi *et al.* [37] in 1994. The system is composed of a PC which acts as the controller of a bank of DAC's. The DAC's are used to convert digitally stored ECG signals into output analogue signals. The analogue

signals are then filtered and simulated artefact can be added to the signal using a bias function. The authors have proposed that DAC's are not suitable for the direct output of signals in the required amplitude range and a PC controlled amplifier attenuation stage is used to attenuate the signals to the required output voltage range. This is an important observation and shall be discussed in more detail later.

Since this design uses stored actual ECG signals it is not suitable for what is known as "absolute accuracy" (i.e. exact measures of distortion) [37] testing or calibration because the generated signals contain recording noise and artefact from the original recording and hence when re-recorded by the ECG machine under test it is not possible to distinguish between noise from the original and that added in the second recording phase. However, the advantage of using actual ECG recordings which have known features, e.g. annotated fiducial points, is such that after re-recording the test signals can be inspected again to see if when re-annotated by an expert or automatic algorithm the resulting fiducial points are the same. If they are not, then an error has presumably been introduced during the re-recording phase.

There are a number of concerns regarding this design. Firstly the D/A and attenuation stages of the architecture are not isolated from the PC. The result is that mains 50 to 60 Hz noise from the power supply of the signal is passed directly to the analogue conditioning circuit. Other PC related noise such as the switching noise of the central PC processor and peripheral circuitry could also spoil the output of the signal generator. The design does not specify what D/A converter or op-amps are used in the analogue stage of the design. No in depth analysis of resulting output noise and temperature characteristics are provided. The minimum output amplitude level is reported as being "in the order of mV" as opposed to the required 100 μV range proposed in Chapter 1. The accuracy of the signal generator is measured by the location of the original recording fiducial points and those found after re-recording of the regenerated signals. The device is not intended as and therefore not suitable for ECG calibration since it contains an array of undefined or unanalysed sources of noise and interference.

3.2.2 PC and MCU Based Design by Mudrov *et al.*

Recognising the requirement of isolation of the analogue ECG output stage of a PC based design Mudrov *et al.* (2004) [38] have proposed a device which communicates

with the host PC by way of an infra-red transmitter and receiver. The design incorporates an 8-bit Microchip PC18F microcontroller (MCU) device that receives simulated ECG test signals from the PC via the optocoupler infra-red device. The MCU also manages user inputs such as selection of required output signal via a 15 button keypad. A flash memory chip is available to the MCU for storing input ECG signals received from the PC.

From a user point of view, the signal generator requires its own power converter to charge the on-board batteries and a PC with an available connection. Although the device has its own microprocessor and power supply on-board its interface with the user is limited to a 15 button keypad which makes operation quite cumbersome. The resulting output signal can be altered using the keypad in terms of sampling frequency although alteration of the actual morphology itself requires reconnection to the host PC. In order to operate the system in a test environment the user requires a PC, a monitor, associated peripheral devices, an RS232 cable to connect to the signal generator and a separate charger for the signal generator batteries.

Figure 3.1 is an excerpt from the schematic layout of the Mudrov *et al.* instrument [38]. The digitally stored ECG recordings are output via an Analog Devices AD5320 12-bit DAC (U6). Similar to the design of Franchi *et al.* [37] the DAC outputs are at a higher output amplitude level than required and are then attenuated. After an amplifier buffer (U7A and U7B), a resistive network (R1-R4 and R6) is used to step the high voltage output which has a maximum reference value of 4.096 V to a differential voltage of ±5mV. The DAC output is unipolar and hence the ±5mV range is with respect to a pair of leads as opposed to a common reference or "ground". In order for the resulting differential signal to correctly represent actual ECG constituent waves the input signal must have been biased positively in software before being passed to the analogue stage. As a result a common mode component is passed to the differential amplifier of the ECG recording machine under test and in this sense it is not a true differential signal. This common mode signal will have to be removed by the ECG recording machine's differential amplifier. A good ECG recording machine should be able to do this but there are two issues with a test signal of this nature. Firstly, the suitability of a test signal should not rely on the performance of the equipment under test since this is in itself contradictory. Secondly, if one wishes to test the ECG recording instrument's ability to remove common mode components from the input differential signal the common mode components should be added in a controlled fashion to the test signal

i.e. have no common mode component to begin with and then specific levels added to the test signal for observation at the output of the ECG recorder.

Apart from the inherent common mode component of the signal, another concern regarding the design is that for the generation of the output signal a resistive network is used as opposed to a voltage source. This may cause signal distortion by a connected test device if the input impedance is not sufficiently high, or it may add to the electrode impedance and hence affect signal quality.

One can also see from the schematic that the output voltage must be altered using the variable resistor, R_6, which has two limitations. Firstly, in order to scale the output signal R_6 must be either manually scaled or perhaps buttons on the keypad have been provided to do this, although no detail has been provided with regard to the nature and access of this variable resistance. The design also means that P and T waves must be fixed in amplitude pre-DAC, i.e. their amplitude is dictated as a factor of the 12-bit DAC input code. This limits the resolution of the P and T wave amplitudes. Consider a case where the required QRS complex amplitude is 10 mV and a P wave scaled to 250 μV which is quite possible in a real life ECG signal. This means that the P wave now only has 4-bit precision as opposed to the 12-bit precision stated, as it only applies to the QRS complex. In theory, the accuracy of the output signal should be consistent for all components of the ECG signal and not just the QRS complex.

The noise and temperature coefficients of the components used in the design are not analysed nor is any figure for measured output noise provided.

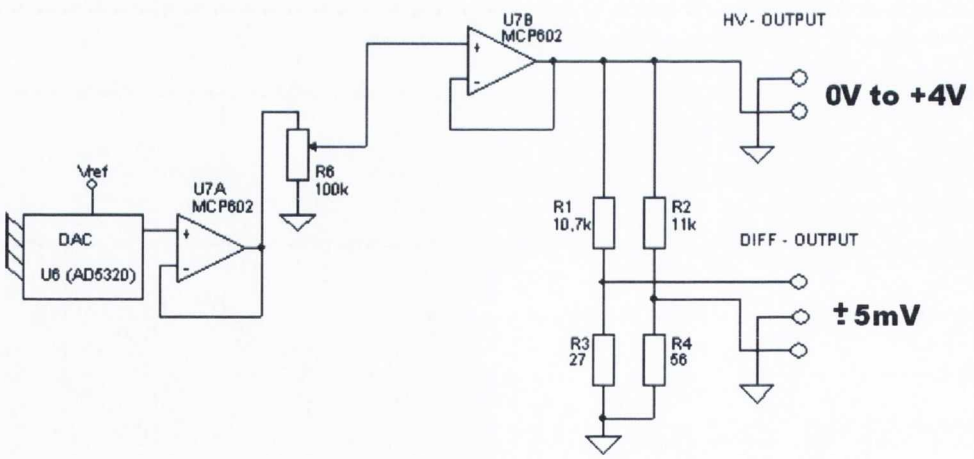

Figure 3.1: Analogue stage design for the Mudrov *et al.* ECG signal generator [38]

The device proposed by Mudrov *et al.* overcomes the isolation issues found in the Franchi *et al.* design. However, the device appears extremely cumbersome to use,

given the requirement of a PC and connection cable to alter the output test signal and independent power supplies for both the PC and signal generator. The analogue output stage has an inherent common mode component, output impedance mismatch, lack of precision for the individual constituent ECG components and no performance measurements or analysis has been performed on the claimed ±5mV output amplitude range.

3.2.3 PC and MCU Design by Martinez *et al.*

A more modern but similar design to that of Mudrov and Franchi *et al.* the microprocessor and PC based design proposed by Martinez *et al.* was published in 2007 [39]. This design is very similar in that it exploits the use of a Microchip PIC16C MCU to control the D/A stage of the signal generator but still requires overall control using a PC. The design suffers similar limitations to both of the previous designs discussed.

The output network for the Martinez *et al.* signal generator is shown in Figure 3.2. The MCU and analogue conditioning circuit is not isolated from the PC and hence suffers from mains generated interference and noise. The DAC arrangement is again unipolar so Q and S waves which are defined as deflections below the iso-electric cannot be generated as such since all signal components must be positive. The resulting output differential voltage hence contains a common mode component as discussed in Section 3.2.2.

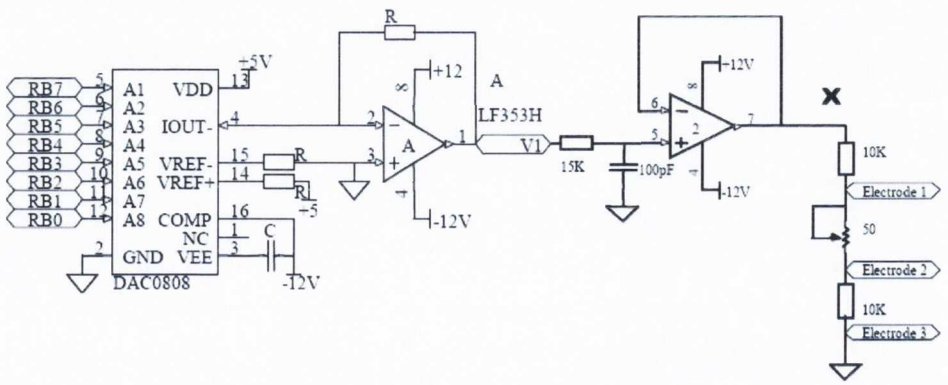

Figure 3.2: Analogue stage design for the Martinez *et al.* ECG signal generator [39]

There are a number of issues concerning this layout. The resistive network used to attenuate the output is said to have been tuned deliberately, presumably to simulate a skin electrode impedance, to 5 kΩ. However, if the ECG machine under test is required to match another impedance or the skin electrodes of the ECG leads used with the

recording machine are not 5 kΩ, this will result in a mismatch. Both Martinez and Mudrov have been shown to provide two different fixed output impedances, while it would be more beneficial in practice to provide a matched very low output impedance i.e. as close to an ideal voltage source as possible to allow versatile connectivity.

Similar to the Murdov design, the output amplitude is varied using a resistor pot and hence the same scaling limitations of the P and T waves are found in this design. In fact Martinez *et al.* use only an 8-bit DAC so the resolution of the P and T waves after scaling using the DAC are more serious.

In terms of testing the accuracy of the signal generator, the authors state that the device has been tuned for test to provide an output voltage of 8 mV which is at the very upper end of the ranges required 100 μ to 10 mV amplitude required. The testing of the signal generator involves only a visual comparison between a real ECG signal with itself after regeneration by the signal generator. The accuracy of the device is not analysed to account for amplifier offset, temperature effects or DAC offset etc.

3.3 Standalone MCU Based Signal Generators

It has been seen in Section 3.2 that using a PC based signal generator has a number of limitations. Isolating the output signal from the PC requires the use of an additional processor such as an MCU to control the ECG analogue generation process. A number of authors have seen the redundancy of using a PC which still relies on a MCU to control the analogue interface and conversely an MCU which is configured in such a way as to require overall control by the PC. As a result, a larger number of signal generators found in the literature exist as standalone instruments where user interfacing, instrument control and signal generation is performed using a single isolated controller i.e. the PC is removed from the process.

Early implementations of these signal generators can be found in the literature from a number of decades ago. Gradually standalone devices have become more sophisticated, although recent research has shown little improvement over previous designs. To gain an understanding of the progression in ECG signal generator design a number of devices dating from 1998 to 2008 are reviewed.

3.3.1 Kontodimopoulos Prototype ECG Simulator

The prototype proposed by Kontodimopoulos *et al.* in 1998 [32] presents an eight output signal generator that allows for the addition of a pacing signal for simulating pace maker pulsing. The reported design of the signal generator is not very clear in that no complete circuit diagram, part numbers (other than the HC11F1 8-bit MCU) or specific details of the circuit layout can be found in the article only a block diagram as shown in Figure 3.3 is given. The user has 4 input buttons available and the output is displayed on a one LCD screen.

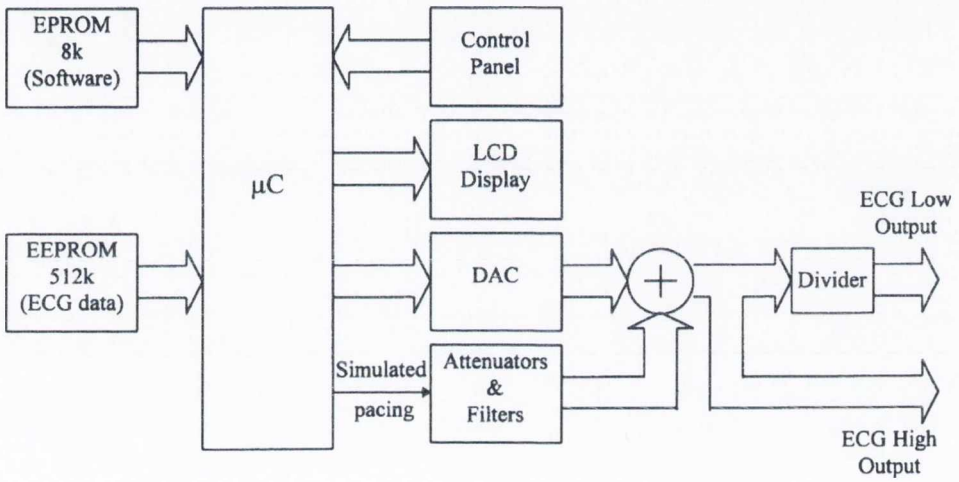

Figure 3.3: The Kontodimopoulos signal generator block diagram [32]

The design appears to be powered via an independent isolated battery supply although the MCU requires a 5 V signal while the technical specification of the device states the use of only two 1.5 V rechargeable batteries. The signal generator is capable of supplying non-ECG like test signals such as sinusoids and triangular waves with amplitudes of 1 to 4 mV peaks in 1 mV increments. ECG signals are also provided, but only in the same 1 to 4 mV amplitude range, the heart rate of which can be selected in multiples of 0.4 to 2.8 times the original heart rate. It is not clear how the alteration in heart rate is accomplished or how the constituent waves are varied to reflect this change in heart rate.

Also seen in Figure 3.3 is how the output signals from the DAC are attenuated by the divider block to achieve the 1 to 4 mV ECG output range. The only portion of a circuit diagram found in the article is of this divider block and is shown below in Figure 3.4.

Since there is no variable resistance in this schematic it can only be assumed that

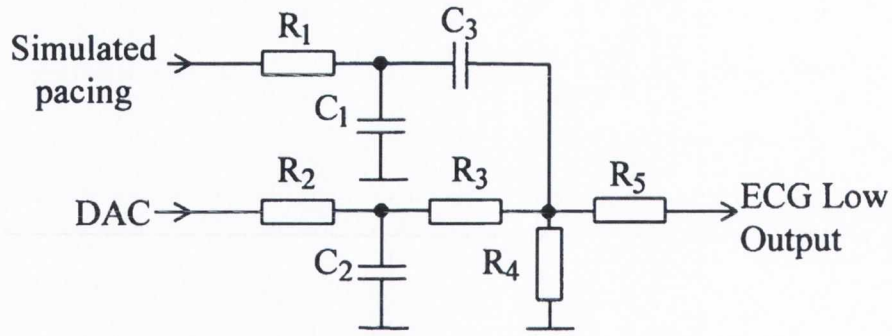

Figure 3.4: The output stage for the "ECG low output" [32]

the QRS amplitude is varied from 1 to 4 mV by altering the input code to the DAC. This results in a lower resolution for signals below 4 mV i.e. an input code of 00111111 to the 8-bit DAC could be used to reduce the peak output by a factor of four. It is not stated how, if at all, P and T wave amplitudes in the test ECG signals can be scaled to a voltage other than their original recorded amplitude. However, if the P and T wave amplitudes do require scaling i.e. to alter the test signal this could only be provided by a further reduction in the input code to the DAC and an accompanying reduction in resolution. It is not made clear if the test signals are bipolar or uni-polar.

This design is described as having been tested by connecting the signal generator to a number of ECG recorders and an oscilloscope to enable the output signal to be viewed. However, no observation of these results or accuracy are reported. No analysis of the output circuitry is provided either. The accuracy and suitability of the signal generator depends on tested and verified accuracy which has not been established. The design is interesting, however, in that it provides an early example of a standalone ECG signal generator.

3.3.2 An Accurate Programmable Simulator by Burke & Nasor

It is clear from the design discussed above that early standalone signal generators required significant improvement and greater consideration of the control and user-ability of the instrument. This necessity is reflected in the instrument originally published in 1998 and in revised form in 2001 by Burke & Nasor [4, 26].

A significant improvement on the other designs, it generates a Lead II signal having a profile that varies with heart rate in a manner which reflects the true *in vivo* variation. The user is provided with adjustment of heart rate, signal amplitude, QRS complex

up-slope, and the relative amplitudes of the P-wave and T-wave. The heart rate can be set within the range 30 to 200 beats min^{-1} in steps of 1 beat min^{-1}. The amplitude of the QRS complex can be verified from 0.1 to 20 mV in 0.1 mV steps, while its up-slope can be set between 10 and 50 ms with a 1 ms resolution. The amplitude of the P-wave can be varied from 5 to 40% and that of the T-wave from 10 to 80% of the amplitude of the QRS complex with a 1% resolution. The design also offers a bi-polar output signal which, as has been discussed, is ideal for an ECG test signal. The user interface is comprised of a LCD display and 16 button keypad.

The design offers a significant improvement over the others discussed thus far in that the output stage is provided using two operational amplifiers as opposed to a resistor network i.e. closer to an ideal voltage source as seen in Figure 3.5. The design is also more accurate in that a three stage DAC process is used to vary the reference voltage to three different DAC's in order to provide full 8-bit resolution for all the constituent waves of the ECG and not just the QRS complex. The device is also fully isolated from mains using an independent battery source.

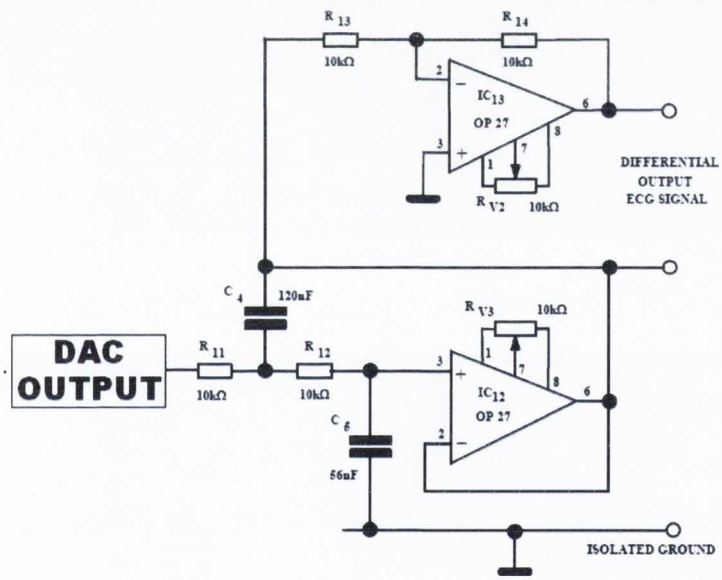

Figure 3.5: Segment of the Burke & Nasor signal generator output stage [4]

Although presenting a significant improvement over the Kontodimopoulos *et al.* design there are still a significant number of shortcomings associated with this design. Firstly, the output signals are not attenuated by any means after digital to analogue conversion so that the DAC must generate the signals in the required 0.1 to 10 mV amplitude range directly. The ability of a DAC to to do this at such a low output level is not defined nor reliable even in modern DACs i.e. they are not suitable to be used

in the sub-mV range. No test results for the output signal in the sub 1 mV range have been reported.

The choice of an OP27 output amplifier, which was the then state of the art precision op-amp allows an offset voltage drift in the order of 20 μV over a temperature change of $\pm 25°C$. When put in the context of a 100 μV QRS complex amplitude this is a significant offset voltage. Other issues such as output noise voltage of the amplifier, input bias current effects and offset voltages were also not considered or compensated for. The design offers some advantages not found in the others discussed thus far and also greater versatility in the user control of output heart rate and constituent component amplitudes. However, one would expect subsequent designs to have improved upon the limitations highlighted here.

3.3.3 An ECG Signal Generator using an MCU and CPLD by Chang Chien *et al.*

A design published in 2006 and 2007 by Chang Chien *et al.* [5, 40], offers little performance improvement over its predecessors and is quite similar to the Burke & Nasor architecture. A complex programmable logic device (CPLD) replaces some of the peripheral components used in the instrument design (a port exapansion chip, tri-state reciever etc) reported by Burke & Nasor.

Some minor changes to the design have been applied to improve accuracy such as the use of the OPA2335 amplifier as the output component shown in Figure 3.6 which provides a lower temperature drift than the OP27 but still suffers from a 5 μV offset per amplifier which is not compensated for. The design by Chang *et al.* removes the multi-stage DAC feature of the original Burke & Nasor design such that P and T waves can only be generated using lower input DAC codes and hence gives reduced resolution of these constituent waves. Consequently, the claimed amplitude rage of 0.1 to 10 mV is misleading in that 1 least significant bit is 0.1 mV i.e. for outputs of 0.1 mV only 1-bit precision is available as opposed to 8-bits using the original Burke & Nasor design. The Chang arrangement is also uni-polar as can be seen from the lack of a negative power supply to the DAC IC_3 in Figure 3.6.

The output stage provided by Chang *et al.* provides less precision in terms of bit resolution and polarity but with a marginal decrease in temperature drift due to the up grading of the available amplifier. However, the system has not been tested nor

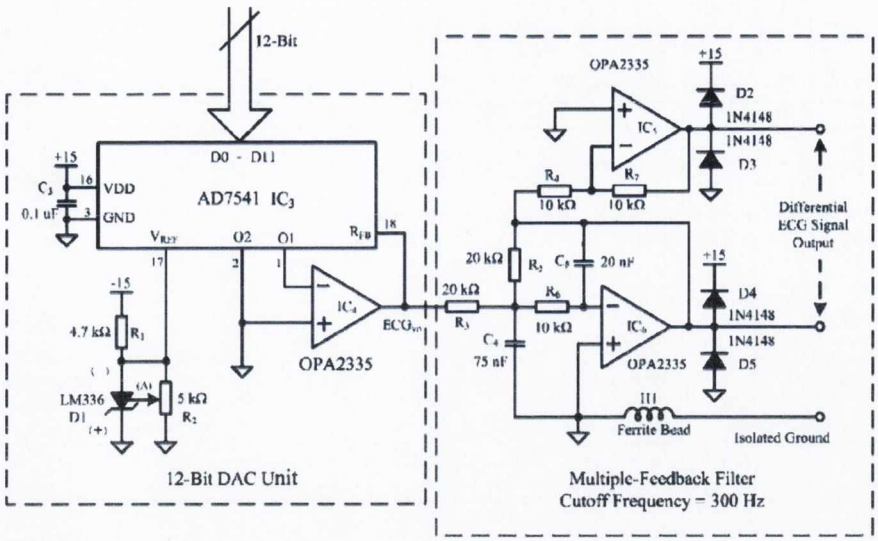

Figure 3.6: Segment of the Chang Chien signal generator output stage [4]

analysed in any more detail than the Burke & Nasor design nor have any of the concerns regarding the low amplitude DAC output, voltage offset compensation, temperature drifts or bias current etc been addressed. The user interface is also identical in the form of an LCD display and 16 button keypad, which by 2007 could probably have been replaced with a cost effective more sophisticated alternative.

3.3.4 The Caner *et al.* ECG Simulator

The programmable ECG simulator proposed by Caner *et al. et al.* in 2008 [41] is based on the use of a Digital Signal Controller MCU device or DSPIC. The DSPIC30F is a modern 16-bit MCU which has been designed to function with essentially two different signal processing cores, one for standard MCU operations and another for enhanced signal processing applications. The DSPIC30F is the fastest operational MCU used in any of the designs discussed thus far. Its enhanced operation over other MCU's is due to its ability to perform multiple operations using both cores at the same time, e.g. to fetch two data operands whilst multiplying two others concurrently. Its processing power allows the processing of over 30 Mega instructions per second (MIPS).

Despite this increased performance MCU, the design still requires all signal processing such as output waveform synthesis to be performed on an external PC with the result passed to the MCU by an RS232 connection. The MCU operation can be controlled by the user using six switches as a keypad. Four of the switches can be used to vary the heart rate from 30 to 120 bpm in four steps. The remaining two switches

start and stop the output signal. The schematic layout of the analogue stage of the design is extremely unclear but it appears to provide a bipolar output signal of ± 5 V. Amplitude noise can be added whilst synthesising the output signal on the PC. Presumably to isolate the signal from the mains supply, the RS232 cable is detached from the signal generator whilst being used.

The performance of the signal generator appears to have only been tested using output signals with a 5 V peak-to-peak amplitude. The only test results reported are three output waveforms with different levels of noise added to the signal with no testing of the device below these amplitude levels presented. Furthermore, no analysis of the component noise or stability has been carried out. The output heart rate range, amplitude level and the users ability to vary the output signal therefore appears limited. It would appear this design offers an instrument which is less sophisticated than its predecessors and its performance in generating actual ECG test signals in the heart rate and amplitude range is undefined.

3.4 Conclusions Regarding Hardware ECG Signal Generators

It has been seen that a number of software ECG simulators can be found in the literature. However, these devices are only suitable for testing ECG processing algorithms since no actual output ECG analogue signals exist. As a result their application is quite limited when put in the context of the entire ECG recording process i.e. from electrode to diagnosis. The majority of ECG signal simulators and generators therefore contain a hardware stage for ECG output.

A number of limitations of PC-based hardware designs have been highlighted. It has been seen that a signal generator composed of a D/A and op-amp PC cards is not appropriate. Shielding and isolating the analogue conditioning stage from the mains and operational noise found in a PC is nearly impossible. This has been reflected by more modern PC based designs which use a second independent controller off site to handle the signal generator analogue signal conditioning circuitry. However, in this case, two processors, i.e. the PC and the MCU, are required to implement the instrument.

Unipolar output signals must be biased positively pre-conversion to provide correct

ECG signal morphology when differentially amplified. This introduces a common mode component into the signal which therefore relies on the ECG recording machine's ability to remove this component. Although the ECG recorder should be able to do this, the fact remains that the test signal essentially contains an artefact which must be removed by the instrument the signal is intended to test. In addition, it was found that output impedances which are dictated by a resistor divider network can cause two problems, a slight mismatch on the output channels and finite output impedance. This could mean that the device may not be connected directly to skin electrodes should the user wish to test the entire ECG recorder accuracy, i.e. from electrode to output recording. It was also shown that many methods of altering the amplitude of the output signal are quite crude since they depend on the variation of a resistor pot. This means that the P and T wave amplitudes must be scaled pre-DAC in software, which and has been shown to decrease their resulting resolution.

The PC based designs require the use of two processors to carry out the required operations. This is quite inefficient since an MCU device is capable of carrying out the entire signal generator operation if designed correctly. Therefore, a number of stand-alone ECG signal generators produced between 1998 and 2008 have been reviewed. It has been found that instrument designs found in the literature have shown no genuine improvement in terms of sophistication, accuracy or user controllability since the Burke & Nasor design published in 1998. No single design has been found which can provide all of the following desirable characteristics of a test ECG signal generator:

(I) An interface which can rival the PC based designs in terms of sophisticated accessibility i.e. not depending on keypads and two line LCD screens.

(II) Verified performance with complete controllability of the output signal i.e. full heart-rate range and amplitude scaling of each constituent component.

(III) An appropriate output stage which provides a near ideal voltage source for connection to any source impedance found in an ECG recorder.

(IV) A pure differential output signal without a common mode component.

(V) Analysis testing to calculate maximum output noise and temperature effects of the signal generator.

(VI) Physical verification and testing of the amplitude and timing accuracy of the output waveforms.

The author is therefore convinced that a new ECG signal generator design is required. The device should be stand-alone, incorporating a modern user interface and providing connectivity to the wider biomedical world i.e. facilities to provide wireless connectivity for remote access and control. Most importantly, the new instrument must overcome the technical and performance limitations which were found repeatedly during review. Claims of increased accuracy must be supported by thorough analysis, testing and verification.

Chapter 4

The Versatile Temperature Stable ECG Signal Generator

4.1 Introduction

The instrument presented in this chapter offers precision across the full amplitude range, with P and T waves measuring as little as 1 μV amplitude and adhering to specific timing parameters. The recreation of low voltage analogue signals is performed using a novel arrangement of low-noise state-of-the art operational amplifiers which are specified to operate with low output noise levels, very low offset voltage and zero temperature drift to ensure optimum signal precision. In terms of accessibility the colour LCD graphical interface, independent battery source and possible internet connectivity make the device user friendly and allow the portable or even remote testing of ECG recording machines and assessment.

Rather than just a design exercise the research problems regarding ECG signal generation introduced in Chapter 1 are systematically overcome. The instrument's output noise voltage, timing accuracy and temperature stability is guaranteed both analytically and in the development of a full working prototype. Results are provided which demonstrate the increased accuracy of the device over those discussed in Chapter 3. Importantly, the final instrument design provides the basis for the subsequent ECG signal modelling and characterisation discussed in the rest of this thesis to be delivered as a real world analogue test signal. Without this hardware platform in place the accuracy of these ECG signal models are of little value in a practical test scenario. It can therefore be used as a basis to implement the models that shall be discussed in the

rest of this thesis for a fully controllable test signal.

The material and results presented in this chapter are based on two peer reviewed publications by the author [42, 43].

4.2 The Hardware Architecture

A number of different technologies were considered during the initial stages of the design. As part of the selection criteria signal-to-quantization-noise-ratio (SQNR) and speed requirements were taken into consideration as discussed later. A USB interfaced approach allows the use of the PC as a user interface. However, such a design still requires electrically isolated peripheral circuitry to perform the actual generation of the low-voltage ECG signal as demonstrated by [38] and [39]. Field-programmable gate arrays offer a high speed alternative but they are significantly more expensive in terms of hardware cost, development cost and power consumption than other commercially available processors. Previous microcontroller (MCU) designs have been limited in terms of processor speed, bit resolution and their inability to provide a modern interface. Investigation however, shows that recent progress with MCU technology has overcome these difficulties.

A number of possible microcontroller devices were compared to find the most suitable for this application. It has been decided that in order to have an adequate signal to quantisation noise ratio and the necessary interface a 16-bit microcontroller is required. Eight possible devices from manufacturers such as Zilog, Siemens, ST Microelectronics, Advanced Mirco Devices, Texas Instruments and Microchip were examined. They were compared in terms of clock speed, programmability, power consumption, input/output pins and available ROM. The PIC24F 16-bit MCU offers a state-of-the-art processor and class-leading performance. This device provides all of the power consumption and flexibility advantages traditionally associated with microcontrollers, whilst also offering the accessibility and functionality usually associated with faster processors. The device is available in a 100-pin TQFP package that contains 84 I/O pins, 128 kB of program memory, 8 kB of data memory and a port known as a Parallel Master Port (PMP). The PMP enables the PIC to be interfaced to LCD's, USB devices and wireless networks. This allows the signal generator to retain the user networking and accessibility advantages normally associated with PC-based designs but at the same time remain battery isolated, portable and inexpensive. The PIC24F has been programmed and developed

using the C programming language and the Microchip Explorer 16 Development Kit. The block diagram shown in Figure 4.1 represents the high level structure of the signal generator.

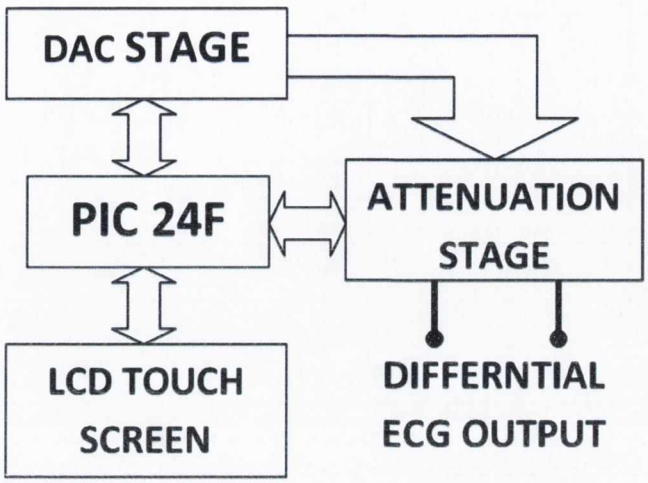

Figure 4.1: Block diagram of the ECG signal generator

4.3 The Graphical User Interface (GUI)

The software design for the signal generator provides the user with a graphical user interface (GUI) to input the required signal parameters and to observe the resulting timing parameters and a representation of the Lead II signal as it is refreshed across the LCD screen. The GUI interface is provided on a 320 x 240 pixel colour TFT LCD touch screen. The advantage of using the TRULY Ltd screen is that it is supported by the Microchip Graphics Solution software as shown in Figure 4.2. Microchip provide both the hardware and software interfaces necessary to develop a GUI interface on the PIC platform.

The lower layers represent the graphics library software that consists of a number of C-language libraries which provide the low level communications code for interfacing the PIC to the LCD and touch-screen. The actual source code which implements the operations of the signal generator and controls its peripheral circuitry uses the graphics library enabling the programmer to create objects (buttons, text boxes etc), draw shapes to represent these objects, control the pixels on the LCD screen and capture messages from the touch screen. The library also aids in the inclusion of animations and icons to be used in the generator's operation.

Figure 4.3 illustrates the user path through the signal generator's operation. Using

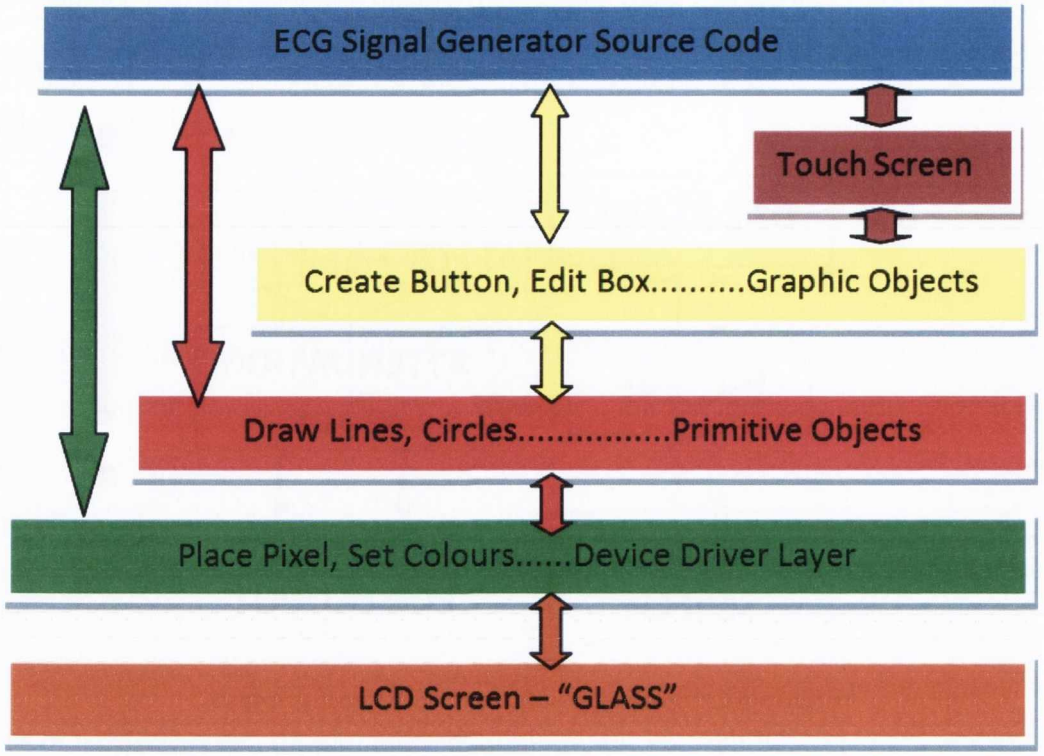

Figure 4.2: GUI Software Architecture

the user inputs the algorithm controls the DAC stage of the signal generator to create a precisely timed and amplitude controlled Lead II signal from a previously synthesized ECG stored in the PIC memory.

4.4 Controlling the Timing of the ECG Signal

For the purposes of development the constituent component durations shall be controlled using the duration equations proposed by Burke & Nasor [10], although these equations are to be replaced with more accurate ones at a later stage. The equations are presented and discussed in detail in Chapter 5.

As discussed in Chapter 2 clinical diagnosis of many cardiac conditions such as hypocalacemia [2] and second degree blockage conduction problems in the AV node [17] can be identified from ECG timing observations such as the decreased duration of the QT interval or a progressive lengthening of the PR interval, respectively. In this case the ECG recording equipment's ability to preserve the signal morphology and timing characteristics of a healthy subject are paramount in the avoidance of clinical misdiagnosis.

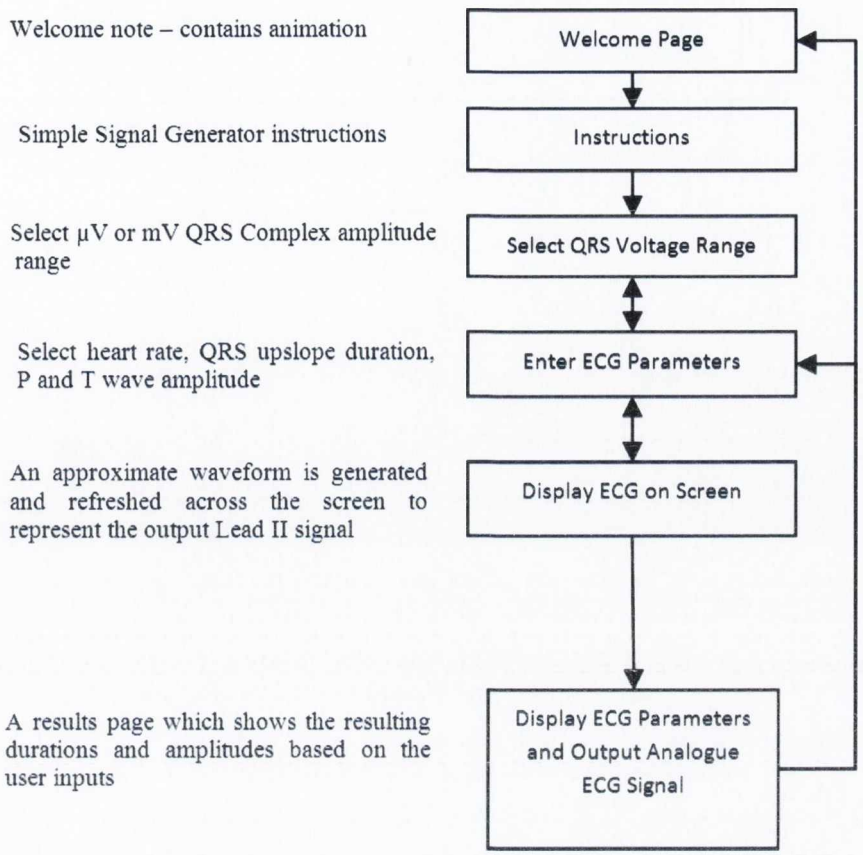

Figure 4.3: Software structure and operation

The ECG signal generator uses a combination of one 16-bit timer TMR1 and one 32-bit timer TMR4/5 (utilizing TMR4 and TMR5) to control the output sampling rates and overall heart rate timing. The timers have a minimum clock cycle of 62.5 ns. The code has been optimized so that the maximum output sample rate error is limited to half a timer clock cycle of 31.25 ns.

Above a heart rate of 163 bpm the P and T waves of successive cardiac cycles begin to merge according to the Nasor equations as demonstrated in Figure 4.4. This merging point is monitored using TMR4/5 to determine where the cardiac cycle time has elapsed and the onset of the next P wave should begin to merge with the outgoing T wave. The output sampling rate for the remainder of the P wave after the termination of the outgoing T wave is adjusted to maintain minimum sampling error. The amplitude of the combined P and T waves during this merging process are calculated as the vector sum of the P and T wave samples, i.e. the square root of the sum of the squares of the amplitudes of the individual components.

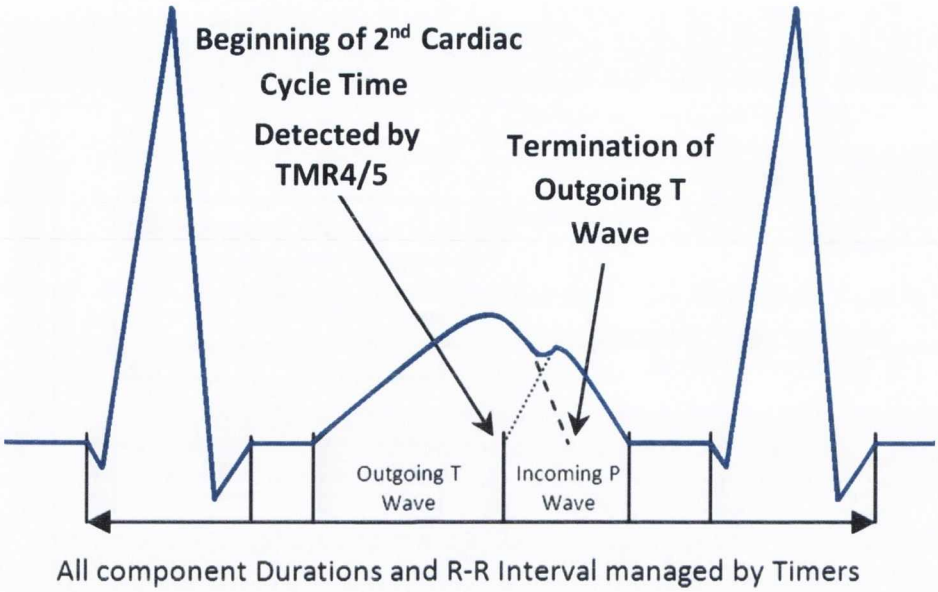

Figure 4.4: Controlling the timing of the synthesised signal

The timers are controlled by placing a "Delay" value in the timer control register (TCON) which must be an integer value. If the calculated delay value is not an integer it must be rounded up or down to create an integer and hence the maximum error is half a clock cycle [44]. The PQ and the ST segments are the most accurately timed as they are treated as a 0V output and hence can be timed to within a half a clock cycle. The generator can guarantee the complete timing accuracy of a full Lead II ECG output to within $\pm 0.3\%$ and can hence be used to measure whether recording equipment distorts the timing of the individual components of the ECG or the R-R interval. The source code consists of 15 functions and initialization code totalling 2,500 lines of C language. The source code also calls upon 16 C files from the graphics library.

4.5 The Hardware Design

4.5.1 Power Regulation and 'Ground' Isolation

Figure 4.5 is a schematic diagram of the signal generator. To isolate the device from mains earth the entire system is run on Li-ion batteries. The voltage regulators ensure that all power sources are low noise and temperature stable. Note that all analogue and digital ground (0V) lines are separate until they are terminated at the battery connection. Both analogue and digital ground lines are also wired with highly conductive low-inductance bus bars to minimize resistivity and induced noise.

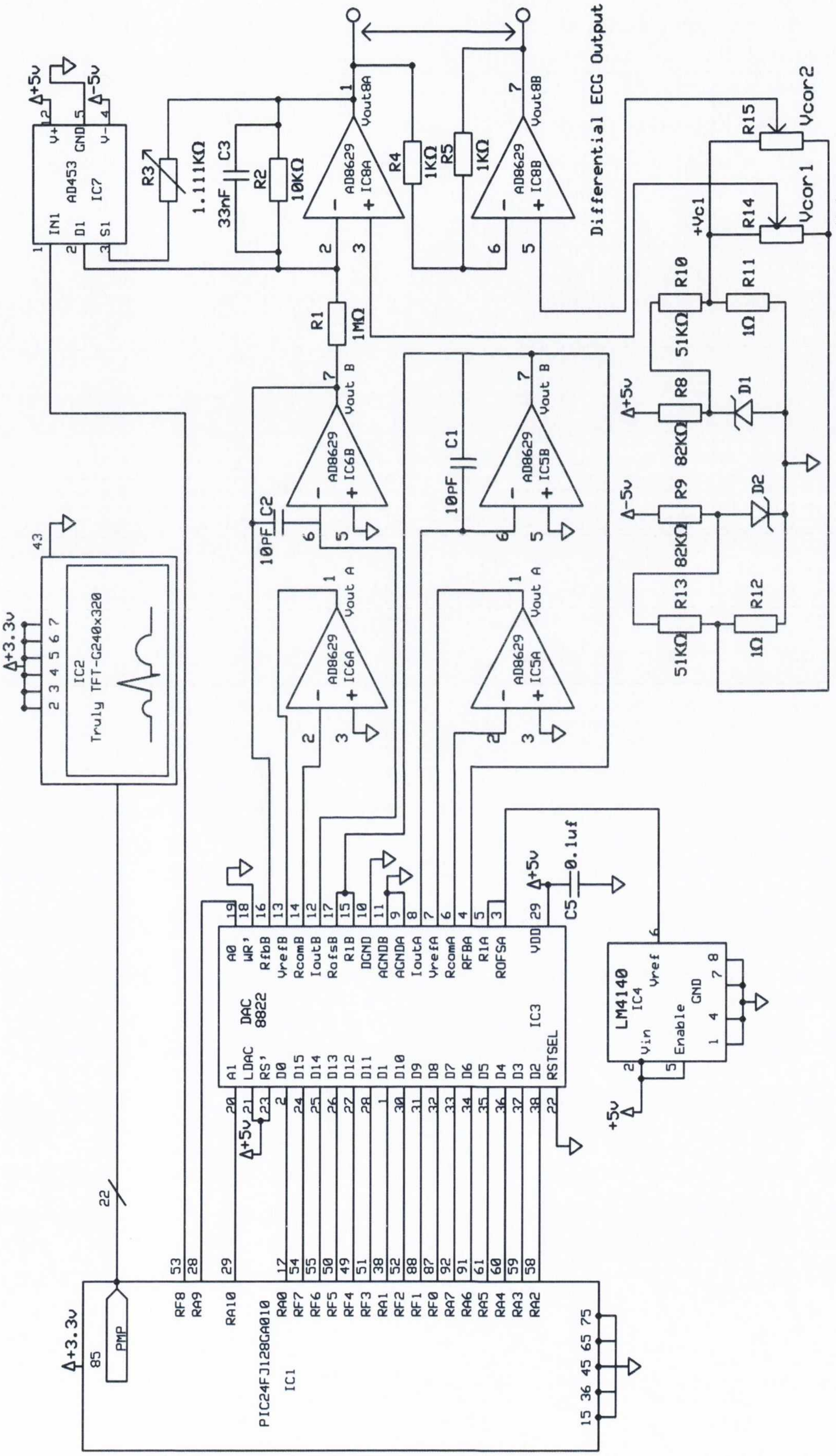

Figure 4.5: Schematic diagram of the signal generator

4.5.2 Digital-to-Analogue Conversion Architecture

Speed and noise calculations formed the basis of the selection criteria used to choose the specific devices employed in the design. It was determined that 14-bit resolution would guarantee a SQNR of 90 dB over the full QRS amplitude range. The DAC comparison process identified the DAC8822 multiplying dual current output 16-bit DAC (IC3) by Texas Instruments as the most appropriate DAC for this application. The DAC provides up to 16-bit resolution (15 data + 1 sign bit), parallel inputs and generates the required QRS ramp from input code 0000-1111 (16,384 steps) within the required minimum QRS upslope duration of 15 ms due to its 2 Mega samples per second (MSPS) conversion speed.

The DAC stage offers full 14-bit resolution to all components of the ECG signal within the voltage range. DAC A is used to step down the 2.048 V reference voltage supplied by the LM4140 precision reference voltage chip IC4 as shown in Figure 4.6. The reference is stepped down to the relative QRS, P and T wave amplitudes as dictated by the analogue conditioning circuit. DAC B receives its reference voltage from DAC A and is then used to process the 14-bit digital samples from the PIC and generate the analogue ECG signal which is subsequently attenuated to the appropriate voltage level in the following analogue conditioning section.

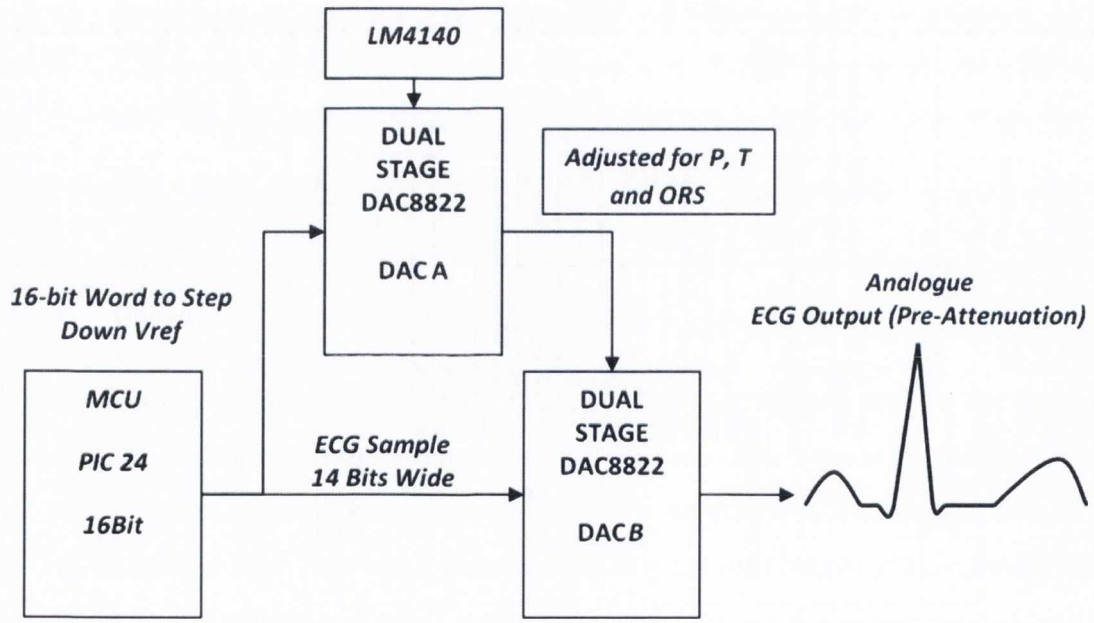

Figure 4.6: The dual stage DAC process

4.5.3 Limitations of Low-Voltage DAC Output Capability

Inspection of DAC datasheets and application notes demonstrates that the performance of DAC's in the sub mV range is not well defined and in general is application and environment specific. This, combined with testing and communication with industrial experts, verified that a multiplying DAC's performance deteriorates as the reference input voltage reduces in amplitude. Tests on a number of DAC's (DAC8822, AD5547 and AD394) have shown that commercially available DAC's are not capable of providing analogue signals at amplitudes lower than 10 mV accurately. The author believes that this is the main source of error in many of the other ECG signal generator designs, and significantly limits their usefulness.

To overcome this problem the ECG signal should be created using devices that have been specifically designed to operate in low voltage ranges and whose behavioural characteristics at these voltage levels are fully defined. In the two DAC stage process used in this design the ECG signal is created at 100 times the required amplitude to generate mV range QRS amplitude signals and 1000 times the required amplitude to generate μV amplitudes. The signal is then attenuated using a low-noise and low-offset novel analogue circuit layout to provide the required QRS output 100 μV to 10 mV range. This system greatly increases accuracy over other architectures. In doing so, characteristics such as output noise voltage, output offset voltage and the effects of temperature drift must be taken into consideration and estimated using fully defined device parameters.

4.5.4 Attenuation Stage and Op-amp Selection

The attenuation stage requires the use of an inverting amplifier to attenuate the output signals appropriately (IC8A). A simple resistive network would not provide a voltage source which the inclusion of IC8A does. Operational amplifiers are also required to convert each of the DAC current output signals to voltage signals (IC5B and IC6B); to invert the reference voltage to allow the bipolar representation of ECG signals (IC5A and IC6A) and to generate the differential output signal (IC8B).

Since the op-amps are generating signals of less than 10 μV, i.e. the scaled P and T waves, it is imperative that the devices used provide the optimum compromise between low-noise performance and minimum offset effects. Modelling the output noise voltage of an operational amplifier configuration can be performed using the data provided by

manufacturers [45, 46]. Note that the DAC and reference voltage output noise levels do not require significant noise modelling. Due to the architecture used here the output noise voltages of these devices, which are in the order of μV's, shall be attenuated by 40-60 dB's along with the output signals by the op-amps discussed previously. Hence the noise becomes negligible when compared to the 100μV to 10mV output amplitude range, the amplifiers responsible for this attenuation however do require noise analysis.

Multiple noise models for the op-amps such as the one shown in Figure 4.7 were created and the resulting output noise voltage equations derived [47]. The resulting equations were applied to 16 different devices selected from commercially available low-noise op-amps. Equation (4.9) is an example of the output noise voltage equation derived for the op-amp arrangement around IC8B in Figure 4.7.

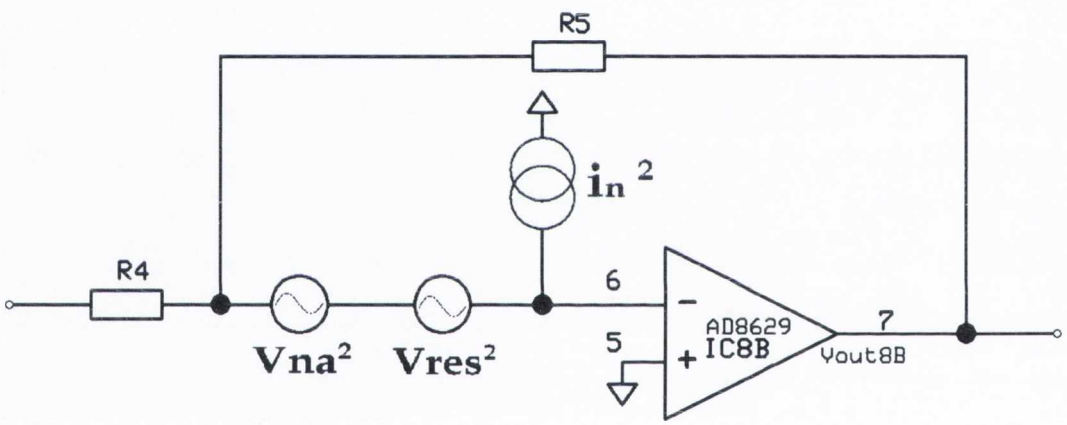

Figure 4.7: Example of the op-amp noise model used

The noise sources shown in Figure 4.7 are specified in root-mean-square values. The average noise powers contributed by each of the noise sources are additive and therefore Superposition can be used to combine the normalised power (voltage squared) contributions of each of the sources to obtain the average normalised output noise power [48, 49].

A voltage based analysis can be used if all terms are squared. The effect of each noise source on the output can be found by considering each in turn and applying Superposition.

The equation for the estimated output noise V_{no} for the output amplifier IC8B:

$$V_{na}{}^2 = V_{nov}{}^2 \left(\frac{R_4}{R_4 + R_5} \right)^2 \tag{4.1}$$

$$V_{nov}{}^2 = V_{na}{}^2\left(\frac{R_4 + R_5}{R_4}\right)^2 \tag{4.2}$$

$$V_{nov}{}^2 = V_{na}{}^2\left(1 + \frac{R_5}{R_4}\right)^2 \tag{4.3}$$

And effect of amplifier noise currents:

$$V_{noi}{}^2\left(\frac{R_4}{R_5 + R_4}\right)^2 = i_n{}^2\left(\frac{R_5 \times R_4}{R_5 + R_4}\right)^2 \tag{4.4}$$

$$V_{noi}{}^2 = i_n{}^2 \times R_5{}^2 \tag{4.5}$$

And the effect of resistors noise:

$$V_{res}{}^2 = V_{nores}{}^2\left(\frac{R_4}{R_5 + R_4}\right)^2 \tag{4.6}$$

$$V_{nores}{}^2 = V_{res}{}^2\left(\frac{R_5 + R_4}{R_4}\right)^2 \tag{4.7}$$

$$V_{nores}{}^2 = V_{res}{}^2\left(1 + \frac{R_5}{R_4}\right)^2 \tag{4.8}$$

Hence the total equation for the output voltage noise V_{no} is :

$$V_{no} = \sqrt{V_{na}{}^2\left(1 + \frac{R_5}{R_4}\right)^2 + (i_n{}^2.R_5{}^2) + V_{res}{}^2\left(1 + \frac{R_5}{R_4}\right)^2} \tag{4.9}$$

However, values for the voltage and current mean square noise V_{na} and i_n respectively are not typically provided directly by manufacturers but can be calculated using values for voltage and current noise spectral density, $V_{ndo}{}^2$ and $i_{ndo}{}^2$, using the following equations [48]:

$$V_{na}{}^2 = V_{ndo}{}^2\left[(f_H - f_L) + 2 \times f_{cv} \times \ln\left(\frac{f_H}{f_L}\right) + f_{cv}{}^2\left(\frac{f_H - f_L}{f_H.f_L}\right)\right] \tag{4.10}$$

$$i_n{}^2 = i_{ndo}{}^2\left[(f_H - f_L) + 2 \times f_{ci} \times \ln\left(\frac{f_H}{f_L}\right) + f_{ci}{}^2\left(\frac{f_H - f_L}{f_H.f_L}\right)\right] \tag{4.11}$$

For the AD8629 Amplifier:

- $V_{ndo}{}^2$ = Voltage Noise Density of Op-Amp = 22 pV$\sqrt{}$Hz.

- $i_{ndo}{}^2$ = Current Noise Density of Op-Amp = 5fA$\sqrt{}$Hz.
- f_H,f_L = The upper and lower limits of the frequency band in question 0.1 Hz to 500 Hz
- f_{cv},f_{ci} = are noise voltage and current corner frequencies

The voltage corner frequency given for the AD8629 = 0.1 Hz. No current corner frequency is given for the AD8629 but was estimated as 200 Hz. Multiple values for f_{ci} ranging from 0.1 Hz to 2k Hz have been used in analysis and it was found that the effects of the corner frequency on the final output noise value are so small as to be negligible. The value of $V_{res}{}^2$ is calculated using:

$$V_{res}{}^2 = 4kTBR \tag{4.12}$$

where k = Boltzmans Constant 1.38×10^{-23}, T = 300°K (approximately 27°C), B = 499.9 Hz and R = Resistance.

The values calculated for the mean square voltage and current noises where $V_{na}{}^2$ = 243 × $10^{-15}V^2$ and $i_n{}^2$ = 10 × 10^{-24}A. The noise due to the resistors R_4 and R_5 (both 1 kΩ) was calculated as $V_{res}{}^2$ = 4.14 × $10^{-15}V^2$. When these values are used in equation (4.9) this yields a total output noise voltage for IC8B of:

$$V_{no} = 0.99\mu V \tag{4.13}$$

The results obtained by using these output noise voltage models indicate that the Analog Devices AD8629 dual op-amp device provides the best balance between low voltage offset of 1 μV, offset temperature drift of 0.002 μV/°C and very low output noise voltage performance.

IC7 is an analogue switch that is used to change the attenuation between 40 dB and 60 dB by altering the resistance in the feedback loop for IC8A. The capacitor C3 is present to low-pass filter the ECG signal and remove the quantization staircase resulting from the DAC process, which has a maximum output sampling frequency of 750 kHz for the construction of the QRS complex. The first order filter has a cut-off frequency of 500 Hz ensuring the ECG signal spectrum is not curtailed or the signal profile distorted.

4.5.5 Voltage Offset Correction

As described in a conference submission of the early stages of this design [42] the output voltage of the signal generator was subject to an accompanying voltage offset. This offset voltage is primarily due to the combined effects of the individual AD8629 offset voltages and results in a total DC offset of 5 μV on the output signal. In order to maximize the precision of the output signal it was necessary to remove this DC offset which exists as an offset on each side of the differential output. The issue is further complicated in that the offset output from IC8A and IC8B are not equal as they are partially independent. A separate programmable voltage offset could be added to the test signal via the DAC in order to test an ECG recorder's ability to remove the polarisation voltage generated by skin electrodes, but this was not included in this design.

The difficulty in removing a μV DC offset lies in the possibility of undermining the zero temperature drift properties of the op-amps. A temperature drift on the offset correction circuitry could lead to an output offset voltage drift larger than the offset which it was intended to remove. Figure 4.8 is an example of a standard bipolar reference voltage diode and voltage divider network used for offset correction.

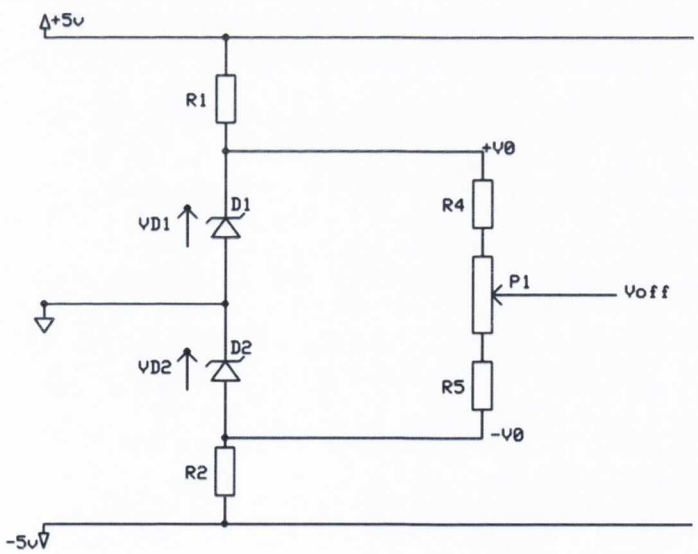

Figure 4.8: Standard Bipolar offset correction circuit

If the diodes have a temperature drift coefficient β so that $\beta\Delta$T is the fractional drift due to temperature of the diode voltage and both diodes have equal nominal voltages of V_{D1} and V_{D2} then:

$$+V_o = V_{D1}(1 + \beta\Delta T) \tag{4.14}$$

$$-V_o = -V_{D2}(1 + \beta\Delta T) \tag{4.15}$$

Consider the case were the circuit has been tuned so that the output V_{off} is 0 V. Now if both diode voltages drift positively with respect to ground by the same $\beta\Delta$T value the output voltage V_{off} is given by:

$$V_{off} = V_{D1} \pm \beta\Delta T(V_{D1}) - V_{D2} \pm \beta\Delta T(V_{D2}) \tag{4.16}$$

where in this case V_{D1} and V_{D2} are the same and can hence be replaced by V_{Dn}

$$V_{off} = V_{Dn} - V_{Dn} \pm 2\beta\Delta T(V_{Dn}) = \pm 2\beta\Delta T(V_{Dn}) \tag{4.17}$$

The design essentially passes whatever drift occurs on the diodes directly to the output of the circuit. Considering that even the most accurate of reference diodes such as the LT1004 used in this design has a temperature coefficient of ±20ppm/°C this could result in a drift of several hundred μV's in the diode voltage and hence the output voltage with just a 5°C change in temperature. For an application where the offset correction required is just a few μV this is clearly unacceptable.

The offset correction circuit shown in Figure 4.5 is based around the diodes D1 and D2 (1.2V) and provides a temperature stable bipolar output voltage that can vary between V_{c+} and V_{c-}. The core difference here is that the voltage divider networks are ground referenced. This arrangement ensures that any change in the diode voltage due to temperature is attenuated by the voltage divider networks R_{10},R_{11} and R_{12},R_{13} along with the diode voltage itself. The correction voltages are taken from the potentiometers P1 and P2 which are much larger in value than R_{10} and R_{12} so that the latter dictate the temperature coefficients of the parallel combinations.

4.5.6 Temperature Stability of the Output V_{out8A}

The temperature effects of the DAC stage, the offset correction circuit, op-amp bias currents and offset voltages on the actual output of the signal generator need to be further assessed. To cover the widest scenario likely the system is analysed with a worst-case temperature variation of ±25°C to demonstrate its stability under extreme

conditions. The model shown in Figure 4.9 identifies the possible temperature effects on V_{out8A}.

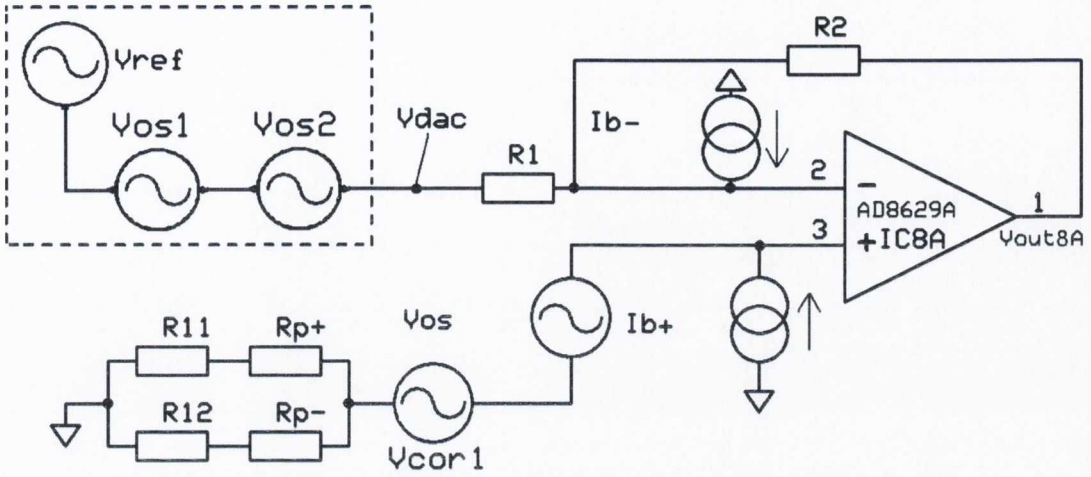

Figure 4.9: Temperature drift noise model for $V_{out}8A$

4.5.6.1 The DAC Stage

The DAC8822 provides full scale temperature tracking when connected to an external conversion op-amp circuit such as IC5B and IC6B via a feedback input on each of the DACs. This provides temperature stability at the output regardless of the temperature characteristics of the external amplifier or the biasing resistors. In addition the inverting voltage reference amplifiers op-amps IC5A and IC6A are used to provide negative reference voltages to the DACs. The operational amplifiers themselves have extremely low offset drift (0.002ppm/°C typical or 0.02ppm/°C maximum) and the biasing resistors used for the unity gain inverting amplifier are internal on the DAC device so they should have similar stable temperature characteristics to the DAC itself. It will be shown by calculation that the effect of these amplifiers is negligible and hence temperature effects on the bipolar output of the signal generator should be essentially the same on a positive or negative output.

The DAC8822 is a multiplying DAC architecture and hence the offsets are modelled as a product of the output DAC offset voltage and temperature coefficients as indicated in the dotted box in Figure 4.9. In theory the reference voltage chip V_{ref} (IC4) should not contribute to the output of DACA when the required output from the DACA is 0V. Similarly DACB takes its reference from DACA so at 0V DACA should not contribute to the output of DACB. In practice however the temperature coefficient of the reference voltage chip may have an impact on the output offset of DACA and also the DACB

output may be affected by the temperature coefficients of both V_{ref} and DACA. The output of DACB is the one connected to the analogue attenuation network and hence it is the offset voltage value at DACB which should dictate any unwanted output voltage offset value at V_{dac}. For the purposes of the temperature drift model we could say that if DACA is set to 0V i.e. to calculate the output drift voltage then V_{ref} and the offset of DACA V_{os1} should be isolated from the final output V_{dac} at DACB. However this is ideal, in order to create the worst case scenario the temperature coefficients for V_{ref} and the offset of DACA (V_{os1}) shall be added to the the offset voltage for DACB which is V_{os2}. This can be seen in the resulting Equation (4.18). Given γ, δ and α are the temperature coefficients of the reference voltage chip IC4, both of the DACs and the resistors respectively and ΔT is the drift from room temperature (25°C) the effect V_{dac} has on the output V_{out8A} is derived as:

$$V_{dac} = V_{os2}(1 \pm \gamma\Delta T \pm \delta\Delta T \pm \Delta\delta T)\left[-\frac{R_2(1 \pm \alpha\Delta T)}{R_1(1 \pm \alpha\Delta T)}\right] \tag{4.18}$$

To aid in simplifying this equation consider the binomial series expansions [50]:

$$\frac{1}{1+x} = 1 + nx + \frac{n(n-1)}{2!}x^2 + \frac{n(n-1)(n-2)}{3!}x^3 ... \tag{4.19}$$

$$\frac{1}{1-x} = 1 + x + x^2 + x^3 + x^4 ... \tag{4.20}$$

and if we consider a case where x$\ll$1 we can neglect the second and higher order terms completely to yield:

$$\frac{1}{1+x} = 1 - x \text{ and } \frac{1}{1-x} = 1 + x \text{ or } \frac{1}{1 \pm x} = 1 \pm x \tag{4.21}$$

Applied to Equation (4.18) the resistor coefficients can be rewritten (note $\alpha \ll 1$ as are all other temperature coefficients used in this chapter, see Section 4.5.6.5) as:

$$V_{dac} = V_{os2}(1 \pm \gamma\Delta T \pm \delta\Delta T \pm \Delta\delta T)\left[-\frac{R_2(1 \pm \alpha\Delta T)(1 \pm \alpha\Delta T)}{R_1}\right] \tag{4.22}$$

As in the case of equation (4.18) the second order temperature coefficients resulting from the simplification of equation (4.22) are negligible compared to the first order coefficients and are hence removed. This can be assumed throughout the derivation of the equations in the rest of this chapter. Equation (4.22) can hence be simplified to:

$$V_{dac} = -V_{os2}\frac{R_2}{R_1}(1 \pm \gamma \pm 2\delta \pm 2\alpha)\Delta T \tag{4.23}$$

4.5.6.2 The Op-amp Bias Currents

The input bias currents for the AD8629 also have an effect on the output voltage. These currents should flow to ground via the offset correction circuit. R_{p+} and R_{p-} can be considered to represent the resistance on either side of the potentiometer wiper. To create a worst case scenario these values should be considered to be half of the pot resistance hence maximizing the parallel resistance and the resulting offset voltage due to bias currents. As an example of deriving a multi-variable equation for estimating the effects of input bias current on the output of IC8A the derivation for V_{bias+} is shown for illustrative purposes. Note that $I_{b\pm}$ are the bias currents, λ and ρ are the temperature coefficients of the potentiometer and bias currents respectively. The equation for V_{bias+} the effect of the temperature drift due to the op-amp bias current on the positive input of the op-amp is:

$$V_{bias+} = I_{b+(1\pm\rho\Delta T)} \times \left[\frac{[R_{11}(1\pm\alpha\Delta T)+R_{p+}(1\pm\lambda\Delta T)][R_{12}(1\pm\alpha\Delta T)+R_{p-}(1\pm\lambda\Delta T)]}{R_{11}(1\pm\alpha\Delta T)+R_{p+}(1\pm\lambda\Delta T)+R_{12}(1\pm\alpha\Delta T)+R_{p-}(1\pm\lambda\Delta T)}\right] \tag{4.24}$$

But $R_p \gg R_{11}$ and R_{12} so the latter can be removed to give:

$$V_{bias+} = I_{b+}(1 \pm \rho\Delta T)\left[\frac{[R_{p^+}(1 \pm \lambda\Delta T)][R_{p^-}(1 \pm \lambda\Delta T)]}{R_p(1 \pm \lambda\Delta T)}\right] \tag{4.25}$$

R_{p+} and R_{p-} have been defined for a worst case as half the pot resistance giving (again neglecting higher order terms):

$$V_{bias+} = I_{b+}(1 \pm \rho\Delta T)\left[\frac{\frac{R_p{}^2}{4}(1 \pm 2\lambda\Delta T)}{R_p(1 \pm \lambda\Delta T)}\right] \tag{4.26}$$

$$V_{bias+} = I_{b+}(1 \pm \rho\Delta T)\left[\frac{R_p}{4}(1 \pm 3\lambda\Delta T)\right] \tag{4.27}$$

Applied to the amplifier:

$$V_{bias+} = I_{b+}(1 \pm \rho\Delta T)\left[\frac{R_p}{4}(1 \pm 3\lambda\Delta T)\right]\left[\frac{R_1 + R_2}{R_1}(1 \pm 2\alpha\Delta T)\right] \tag{4.28}$$

$$V_{bias+} = I_{b+}\left(\frac{R_p}{4}\right)\left(\frac{R_1+R_2}{R_1}\right)(1 \pm 3\lambda \pm 2\alpha \pm \rho)\Delta T \tag{4.29}$$

The "1+" term can be removed as for equation (4.36) if only the drift due to temperature is required giving the final equation :

$$\Delta V_{bias+} = I_{b+}\left(\frac{R_p}{4}\right)\left(\frac{R_1+R_2}{R_1}\right)(\pm\rho \pm 2\alpha\Delta T \pm 3\lambda)\,\Delta T \tag{4.30}$$

The equation for V_{bias-} is:

$$V_{bias-} = I_{b-}(R_2)(1 \pm \rho \pm \alpha)\Delta T \tag{4.31}$$

4.5.6.3 The op-amp offset voltage V_{offset}

The AD8629 amplifier has an offset voltage which is modelled as a voltage source on the non-inverting input of the device. The effect of this offset voltage on the output is given by:

$$V_{offset} = V_{off}\left(\frac{R_1+R_2}{R_1}\right)(1 \pm 2\alpha \pm \varepsilon)\Delta T \tag{4.32}$$

where ε is the temperature coefficient of the offset voltage of the AD8629 op-amp.

4.5.6.4 The Offset Correction Output Voltage

The output of the offset correction circuit V_{cor1} also suffers from temperature variation effects. It can be assumed that regardless of where the wiper on the potentiometer is placed the maximum output voltage is equal to $\pm V_{c1}$. Therefore, the effect of V_{cor1} on the output is given by:

$$V_{cor1} = V_D\frac{R_{11}}{R_{10}}\left(\frac{R_1+R_2}{R_1}\right)(1 \pm 4\alpha \pm \beta)\Delta T \tag{4.33}$$

Where β and V_D are the temperature coefficient and voltage (1.024V) of the LT1004 diode respectively.

4.5.6.5 The Total Temperature Effect at the Output of IC8A

The offset correction circuit will be tuned to remove all the nominal DAC offsets, op-amp bias currents and voltage offsets from the output signal. It is only when the

temperature drifts from this tuning temperature that an error on the output will materialize. In this event the "1" term within each equation can be removed so that only the drift due to the temperature change remains as shown in the derivation of Equation (4.30). The equations now represent the voltage drift from zero of each component. In the analysis conducted throughout this chapter some offset contributions will be significantly larger in magnitude than others. Note how the result of of Equation (4.36) is significantly smaller than the other offset contributions. The value of ΔV_{bias+} could be ignored during calculation of the overall offset given that it is several orders of magnitude smaller than the other sources. However, for the sake of completeness the author has decided to include all contributions of noise and offset voltages in the analysis reported in this chapter.

Given $R_1 = 1M\Omega$, $R_2 = 10k\Omega$, $R_p = 1k\Omega$, $R_{11} = 1\Omega$, $R_{10} = 51k\Omega$, $\gamma = 3ppm/°C$, $\delta = 2ppm/°C$, $\alpha = 50ppm/°C$, $V_D = 1.204V$, $\rho = 500ppm/°C$, $\lambda = 100ppm/°C$, $\varepsilon = 0.02ppm/°C$, $\beta = 20ppm/°C$, $V_{off} = 1\mu V$, $V_{os2} = 1mV$, Ib+ = Ib- = 30pA, and $\Delta T = 25°C$.

The contribution of each individual effect to the output IC8A are:

$$\Delta V_{dac} = -V_{os2}\frac{R_2}{R_1}(\pm\gamma \pm 2\delta \pm 2\alpha)\Delta T = \pm 26.75nV \tag{4.34}$$

$$\Delta V_{bias-} = I_{b-}(R_2)(\pm\rho \pm \alpha)\Delta T = \pm 4.125nV \tag{4.35}$$

$$\Delta V_{bias+} = I_{b+}\left(\frac{R_p}{4}\right)\left(\frac{R_1 + R_2}{R_1}\right)(\pm 3\lambda \pm 2\alpha \pm \rho)\Delta T = \pm 0.169nV \tag{4.36}$$

$$\Delta V_{offset} = V_{off}\left(\frac{R_1 + R_2}{R_1}\right)(\pm 2\alpha \pm \varepsilon)\Delta T = \pm 2.5nV \tag{4.37}$$

$$\Delta V_{cor1} = V_D\frac{R_{11}}{R_{10}}\left(\frac{R_1 + R_2}{R_1}\right)(\pm 4\alpha \pm \beta)\Delta T = \pm 129nV \tag{4.38}$$

Therefore, the total voltage drift for IC8A is given as the sum of all contributions as follows:

$$\Delta V_{out8A} = \Delta V_{dac} + \Delta V_{bias-} + \Delta V_{bias+} + \Delta V_{offset} + \Delta V_{cor1} \tag{4.39}$$

$$\Delta_{Vout8A} = \pm 162.5nV \tag{4.40}$$

With a 25°C change in temperature the maximum output voltage drift is ±162.5 nV. The largest contribution comes from the offset voltage correction circuit itself as ±129 nV. However, the circuit is in place to correct an error of over 5 μV so this error is negligible by comparison. It is also apparent that because the required offset voltage correction is just 5 μV the potential divider within the correction circuit has an attenuation 51 × 10^3 which also greatly attenuates the drift of the voltage reference diode and potentiometer.

4.5.7 Temperature Stability on the output V_{out8B}

V_{out8B} is generated by inverting the output from V_{out8A} hence the drift voltage from V_{out8A} is passed to the inverting input of IC8B. The model for IC8B is essentially the same as for IC8A with the exception that V_{dac} is replaced by V_{out8A} and the offset correction is now V_{cor2}. The equation for the effect of V_{out8A} on the output of V_{out8B} is hence given by:

$$\Delta V_{out8A}{}' = -\Delta V_{out8A}\frac{R_5}{R_4}(1 \pm 2\alpha)\Delta T = \pm 162.9nV \tag{4.41}$$

Given previous component values and R_4 = 1K, R_5 = 1K, R_{12} = 1Ω, R_{13} = 51KΩ the contribution of each effect to the output V_{out8B} is:

$$\Delta V_{bias-} = I_{b-}(R_5)(\pm\rho \pm \alpha)\Delta T = \pm 0.4125nV \tag{4.42}$$

$$\Delta V_{bias+} = I_{b+}\left(\frac{R_p}{4}\right)\left(\frac{R_4 + R_5}{R_4}\right)(\pm 3\lambda \pm 2\alpha \pm \rho)\Delta T = \pm 0.675nV \tag{4.43}$$

$$\Delta V_{offset} = V_{off}\left(\frac{R_4 + R_5}{R_4}\right)(\pm 2\alpha \pm \varepsilon)\Delta T = \pm 5nV \tag{4.44}$$

$$\Delta V_{cor2} = V_D\frac{R_{12}}{R_{13}}\left(\frac{R_4 + R_5}{R_4}\right)(\pm 4\alpha \pm \beta)\Delta T = \pm 259nV \tag{4.45}$$

The total voltage drift for IC8B is:

$$\Delta_{Vout8B} = \Delta V_{outA}{}' + \Delta V_{bias-} + \Delta V_{bias+} + \Delta V_{offset} + \Delta V_{cor2} \tag{4.46}$$

$$\Delta_{VoutB} = \pm 427.7nV \tag{4.47}$$

With a 25°C change in temperature the maximum output voltage drift is ±427.7 nV. The error on this output IC8B is larger than the IC8B output due to the fact that all sources of drift on the positive input of the op-amp are doubled due to the non-inverting gain and that the error from IC8A is passed on to IC8B. The worst case differential output drift error is the sum of the separate drifts giving ±590 nV or approximately 24 nV/°C. If the user of the signal generator required a P wave output voltage which was 1% of the minimum 100 μV QRS complex available, then this error is approximately half that 1μV amplitude. Also given that the calculated output noise voltage of the AD8629 amplifier is 0.99 μV, the voltage offset drift should not be observable at the output. This provides a comprehensive analysis of the effects of offset and temperature drift for the authors instrument which has been lacking in the literature reporting previous designs.

4.6 Verification and Test Results

The primary measure of the usefulness of any signal generating instrument lies in its accuracy and precision. For an ECG signal generator this accuracy must be defined as a function of time, temperature and amplitude. The device must be tested at the full range of amplitudes, heart rates and operating temperature range. The expected amplitude performance of this design has been rigorously investigated from a theoretical point of view in the previous section. It is necessary to test and provide output waveforms and results for signals created at amplitudes and heart rates typical of those an ECG machine is required to handle in everyday use. A working prototype has been constructed by the author and is shown in Figure 4.10. The prototype has been constructed manually by the author by interfacing with the development kit for the PIC24F which is shown as the green printed circuit board (PCB) in Figure 4.10. The development kit houses the PIC itself and interfaces with the touch screen however the ribbon cable shown on the left of the figure shows the bus which is used to connect the MCU to the DAC and analogue conditioning stages which have been developed on breadboard. The device was developed incrementally on breadboard because the necessities of the design i.e. the multi-stage DAC architecture, the use of the analogue switch, offset correction circuit etc could only be discovered during development

and piecewise testing of the instrument. Ideally, now that the entire system has been designed and without the time restrictions associated with the authors research the device could be built on a single PCB.

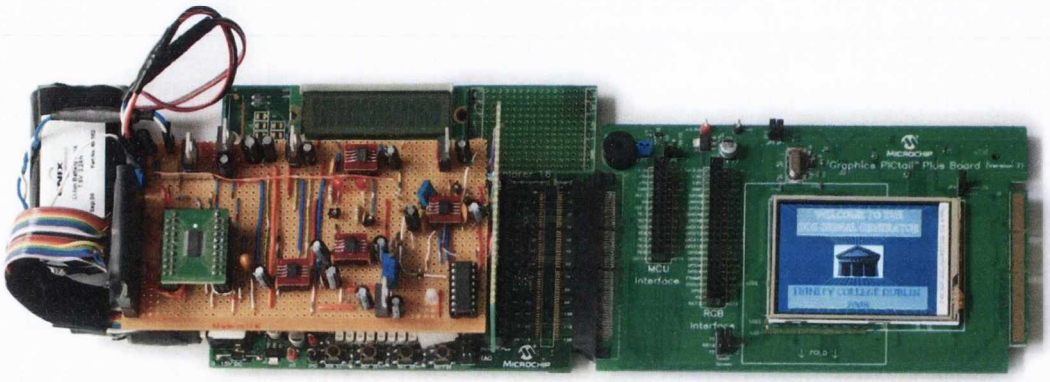

Figure 4.10: Signal generator prototype

4.6.1 Verification of Individual Component Timing Accuracy

The calculated component durations using the duration equations of Burke & Nasor are displayed on the LCD screen. The actual output timing accuracy of each of these components is shown in Table 4.1 for a heart rate of 85 bpm. A heart rate of 85 bpm was chosen for expressing the error as a percentage of T_{RR}, since at this heart rate the largest possible timing error for the QRS complex is formed. At 85 bpm a QRS complex duration of 77.1 ms as dictated by Equation (5.11), is required to time the wave correctly. As a result of this, a delay value of 35.49 would require placement in the TCON register (as described in Section 4.4), however the delay figure must be an integer value. This means that when a rounded integer delay figure of 35 is placed in the TCON register of the PIC timer. Every output sample has a timing error of approximately half a clock cycle or 31.25 ns which is the maximum possible timing error per sample. The results in Table 4.1 have been measured using the cursors on the battery isolated digital scope. The QRS complex is always the most significant contributor to timing error because it has the largest number of samples.

The QRS duration is always created within ±1.5% of the required output QRS duration and ±0.336% of the overall ECG duration. By expressing the error of the output QRS duration as a percentage of the required QRS duration it can be used as a basis by the user to determine the accuracy of the recording apparatus under test to within these defined bounds. Figure 4.11 demonstrates how accurately the

Table 4.1: Timing Accuracy of ECG Components

Component	Number of Samples	Measured Error (s)	Error % of Total Trr Duration (@ 85 bpm or Trr = 324ms)
P Wave	300	±9.38μs	±0.003%
PQ Segment	1	±31.25ns	±0.00001%
QRS Complex	34768	±1.09ms	±0.336%
ST Segment	1	±31.25ns	±0.00001%
T Wave	300	±9.38μs	±0.003%

QRS duration is generated over the full heart rate range, compared with the values determined by the equations. The maximum error over the outlined range is ±1.09 ms or ±0.336% of T_{RR}.

Note that the error in the timing of the QRS complex could be reduced by a reduction in the number of samples used to create it. For test purposes in this example the QRS was created by using all 14 bits for the ramp up and down of the QRS slopes, and another 2000 samples used to create the S wave of the QRS complex. In reality the number of samples used to create the up and down slopes of the test signal could be significantly less without an observable deterioration in signal quality.

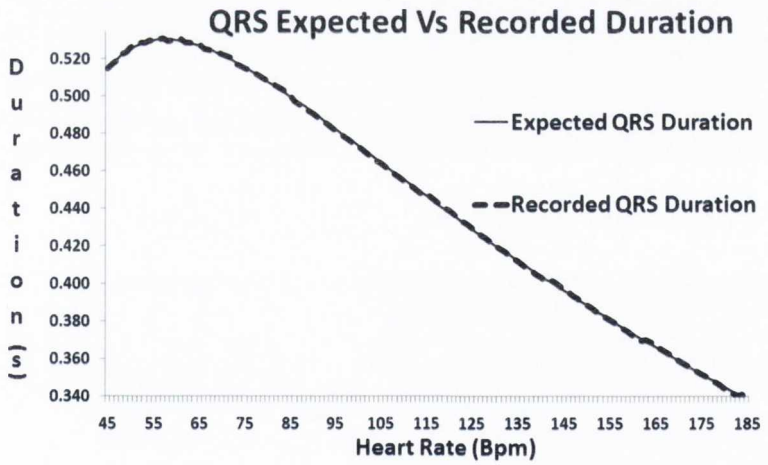

Figure 4.11: QRS duration accuracy

4.6.2 Verification of the R-R Interval Duration

Figure 4.12 is an example of a recorded 60 bpm output signal. It is important to note that the output waveforms shown here were recorded via an amplification stage which re-amplified the output of the signal generator to ranges that an isolated oscilloscope can detect. This will have introduced additional noise to the output. The oscilloscope is also limited in that it samples waveforms at a maximum frequency depending on

the set time per division and has limited resolution in the amplitude domain also i.e. the resolution of the screen on the oscilloscope in both the X and Y planes limits the clarity of the displayed waveforms. A more accurate oscilloscope is unavailable for test at this time.

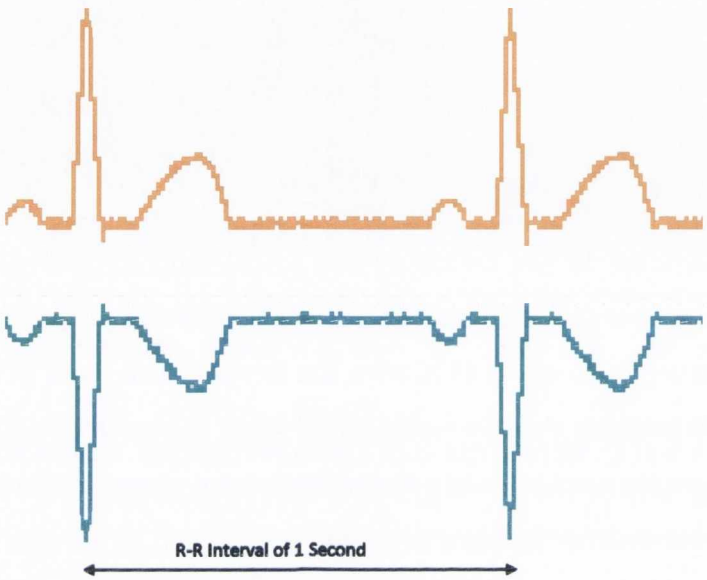

Figure 4.12: R-R accuracy at 60 bpm with P and T waves scaled below 10% and 30% of the QRS amplitude, respectively

4.6.3 Amplitude Accuracy of the ECG Components

Figure 4.13 demonstrates the accuracy of the signal generator at a high heart rate of 185 bpm and an amplitude of 500 μV. Note how the P and T waves are merged together by generating the output amplitude as the root mean square of both P and T wave samples taken individually. This recorded signal was also measured and found to have preserved the R-R interval of 324 ms by maintaining the required sampling rate for both the P and T wave components despite the merging process.

Figure 4.14 is an example of the output of the signal generator at the intermediate heart rate of 120 bpm and amplitude of 100 μV. The R-R interval was measured at 500 ms.

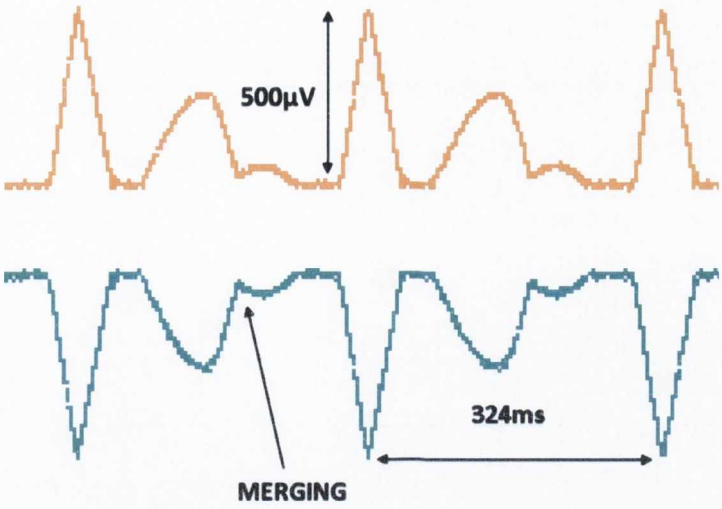

Figure 4.13: Signal at 185 bpm with a 500 μV QRS amplitude with P and T waves scaled at 10% and 50% of the QRS respectively

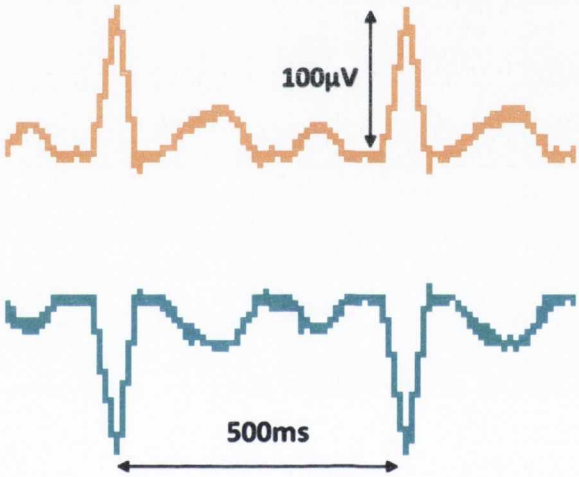

Figure 4.14: Signal at 120 bpm with a 100 μV QRS amplitude with P and T waves scaled at 25% and 40% of the QRS respectively

4.6.4 Testing Temperature Stability

The prototype underwent temperature stability testing at temperatures of 0°C, 25°C and 50°C and at heart rates of 45 ,100 and 185 bpm for each temperature. Again additional amplifiers were required to enable viewing of the signal on the isolated oscilloscope.

Firstly, the offset was tuned to 0 V at 25°C and then the temperature varied using an oven. It was found that any drift from 0 V was in fact buried in the noise band of the output signal, as predicted by Equations (4.40) and (4.47) and consequently cannot be quantified. Secondly an output signal at each of the heart rate was generated to find

any QRS complex amplitude variation due to temperature. There was no observable variation on the R peak amplitude of the signal. These results support those obtained from the theoretical analysis of the temperature variations.

4.7 Conclusion

The author believes that the limitations of modern ECG signal generator designs as discussed in Chapter 3 have been overcome by the design presented here.

In software terms the signal generator operating system provides a user interface with an easy-to-use industry standard colour GUI similar to those found in high-end commercial biomedical instruments. The signal generator output timing accuracy can be guaranteed to within half a processor clock cycle of ± 32.5 ns per sample or a maximum error of approximately $\pm 0.3\%$ of the total ECG waveform duration. This allows the signal to be used to test recording equipment performance within well defined performance limits.

The hardware architecture uses a high bit resolution that provides for a SQNR of 90 dB. This SQNR applies to the P wave, QRS complex and T wave components by virtue of the two stage DAC process. The use of operational amplifiers to control the attenuation of the ECG signal to the required low output levels maintains minimum output voltage noise (0.99 μV). The design also includes an analogue switch that allows the DAC to generate signals at a higher mV voltage range with the signal being attenuated subsequently to achieve lower μV output signals. Total output offset voltage (previously 5 μV) is corrected using a thermally stable correction circuit and is guaranteed to be less than ± 0.6 μV.

The instrument's timing accuracy, low noise output signal and temperature stability has been analyzed and tested. Recorded waveforms show the output signal at various amplitudes and heart rates. While the maximum offset differential voltage drift calculated is just ± 590 nV over ± 25°C it is not observable on the battery isolated scope during test and is therefore approximated to be less than ± 100 nV since any offset larger than this would begin to exceed the observable noise around 0 V on the scope. The author believes the analytical error is larger than observable during test because the analysis has been performed to find the worst case scenario. The output voltage and timing information of the waveform being supplied to the user allow the signal to be used to test hospital, Holter monitor and ambulatory ECG recording devices. The

output signal is intentionally synthetic and therefore, it can also be used to test ECG analysis software which annotates the onset and termination of ECG components given that the location of these characteristics are known in the synthetic signal.

With the user interface and precision hardware platform presented here the signal generator could be expanded to provide multiple ECG leads and different ECG arrhythmia conditions. A synthetic signal was used since a recorded ECG would inherently contain recording noise which would limit its usefulness as a test signal. The synthetic signal used could also be replaced by a modelled signal that reflects the profile of an actual ECG more closely over the heart range required. Such a signal would provide the noiseless accuracy of the synthetic signal but also the behavioural characteristics of a real ECG.

The instrument presented is not only low cost, accurate and portable but the choice of the PIC24F as a central processor means that the device could be readily interfaced to a PC or wireless network using the PMP and other C libraries similar to the Microchip Graphics Library used in this design which are available from Microchip on-line.

Chapter 5

A Review of ECG Characterisation and Modelling

5.1 An Overview

A review of ECG characterisation and modelling uncovers a wide range of approaches to the subject which have been driven by the intended application of the models. The characterisation and subsequent modelling of the ECG can be broadly grouped into three categories:

1. Clinical Definition and Characterisation: Fundamentally the ECG signal is a tool to be used by a cardiologists to perform a diagnosis. In this context any model for the shape or duration of the ECG components should serve to provide clinical definitions for normal and abnormal behaviour of the human ECG.

2. The Inverse ECG Model: In this case the intention is to model or compute the potential at the location of the heart from observation of the recordings on the surface of the body.

3. Empirically Derived Models: The actual output of ECG recordings are analysed and subsequent observations made regarding the ECG signal which are used to characterise and model the ECG signal itself with a view to replicating this signal in a controlled environment.

In this chapter each category of ECG modelling and characterisation shall be discussed in order to understand the strengths and weaknesses of the state of the art research in the field and to explore their degree of alignment with the author's aims.

5.2 Clinical Definition and Characterisation

The ECG has been the subject of an enormous amount of on-going research not only in the clinical domain, but also in the industrial and academic fields aimed at supporting and assisting the clinician. The purpose of this research in a clinical sense is to provide indices or metrics from which the normal or abnormal behaviour of a subject's cardiovascular system can be assessed. The indices have been created from the observations by cardiovascular experts of vast numbers of ECG recordings, subject symptoms and invasive explorations in order to find a correlation between the shape and duration of the constituent components of an ECG and the subject's cardiac state as discussed in Chapter 2. The ECG itself is only useful when used in conjunction with the accepted interpretations of the ECG behavioural characteristics.

The number of normal and abnormal variations found in the ECG and defined in the clinical literature are too numerous to mention. However, it is very important that any model which is to be used to test or calibrate a biomedical signal processing technique or instrument should reflect the clinical definitions of normal and abnormal behaviour of the ECG. One example of such a metric is the clinical definition of the QT interval duration. It is commonly accepted that a normal or healthy QT interval should vary inversely with heart rate [2] or directly with cardiac cycle time T_{RR} as shown in Figure 5.1.

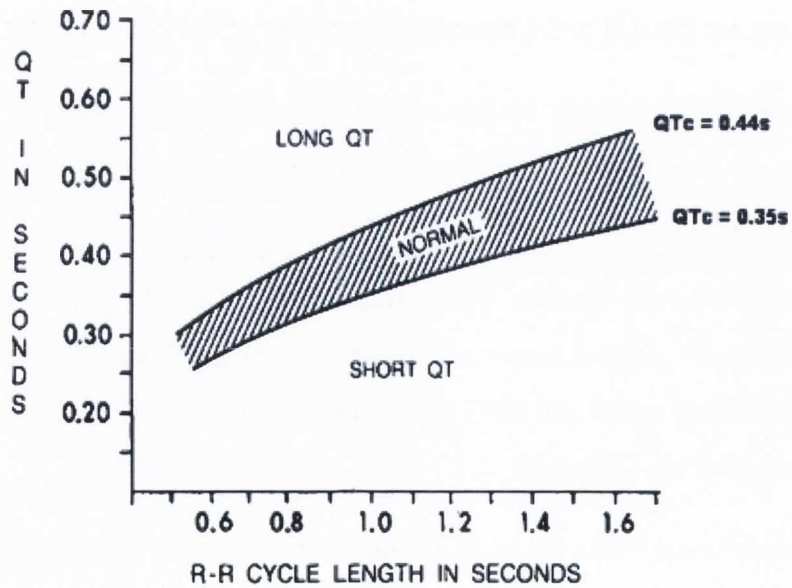

Figure 5.1: The Goldenberg characterisation of the healthy QT interval duration [51].

Figure 5.1 is the result of a study of 581 healthy subjects by a team of cardiologists in the University of Rochester Medical Center, New York and shows their definition of the normal QT interval duration and is illustrative of the clinically accepted definition of this interval [51]. Any mathematical model for the QT interval should yield results in keeping with this characterisation.

Not all of the ECG constituent components have such a strong correlation with heart rate as the QT interval. However, they do consistently alter with respect to heart rate. The QRS complex, for example, has been found to increase in duration at lower heart rates (higher T_{RR}) in a number of studies [52–54].

The author believes that any model of the variation of the ECG should be placed in the context of large clinical studies such as the Goldenberg study and the wider world of cardiac metrics where possible. In doing so, one can ensure that the models created and used in the science and engineering fields of biomedical research which aim to assist the clinical experts reflect the same understanding and characteristics used by these experts. In Chapter 8 a number of other clinical characterisations and studies shall be used to verify the timing model proposed in this thesis.

5.3 The Inverse ECG Model

The second approach to ECG modelling involves attempting to create a model of the electrical activity at the location of the heart by observation of the activity on the surface of the body. This problem is commonly known as the Classical Inverse ECG Problem and is illustrated in Figure 5.2.

This more complex approach to modelling the ECG signal aims to model the source of the signal i.e. the cells and tissues within the heart muscles and hence replicate the resulting surface potential. Multiple approaches have involved modelling the cells as a three-dimensional cubic lattice [55], as a difference of two sigmoid functions [56] and as a series of wave-fronts emanating on the heart surface [57]. These types of complex mathematical models are still very much an ongoing area of research but the ability to model each cell or cluster of cells is limited and they are aimed more at understanding and capturing the internal activity of the heart than at directly characterising the ECG signal produced at the body surface.

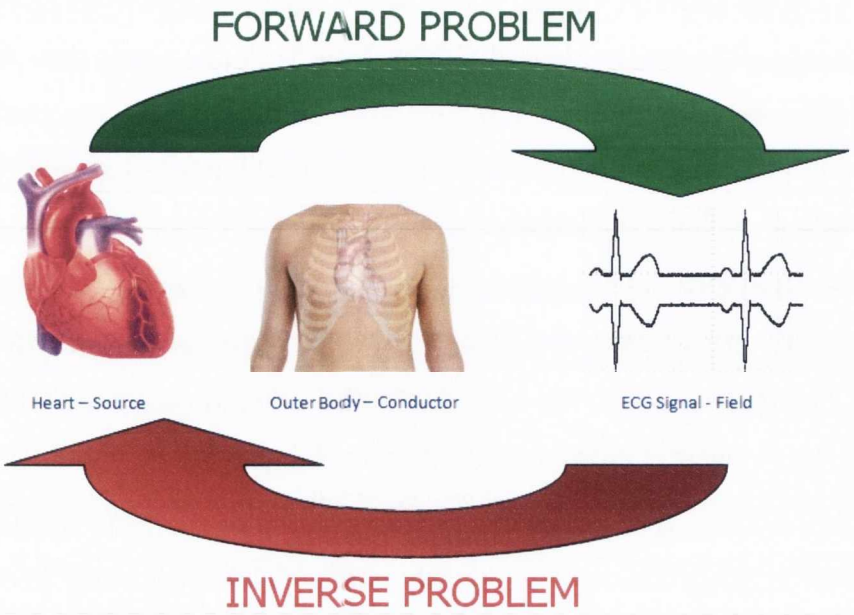

Figure 5.2: The Inverse ECG Problem

In terms of the objective of this study, i.e. the synthesis of an accurate ECG test signal, inverse modelling is not useful and consequently the rest of this review will focus on models aimed at characterising the "field" or ECG signal itself as recorded on the surface of the body.

5.4 Empirically Derived Models based on Actual Recordings

An alternative to inverse ECG modelling involves the observation of real ECG recordings, empirically matching or characterising their amplitude and timing characteristics and incorporating them into a model.

5.4.1 Gaussian Pulse Decomposition Models

Early researchers used mathematical basis functions [58], polynomials [59] and cosine waves [60] to synthesis the ECG signal. However more recently a number of more accurate and practical algorithms have been used to decompose the ECG signal into Gaussian pulses. The methods typically involve selecting a portion of the signal e.g. the P wave, and fitting a single Gaussian pulse to that portion of the signal. This pulse is then subtracted from the original ECG waveform and the process is repeated iteratively

until the residual waveform is below a given error threshold [61]. Continuing research has extended this method to model the asymmetrical T wave using an asymmetric Gaussian function and increase the accuracy in capturing the elevation and depression of waves subject to baseline wander [62]. The process is illustrated in Figure 5.3.

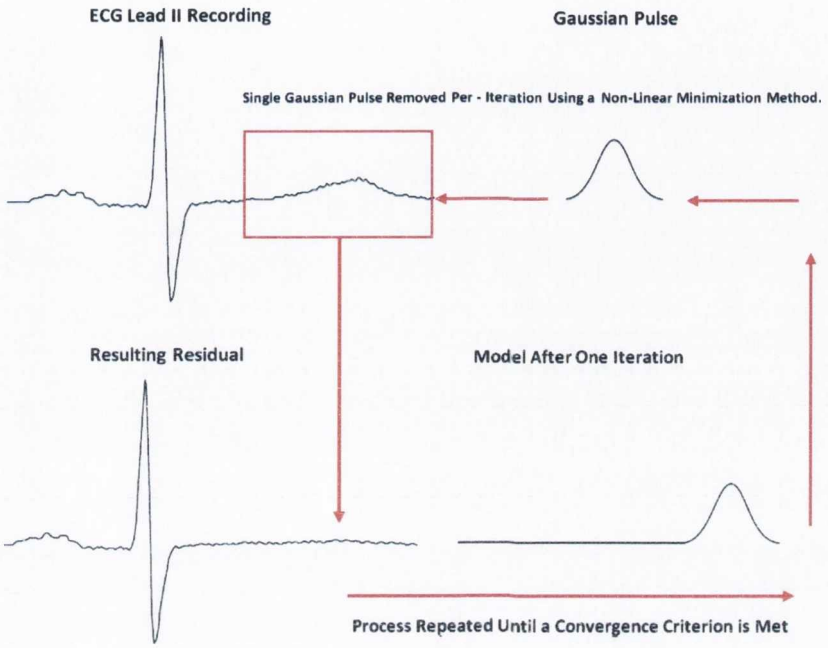

Figure 5.3: The Gaussian Pulse Decomposition Method as Proposed by Suppappola *et al.* [61]

The algorithm has been verified as accurately capturing the morphology of the signals under test. However the limitation or shortcoming of the Guassian models found in the literature is the lack of timing information included in the model. Details are given for modelling existing ECG recordings, but a method of generating the synthetic Gaussian pulses over the full range of cardiac cycle times in a way typical of *in-vivo* recordings is not described or incorporated into the model.

5.4.2 A Dynamical Model for Generating Synthetic Electrocardiogram Signals

A dynamical model proposed by McSharry *et al.* [8] involves the creation of a three-dimensional state space in which to generate synthetic waveforms. The quasi-periodicity of the ECG signal is reflected in the (x,y) planes and the amplitude variations in the (z) plane. Each beat duration or limit cycle is reflected by one revolution through the three dimensional state space as shown in Figure 5.4.

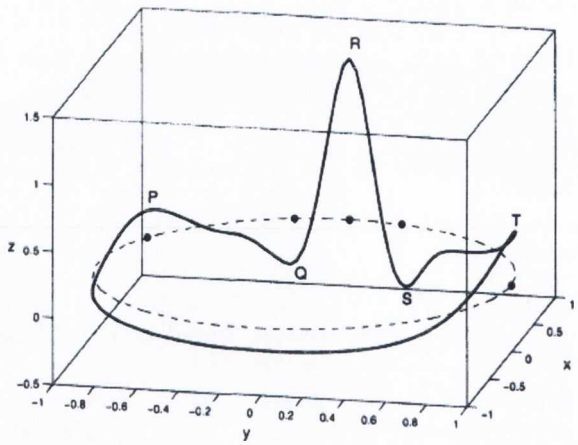

Figure 5.4: The McSharry *et al.* three dimensional state space model [8]

The model allows for the addition of baseline wander and other phenomena such as Mayer waves, or heart rate variability into the signal as well as coupling it with blood pressure [63]. The model can also be used in conjunction with Gaussian pulses to mimic a given recorded ECG signal by varying three parameters - amplitude, width and phase for the pulse to achieve a best fit to the beat under analysis. Once the best fit has been achieved the constructed representation of the signal can be regarded as a filtered [9, 64] or compressed [65] version of the original.

This model is described by McSharry *et al.* as having been designed as a tool for assessing biomedical signal processing techniques. One limitation of the model is that it does not specify or define the timing of the onset and termination points of the constituent waves clearly with respect to heart rate. In fact, it has been reported [66] that when the model is calibrated to recreate the heart rate variability and other timing characteristics observed in a set of actual ECG signals, the resulting P, R and T wave locations are different than in the original ECG recording.

This type of model has been suggested primarily as an alternative to using reference databases of real ECG recordings to test signal processing techniques and their ability to detect and remove artefact from the ECG. The advantages and benefits of this dynamical model are clear when attempting to recreate ECG signals with controllable artefact included in the morphology. It can be trained or adjusted to mimic a specific set of artefactual conditions found in real ECG recordings. However, it is not aimed at allowing the design of hardware to generate ECG test signals since the durations of the components are defined by manual observation rather than by empirical or theoretical simulation.

5.4.3 Data Flow Graph based ECG Signal Synthesis

An alternative model and one more closely correlated with generated ECG test signal is that of the Data Flow Graph (DFG) based model [67]. Essentially this model involves taking an actual ECG recording and segmenting it into a series of distinct time domain signals with each wave becoming a separate node in the system. The reconstruction of these segments can then be controlled by the output sampling rate to alter the duration of each component to simulate a change in heart rate and the timing of individual components. The DFG model has also been extended to allow interpolation of the original data points to limit any distortion of the signal when its time scale is altered with the sampling rate [68]. The limitation again found in this model is the lack of time characterisation that the output constituent components of the wave adhere to if the heart rate of the ECG signal is changed. In the literature cited here the durations are merely numerical estimates and cannot be varied automatically with heart rate.

5.4.4 ECG Synthesis Based on Morphing

ECG synthesis by morphing is based on having two parent ECG recordings and the creation of a third signal which has some of the characteristics of the parent ECG recordings but is in itself a different ECG waveform [69]. The two parent signals are manually segmented using the key feature points of the ECG as defined in Figure 1.1. Between these points a cubic spline interpolation is performed and the periods between features are oversampled so that both of the parent signals have the same number of points. Using the process known as "morphing" the two parent signals are weighted in terms of their contribution to a third new signal which is a combination of both parent signals.

If the two parent signals are designated ECG1 and ECG2 then the position in time and the resulting amplitude of the synthesised signal ECG_{out} is given by Equation (5.1) for the time alignment during morphing and (5.2) for the resulting amplitude of the points in the new signal.

$$tn = t(n)_{ECG2} + \varepsilon \times (t(n)_{ECG1} - t(n)_{ECG2}) \tag{5.1}$$

$$ECG_{out}(t) = \varepsilon \times (ECG1) + (1 - \varepsilon) \times ECG2 \, \forall \, n \tag{5.2}$$

where t(n) is the advancement in time for the new sample, $t(n)_{ecg1}$ and $t(n)_{ecg2}$ are the corresponding points in time of the parent signals and ε is a user defined weighting factor.

The resulting ECG signal provides a realistic waveform which is within the amplitude and temporal constraints of the original ECG recordings as shown in Figure 5.5.

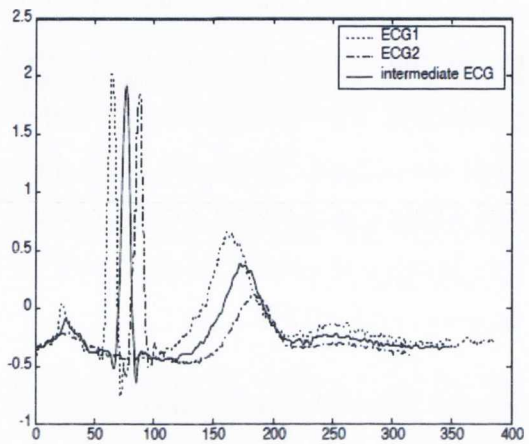

Figure 5.5: The results of ECG synthesis by morphing [69]

The original motivation for synthesis by morphing was concern regarding the unrealistic output from the dynamical model discussed in Section 5.4.2 where Nimunkar and Tompkins state "one needs to be very careful in order to generate realistic ECG's using these techniques". The author assumes that this "care" regards the arbitrary method used in designating the timing parameters of the synthetic ECG signal. The timing of the output samples in the waveform synthesised waveform by morphing are based on Equation (5.1) which is varied using the variable ε. Although it is clear that there is a correlation between the resulting output component durations and the parent signals there is no direct comparison with respect to cardiac cycle time during the morphing process since it is based on the arbitrary scaling variable used to weight the contribution of each parent signal to the output. Although useful for creating realistic looking signals the synthesised output is not actually based on any physiological phenomena but simply an arbitrary combination of only two parent signals. Given that it requires two parent ECG signals in the first instance, its targeted applications are somewhat unclear to the author.

5.4.5 Classical Component Duration Modelling of the ECG signal

In Chapter 2 it was illustrated how the core diagnostic value of the ECG recording lies in the observation of the durations of constituent component and in some cases their components variation with respect to heart rate. It has also been seen in Section 5.2 that clinical studies of the ECG signal attempt to characterise healthy and unhealthy subjects by the creation of indices to measure normal and abnormal component durations. Yet it can be observed thus far in this review that the models reported are focused mainly on synthesising the amplitude characteristics of the ECG signal or the effects other phenomena may have on the ECG signal. They do not include a basis for altering the duration of each constituent component in a manner consistent with *in-vivo* ECG recordings.

A number of studies have been conducted in an attempt to mathematically characterise the variation of the ECG constituent components and in particular the QT-interval with respect to heart rate as seen below. The earliest research involved relating the QT interval duration to cardiac cycle time T_{RR} using various functions (not to be confused with the correction formula as will be discussed in Chapter 8), note all K variables are constants (*Int* blow denotes interval):

Bazett's Equation [6] :

$$T_{QT-Int} = K_B\sqrt{T_{RR}} + A_B \tag{5.3}$$

Fredricia's Equation [26]

$$T_{QT-Int} = K_F(\sqrt{T_{RR}})\frac{1}{3} \tag{5.4}$$

Shlamovitz and Simonson et al also proposed a linear relationship [70]:

$$T_{QT-Int} = K_{S1}(T_{RR}) + K_{S2} \tag{5.5}$$

Ashman and Hull [71]:

$$T_{QT-Int} = K_A log[10(T_{RR} + 0.07)] \tag{5.6}$$

These classical equations, and in particular Bazett's equation, have been used to characterise the QT interval duration and its relationship to heart rate [2] for decades, despite the well documented limitation of the equations at low heart rates [26, 72].

5.4.6 Wavelet Based Analysis of the ECG Component Durations

In order to perform a more thorough investigation of the ECG components and their relationship with heart rate a more in-depth study was undertaken by M. Nasor [26]. Nasor found that the first order equations being used to characterise the variation of any ECG component with respect to T_{RR} could be replaced by a more accurate formula of the form shown in Equation (5.7). It was verified as being a more accurate representation of the time components using the same data as Bazett and Ashman & Hull:

$$T_{Comp} = AT_{RR} + B\sqrt{T_{RR}} + C \tag{5.7}$$

Using the new second order Equation (5.7) in $\sqrt{T_{RR}}$, Nasor decided to derive a complete timing model for each component of the ECG signal with respect to T_{RR}. The purpose of the model was to enable the creation of a synthetic ECG test signal that could be generated across the full range of heart rate and have constituent components that varied with respect to heart rate in a fashion typical of normal healthy subjects [4]. In theory, this time model could be used to increase the usefulness and validity of each of the models discussed in Sections 5.4.1 to 5.4.3 and allow them to provide more realistic ECG signals.

The method chosen by Nasor to segment the ECG signal for the purposes of characterisation was based on the wavelet transform. Previous segmentation techniques based solely in the time domain had relied on thresholding, slope detectors and template matching. The shortcoming of these methods is that they do not allow for the time-varying features of the ECG signal. Choosing the Mexican Hat wavelet, Nasor demonstrated how one can convolve the wavelet signal with an ECG database of recordings and delineate the signal into its constituent components based on this comparison. The Mexican Hat wavelet was chosen due to its similarities with the ECG component morphologies as seen in Figure 5.6.

The process involves decomposing the ECG signal into multiple wavelet transform bases with different frequency bandwidths. Within these time-frequency based signals the onset and termination points of the P, QRS and T waves can be found by observing the appearance of the components in different transform base bandwidths. By connecting the location of these points or modulus maxima across the multiple levels

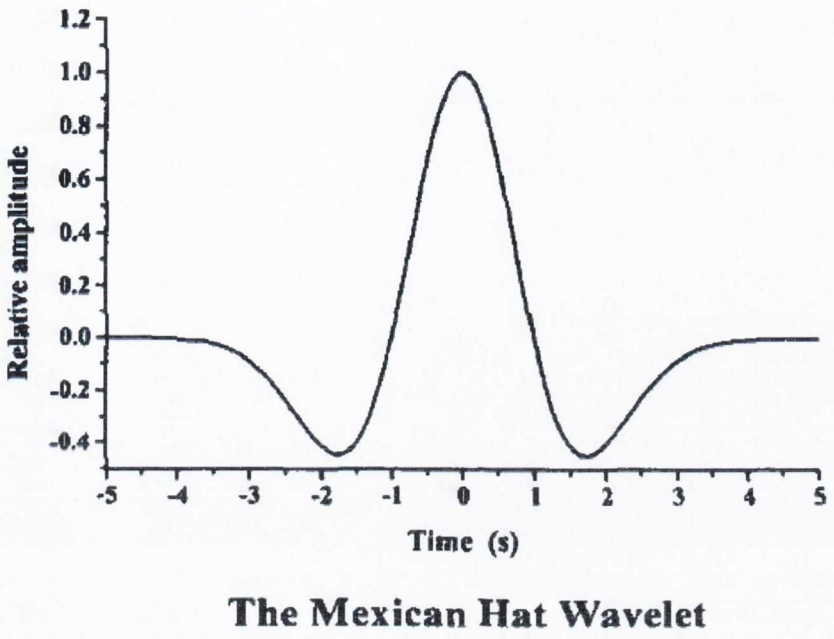

Figure 5.6: The Mexican Hat Wavelet used during Nasor's study [10]

to create ridge vectors their final locations were found by convergence in a skeleton diagram of the modulus maxima. Using thresholding the P, QRS and T waves could be isolated based on the expected level or bandwidth they were estimated to appear within. An example of one such skeleton of modulus maxima from [10] is shown in Figure 5.7.

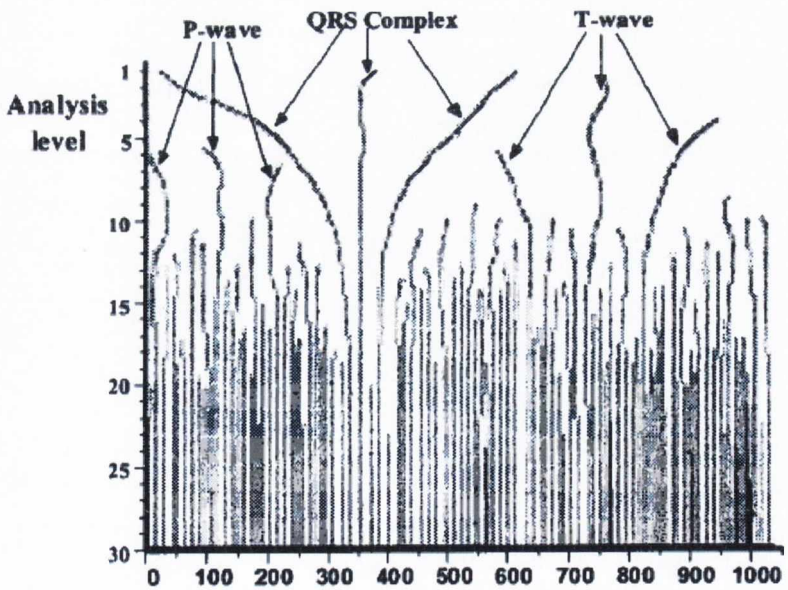

Figure 5.7: The skeleton of the modulus maxima of one cardiac cycle [10]

Nasor derived a set of equations for each component as defined in Figure 1.1 of the ECG signal with respect to T_{RR}. It was suggested in subsequent publications by Burke

& Nasor that the equations could be accurately used over a range of cardiac cycle times of 0.3 to 2.0 seconds. The equations originally reported in [26] were revised and the final versions reported in the most recent publications [4, 10] are:

$$T_{P-Wave} = 0.37\sqrt{T_{RR}} - 0.22T_{RR} - 0.06 \tag{5.8}$$

$$T_{P-QSeg} = 0.33\sqrt{T_{RR}} - 0.18T_{RR} - 0.08 \tag{5.9}$$

$$T_{P-QInt} = 0.69\sqrt{T_{RR}} - 0.39T_{RR} - 0.14 \tag{5.10}$$

$$T_{QRS} = 0.25\sqrt{T_{RR}} - 0.16T_{RR} - 0.02 \tag{5.11}$$

$$T_{Q-TInt} = 1.21\sqrt{T_{RR}} - 0.53T_{RR} - 0.31 \tag{5.12}$$

$$T_{T-Wave} = 1.06\sqrt{T_{RR}} - 0.51T_{RR} - 0.33 \tag{5.13}$$

$$T_{S-TSeg} = -0.09\sqrt{T_{RR}} + 0.13T_{RR} + 0.04 \tag{5.14}$$

5.4.6.1 Limitation of the Burke & Nasor Equations

The results of the Burke & Nasor equations offer a significant benefit not found in the other models discussed in this review in that they provide a comprehensive modelling of each component duration within the healthy Lead II ECG signal with respect to heart rate. The application of the then state-of-the-art wavelet technique to ECG component duration calculation was a novel approach to the problem.

However, some limitations of the equations can be identified by observation of the equation for the QT interval and QRS duration when plotted over the 30 to 200 bpm or T_{RR} range of 0.3 to 2.0(s) as suggested in [4].

When one compares the plot in Figure 5.8 to the clinical definition and figure for the QT interval presented in Section 5.2 it is clear that the mathematical model suggested by Burke & Nasor in Equation (5.12) does not accurately characterise the variation of the QT interval with respect to heart rate at lower heart rates as shown by the approximated inconsistency region in Figure 5.8 i.e. T_{RR} >1.3 s or heart rates <46

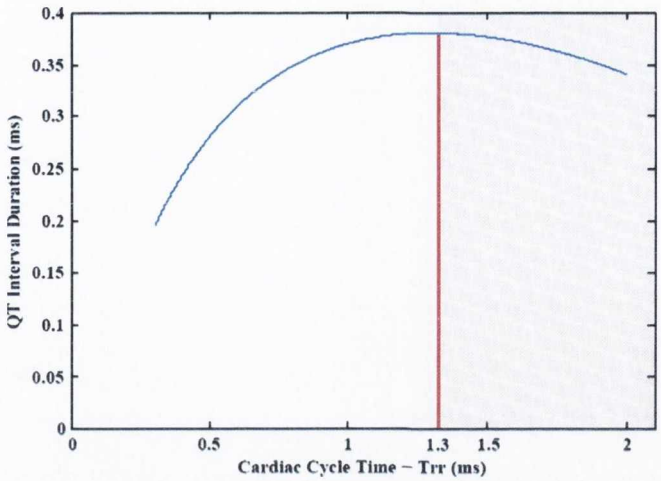

Figure 5.8: The QT interval duration according to Burke & Nasor's Equation (5.12)

bpm. This limitation was also acknowledged in the original form of the equations [26]. The clinical definition states that the duration should increase continuously with respect to lower heart rates [2].

A plot of Equation (5.11) over the same range of T_{RR} also shows an inconsistency when placed in the context of other studies of the QRS duration during exercise and rest as shown in Figure 5.9. The QRS duration as discussed in Section 5.2 should have an inverse relationship with heart rate i.e. the duration increases the lower the heart rate (higher the T_{RR}). Equation (5.11) however results in the opposite trend with respect to T_{RR} at lower extremes of heart rate the duration decreases.

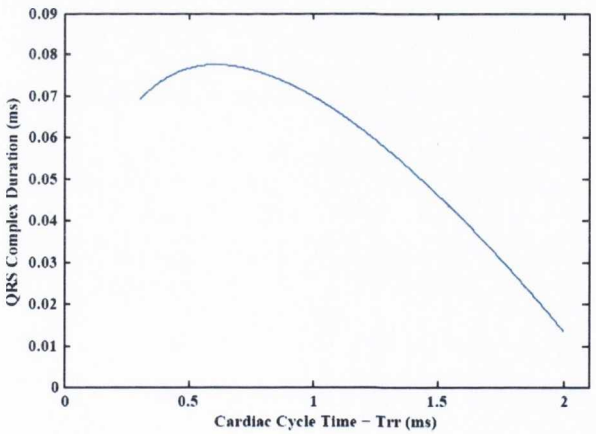

Figure 5.9: The QRS complex duration according to Burke & Nasor's Equation (5.11)

Firstly, it is possible that the database used to create Equations (5.8)-(5.14) does not contain a large enough cohort of subjects to adequately assess the variation of the components with respect to heart rate. With this in mind, the manner in which the data were averaged before the equations were fit to the results of the wavelet analysis

could also have had a profound effect on the end result particularly at the extremes of heart rate where less recordings would have been available i.e. < 50 bpm. To examine this possibility one could use the same dataset but a different technique for the detection of the onset and termination of each wave and the averaging method applied before attempting to characterise the results. It would then be possible to see if the errors observed in Figures 5.8 and 5.9 are reproduced by the results of the new study.

Another possibility may be that the wavelet based method for delineating the signal was not accurate enough for the application.

5.4.6.2 Synthetic Testing of the Wavelet Technique

Nasor argued that the onset and termination points of the constituent waves could be accurately resolved by tracing the appearance of these points across the different frequency bands of the resulting wavelet basis functions which also retain the temporal information of the original signals. He also pointed out that the wavelet transform had previously been used to great effect in the removal of noise and detection of the P,R and T wave peaks since they have distinctive frequency features when compared with the rest of the ECG beat. To investigate the wavelet transforms ability to detect the onset and termination points of the constituent waves a synthetic signal with clearly defined and known onset and termination points was used. The synthetic signal is shown in Figure 5.10.

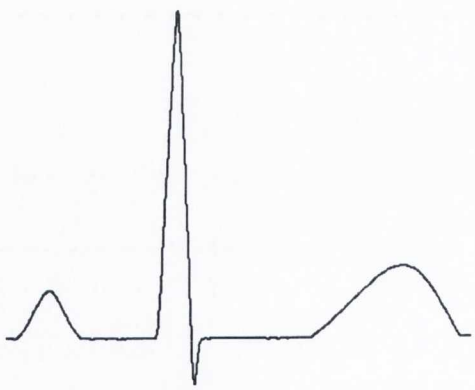

Figure 5.10: Synthetic Test Signal Used by Nasor [26]

Using this test signal synthesised at different heart rates Nasor investigated the wavelet technique's ability to find the onset and termination points of the P, QRS and T waves in the synthetic signal and found the maximum error to be just 3 ms for the

measured T wave duration. This test signal offers an adequate insight into the wavelet techniques ability to resolve clearly defined points in an ECG signal. However, this test signal does not test the the wavelet techniques accuracy when trying to find less obvious alterations in the signal. The Mexican Hat wavelet and the synthetic signal should offer very good results when decomposed into wavelet transform bases functions since the user is attempting to match a synthetic wavelet with clearly defined properties to a synthetic signal with clearly defined properties. However, in actual ECG recordings the onset or termination points of the constituent waves are not so clear.

Figure 5.11 shows actual ECG signals taken from the Physionet QT Database of expertly annotated ECG signals [73] and shall be discussed in more depth in Chapter 6. The Physionet database is an open source and available on-line, making it the most popular and comprehensive research database of physiological signals worldwide. It has been compiled by experts at the National Institute of Biomedical Imaging and Engineering, National Institute of Health, The National Institute of General Medical Sciences and M.I.T. PhysioNet is an actively updated archive.

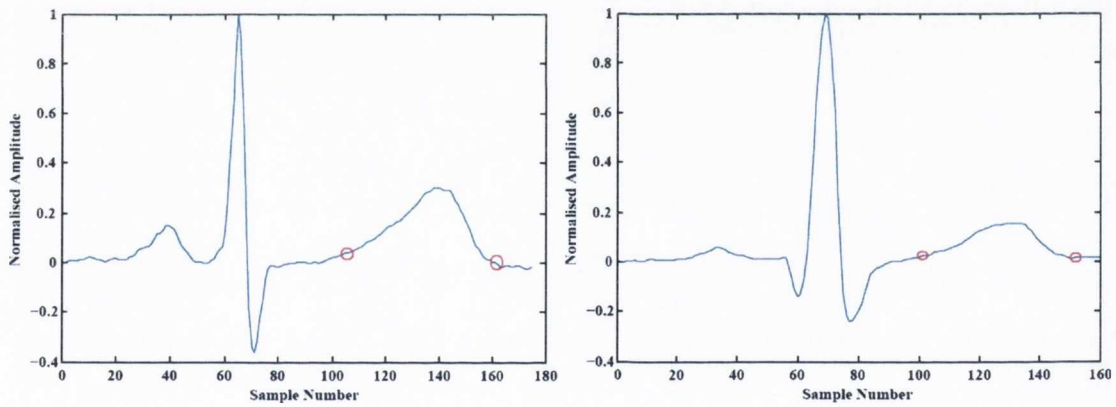

(a) (b)

Figure 5.11: Actual ECG recordings as annotated by an expert cardiologist.

The purpose of the example signals in Figure 5.11 is to demonstrate that even very clean ECG recordings with stable baselines do not have clearly defined onset and termination points. As indicated by the red circles in Figure 5.11a the expert annotation does not appear at any identifiable characteristic deflection from the isoelectric line. In Figure 5.11b one can also see that sometimes there is no isoelectric zero or definite baseline between the ST segment and the T wave but rather a continuous slope from the end of the QRS complex. The cardiologist has used his expertise to annotate the signal when no definite deflections are clear. This is extremely common in real

ECG recordings and is observable in many ECG recordings within the Physionet QT database. The performance of the wavelet technique is based on its ability to decompose the signal into frequency bases, which is most accurate in the detection of peaks and high frequency noise as described by Nasor *et al.* However, its ability to find the onset and termination points in morphologies that have very subtle variations such as those shown in Figure 5.11 is questionable. It is most likely that a reference database of signals such as the Physionet QT database was not available at the time, so the use of a synthetic signal was the only method available to Nasor *et al.* It is possible that this may have led to the error observable in Equation (5.12), especially when one considers that the significant error occurs at low heart rate or high cardiac cycle time where the variations in the ECG morphology are more gradual due to the lower frequency of the heart beat.

5.5 Summary and Conclusions

5.5.1 Clinical Review:

The use of the ECG signal by cardiologists for diagnosis depends on their ability to discern the morphology and timing characteristics observed in a subject's ECG recording with their a priori knowledge of normal and abnormal ECG signals. As such, the largest and most important characterisations of the ECG signal and its constituent components are found in the clinical research. Any amplitude or timing model, particularly one claiming to characterise the normal variation of the ECG, should be comparable to the indices and metrics for normality as defined by clinicians.

5.5.2 The Inverse Problem:

Also discussed in this review is the inverse approach to characterising the ECG signal whereby the researcher is modelling the activity at the location of the heart by observation of the ECG signal on the surface of the body. The alternative approach finds its roots in more of a biological setting than an engineering one. Although not directly relevant to the objectives of this research project it is still important to be aware of in terms of the research field.

5.5.3 Empirically Derived Models based on ECG Recordings:

The most common approach to the creation of synthetic ECG signal involves the modelling of the ECG morphology and its time variations. A number of models where shown to enable the user to model the morphology of a given ECG recording using Gaussian pulses to include realistic controlled artefacts on the resulting output ECG signal. However, the models include no information for the creation of synthetic signals which morphologically vary with heart rate of in a fashion reflective of *in-vivo* recordings.

To address this limitation other models analyse the time variation of the ECG components, and in particular the QT interval with respect to heart rate. The most comprehensive study of the variation of the ECG components with respect to heart rate by Nasor *et al.*, presents a mathematical model for each component which is very useful. The results of the model present a significant contribution to the characterisation of each components duration with respect to heart rate. Unfortunately, when the equations for generating certain component durations are examined in the context of clinical observation of the component durations there are some inconsistencies between the two. At the time the research was conducted, the only method available to test the wavelet techniques ability to identify the fiducial points within the ECG may have been limited to synthetic signals. The researcher was also limited to a relatively small cohort of subjects which probably should have been considered when averaging the results before attempting to characterise them, particularly at extremes of heart rate where a smaller number of samples would have been available.

A reinvestigation of the component variation with respect to heart rate is required. The technique used to derive this new characterisation should be able to operate with the time variant nature of the ECG signal but not suffer from the same possible limitations of the wavelet based technique. Its accuracy should be tested using real ECG recordings and the final results placed in the context of known clinical research regarding the variation of the component durations with respect to heart rate. The principle idea of a complete time model as proposed by Nasor *et al.* is an extremely useful one in the context of this authors work. The author will hence attempt to re-derive the equations for the durations using a different technique, known as Dynamic Time Warping to segment the ECG signal, and examine the possible effects of alternative averaging of results before fitting equations to them.

With the beginning of more advanced ECG modelling and simulation, in the late 1980's and early 1990's research raised concern regarding the suitability of subsequent models when applied in a realistic test setting. The necessity for models derived empirically to reflect medical knowledge gained both through quantitative and qualitative research was also highlighted [74]. The author believes that a model of the variation of the constituent ECG components such as that proposed by Nasor *et al.* is an invaluable tool because it is relatively easy to implement in hardware. It can also be combined with morphological based models such as those discussed in this review. The validity of the timing model however must be established in the context of larger clinical trials and definitions as expounded by cardiology experts.

Chapter 6

The Dynamic Time Warping Algorithm

6.1 Introduction

In this chapter the use of the dynamic time warping algorithm is proposed to investigate the timing of the ECG components. Dynamic time warping fundamentally aligns two signals of differing frame length, typically one a known reference signal and the other a signal we wish to characterise, which shall be called a query signal for the purposes of this thesis. Dynamic time warping (DTW) is a method of pattern recognition used in many different applications, having originated from the area of speech recognition [75]. It is used in many applications including robotics [76], manufacturing [77], biometric identification [78] and biomedical signal analysis [79]. The different variations of the algorithm can be sorted into three classes: value based (DTW), derivative based (DDTW), and feature based (FBDTW). One of the issues surrounding ECG pattern recognition is that the ECG itself is a non-stationary signal. As such, a direct comparison between two different signals cannot be done directly using a Euclidean distance measurement between them. Linear time warping (LTW) is hence not applicable to ECG classification or comparison. DTW offers a solution to this issue in that it uses a set of specified parameters for non-linear time-normalisation to minimise the difference between the two ECG recordings. The choice of DTW method is very much application and environment specific. For the purposes of this chapter the algorithms shall be discussed on the assumption that the objective is to identify the fiducial points for the P, QRS and T wave onset and termination in a Lead II signal since that is the

intended application of the algorithm in this research.

In order to examine the accuracy of the DTW algorithm and its variations a large database of ECG signals is required. The database of test signals introduced in this chapter shall also form the database of reference signals used to characterise the ECG signals in Chapter 8. The selection, filtering and formatting of the reference signals before being used with DTW is also presented in this chapter. For each form of the algorithm the advantages and disadvantages are explored. In the course of this exploration, an in depth study of the effects of approximation of the ECG signal (as used in DDTW) is performed and an alternative method of measuring the accuracy of such approximations is presented. The chapter concludes with the selection of a type of dynamic time warping and proposals to refine and increase the accuracy of the algorithm are made. Note that all signal processing was performed using the Matlab software package.

6.2 Formatting Test Signals

Throughout this thesis various digital signal processing algorithms for ECG signal analysis shall be tested. In order to test these algorithms a database of reference signals is required. The largest and most frequently used database of biological signal archives is that of the MIT PhysioNet database available as an open source on-line [73]. The largest and most widely referenced database of ECG signals from this signal archive is the QT database. Within this database are included ECG recordings with normal sinus rhythm and various arrhythmia.

6.2.1 Formatting The QT Database Reference Signals

The QT database compiled by Laguna et al. [80] contains 105 fifteen minute excerpts of two-channel digitized ECG's. The records were selected from a variety of other databases to represent a wide variety of QRS, ST segment and T wave morphologies. Each record in the database has between 30 and 100 representative beats which were manually annotated by cardiologists who identified the beginning and end of each P, QRS and T wave of each cardiac cycle in the recordings.

In the final results chapter, Chapter 8, comparisons between these reference signals and those from a database of healthy exercise ECG signals shall be made in order to

characterise the time variation of the constituent components of the ECG signal. A set of 719 ECG Lead II beats were selected by the author from the manually annotated beats described as normal Lead II ECG recordings, originally belonging to subsets of the Normal Sinus Rhythm and MIT-BIH-Arrhythmia databases as detailed in Table 6.1. The original data from the QT database has a 250 Hz sampling frequency and hence a sampling period of 4 ms. Unfortunately, many of the annotated beats available in the database are fragmented across each selection, and some annotations are incomplete in that they do not possess manually annotated T-onsets. An algorithm was written to read each of the manual annotations and create 719 records each with a complete single cardiac cycle recording, and a full set of P, QRS and T wave onsets, peaks and terminations. Where manually assigned annotations were incomplete, automatically generated annotations also available for each selection from the QT database were used to complete the records.

Table 6.1: The selection of reference signals from the QT database

MIT-BIH-Arrhythmia	Normal Sinus Rhythm
Sel 103: 30 beats	Sel 16265: 30 beats
Sel 114: 50 beats	Sel 16272: 50 beats
Sel 116: 50 beats	Sel 16273: 50 beats
Sel 117: 30 beats	Sel 16420: 30 beats
Sel 123: 30 beats	Sel 16483: 30 beats
Sel 213: 71 beats	Sel 16539: 30 beats
Sel 223: 31 beats	Sel 16773: 30 beats
Sel 230: 50 beats	Sel 16786: 30 beats
Sel 231: 47 beats	Sel 16795: 30 beats
Sel 233: 30 beats	Sel 17453: 30 beats

The test data comes from 20 subjects, with each beat having been fully annotated by an expert cardiologist and confirmed as being a "Normal" ECG beat.

6.2.2 Filtering the ECG signals

The ECG recordings require filtering to remove some of the sources of contamination from them as discussed in Chapter 2. All filters have been designed and tested to ensure

they satisfy the constraints of the most recent European standard for ECG recording [28] by Dozio [19].

6.2.2.1 The Low Pass Filter (LPF)

The signal was first low pass filtered to remove any unwanted high frequency interference on the signal such as muscle contraction. The European standard [28] requires a 3 dB cutoff frequency of greater than 100 Hz. A second order, analogue Bessel filter with a cut off frequency of 118 Hz was created in Matlab using the "Besself" function and all signals have been filtered using the resulting transfer function and the "lsim" function in Matlab which constructs the filter in software. The Bessel filter was chosen as it offers a maximally flat group delay (maximally linear phase response) in the pass band. The frequency response and 3 dB point are shown in Figure 6.1.

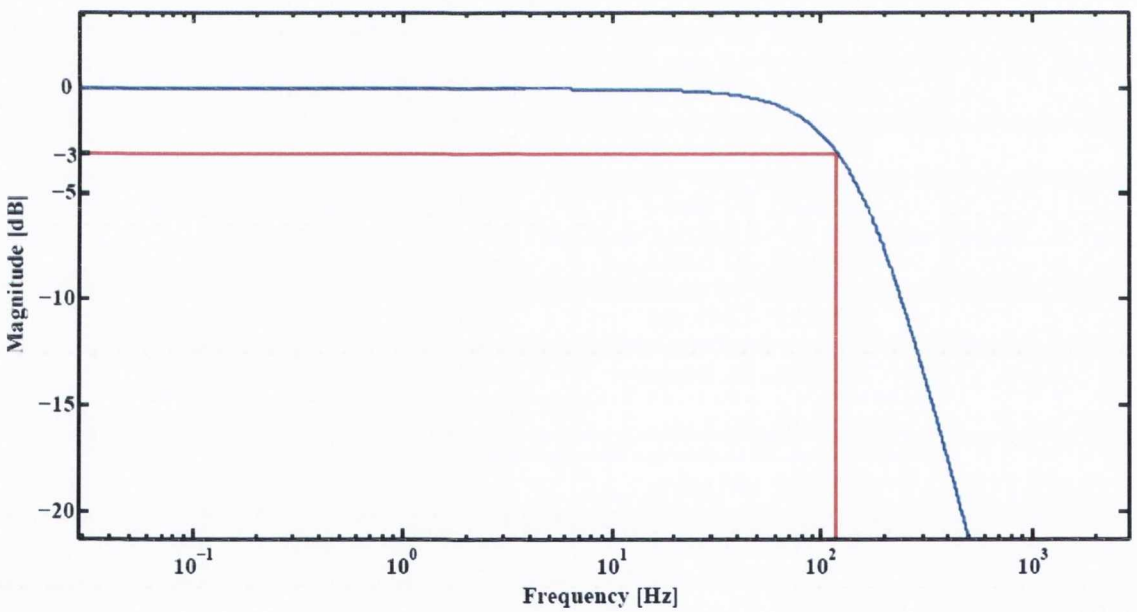

Figure 6.1: Second order low pass filter frequency response

The result of filtering high frequency noise for a typical ECG signal is shown in Figure 6.2. Other filters such as smoothing or median filters could have been used to remove the remaining high frequency noise but they have not been applied to avoid adding any unquantifiable distortion to the signal.

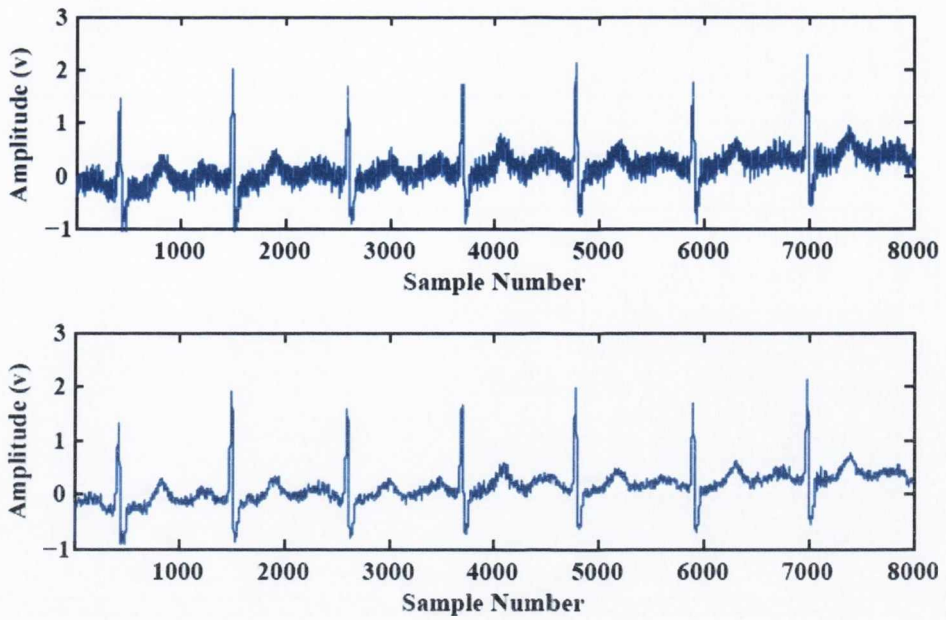

Figure 6.2: ECG signal before and after filtering with the LPF

6.2.2.2 The High Pass Filter (HPF)

The low frequency noise is filtered using a filter with symmetric time response to ensure no phase shift within the ECG signal. Low frequency shifts due to high pass filtering, can be significant because time displacements can occur due to phase non-linearity in the vicinity of the filter corner frequency. As a solution to the problem of phase shifts during high pass filtering Longini et al. [81] proposed that a signal may be filtered once through a high pass filter and then reversed and passed through the same high pass filter. The net phase displacement from the double filtering process is zero.

This process was again investigated by Dozio and it was proven that a second order Butterworth base filter with a corner frequency of 0.15 Hz satisfies the constraints of the standard [28] when used as a basis for the double filtering technique proposed by Longini [81]. The analogue filter was again simulated in Matlab using the "Butter" function to create the filter transfer function and "lsim" to filter each sequence using the filter. The frequency response of the zero phase shift Butterworth Filter is shown in Figure 6.3

The filter removes the majority of low frequency artefact such as baseline wander below 0.15 Hz as seen in Figure 6.4.

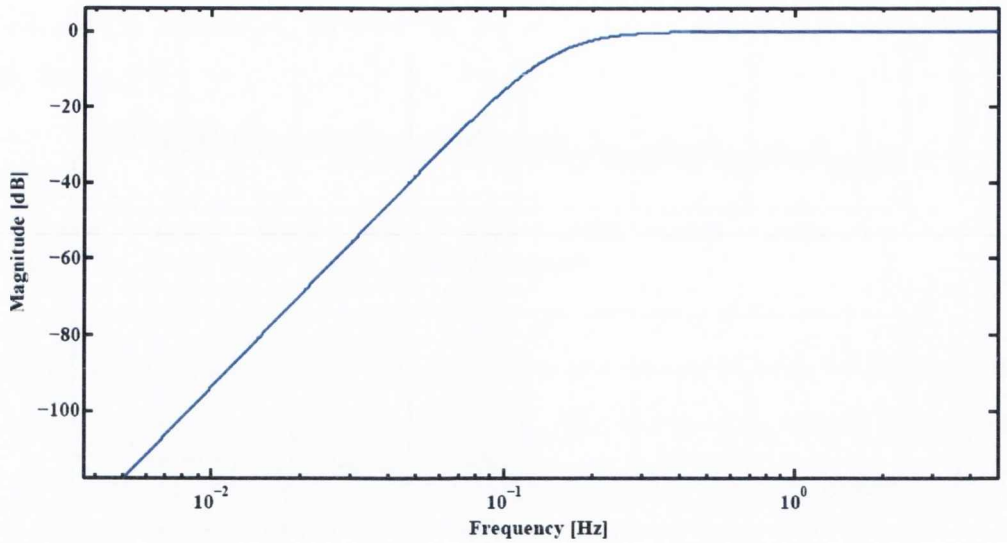

Figure 6.3: The Butterworth high-pass base filter frequency response

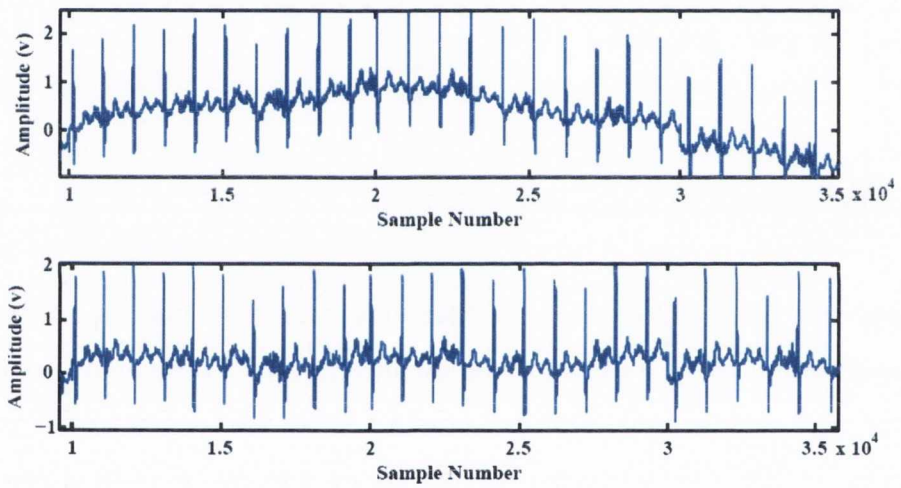

Figure 6.4: ECG signal before and after filtering with the HPF

Additional in-band filters such as a notch filter were not used to filter the signal as they have been found to remove in-band noise at a cost of introducing amplitude and phase distortion into the clinically significant signal [82]. As a result of this, the standards for diagnostic ECG recording [28] provide no criteria for in-band filtering, and as discussed above the minimum low pass corner frequency is specified as 100 Hz.

6.2.3 Formatting The Reference Signals

In order to format the ECG signals to be used as test reference signals, individual beat records are required. The creation of these records includes finding the peaks in a given ECG recording and segmenting each beat individually. The author has

designed a simple amplitude peak detector with a variable threshold which can be altered empirically to find all of the R peaks in a given ECG recording. When run the peak detector displays the detected peaks and allows the user to, change the threshold and add any peaks that are not found by the peak detector or remove false peaks. An example of the peak detectors output is shown in Figure 6.5

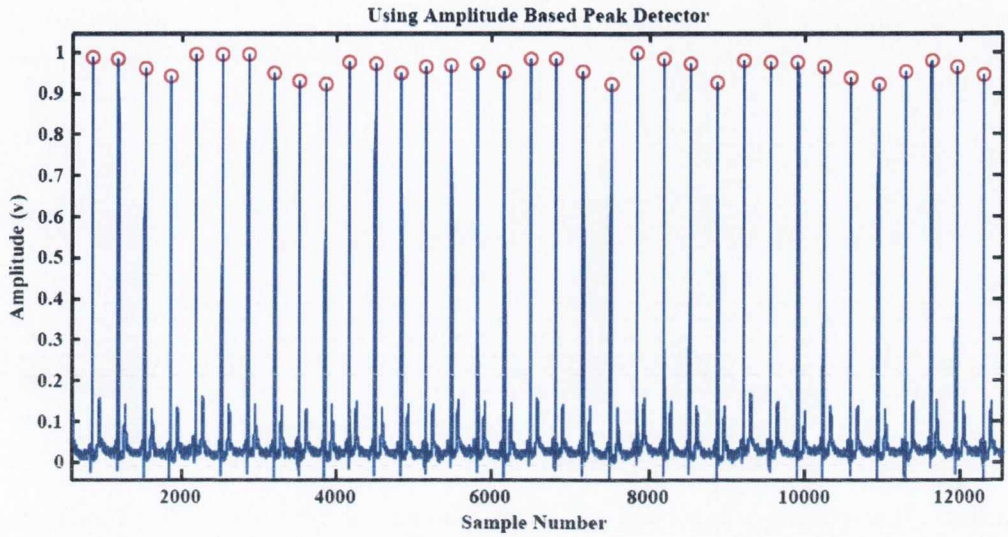

Figure 6.5: Example of the peaks found using the amplitude based peak detector

A more automated or sophisticated peak detector is not required because each signal from the reference database and later each test signal from an exercise ECG database must be visually examined by the author to ensure poor quality signals that are a result of a bad skin-electrode contact are excluded from the analysis.

Once the peaks are detected, the heart rate for each beat can be determined as discussed in Chapter 2. Using the R-peak each recording can be segmented by windowing around the R-peak to include the P and T waves of the beat. As a measure of the required window length the Burke & Nasor equations presented in Section 5.4.6 can be used estimate the required window length around the complete ECG beat. The algorithm for windowing allows the user to alter the window size empirically during viewing of the signals to ensure the full ECG beat is included. The heart rate, expert annotation values and the windowed single ECG cycle sequence are saved for each of the reference beats. The process is illustrated in Figure 6.6. To detect and remove spurious heart cycles or ectopic beats, the median heart rate for each 10 beat sequence can be found, any heart rate found to lie outside three median absolute deviations of this median is removed from the database. The median and median absolute deviations are robust and well-established outlier removal criteria [83].

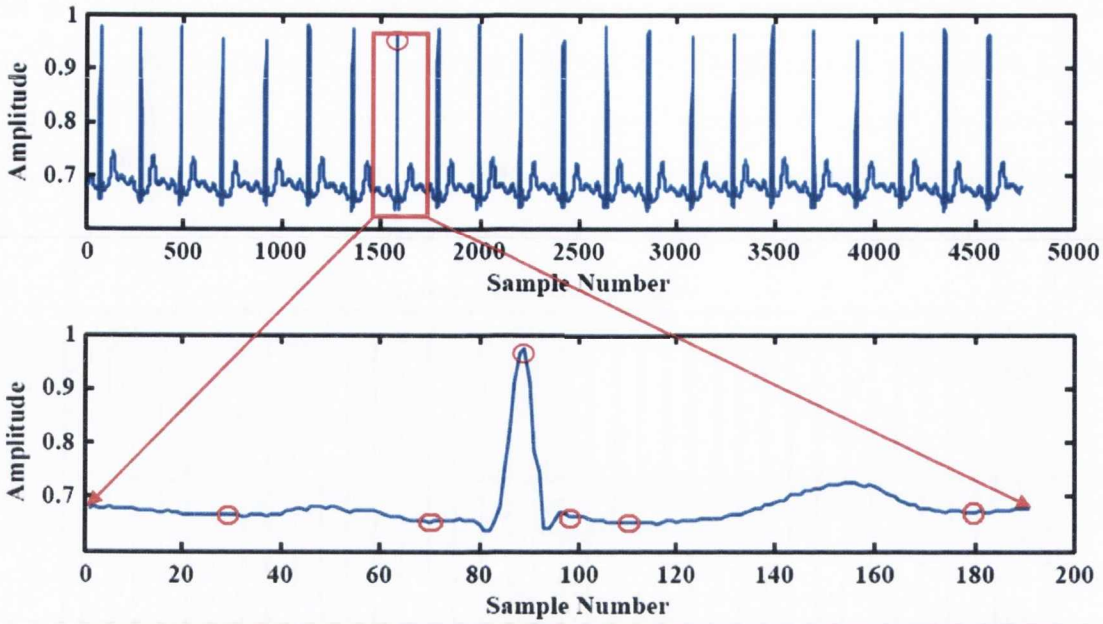

Annotation	P Onset	P Termination	QRS Onset	QRS Termination	T Onset	T Termination
Sample Number	31	70	78	98	111	180

Figure 6.6: The creation of reference record including individual beats and annotations

6.3 Value Based Dynamic Time Warping

Dynamic Time warping is a process whereby two signals are time aligned with one another through expansion or compression of sample points. By matching an unknown ECG signal to a signal with known characteristics it is possible to identify similar characteristics in the unknown signal. The value based DTW algorithm used by the author is based on that described by Theodoridis & Koutroumbas [84] which has been successfully applied to ECG analysis in its "classical" form and combined with application-specific changes to the algorithm by a number of authors in recent years [78, 85–87]. For illustrative purposes the value based DTW algorithm shall be discussed in depth since the DDTW and FBDTW variations of the algorithm are based on the same principles. The algorithm has been implemented in Matlab based on the open-source DTW code created by Felty [88]. Note that the notation and terminology used to describe the DTW process varies in the literature and the author has used the notation which he feels provides the greatest clarity.

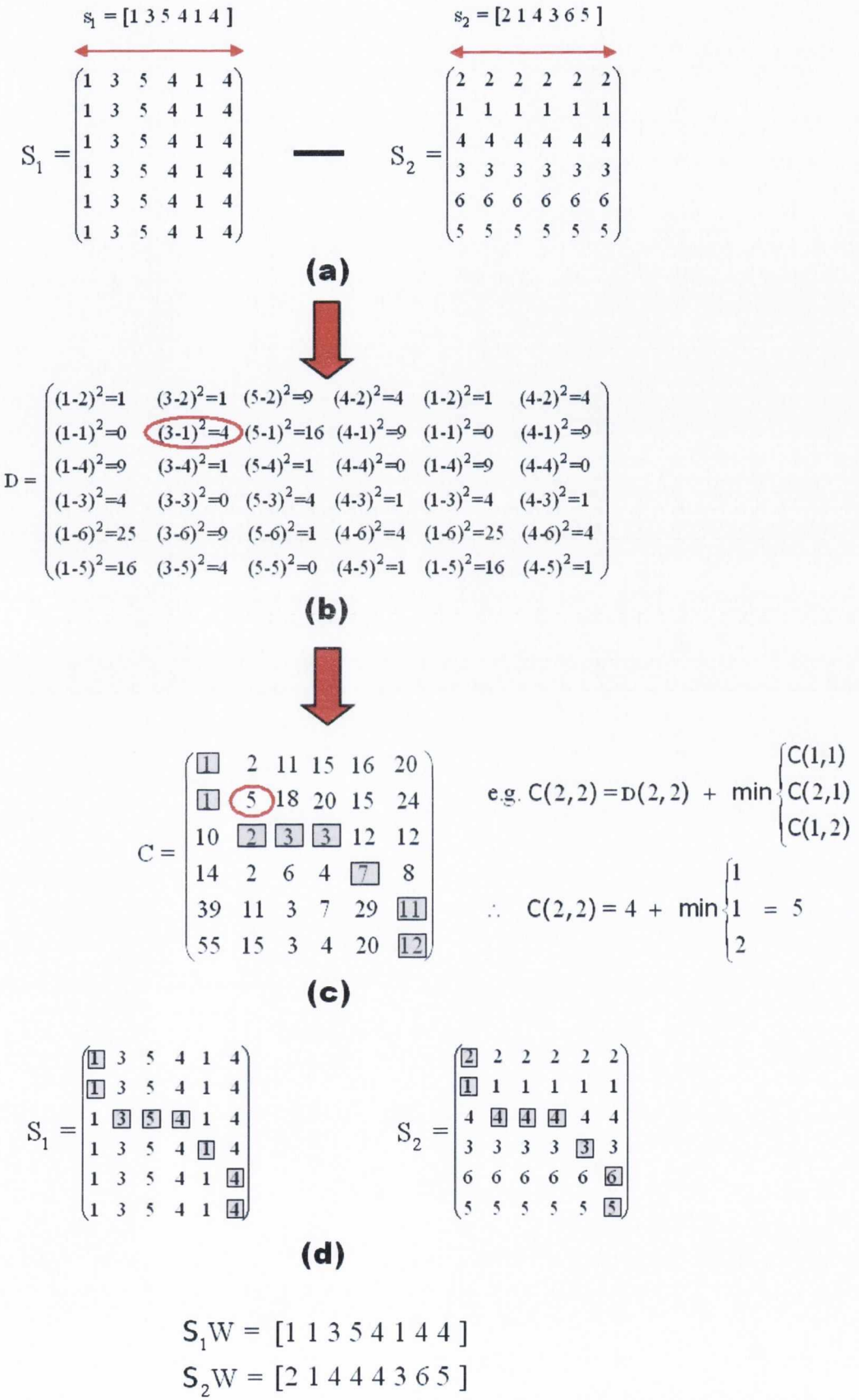

Figure 6.7: The dynamic time warping of two arbitrary signals

Consider the two input signals, the known signal s_1 of length n samples and unknown signal s_2 of length m samples. From the input signals two matrices are created, S_1 an $m \times n$ matrix which contains the known signal repeated on each row and S_2 an $m \times n$ matrix which contains the unknown signal repeated in each column as shown in Figure 6.7a. A distance matrix D can now be calculated as a single dimension Euclidean distance also shown in Figure 6.7b:

$$D(a,b) = [S1(a,b) - S2(a,b)]^2 \tag{6.1}$$

where $1 \leq a \leq m$ and $1 \leq b \leq n$.

The next step calculates a cumulative distance or cost matrix C, which measures the minimum cost of matching each sample in the two signals to each other, it is based on Bellman's Optimality Principle [89] which shall be discussed later. The cost function used in this case is a cumulative measure of the commonly used Euclidean distance measurement as calculated by Equation (6.1). The cost matrix in this sense is essentially a map showing the total resulting distance between the two test signals when the sample points in each are matched in all possible combinations. The cost matrix C is created by starting at location (1,1) of matrix D and calculating the cumulative distance of row one and column one of the matrix D and storing the results in the corresponding locations of the new cumulative distance matrix C (an m x n matrix also). The remaining cumulative values to be stored in the cost matrix are calculated by following the recursive equation below as shown in Figure 6.7c:

$$C(a,b) = d(a,b) + \min \begin{cases} C(a,b-1) \\ C(a-1,b-1) \\ C(a-1,b) \end{cases} \tag{6.2}$$

where $1 \leq a \leq m$ and $1 \leq b \leq a$.

Note that when template matching a reference and query signal often the most suitable reference or template match is based on the one which yields a minimum cost during warping. It shall be shown later that this approach is used frequently in ECG template matching, although it does not consider a number of possible issues regarding the suitability of classifying the best template match. In matching reference and query signals "something more is needed" [84] which is discussed further throughout this and the next chapter.

The final stage in the process involves starting at location *C(m,n)* of the cumulative distance matrix and moving to the smallest "cost" value stored in any one of the indicated adjoining locations. If all adjoining locations have the same value then the node diagonally adjacent, *C(a-1,b-1)* is chosen i.e. no repetition of points is required. One can traverse all the way back to location (1,1) of the matrix C, recording the path 'W' used which results in the minimum accumulated difference. Now that the optimal path across the matrix C has been found which yields the best alignment of the query and reference signals they can be recreated by following the same path across the original signal matrices S_1 and S_2 to create the two optimally time aligned signals S_1W and S_2W as shown in Figure 6.7d.

These two new signals are called the warped signals and are the same length as each other. The optimal path traced through the minimum cost of adjoining cells may dictate that certain samples of each signal be repeated (padding as in Figure 6.7) to optimally match a corresponding point in the other signal during the warping process. Figure 6.7 demonstrates the entire warping process for two arbitrary signals.

The DTW process and the warping path as described above is based on Bellman's Optimality Principle [89] and is subject to a number of constraints [84, 90].

6.3.1 Bellman's Optimality Principle and Dynamic Programming

Consider the optimal path between two points or nodes in the cost matrix C above, an initial node (m_0,n_0) and a final node (m_f,n_f). The optimal path can be expressed as:

$$(m_0, n_0) \overset{opt}{\longrightarrow} (m_f, n_f) \tag{6.3}$$

If another intermediate node (m_d,n_d) is between (m_0,n_0) and (m_f,n_f), then the optimal path from (m_0,n_0) to (m_f,n_f) constrained to pass through the intermediate node (m_d,n_d) is defined as:

$$(m_0, n_0) \underset{(m_d,n_d)}{\overset{opt}{\longrightarrow}} (m_f, n_f) \tag{6.4}$$

Bellman's principle [89] states that:

$$(m_0, n_0) \underset{(m_d,n_d)}{\overset{opt}{\longrightarrow}} (m_f, n_f) = (m_0, n_0) \overset{opt}{\longrightarrow} (m_d, n_d) \oplus (m_d, n_d) \overset{opt}{\longrightarrow} (m_f, n_f) \tag{6.5}$$

where $\oplus$ denotes the concatenation of paths. In other words the optimal path from the initial to final node is the concatenation of the optimal path from the initial node (m_0,n_0) through the intermediate node (m_d,n_d) and the optimal path from (m_d,n_d) to the final node (m_f,n_f). The conclusion which can be formed from this, is that if one finds the optimal path from the initial node to an intermediate one, one need only search for the optimal path from this intermediate node to the final node in order to find the overall optimal path from initial to final node via the intermediate node. If this procedure is carried out for every node in the matrix the optimal path is found across the entire matrix as required. Algorithms based on this principle are known as dynamic programming algorithms, and it is the basis of dynamically solving Equation (6.2)as illustrated in Figure 6.7c which yields the optimum match between the two test signals.

6.3.2 End Point Constraints

In the example illustrated in Figure 6.7 an optimal path was found which matched the entire sequence of the two signals S_1 and S_2 to each other by starting and location C(m,n) and working back to C(1,1). In the case of ECG matching, this is typically the case because it is known that in a given ECG beat sequence there should be a complete wave for both the query and reference signals. Therefore, it is appropriate to align the beginning and end of both the query and reference signal sequences. Although not appropriate in this application, an alternative to the complete path constraints can be created if the end point of the optimal path is not defined *a priori* and it is left to the optimisation algorithm to find it.

6.3.3 Local Constraints

A number of local constraints have been imposed on the process to ensure a logical matching of the two signals during the DTW process.

6.3.3.1 Continuity

If a given step in the path w_k = (a,b) then w_{k-1}= (a',b') where a-a'$\leq$1 and b-b'$\leq$1 i.e. each step through the path must be to an adjacent cell as shown in Figure 6.7 and in a progression towards C(1,1).

6.3.3.2 Monotonicity

Given w_k = (a,b) then w_{k-1} =(a',b') where a-a'$\geq$0 and b-b'$\geq$0 i.e. the points in the resulting path are monotonically spaced in time.

6.3.3.3 Other Local Constraints

There are a series of alternative constraints that are used in other applications of DTW. For example in the local constraints proposed by Itakura for speech signal processing [7, 84], two successive horizontal transitions during the optimal path establishment shown in Figure 6.7c would not be allowed. Moreover, if using the Itakura constraints, a single point in the query vector could be skipped during a transition. These constraints are inappropriate in the application of DTW to ECG signals since firstly segments, e.g. the PQ segment, between waves may require significant expansion in time (horizontal or vertical transitions in the C matrix) to accurately align the P and QRS waves should the query and reference have different heart rates and hence frame lengths. Also points from the query and reference signals should not be skipped in the application of DTW to delineate the ECG signal, since these points could in fact be onset and termination points the user is attempting to establish in the query. Other constraints have been proposed by Sakoe & Chiba [75].

6.3.4 Global constraints

Global constraints can be added to the process such as windowing, which effectively removes the corners of the cost matrix and slope weighting, which biases the warping path towards the diagonal of the matrix. Itakura [7] proposed a global constraint that ensures the maximum expansion or compression of the query signal is by a factor of two compared to its original length. One purpose of these global constraints is to essentially remove what are known as "singularities". A singularity occurs when one sample in one of the signals is warped to multiple samples in the other signal. An example of a singularity is shown in the warping of two ECG signals and their accumulated cost

matrix C and path 'W' in Figure 6.8 and the resulting warping of the two signals in Figure 6.9. Two corresponding singularities evident in the cost matrix and the time domain representation of the two signals are identified in each figure.

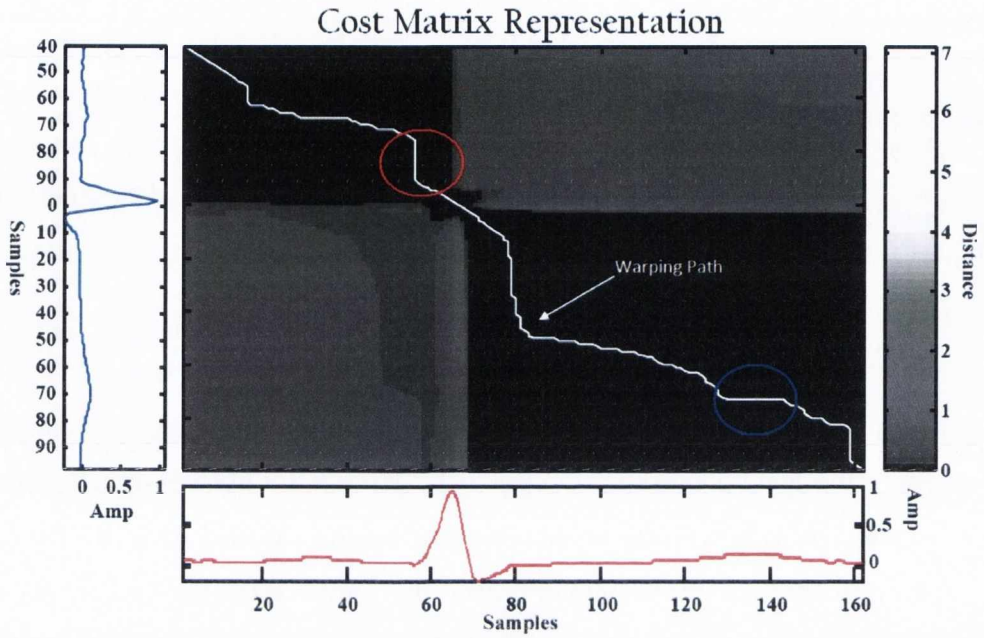

Figure 6.8: Finding the optimum path through the cost matrix for the alignment of the two signals with singularities shown

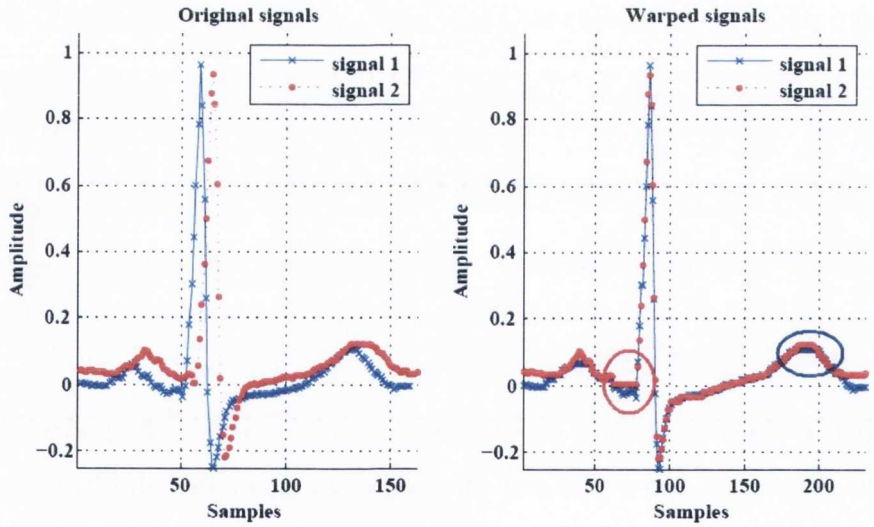

Figure 6.9: The original and resulting warped signals in the time domain with singularities shown

6.3.5 Limitations of Value Based DTW

Singularities in the warped signals are a concern since they result in an unintuitive alignment of the two signals. Note how the termination of the P wave in Signal 1 and

Signal 2 have not been aligned correctly. Introducing global constraints can reduce the occurrence of singularities by manipulating the warping path to create the warp with minimal padding. However, such manipulation means that the path solved for dynamically using an altered version of Equation (6.2) is now no longer the optimal path. The use of global constraints has been criticised for that reason [90] and the author does not feel they are suitable for this application.

A critical limitation of the value based DTW algorithm has been identified. In attempting to minimise the difference between the two signals in the amplitude domain the algorithm inserts padding or repeats a single value, to a point where the time features of the two signals are aligned in an inappropriate manner. The algorithm performs the optimal alignment of the two signals based on minimising the Euclidean distance between the signals but with no consideration of the position of each feature e.g. the P waves within the global signals. One method of reducing the occurrence of these singularities involves aligning some of the features of the two signals before warping. This involves removing the offset at the beginning of each signal and amplitude aligning their R peaks [90, 91]. With these two features aligned the DTW algorithm will tend to warp them to each other since they have the same amplitude values to begin with. Figures 6.10 and 6.11 show the result of warping the same two signals as before but having removed the initial offset of each signal and aligning the R peak of both signals before warping.

It is visibly clear from both Figures 6.10 and 6.11 that there has been a significant improvement in the accuracy of the warping than in Figures 6.8 and 6.9. The regions where singularities existed previously are highlighted and it can be seen that the singularities in both the P and T wave regions have been significantly reduced, although not eliminated altogether. One can see that the path 'W' is much closer to the ideal of a diagonal path from C(1,1) to C(m,n), which could only be achieved by warping a signal to itself. The pre-processing of the signal involves only the removal of the offsets of each signal and a linear scaling of each to align the R peak of each QRS complex. The signals were not distorted in any way but merely scaled and the DTW algorithm used to warp the signals is identical in both cases. Critically, no global constraints were used to interfere with the dynamic optimisation Equation (6.2). Although this pre-processing has increased the accuracy significantly in this example, its ability to do so in an ECG signal with more variable characteristics such as baseline wander may be limited and may require a more complex pre-processing technique. An alternative

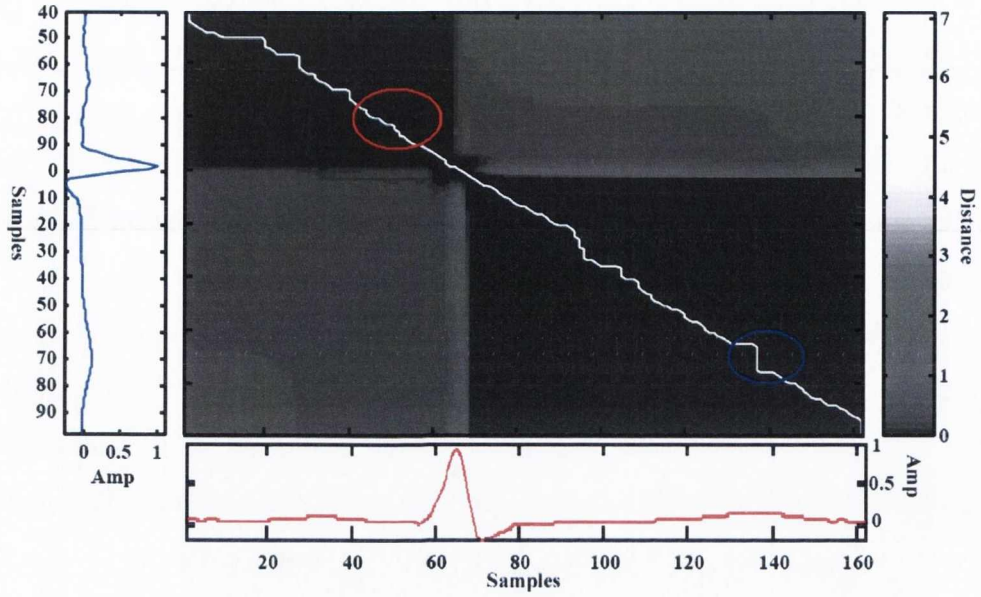

Figure 6.10: Finding the optimum path through the cost matrix for the alignment of the two signals after additional pre-processing

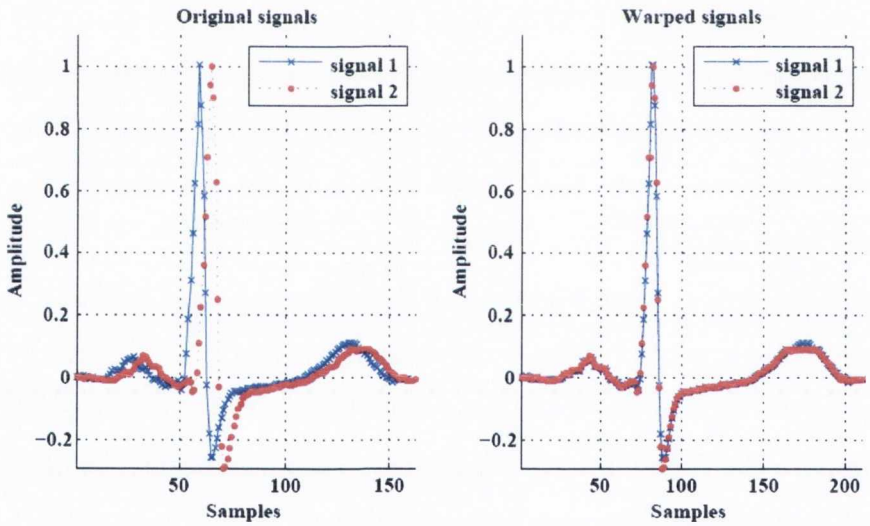

Figure 6.11: The original and resulting warped signals in the time domain after pre-processing

method of overcoming these limitations is DDTW.

6.4 Derivative Dynamic Time Warping

An alternative to value based DTW, derivative based DTW (DDTW) attempts to characterise regions or segments of the signals before attempting to warp them together. Derivative DTW uses the shape of the sequence of data rather than the absolute values

of each data point to find the difference between the two signals. The derivative of each data point to data point line within the signal will give an indication of the shape of the wave between the two data points. The derivative is estimated in many different ways, one example of which is by Equation (6.6) as proposed by Keogh and Pazzani [90]:

$$D_x[q] = \frac{(q_i - q_{i-1}) + [(q_{i+1} - q_{i-1})/2]}{2} \tag{6.6}$$

where D_x is the average of the slope of the line through the current point q_i and its left neighbour q_{i-1} and the slope of the line through its left neighbour, the point in question and its right neighbour q_{i+1}.

However, on a point by point basis the ECG signal will vary with noise or interference and the slope of a line on either side of a single point offers little insight into the actual shape in a wider region of the signal and can hence fail to characterise significant features in the signal [91]. To improve on this an approximation of the signal is usually performed. The result of this approximation is a series of splines approximating groups of points in the original signal, which are combined on a piecewise basis to recreate an approximated version of the original signal. By decomposing the ECG signals into splines or linear segments the slope of each segment of the original two signals can be used as a measure of difference between the shape of the two segments in each signal. So instead of a Euclidean distance measurement between two points as in Equation (6.1), the difference between each segment of the two approximated waves is measured as a difference of the slopes or derivatives of these segments. This method of characterising the shape is favoured by many users of DDTW [92–94] over the point-by-point derivative given in Equation (6.6). The assumption made in each of these articles is that each fiducial point in the signal will lie "near to" the end of one of the approximation splines. In principle, the concept of characterising the shape of the signal and using this to warp the signals, as opposed to the value point by point based DTW method is very appealing. However, the author is concerned with two issues regarding DDTW.

Firstly, the accuracy of the process is highly dependent on the approximation algorithm's ability to remove the unwanted and insignificant variations in the original signal whilst maintaining the shape of the original signal itself. The approximation splines need to be large enough to characterise the shape of a given region but the

longer the spline the larger the approximation error. Secondly, it is not necessarily safe to assume that a fiducial point will lie near to the end point of an approximation spline. An approximation or linearization technique will end an approximated segment where variations in the signal cause the difference between the approximation and the original signal to exceed a defined error threshold. The T wave shown in Figure 6.12 has been annotated by an expert cardiologist [73] and demonstrates how a fiducial point may not be near a significant variation in the signal and hence will not necessarily be located near to the beginning or end of a spline.

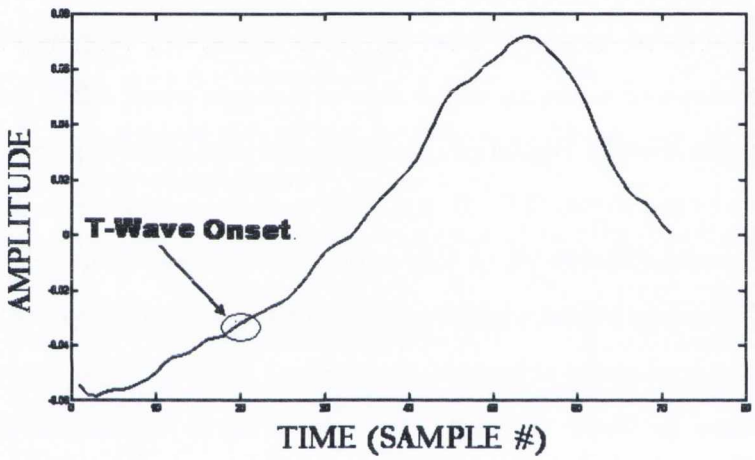

Figure 6.12: T wave onset annotation

The only way in which this T wave onset would be located close to the beginning or end of an approximation spline is if the error threshold is extremely small, resulting in a larger number of approximation splines and hence defeating the purpose of using derivative DTW in the first place. If the true T wave onset is not located near the end of a spline but is assumed to be as is the case in DDTW, then the reference signal has been distorted and the original T onset location and its associated annotation is no longer being used as a fiducial point.

With these concerns in mind the author decided to conduct a thorough investigation the effects of approximation on the ECG signal and in particular the fiducial points of the original reference signal.

6.5 Measuring the Effect of Approximating ECG Signals for DDTW

The material and results discussed in this section are based on two peer reviewed publications by the author [95, 96].

6.5.1 An Introduction to ECG Compression-Approximation

The use of ECG compression and/or approximation is as prevalent today as it was during the 1960s when research into ECG compression techniques began. ECG compression methods are classed into three distinct groups: direct data compression, transforms and parameter extraction. Direct data compression algorithms detect redundancies in the data by analysing the actual samples of the signal and discarding the redundant data. Numerous direct data compression techniques have been developed with increasing complexity including the AZTEC algorithm [97, 98] the SAPA algorithms [99, 100] and piece-wise approximation algorithms [101, 102]. There is also a range of transformation and parameter extraction methods having varying levels of complexity utilizing Fourier, Wavelet and Principal Component Analysis techniques [103–108]. In general, direct methods are considered superior to transforms in terms of system simplicity and approximation error [105], although transform methods typically provide a higher compression ratio and are not as sensitive to original sampling frequency [109].

The objective of this investigation is to analyse the effects of data compression algorithms on the morphology of the original ECG signals and to determine if approximation of these signals for DDTW is advisable. Many comparative studies of approximation methods and algorithms use a percentage root-mean-square difference (PRD) between the original input signal and the reconstructed approximate version as a test of accuracy [100]. However, the PRD provides very limited insight into the ability of a compression algorithm to preserve diagnostically significant information contained within the recording [109, 110]. Indeed the final decision on the clinical acceptability of the approximation often depends on the reconstructed signals being visually inspected by a cardiologist [111].

The author proposes that the accuracy of a reconstructed approximation in terms of preservation of the original signal morphology and the location of its fiducial points (P wave onset and termination etc) can be better measured using a two pronged method.

First of all the original and approximated signals are divided into ECG components and inter-beat isoelectric segments with partial PRDs calculated over the two groups separately. In theory, one would wish to maximize the PRD of inter-beat segments and minimise it over the actual ECG component durations and this test gives an insight into where the resulting compression is obtained. It was demonstrated in Section 6.3 that when two signals which are similar to each other i.e. have the same offset voltage, R-peak amplitude etc., value based DTW can warp the two signals very accurately. Using DTW, an insight into the effects of approximation, particularly on the fiducial points of the original ECG signal can be gained. Note that in the case of comparing a signal with its approximated version the concerns of applying value-based DTW to the ECG signal which have been highlighted in Section 6.3.5 such as baseline wander, constituent component offsets etc. are not a concern. In this scenario the two signals under test are very similar and will have essentially the same offsets, amplitude levels etc. As such value-based DTW, as presented thus far, is an appropriate algorithm for measuring ECG compression accuracy.

6.5.2 Direct Data Compression-Approximation of ECG Signals

For the purposes of this investigation, the accuracy of six direct data compression methods are compared, although dynamic time warping could also be applied to any reconstructed approximation from the range of transform compression methods. Three of the approximation algorithms examined are novel in that they combine existing fixed error threshold algorithms with variable error threshold calculation techniques. The results demonstrate that DTW can be used to identify accuracy differences not only between completely different algorithms but also subtle variations of the same algorithm e.g. with fixed and variable error thresholds. Indeed, when selecting an approximation technique, the user must find a balance between compression ratio and accuracy, a process that simple PRD calculation makes extremely difficult. Approximations yielding the same total PRD value from each algorithm will be tested and the results compared using partial PRDs and DTW to demonstrate the limitations of the PRD and the benefits of the new DTW approach.

The algorithms chosen for analysis include the piecewise linear approximation algorithm (PLA) as proposed by Koski et al. [101] which has been applied pre-DTW

in [92, 94] and other piecewise based modelling more recently in [102]. Secondly the scan along polygonal algorithm as outlined by Ishijima et al. [99] which continues to be used in modern ECG compression research [100] shall be examined. Three novel techniques based on a combination of the scan along polygonal algorithm and Furhts Amplitude Zone Time Epoc Coding [97] algorithm with variable threshold shall also be assessed.

6.5.2.1 The Piecewise Linear Approximation Algorithm (PLA)

The PLA algorithm presents a method of dividing the ECG into segments without the necessity of defining a large number of parameters to control the segmentation process [92, 101]. Segmentation methods such as this are used in pulse wave recognition, signal compression and pre-processing for pattern recognition applications as the fundamental principle is the same in each case [101].

The algorithm starts with the first sample *S(n)* in the signal to be approximated and windows to a higher sample number in the signal *S(n+L)* where L is the window length in terms of samples. It connects the two points with a line to form the new approximated segment of the signal and then calculates the error ε as the Euclidean distance between the approximated line and each sample of the original signal sequence. If an original data point is inside the normals at either end of the approximation segment a modified Euclidean distance formula is used to calculate the distance from the spline. If however the original data point under test is outside the normals at the endpoints of the line the standard Euclidean distance formula is used. If the error exceeds a predefined threshold (V_{th}) at any particular sample the segment is terminated at the intermediate point with the largest error distance and the process is repeated. If not, as in Figure 6.13, the algorithm would then extend the endpoint to *S(n+2L)* and the process is then repeated until all point to approximation distances are less than V_{th}. The window length L is fixed at a predefined number of samples but the resulting overall spline length is reduced dynamically to ensure the error criteria is satisfied.

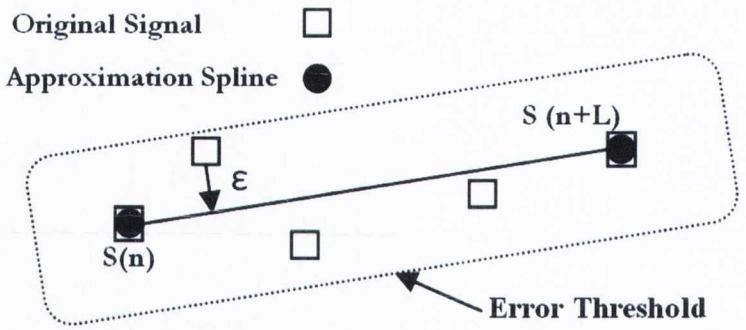

Figure 6.13: The PLA Algorithm

The overall result is that the approximated signal shall always be maintained within a predefined error threshold of the original signal. The sample number of the beginning, end and length of the segment can be recorded and used to reconstruct the approximation of the signal.

6.5.2.2 Scan Along Polygonal Approximation (SAPA)

The SAPA technique is based on calculating the slope from one data point (the current vertex) to another the current end point of the spline ± the threshold error [99]. Initially the slopes from the vertex S(n) to the next point S(n+1)$\pm V_{th}$ are recorded as M1 and M2. As the end point of the spline is extended from one point to the next, the smallest slope value from the vertex to an endpoint plus V_{th} is saved as M1 and the largest slope value from the vertex to an endpoint minus V_{th} is saved as M2. Note that as the slopes from the vertex to the candidate endpoint ± the error threshold are calculated, they are only recorded if the slope from vertex to current candidate endpoint plus threshold is smaller than a previously saved value of M1 or if the slope from vertex to current endpoint minus the threshold is larger than the previous value of M2. At all times the following slope criteria must hold:

$$M1 \geq M2 \tag{6.7}$$

If for any candidate end point of the spline the criteria defined in Equation (6.7) does not hold, as in Figure 6.14, the spline is terminated at the previous endpoint, S(n+1) in Figure 6.14 which will then act as the vertex of the next spline. The process is repeated on a sample by sample basis for the entire recording with the vertices and length of each spline recorded for reconstruction of the approximated signal.

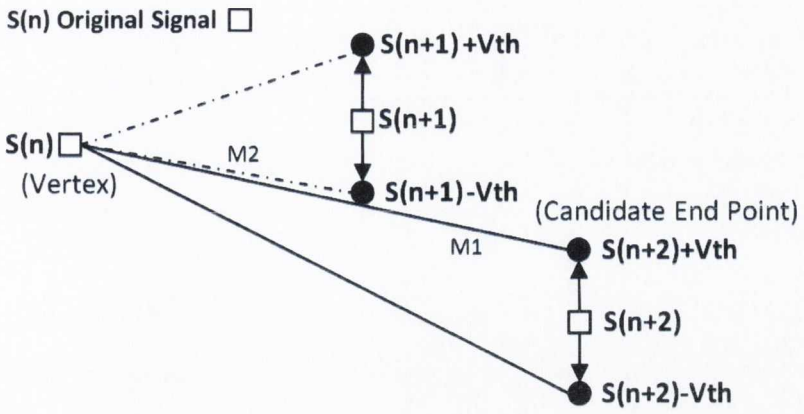

Figure 6.14: The SAPA Algorithm

6.5.2.3 Scan Along Polygonal Approximation with Centre Line Criterion (SAPA-2)

An extension of the first scan along polygonal compression method SAPA, the SAPA-2 algorithm is an ECG compression technique also presented by Ishijima et al. [99]. It is based on calculating a number of slopes from a selected vertex (start point of a segment S(n) in Figure 6.15.) to a candidate end point of the segment. The algorithm initially selects the next data point S(n+1) as the candidate endpoint and calculates a slope to points at a predefined threshold above and below the sample value. It then calculates a slope from the selected vertex to the candidate end point forming a centre line. The next point in the data, S(n+2) in Figure 6.15, is now selected as the new candidate end point and the slopes are again calculated. The smallest slope value from the vertex to the endpoint plus V_{th} is again saved as M1 and the largest slope value from the vertex to the endpoint minus V_{th} is saved as M2 as shown in Figure 6.15. As the endpoint is incremented and the segment length increases the following criteria must always apply:

$$MC \leq M1 \; and \; MC \geq M2 \tag{6.8}$$

If they do not, the segment is terminated at the previous sample, S(n+1) in Figure 6.15, forming the end of the current segment and the vertex for the next.

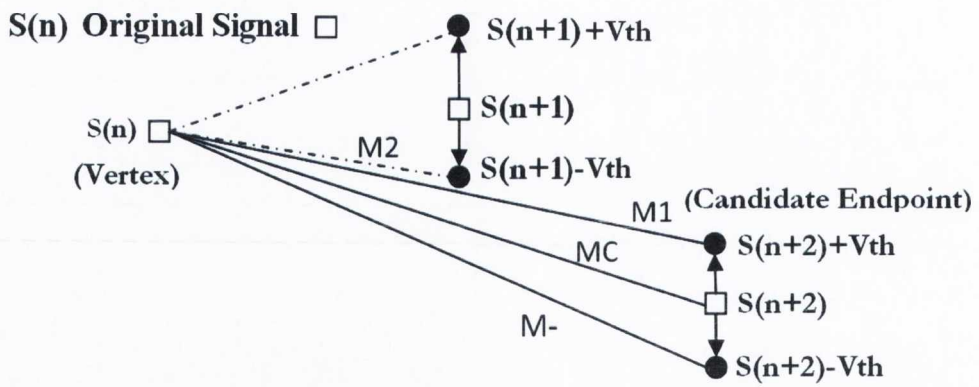

Figure 6.15: The SAPA-2 Algorithm

6.5.2.4 Variable Error Threshold Approximation - The Amplitude Zone Time Epoc Algorithm (AZTEC)

The AZTEC algorithm [97, 98] is intended for real time ECG data compression and typically offers a less accurate representation of the ECG signal than the other algorithms discussed above. It effectively uses a sample-and-hold process to linearise the ECG by holding a sample value until the approximation error exceeds the acceptable threshold error voltage. It generates a high-compression-ratio, low-accuracy, approximated signal as demonstrated in Figure 6.16.

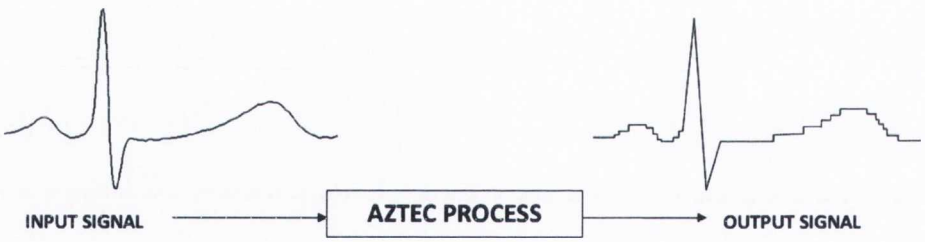

Figure 6.16: The AZTEC Algorithm

Since the AZTEC algorithm typically provides a low accuracy approximation, it shall not be included in the analysis here. AZTEC does however provide a variable error threshold not found in the other processing techniques discussed thus far which shall be applied to more accurate methods. For approximation one would like to use a low error threshold for the ECG components themselves but a larger error threshold for the inter-beat segments in order to remove high frequency random spikes and noise which possess no clinically significant information, which is precisely what the AZTEC algorithm attempts to achieve. The AZTEC algorithm uses a statistical measurement known as the third moment along with the signal mean and standard deviation to vary

the acceptable error threshold whilst the input signal is being processed. The error threshold is calculated recursively for a signal X with n samples as follows:

$$Mean\ \ Value : \bar{X}_k = \frac{(k-1)\bar{X}_{k-1} + X_k}{k} \tag{6.9}$$

$$Standard\ \ Deviation : \sigma_k = \sqrt{\frac{(k-1)\sigma^2{}_{k-1} + (X_k - \bar{X}_k)^2}{k}} \tag{6.10}$$

$$Third\ Moment: M_k = \left[\frac{(k-1)M^3{}_{k-1} + (X_k - \bar{X}_k)^3}{k}\right]^{1/3} \tag{6.11}$$

$$CF_k = C_1(\sigma_k + M_k) \tag{6.12}$$

$$V_{thk} = V_{thk-1} - C_2(CF_k - CF_{k-1})V_{thk-1} \tag{6.13}$$

where $1 \leq k \leq n$, CF_k is the criterion function, C_1 and C_2 are pre-defined constants which can be selected to alter the variation of the error threshold as desired and V_{thk} is the resulting error threshold.

Although the AZTEC algorithm itself is intended for real-time, relatively low-accuracy applications its method of calculating a variable error threshold could be applied to more accurate algorithms that analyze the input signal on a sample by sample basis such as the SAPA algorithms.

6.5.2.5 Variable Threshold SAPA Algorithms (VTH-SAPA)

If the variable threshold calculation originating from the AZTEC algorithm is incorporated into the SAPA and SAPA-2 compression techniques it may increase the usefulness of the SAPA algorithms by taking advantage of a variable error threshold combining it with the better accuracy of the SAPA methods of compression. These new variations of the SAPA algorithms shall be known as VTH-SAPA and VTH-SAPA-2. Figure 6.17 demonstrates how the threshold dynamically varies with the variation of the ECG input signal.

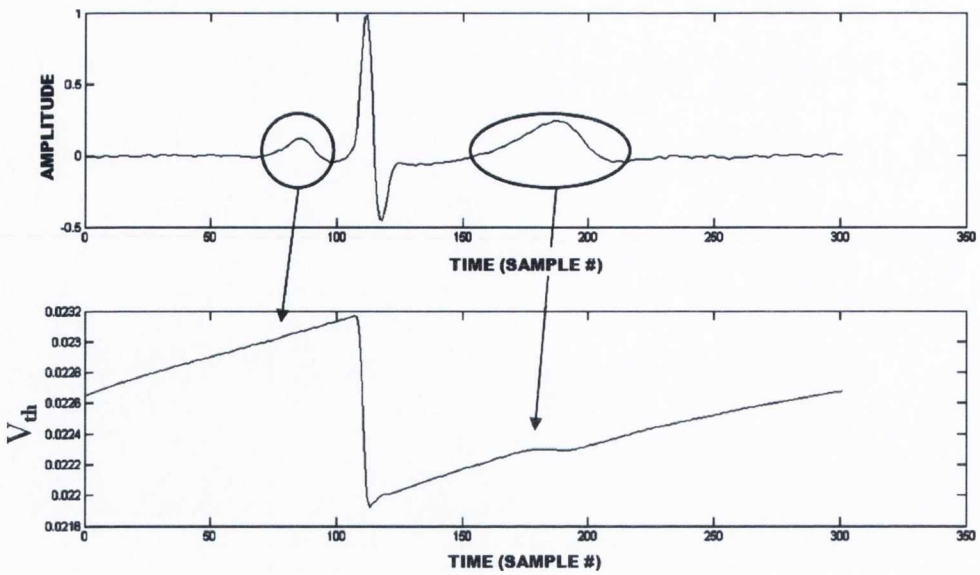

Figure 6.17: Variable voltage error threshold ($C_1 = 1$ and $C_2 = 4$)

The constants C_1 and C_2 control the effect that CF_K has on the error threshold V_{th} but not the variation of CF_K itself i.e. its sensitivity to spikes in the signal. Although some variation of the voltage error threshold is visible in Figure 6.17 the author believes a more significant variation of the threshold due to the P and T wave is desirable since the goal is for the error threshold to be sensitive to significant variations in the signal i.e. the P, QRS and T waves. To achieve this, a new constant C_3 is introduced to the third moment Equation (6.11) to accentuate the effect that the difference between the current sample X_K and the cumulative mean has on the third moment. Now a modified third moment is calculated as:

$$\textit{Modified Third Moment: } Mod_k = \left[\frac{(k-1)(M_{k-1} \times C_3)^3 + (X_k - \bar{X}_k)^3}{k} \right]^{1/3} \tag{6.14}$$

and the criterion function uses the modified third moment:

$$CF_k = C_1(\sigma_k + Mod_k) \tag{6.15}$$

With C_3=0.02 the increased sensitivity of the variable threshold to the presence of the P, QRS and T waves is demonstrated in Figure 6.18.

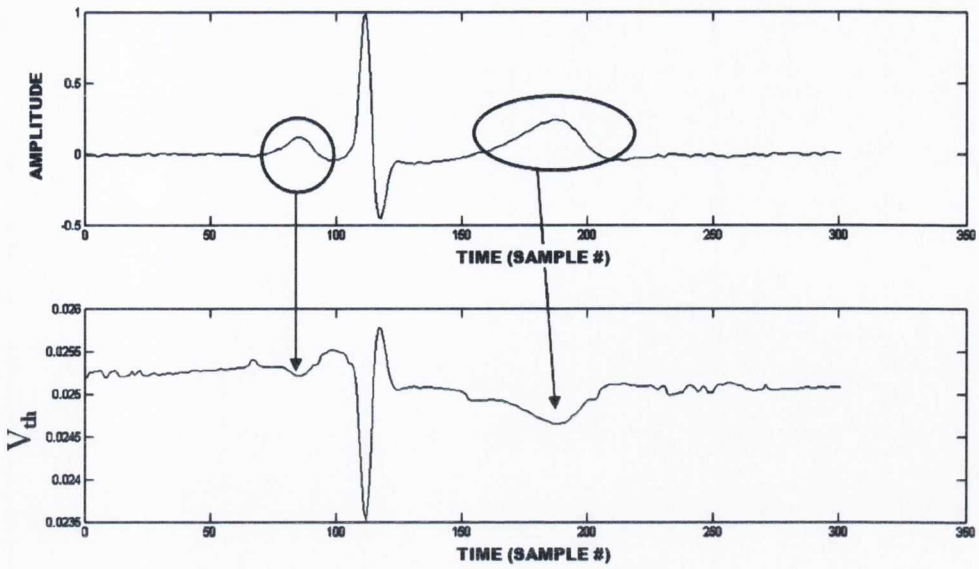

Figure 6.18: The modified variable error threshold

This final modified variable threshold calculation shall be applied to the SAPA-2 algorithm, and shall be known as the MOD-VTH-SAPA-2 algorithm.

There are an enormous number of algorithms available to approximate the ECG signal and indeed more accurate methods may be available than the six chosen here. However, the variety of the algorithms and the fact that the AZTEC, PLA and SAPA algorithms are still being used in recent research into ECG signal approximation makes them convenient and adequate choices for this investigation [98, 100, 105, 112]. Having selected six algorithms to test the effects of approximation on the resulting ECG signal a measure of accuracy must now be discussed.

6.5.3 Measuring The Accuracy of ECG Compression

In some of the DDTW articles the effects of approximation with regard to the location of the fiducial points are simply stated as minimal [93] or as "the error introduced" by the approximation algorithm for each fiducial point [92]. It is not made clear how this error was measured nor how the acceptable error threshold (V_{th}) for the approximation algorithm were set accurately. The amount of approximation i.e. a compression ratio is not stated. The error due to approximation is stated for each fiducial point, and although it is not clear how this error has been measured, it is implied that this error is the difference between the annotated fiducial point and the end of the nearest spline to that point, since the assumption is that they are close to each other. Figure 6.19 shows the P wave and QRS onset of a highly approximated ECG beat from the test

database discussed.

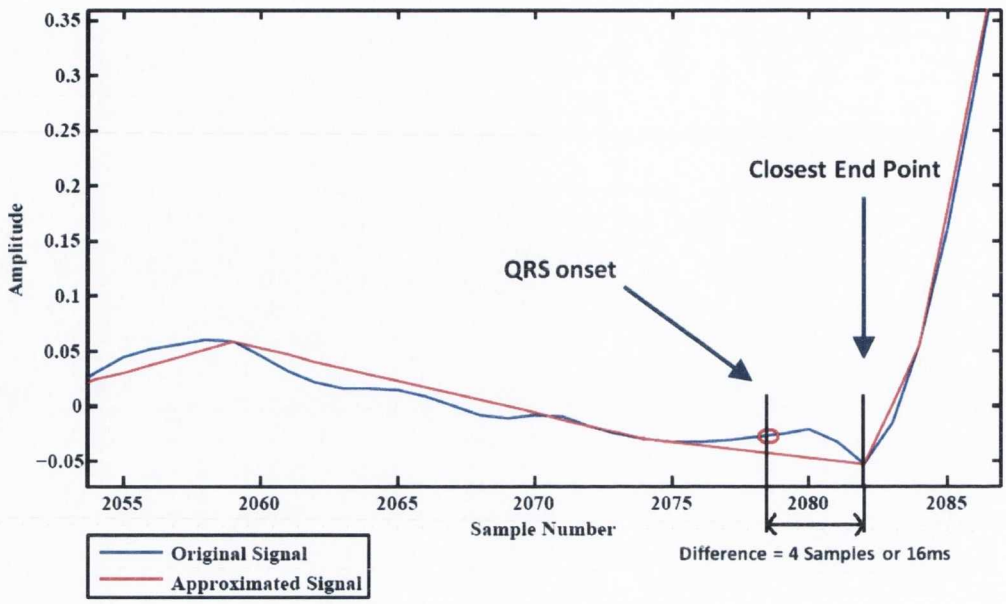

Figure 6.19: P and QRS Complex of a signal and its approximation

The signal has been approximated using the SAPA algorithm and a large error threshold to show the limitations of assuming the error of approximation is the difference between the actual location of a fiducial point and the nearest spline end point. The difference between the QRS onset and the nearest spline endpoint in Figure 6.19 is just 4 samples or, at the recording sampling frequency, 16 ms. However, one can clearly see that the slope of the spline in this region is not at all representative of the shape of the QRS complex onset to the extent that the Q wave has been removed, and any subsequent matching of this approximated slope to a reference signal with a similar slope in this region, would be inaccurate. ECG compression algorithms are hence not typically tested for accuracy in such ways.

6.5.4 Percentage RMS Difference Calculation

The error introduced by compression of ECG data is frequently measured using the percentage root-mean-square difference (PRD) [113] . Even though it is acknowledged by many authors as not guaranteeing the preservation of clinical information [96, 109, 111], it is still used as a measure of accuracy in most of the compression articles referenced here.

$$PRD = \sqrt{\frac{\sum_{i=1}^{n} [X(i) - A(i)]^2}{\sum_{i=1}^{n} X(i)^2}} \times 100\% \tag{6.16}$$

Where X(i) and A(i) are corresponding samples of the original and approximated signals respectively.

6.5.5 Partial Percentage RMS Difference Calculation

In simplistic terms a compression algorithm should remove as much inter-beat noise as possible since it provides no clinically significant information whilst preserving the actual waves of the ECG as accurately as possible. A method of measuring this would be to calculate PRD values across the wave components of the ECG and then the inter-beat durations separately using annotations to divide the signals appropriately. The algorithm which minimises the PRD for the ECG components (P-onset to T-termination), whilst providing a higher PRD for inter-beat durations (T-termination to next P-onset) can therefore be regarded as the most accurate. Note that in the absence of a set of annotations the user can segment the signal by visual inspection. Although this does not guarantee that the beat and inter-beat durations are exactly as described it should still offer a good approximation for the segmentation of the signal under analysis.

The application of partial PRD calculation shall be demonstrated using two test signals chosen from the PhysioNet QT Database of fully annotated ECG recordings discussed in Section 6.2. The two signals were originally contained in the Normal Sinus Rhythm Database as detailed by [80]. It is intended to demonstrate how two approximations can yield the same total PRD value but significantly different partial PRD results. Approximations using the PLA and each variation of the SAPA-2 algorithms are generated for several signals that yield the same total PRD value. Each original signal and its corresponding approximation are then segregated into accumulated ECG beat and inter-beat durations. The waveforms shown in Figure 6.20 are created by connecting the signals at annotated points.

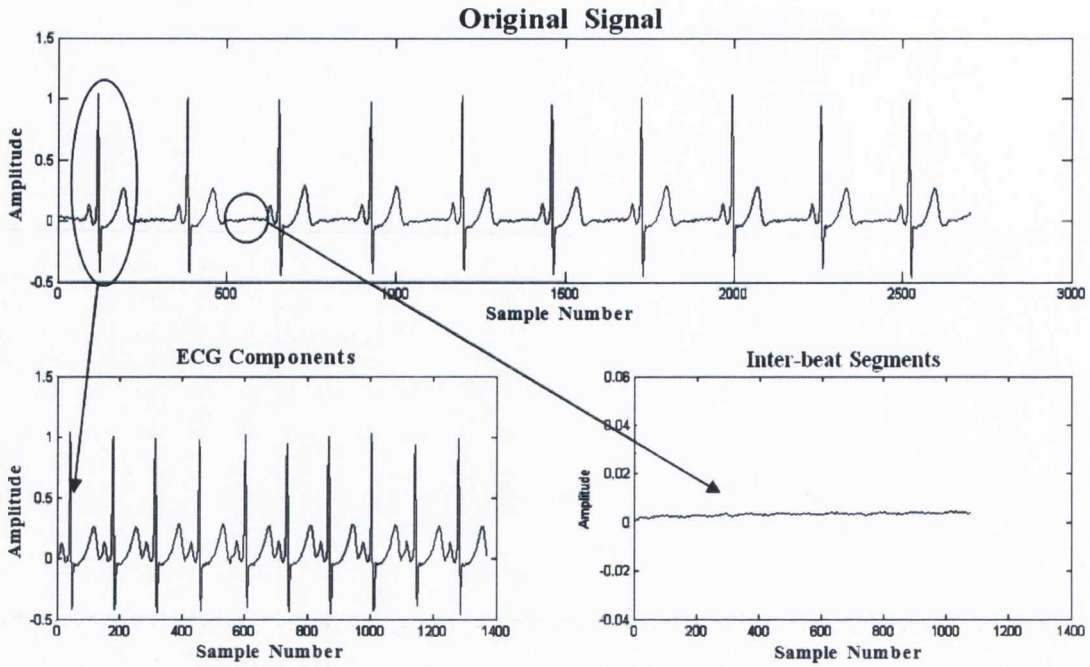

Figure 6.20: Segmented signal for partial PRD calculation

Partial PRD's are calculated between each beat component of the original and approximated signals and each inter-beat segment of the original and approximated signals separately. The data shown in Tables 6.2 and 6.3 demonstrate how approximations which yield the same total PRD value can in fact provide significantly different partial PRD results.

As can be seen from Tables 6.2 and 6.3, despite each algorithm producing the same total PRD, they actually preserve the ECG beats and compress outlying inter-beat noise to quite different extents. The partial PRD can be used to observe not only how different approximation methods i.e. the PLA and SAPA algorithms preserve the signal but also to make observations with regard to variations of the same approximation technique (SAPA-2 in this case).

Observe from Table 6.2 that for low total PRD values of 0.5 to 1.0% the SAPA-2 algorithm results in a lower component PRD and a higher inter-beat PRD value than the PLA algorithm as required. However as the total PRD increases beyond 1% the PLA algorithm results in lower component PRD values than any of the SAPA-2 algorithms. The conclusion can be drawn that for the #16272 signal the algorithm chosen for approximation depends on the overall amount of compression required.

Partial PRDs can also identify the subtle performance changes introduced by adding the variable error threshold and its modified version to the SAPA-2 algorithm. From

Table 6.2: Partial PRDs for Test Signal # 16272

Total PRD %	PLA Beat PRD %	PLA Inter-Beat PRD %	SAPA2 Beat PRD %	SAPA2 Inter-beat PRD %	VTH-SAPA2 beat PRD %	VTH-SAPA2 Inter-beat PRD %	MOD-VTH-SAPA2 Beat PRD%	MOD-VTH-SAPA2 Inter-beat PRD%
0.5	0.3	4.6	0.14	5.1	0.18	5.6	0.16	5.7
1	0.7	10.5	0.47	13.6	0.47	13.5	0.49	13.1
5	3.5	55	4.28	40	4.19	40.4	4.21	40.1
7	4.39	83.4	6.3	45	6.42	45.7	6.22	44.3
10	6.25	98	9.3	58	9.23	58.6	9.38	53.8

Table 6.3: Partial PRDs for Test Signal # 16539

Total PRD %	PLA Beat PRD %	PLA Inter-Beat PRD %	SAPA2 Beat PRD %	SAPA2 Inter-beat PRD %	VTH-SAPA2 beat PRD %	VTH-SAPA2 Inter-beat PRD %	MOD-VTH-SAPA2 Beat PRD%	MOD-VTH-SAPA2 Inter-beat PRD%
0.5	0.4	5.56	0.28	8.19	0.28	7.65	0.28	7.68
1	0.85	11.2	0.74	12.5	0.76	12.7	0.69	12.7
5	3.91	49.8	4.57	40.6	4.81	41.4	4.55	45.3
7	5.32	73.8	6.44	50.2	6.33	49.9	6.18	53.6
10	8.32	87.3	9.1	67.8	9.06	71.1	9.09	65.9

Table 6.3 for example, it can be seen that the VTH-SAPA-2 algorithm provides similar component PRD values and some higher inter-beat PRD values than its original SAPA-2 and the MOD-VTH-SAPA-2 forms for most of the total PRD percentages.

Using only the total PRD calculation each of the approximations detailed in Tables 6.2 and 6.3 would have been regarded as providing the same level of accuracy. It is thus shown how using partial PRDs further insight into approximation can be gained. The issue remains, however, that a low partial or total PRD value means that both of the signals had similar amplitude profiles overall but that does not ensure that the area around the fiducial points has not been distorted by the approximation.

6.5.6 DTW to Establish the Effects of Approximation

In annotating an ECG signal, a cardiologist will annotate the onset and termination of each component based on the shape and profile of the signal as observed simultaneously in one or many of the ECG recording leads. In order to achieve a genuine measure of what effect each algorithm has on the fiducial points and the ECG morphology around the fiducial points; dynamic time warping can be applied. The dynamic time warping

algorithm shall seek to match the two test signals and their approximations using the PLA, SAPA, SAPA-2 algorithms and variable error threshold algorithms VTH-SAPA, VTH-SAPA2 and MOD-VTH-SAPA2. After the two signals have been warped, the location of the fiducial points from the original signal should ideally match with the corresponding sample number in the approximated signal, provided no significant altering of the signal morphology has occurred. The warping algorithm by its very nature will match the fiducial point in the approximation and the points surrounding it optimally to a similar section within the original signal.

If the warping algorithm matches the approximated fiducial point to a different point in the original signal then the morphology has been altered by the approximation such that the locations of the fiducial points originally identified by the cardiologist have now been changed in the approximated signal.

All ten of the Normal Sinus Rhythm signals available in the QT database were used to test the dynamic time warping algorithm. Five approximations yielding the same total PRD value for each algorithm and test signal were created and warped to the original signal. The mean error between the location of the original fiducial point and the optimum match in the approximated signal was calculated and along with the standard deviations of cardiologist annotation are shown in Table 6.4. Also provided in Table 6.4(g) is an estimate of the average compression ratio provided by each algorithm for each total PRD value. These compression ratios are calculated as the original number of sample points divided by the number of sample points retained for reconstruction after approximation.

6.5.6.1 Distortion of Clinically Significant Fiducial Points

The results in Figure 6.4 demonstrate that the algorithms have different mean error figures with regard to each fiducial point despite all approximation methods yielding the same total PRD calculation. To quantify the possible consequences of this section (f) in Table 6.4 is a measure of the clinical standard deviation in the annotation of the same ECG recording by different cardiologists as reported by Jane et al. [114].

Using the PRD versus compression ratio decision method all algorithms would have been classed as having maintained the same level of accuracy for a total PRD of 3.5% with the PLA providing a higher average CR of 8.4, more than any of the other algorithms [see section (g)]. The PLA algorithm would hence be chosen as the

Table 6.4: Mean ± standard deviation errors due to approximation

	(a) P-Onset						(b) P-Termination					
Total PRD %	PLA (ms)	SAPA (ms)	VTH-SAPA (ms)	SAPA-2 (ms)	VTH-SAPA-2 (ms)	MOD-VTH-SAPA-2 (ms)	PLA (ms)	SAPA (ms)	VTH-SAPA (ms)	SAPA-2 (ms)	VTH-SAPA-2 (ms)	MOD-VTH SAPA-2 (ms)
0.01	-0.1±0.6	-0.1±0.6	0.0±0.0	0.0±0.0	0.0±0.0	0.0±0.0	0.0±0.0	0.0±0.0	0.0±0.0	0.0±0.0	0.0±0.0	0.0±0.0
0.5	0.2±3.8	-0.2±3.2	0.3±3.7	0.7±4.2	0.9±5.3	0.8±4.3	0.0±0.9	0.0±1.1	-0.1±1.2	-0.1±0.9	0.0±0.4	-0.2±1.0
1.5	1.2±16.3	1.1±16.3	1.4±16.8	2.1±9.7	3.0±11.4	1.9±9.6	-0.3±3.5	-0.8±2.4	-1.0±2.6	-0.7±2.9	-0.7±3.0	-0.8±3.0
2.5	3.6±17.4	11.8±22.9	11.0±24.8	3.0±14.9	2.9±14.9	1.1±14.2	-2.2±7.7	-3.1±5.8	-3.2±6.0	-1.2±4.0	-1.2±4.5	-1.4±4.6
3.5	2.2±18.0	19.6±23.7	17.0±25.1	4.8±15.3	8.6±15.8	7.0±14.5	-4.0±13.8	-4.8±7.8	-5.3±10.4	-1.8±5.4	-1.6±5.3	-1.6±6.4

	(c) QRS-Onset						(d) QRS-Termination					
Total PRD %	PLA (ms)	SAPA (ms)	VTH-SAPA (ms)	SAPA-2 (ms)	VTH-SAPA-2 (ms)	MOD-VTH-SAPA-2 (ms)	PLA (ms)	SAPA (ms)	VTH-SAPA (ms)	SAPA-2 (ms)	VTH-SAPA-2 (ms)	MOD-VTH-SAPA-2 (ms)
0.01	0.0±0.0	0.0±0.0	0.0±0.0	0.0±0.0	0.0±0.0	0.0±0.0	0.0±0.0	0.0±0.0	0.0±0.0	0.0±0.0	0.0±0.0	0.0±0.0
0.5	0.3±2.6	0.0±2.5	-0.2±2.8	0.0±0.4	0.0±0.4	0.0±0.4	0.0±0.0	0.0±0.4	0.0±0.4	0.0±0.0	0.0±0.0	0.0±0.4
1.5	1.0±6.9	0.3±8.4	0.4±8.9	0.6±2.2	0.8±2.5	0.7±2.3	0.1±0.8	0.0±0.7	0.0±0.9	0.0±0.6	0.1±0.8	0.0±0.6
2.5	1.8±13.4	2.0±12.3	0.0±9.9	1.3±4.1	1.6±4.2	1.2±3.6	-0.5±3.7	-0.1±0.9	-0.1±0.6	-0.2±1.3	-0.2±1.3	-0.1±1.2
3.5	2.7±16.3	-1.1±10.3	-0.6±10.8	1.3±5.4	2.4±7.2	2.0±5.8	-0.7±4.0	-0.2±1.9	-0.5±2.1	-0.4±1.8	-0.4±1.7	-0.6±1.7

	(e) T-Termination					
Total PRD %	PLA (ms)	SAPA (ms)	VTH-SAPA (ms)	SAPA-2 (ms)	VTH-SAPA-2 (ms)	MOD-VTH-SAPA-2 (ms)
0.01	0.0±0.4	0.0±0.4	0.0±0.4	0.0±0.0	0.0±0.0	0.0±0.0
0.5	0.0±1.1	0.0±0.9	0.1±1.0	-0.1±1.1	-0.2±1.4	0.0±1.0
1.5	-1.0±4.9	-1.7±4.1	-1.5±4.6	-1.0±2.6	-1.0±2.6	-1.1±2.8
2.5	-2.0±6.5	-4.4±7.0	-3.8±6.0	-3.2±4.8	-3.0±4.5	-2.6±3.9
3.5	-1.7±6.9	-4.3±7.4	-4.2±7.5	-5.0±7.5	-5.4±8.4	-5.4±7.8

(f) Standard Deviation in Cardiologist Annotations	
P-onset (ms)	±10.2
P-termination (ms)	±12.7
QRS-onset (ms)	±6.5
QRS-termination(ms)	±11.6
T-termination (ms)	±30.6

	(g) Mean Compression Ratio (C.R.)					
PRD %	PLA (ms)	SAPA (ms)	VTH-SAPA (ms)	SAPA-2 (ms)	VTH-SAPA-2 (ms)	MOD-VTH-SAPA-2 (ms)
0.01	1.2	1.2	1.1	1.0	1.0	1.0
0.5	2.5	2.2	2.0	1.2	1.2	1.2
1.5	4.9	4.3	4.1	1.8	1.8	1.8
2.5	7.3	6.2	5.8	2.5	2.5	2.4
3.5	8.4	7.1	7.3	3.2	3.0	3.2

optimum algorithm as it yields a higher CR and the same PRD accuracy.

However, it can be observed that for a total PRD of 3.5% the SAPA-2 algorithm preserves the QRS-onset with a mean and standard deviation error of 1.3±5.4 ms from its original location while the PLA preserves it to within 2.7±16.3 ms. The acceptable standard deviation around the resulting mean location of a fiducial point as assigned by expert annotators in the location of a QRS-onset point in an ECG recording is ±6.5 ms. The SAPA-2 algorithm preserves the location of the QRS-onset to a lower mean error than the PLA and also has a lower standard deviation than the cardiologists while the PLA algorithm does not. Due to its higher compression ratio the PLA algorithm has in fact altered the location of the fiducial point beyond the range that applies to its annotation by different cardiologists, altering the clinically significant information. The PRD measure fails to detect this. It is also now possible to quantify the distortion introduced to the location of the fiducial points in a meaningful fashion. With a CR of 3.2 for the SAPA-2 algorithm, which equates to an average spline length of just three samples the distortion introduced into the signal is becoming significant when placed in the context of measured deviations in expert annotations. Conclusions regarding the effects of approximation for DDTW on the fiducial points can now be made.

6.5.7 Conclusions Regarding the DDTW Algorithm

The principle of approximating or compressing a signal involves reducing the number of data points either to decrease transmission loads or in the case of DDTW to create shape features of the signal under test. However, any approximation results in an inherent introduction of distortion within the signal. Having conducted a review of all DDTW methods which approximate signals, concerns have been raised regarding the effects of approximation. As such, a study of several ECG signal compression algorithms has been conducted to attempt to establish the possible adverse effects of approximating an ECG signal for use in the DDTW algorithm.

In order to quantify the loss of accuracy resulting from approximation, accuracy metrics were reviewed. PRD calculation vs CR has been criticised as a metric for comparing compression algorithms although it is the most commonly used. Using the author's suggested partial PRD calculation it has become clear that two methods of approximation which yield the same total PRD value do not preserve the signal morphologies with the same level of accuracy. As such a more complex method of measuring distortion was required. The advantages of using DTW as proposed by the author are clear when one observes the insight gained into the accuracy of each approximation algorithm in Table 6.4.

From this study the author has decided that an approximation which would yield large enough spline lengths to capture the shape of a given region in an ECG signal would introduce distortion levels that exceed the variation between experts in the annotation of the fiducial points i.e. beyond clinically acceptable variation levels shown in section (f) Table 6.4. Admittedly, more accurate approximation algorithms may be available than those used here, but a much better algorithm would be required in order to reduce the distortion significantly whilst maintaining spline length. Even with increased accuracy the fact remains that approximation adds uncertainty as to the location of the fiducial points. The value based DTW algorithm, as with any pattern recognition method, contains its own measure of error as discussed. However, when warping the original and approximated signals to each other this is limited by the fact that the approximated signal is a relatively accurate representation of the original signal so that they will have similar offsets, peak amplitudes etc and hence the measured distortion of fiducial points when the original and approximated signals are aligned is as a result of approximation. The correlation between increased CR, total

PRD level and resulting fiducial error imply that the error is indicative of increased approximation i.e. CR and not a systematic error of DTW.

The author believes DDTW is more suited to cases where shape matching of ECG signals i.e. for comparing shape variations of subjects with known arrhythmia to other subjects for diagnosis as opposed to the location of fiducial points. In this case the more accurate characterisation of the overall shape features of each wave and segment of the ECG signal at a cost of fiducial point position is more acceptable than in the author's application. More modern applications of DDTW for shape matching reflect this [115].

6.6 Feature Based Dynamic Time Warping

In other fields of digital signal processing such as speech analysis and synthesis features of the recording under test are extracted to gain more useful knowledge of the signal. These features typically involve transformation into another domain, such as the frequency domain and measures of power content in spectral bands are then used to find the occurrence of different sounds etc within the speech signal. Frequency domain analysis is not usually applied to ECG signals since all constituent features of the components lie within the same narrow band of 0.5-150 Hz approximately. The features of interest to the cardiologist or engineer working with the ECG signal are present and clear in the time domain (fiducial points, segments offsets etc), and for this reason the ECG signal is presented in the time domain for inspection. In essence value based DTW and DDTW are also a type of feature based DTW algorithm in that they warp the amplitude features or shape features of the two signals under test. However, extraction of time domain features beyond first derivatives, spline slopes or sample values of the signal to increase the accuracy of DTW has become the focus of resent research which are named feature based DTW (FBDTW).

Feature based DTW is an attempt to overcome the limitations of the value DTW and DDTW methods. During the comparison of samples in each of the two signals, feature based DTW takes into consideration both the local and global features of the two signals. In doing so, it increases consideration of not only the overall shapes of the signals but also the local trend around the samples. The main issue with the use of feature based DTW is that it is very specific to the application and the signals under test. As such, it must be adapted and retrained by the user to suit the changing

conditions and is computationally expensive. The trade off in the use of FBDTW remains between accuracy and computational speed. Feature based DTW is not yet suited to applications where the user is performing a significant amount of analysis, e.g. evaluation of an ECG database, or requires near real time results [78] although research is under way into increasing the speed of the process as reported by Xie et al. [91]. No results regarding the increased accuracy of FBDTW over the other methods on a significant number of ECG recordings are available, although Xie et al. have compared a modified value based DTW, DDTW and FBDTW algorithms for ECG using a small set of test signals from control, microelectronics, fabrication and video surveillance sources. In the course of early results DDTW provided "much worse performance" than the improved value based DTW and FBDTW algorithms and was omitted from the majority of their comparisons.

For the purposes of this research project the application of DTW is required in establishing the onset and termination of the fiducial points in the analysis of the timing information found in a significant volume of ECG recordings. Given this, the fact that there are not a large number of FBDTW algorithms available and the one which was found has not been tested extensively the author considers FBDTW less appropriate than the other forms of DTW for this research project.

6.7 Summary of DTW Investigation

In this chapter three types of DTW algorithm have been reviewed. The first type of value-based DTW, was found in the largest number of references particularly in the area of ECG analysis. The errors associated with value based DTW were highlighted and are based around the fact that the optimum alignment between the two signals under test is based on a Euclidean distance measurement of each sample in the signals. Without incorporating the local trends and global position of samples within the ECG wave value based DTW can provide unintuitive alignment as shown in Figure 6.9. However, this error can be greatly reduced by aligning features of the two signals such as aligning the start of each beat and scaling the peaks of the R waves pre-DTW. In doing so the user reduces the Euclidean distance difference of these features between the two signals to zero and hence ensures they are properly aligned in the two warped signals. When pre-processed correctly as in Figure 6.11, the unintuitive alignment of the P termination points was removed. The author believes that this pre-processing

could be extended to a type of composite normalisation to ensure similarity of other features in the signal such as P and T wave onset regions and peaks. Any singularities remaining in the signal should then be due to morphological differences between the two signals.

DDTW is based on extracting the principal shapes of the waves under test using first derivatives of points or approximation splines to characterise the shape of regions. Although theoretically this is an intuitive improvement of DTW, concerns regarding the loss of signal integrity due to approximation are not addressed in the literature. To investigate the effects of approximation on the true location of the fiducial points in an ECG signal a number of accuracy measurements were undertaken. The standard PRD calculation is heavily criticised in the literature but continues to be the most commonly used metric. The inaccuracies of the PRD method were exposed by partial PRD calculation. To measure the effects of approximation on the fidelity of identifying the fiducial points after approximation value based DTW was applied. This novel approach to testing the accuracy of ECG compression highlighted that even at relatively low CR's the standard deviation of the error between the original and approximated location of the fiducial point approached the bounds of acceptable deviation between expert annotations. DDTW is better suited to cases where the objective is to characterise the overall shape of components within the signal rather than for the location of specific points.

A little misleading in its name, since value and DDTW warp features of each signal also, FBDTW attempts to characterise each point with respect to the points around it and its position in the global or overall signal. The literature explains that the algorithm must be retrained to work adequately with different signals which increases time constraints of using the algorithm. This is a concern the creators of FBDTW for ECG's are currently trying to address. Suitability of this variation of the algorithm to ECG processing has not been found in a large number of cases in the literature. Given the intention to apply the algorithm to a large cohort of subjects and recordings in this research FBDTW is not considered appropriate.

Another note to be taken from review of the DTW literature is that the most appropriate match between the unknown query and reference signal for classification is typically found by choosing the one with the minimum cumulative difference between the two signals, be it a Euclidean distance difference or a difference in first derivative or slope, or a residual voltage measure after DTW has been applied. The author believes

that the choice of the best match between a query and a number of reference signals could also be based on other features such as the amount of time warping required and perhaps features of the two signals known *a priori* such as the heart rate of the two signals. A classifier incorporating the residual difference after warping, amount of time alignment required and *a priori* knowledge of the signals could increase the accuracy of any DTW process be it value, derivative or feature based.

The author believes that value-based DTW can be used very accurately for the objective of this research if the signals are pre-processed correctly and a multiple feature based classifier is used to find the the best match possible between the query and reference signals. Improved methods of pre-processing the signals and classifying the results of DTW shall be explored in the next chapter.

Chapter 7

Improved Pre-Processing and Classification for Value Based DTW

7.1 Introduction

In this chapter a method of pre-processing the query and reference signals known as "Composite Normalisation" is proposed to overcome the limitations of value based DTW. The benefits of composite normalisation are tested using the 719 reference beats available for test as discussed in Chapter 6. Using composite normalisation singularities and ensuing unintuitive errors are greatly reduced by minimising the Euclidean distance between distinct features of the two signals pre-DTW. Remaining differences between the two signals are hence mostly inherent morphological differences which exist between them.

Pre-processing composite normalisation increases the accuracy prior to DTW. However, the accuracy of DTW can also be increased by classifying the best match between a query and reference on the basis of multiple features of the two signals. A time domain based classifier which includes a measure of similarity between the signals based on heart rate, required time alignment during DTW and resulting residual amplitude difference between the two after DTW is presented. The benefit of using this multi-feature classifier over just a single difference measurement is examined by tests using the 719 reference signals. A method of further increasing the accuracy of finding the fiducial points for the QRS complex is also suggested.

The chapter concludes having combined the value based DTW algorithm with composite normalisation and a multi-feature classifier to optimally find the location of the

fiducial points in a query signal. This process shall be used in Chapter 8 to investigate the time characteristics of the constituent ECG components in the Nasor exercise ECG signal database discussed in Chapter 5.

7.2 Composite Normalisation

Some of the theory and results in this section are included in an article published by the author in [116].

In most of the DTW articles discussed in Chapter 6 both the query and reference signals are amplitude normalised such that the R-peak of each signal have the same value. This method of standard normalisation which was illustrated in Chapter 6 is shown in Figure 7.1. For illustrative purposes the same two signals shall also be warped having undergone composite normalisation.

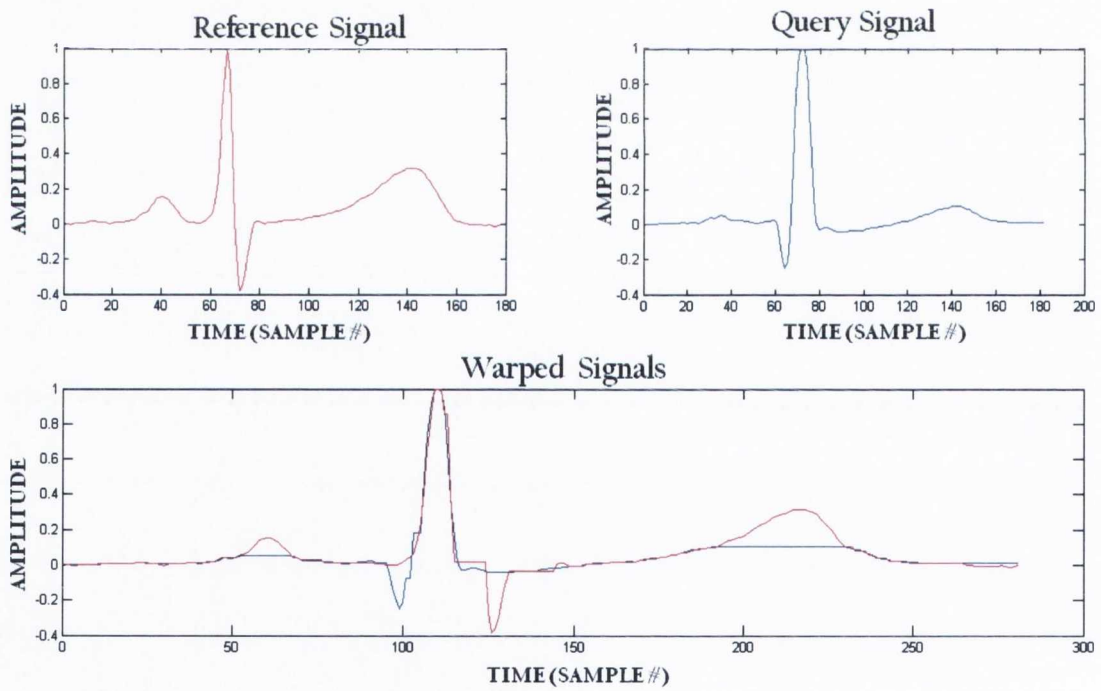

Figure 7.1: Standard Normalisation

This is a linear amplitude normalisation given by Equation (7.1) and does not distort the morphology but merely increases the match between the two QRS complex amplitude profiles pre-DTW. For the single beat query and reference signals q(t) and r(t) in Equation (7.1) the amplitude normalisation is given by:

$$q_{Normalized}(t) = \left| \frac{\max[r(t)]}{\max[q(t)]} \right| q(t) \tag{7.1}$$

This standard normalisation will not however, serve to minimise the difference between the P and T waves of reference and query signals. So, even if the shape and profile of the two signals are similar, the R-peak normalisation process could infact change their amplitudes in such a way as to increase the Euclidean distance between them pre-DTW.

By the same token it can be argued that the normalisation process should normalise the P, QRS and T waves and warp the resulting query and references signals separately for each. The ECG signal can be segmented into regions approximately around each of its constituent components using a segmentation technique suggested by Olmos et al. [117], and the value of the extrema features of the P and T waves used to amplitude align the signals for composite normalisation. Note it cannot necessarily be assumed that the maximum value of the waves can be used for normalisation, as there are also signals with inverted components such as the T wave inversion shown in Figure 7.2. Segmentation into windows is only required to find the extrema for composite normalisation. The signals are not segmented before DTW i.e. complete ECG cycles are still warped to each other at this stage as shown in Figures 7.1, 7.3 and 7.4.

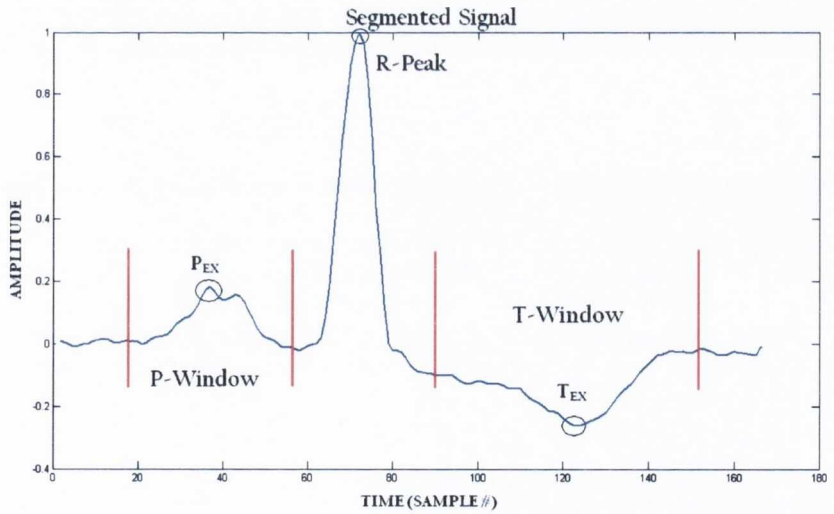

Figure 7.2: Composite Normalisation feature extraction

Composite normalisation is accomplished using three different amplitude aligned query signals:

$$q_{Pnorm}(t) = \left| \frac{r(P_{EX})}{q(P_{EX})} \right| q(t) \tag{7.2}$$

$$q_{Rnorm}(t) = \left| \frac{r(R_{pk})}{q(R_{pk})} \right| q(t) \tag{7.3}$$

$$q_{Tnorm}(t) = \left| \frac{r(T_{EX})}{q(T_{EX})} \right| q(t) \tag{7.4}$$

Figure 7.3 is an example of the same two signals as in Figure 7.1 but with the P waves of the query and references normalised together using Equation (7.2).

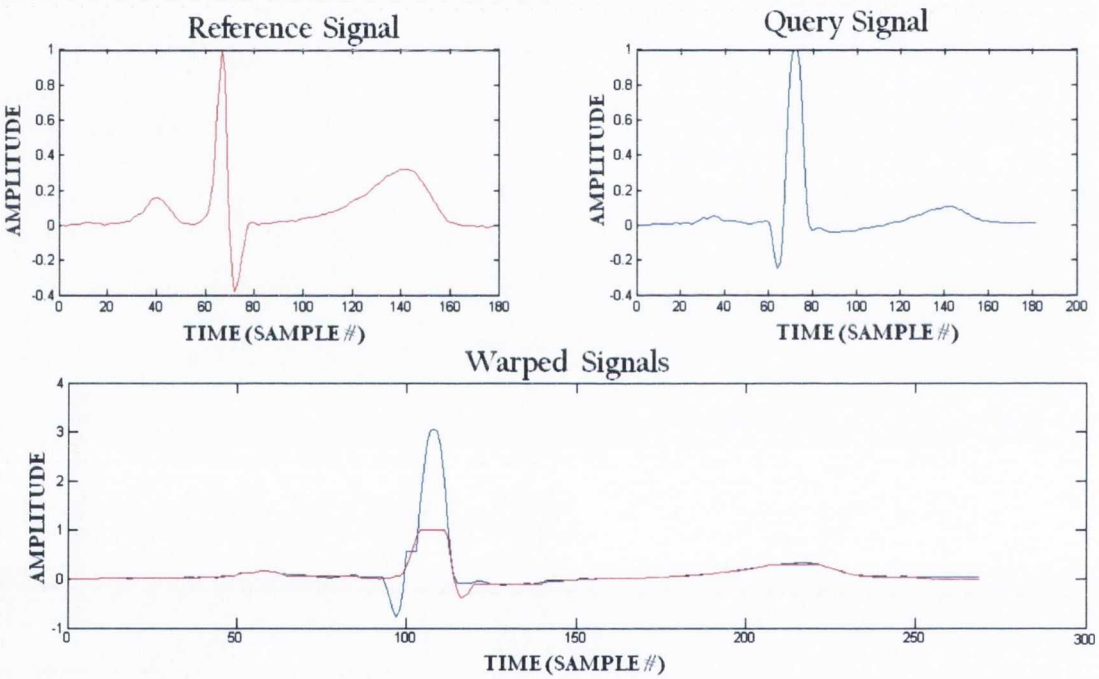

Figure 7.3: Warping of q_{Pnorm} with reference signal

It is clearly evident from Figure 7.3 that normalising the P waves has resulted in a better warping of the query and reference P waves. R-peak normalisation by Equation (7.1) is identical to standard normalisation so its resulting output is the same as in Figure 7.1.

Figure 7.4 shows the result of warping query and reference signals with normalised T waves using Equation (7.4). Again it is clear that normalising the T waves has improved the accuracy of the warping of these components.

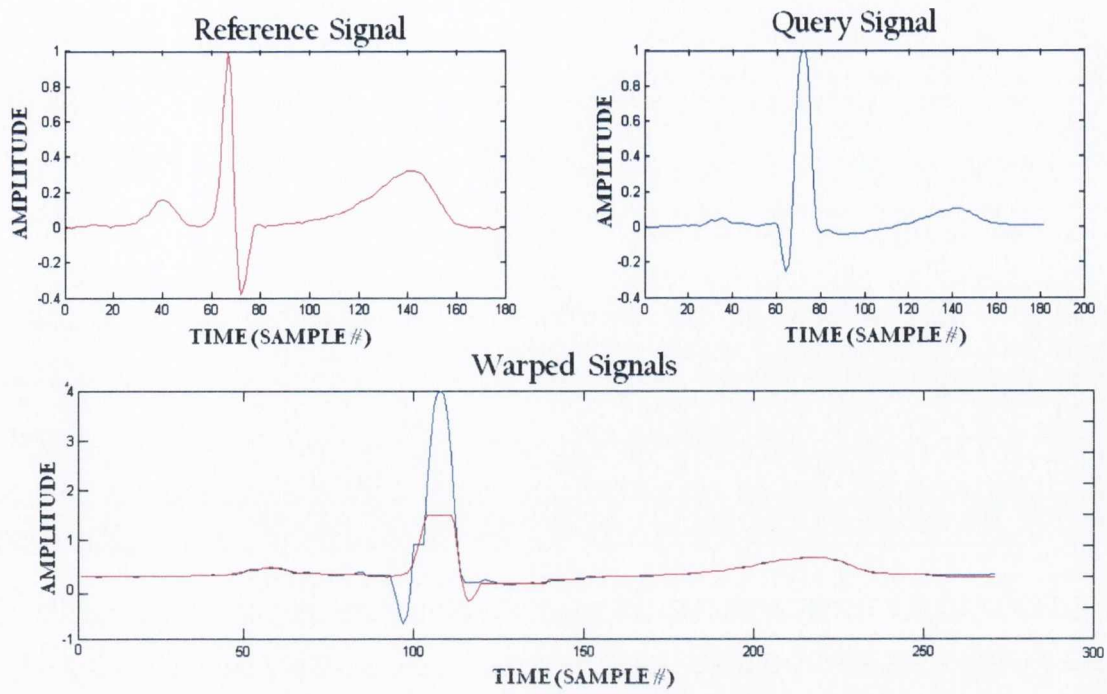

Figure 7.4: Warping of q_{Tnorm} with reference signal

This composite method of amplitude normalising the signals pre-DTW appears visually to increase the accuracy of the warping process.

7.3 Increased Accuracy due to Composite Normalisation

The benefit of the composite normalisation technique being applied pre-DTW shall be investigated by taking each of the reference beats and comparing them with the other beats available in the same recording from the reference database and then with all other signals in the database. The two test signals are normalised pre-DTW first using standard R-peak normalisation and then using the composite normalisation technique.

7.3.1 Warping using Similar Signals

In this case, the true fiducial points as annotated by the expert cardiologists are known for both the reference and query signals so the error between the true fiducial points and the fiducial points identified by the DTW algorithm in the query signal can be measured. In order to observe the effects of the alternative pre-processing techniques we approach it in two steps. The mean and root-mean-square-error (RMSE) in the

estimated location of each fiducial point resulting firstly, from comparisons with each signal in the same recording (see Table 7.1) and secondly, with every other beat in the reference database were calculated separately. This examines the proposed benefit of composite normalisation for constituent waves with similar and significantly different amplitudes. The signals from the arrhythmia and normal sinus rhythm databases are morphologically quite different and hence results are divided into P, QRS, T wave onset and termination points for each database. The results below are measured as mean ± root-mean-square-error (RMSE) values. RMSE is used here because it is a measure of variance around the expertly annotated estimate of the fiducial point location as opposed to mean ± standard deviations, where standard deviation is a measure of variance around the mean error in the locating of the fiducial point as determined by the algorithm [83]. Standard deviation and RMSE are often used interchangeably since in an unbiased system they are the same.

Table 7.1: Results for Arrhythmia signals within the same recording

Fiducial Point	Standard Normalisation	Composite Normalisation
P-Onset(ms)	-4.35±44.8	2.00±41.35
P-Termination(ms)	2.37±51.7	-1.09±42.63
QRS-Onset(ms)	-16.55±51.83	-16.55±51.83
QRS-Termination(ms)	-16.21±53.37	-16.21±53.37
T-Onset(ms)	1.23±67.80	5.13±56.58
T-Termination(ms)	0.53±45.74	-1.61±41.86

Table 7.2: Results for Normal Sinus Rhythm signals within the same recording

Fiducial Point	Standard Normalisation	Composite Normalisation
P-Onset(ms)	7.01±28.43	6.92±27.74
P-Termination(ms)	-3.33±23.20	-3.57±22.94
QRS-Onset(ms)	5.98±23.72	5.98±23.72
QRS-Termination(ms)	-4.48±22.18	-4.48±22.18
T-Onset(ms)	4.04±37.43	4.82±37.21
T-Termination(ms)	-6.50±28.50	-6.18±28.01

When analysing the data one must take into consideration that the sampling period of the signals is 4 ms. With this in mind the mean estimate errors shown in Tables 7.1 and 7.2 have very little difference (less than one sample in each case) using either pre-processing technique. One can however, see that the composite normalisation technique does yield a lower RMSE for each fiducial point, significantly so by >9 ms in the case

of the arrhythmia P termination and T onsets which would indicate increased stability of the algorithm. The benefits of composite normalisation should become more clear when signals with significantly different P and T wave amplitudes are warped to each other.

7.3.2 Warping all Reference Signals

The results in Tables 7.3 and 7.4 are again divided into signals taken from the Arrhythmia and Normal Sinus Rhythm databases to enable a more specific view of the effects of the pre-processing techniques.

Table 7.3: Results for warping to all Arrhythmia signals

Fiducial Point	Standard Normalisation	Composite Normalisation
P-Onset(ms)	-8.23±58.00	-2.25±46.00
P-Termination(ms)	9.66±58.83	1.13±53.50
QRS-Onset(ms)	26.17±62.84	26.17±62.84
QRS-Termination(ms)	-61.10±118.54	-61.10±118.54
T-Onset(ms)	-19.65±120.17	13.23±108.20
T-Termination(ms)	10.45±89.15	6.44±75.32

Table 7.4: Results for warping to all Normal Sinus Rhythm signals

Fiducial Point	Standard Normalisation	Composite Normalisation
P-Onset(ms)	13.44±56.68	6.52±41.68
P-Termination(ms)	-18.45±48.81	-16.92±46.46
QRS-Onset(ms)	2.79±41.46	2.79±41.46
QRS-Termination(ms)	-16.34±67.66	-16.34±67.66
T-Onset(ms)	23.79±95.80	10.79±84.60
T-Termination(ms)	20.53±83.35	5.21±63.91

As predicted, the composite normalisation technique has produced mean error and RMSE values significantly lower than standard normalisation. It allows reference and query signals of similar morphology but significantly different amplitudes to be warped more accurately. This is achieved by aligning the common features within the two signals pre-DTW such as the initial offset at the beginning of each beat, the P, R and T peaks. The remaining error is primarily due to differences in the actual signal morphologies.

7.3.3 Conclusions Regarding Composite Normalisation

The database of reference real ECG recordings with significant morphological variation has been used to test the composite normalisation method. Pre-processing the signal using standard and composite normalisation has been compared when warping signals of similar morphologies and signals with significantly different P and T wave amplitudes. For signals of similar amplitude and morphology the mean estimate errors have less than one sample difference for any fiducial point using either method. There is a significantly lower RMSE for the composite normalisation method in the case of the P wave termination and T wave onset. The true benefit of the composite method of normalisation becomes apparent when warping signals of different amplitude levels, where improved mean estimate and significantly lower root-mean-square errors are recorded for all fiducial points.

7.4 Classifying the Results of DTW

A peer reviewed paper published by the author [118] is based on the material and results discussed in this section.

The process of establishing which reference signal the query is most similar to is known as classification. There are a number of methods used to classify the most accurate match between the query and a reference signal. Many researchers [92, 93] use a multi-layered approach whereby, when warping the signals, the reference signal identified as the closest match is the one which provides the minimum slope differences between approximation splines during warping. Others [85] use the residual difference between the query and reference to perform the classification of the signals post-DTW. Although these methods of classification are popular, they have the limitation of being dependent on just one feature of the signals.

To overcome this limitation some users have combined other analysis techniques with DTW such as Fisher's Linear Discriminant Analysis [78] to further increase the accuracy of the classification process. In this section it shall be shown how using a classifier that takes into account the signal heart rates, the amount of time alignment required around the fiducial points of the ECG signal during DTW and the resulting residual amplitude difference between the query and reference signals can aid in the classification process. The classification is not unduly complex, as all of the features

used are based in the time domain and hence, is not computationally intensive.

7.4.1 The Classifier Features

The classifier consists of three time domain features with respect to the query and reference signals. Each must be combined with a weighting constant before being used in the classifier equation. The assumption before using the classifier is that the query has been warped to every signal in the reference database and the objective is to analyse each template match and select the most similar reference signal.

7.4.1.1 Heart Rate of the Query and Reference Signals

The first feature to be included is the relationship between the heart rate of the original signal and the reference signal. This can be considered as a global feature of both signals since the total frame length and duration of each component is correlated with the cardiac cycle time for the particular beat. The difference between the heart rate of the current query and reference is expressed as a fraction of the maximum heart rate difference between the current query signal and the reference with the least similar heart rate in test database. The heart rate variable X is given by:

$$X = \frac{|Q_{HR} - R_{HR}|}{\max |Q_{HR} - Rd_{HR}|} \tag{7.5}$$

Where Q_{HR} and R_{HR} are the heart rates of the query and reference signals respectively, and Q_{HR}–Rd_{HR} is the difference between the current query beat heart rate and the reference signal with the least similar heart rate i.e. the maximum difference.

7.4.1.2 Time Alignment Required around the Fiducial Points

The second feature to be included in the classification criteria accounts for the alteration of the test signal's time scale around the fiducial points, i.e. onset or termination of a constituent wave during time alignment. The duration of each constituent wave and hence the location of these points is diagnostically significant [2]. Identification of these points is the objective of applying DTW in this instance, hence, it is desirable that the query and reference signal are similar to each other in these regions before alignment.

Of course it is possible that the morphologies are similar but require compression or expansion to align them in time as is the purpose of the DTW algorithm. However, significant alignment or repeated singularities would imply that the morphologies of

the two signals are in fact very different, given that all waves are normalised pre-DTW using composite normalisation. The variable Y is calculated for each constituent wave of the current signals under comparison and is defined as the total padding inserted within ±6 samples of the onset and termination of the P, QRS and T waves of the current query and reference signal. The variable is expressed as a fraction of the maximum padding inserted during warping of the current query to the reference signal in the database which required the most time alignment around the fiducial points during DTW.

$$Y = \frac{|P_O + P_T|}{|P_{MO} + P_{MT}|} \tag{7.6}$$

Where P_O and P_T is the time scaling or number of samples inserted within ±6 samples of the onset and termination of the current query and reference signal respectively during DTW. P_{MO} and P_{MT} are the total padding required during time alignment between the current query and the reference signal from the database that required the maximum amount of time alignment around the fiducial points.

7.4.1.3 Residual Difference of Query and Reference after DTW

The purpose of this feature in the classifier is similar to the residual or difference measurements used in [85, 92, 93]. The peaks of the query and reference signals should be amplitude normalised by composite normalisation pre-DTW. After dynamic time warping has been performed one can measure the remaining amplitude difference between the query and reference signal components and take this as a measure of similarity between the two signals. In this case the root-mean-square difference (RMS-difference) is used to measure the amplitude difference between the time aligned query and reference signals. For each of the constituent waves of the signal i.e. the P, QRS and T waves of the heart beat under analysis a RMS-difference variable Z is calculated as:

$$Z = \sqrt{\frac{\sum_{i=k}^{n} [R(i) - Q(i)]^2}{\sum_{i=k}^{n} R(i)^2}} \times 100 \tag{7.7}$$

where Q and R are the query and reference signals respectively, k is the onset sample number and n the termination sample number of the ECG constituent component being analysed. The RMS-difference provides a measure of the similarities of the two signals in amplitude terms after they have been time aligned.

7.4.2 The Classifier Equation

The classifier uses a root of the sum of the squares of the features X,Y and Z to rank each of the results between the query and the signals in the reference database as shown in Equation (7.8):

$$C_R = \sqrt{C_1(X) + C_2(Y) + C_3(Z)} \tag{7.8}$$

Where C_R is the resulting classifier rank, X, Y and Z are the feature variables and C_1, C_2 and C_3 are the feature weights. The feature values X,Y and Z are fractions of independent measurements and hence will have very different scales. To scale the feature coefficients correctly the feature scalars or weights can be used to find a balanced combination of the coefficients [84]. A classifier rank is created for the P, QRS and T wave of each query to reference match. The match which yields the minimum ranking for a particular component is selected as the best match for that component. Before testing the classifier's ability to discriminate between the good and poor query to reference matches the coefficients must first be weighted optimally.

7.4.3 Optimising the Scaling Coefficients

In order to find the most accurate combination of scalars to weight the contribution of each feature, the coefficients C_1, C_2 and C_3 shall be adjusted from 0 to 1 in 0.167 increments. Starting with C_3, C_2 and finally C_1 all combinations of the scaling weight coefficients can be tested. For each combination of scaling coefficients each one of the 719 reference signals is warped to the other 718 samples in the annotated database. The best match is selected using the classifier with each set of weights. The error between the location of the expertly annotated fiducial points and the ones from the query to reference warp selected by the classifier is then recorded.

Figure 7.5 is a plot of the total root mean square error (RMSE) in the identification of the fiducial points in all of the 719 test signals for each combination of the scaling coefficients. It can be clearly seen that each feature has an effect on the accuracy of the classifier. Note how after the 49^{th} combination, where C_1 (X) is increased from 0 to 0.167, there is a large reduction in the RMSE because the heart rate constraint has been introduced to the classifier. One can also see that at every 49^{th} combination from here on the error spikes to a peak as C_2 (Y), the measurement of padding around the fiducial point is removed when C_2 returns to zero. The final constraint Z, the

RMS-difference or residual between the query and reference constituent P, QRS and T waves is reset to zero every 7^{th} combination as the coefficient C_3 is returned to zero. By observation of the resulting RMSE in Figure 7.5, it was found that to achieve minimum RMSE (providing minimum error and maximum stability) a coefficient combination C_1=0.333, C_2=0.833 and C_3=1.0 should be used to scale or weight the contribution of each feature to the classifier. If the process was repeated with a larger database and a larger variety of morphologies at different heart rates one might expect the weights to vary accordingly.

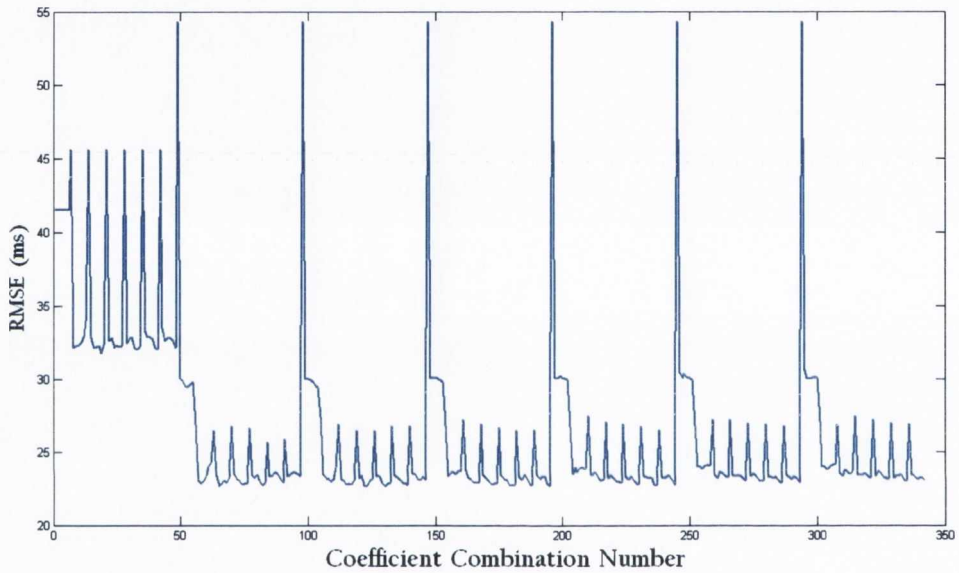

Figure 7.5: Training the feature weight scaling coefficients

7.4.4 Accuracy of the Improved DTW Process

The test signals originating from the Normal Sinus Rhythm and Arrhythmia Databases are again examined separately since they offer significantly differing morphologies. The value based DTW algorithm combined with composite normalisation and the classifier is tested for its ability to locate fiducial points and resulting P, QRS and T wave durations. Note that 1.5% of the query/reference matches were deemed as obvious errors and removed before the subsequent analysis shown here.

The results in Table 7.5 are the mean and standard deviation of error between the annotated location of the fiducial points and those identified using DTW. Mean $\pm$ standard deviation is used as a measure of accuracy here to allow comparison to previously published estimates of acceptable standard deviations found in expert annotations of the same fiducial points. These deviations are regarded as acceptable by

different cardiologist assessors of the same points as reported by Jane et al. which serve as a bench mark for assessing the performance of the automatic algorithm [114].

Table 7.5 demonstrates that the mean errors resulting from the algorithm are low, particularly if one considers that with a sampling frequency of 250 Hz a mean error of 4 ms is just one sample. Comparing the standard deviations of error for the algorithm with the deviation of expert cardiologist opinion one can see that the algorithm deviations are within ±12ms or ±3 samples. The algorithm deviations are higher for some of the fiducial points. This is because the expert deviations are those of experts viewing the same beats while in the case of the algorithm it is matching a different annotated reference beat. The component with the least accurate results when put in terms of acceptable deviation is the QRS complex and this shall be explored further in the next section.

Table 7.5: Mean and standard deviation of the DTW and classifier error compared with expected expert deviation

Fiducial Point	Expert (ms)	Normal-Sinus Rhythm (ms)	Arrhythmia (ms)
P-Onset	±10.2	-2.05±17.23	-0.64±16.44
P-Termination	±12.7	2.48±13.30	5.23±17.47
QRS-Onset	±6.5	0.71±11.20	2.11±18.38
QRS-Termination	±11.6	1.75±10.83	5.07±14.78
T-Onset	N/A	-11.39±29.0	12.1±31.71
T-Termination	±30.6	6.76±14.87	6.03±27.62

To further investigate the accuracy of the DTW classifier process an investigation how well the duration of the P, QRS and T waves from each signal can be measured is required. In Figure 7.6 the duration of each component as annotated by the expert cardiologists for each wave has been averaged over 6 bpm intervals. Also shown is the mean ± one standard deviation of the durations for each heart rate interval to give an idea of the variation in how the expert annotated the different waves for the same heart rate interval. One would hope the results of the warping process would lie within the deviations that exist between expertly annotated durations to provide comparable accuracy to annotation by cardiologist experts.

The results in Figure 7.6 prove that the combination of composite nomralisation, value based DTW and the time domain classifier enable an accurate automatic measurement of the duration of each constituent waveform for the signals in the database. Similar results for the Normal Sinus Rhythm test signals are shown in Figure 7.7. The

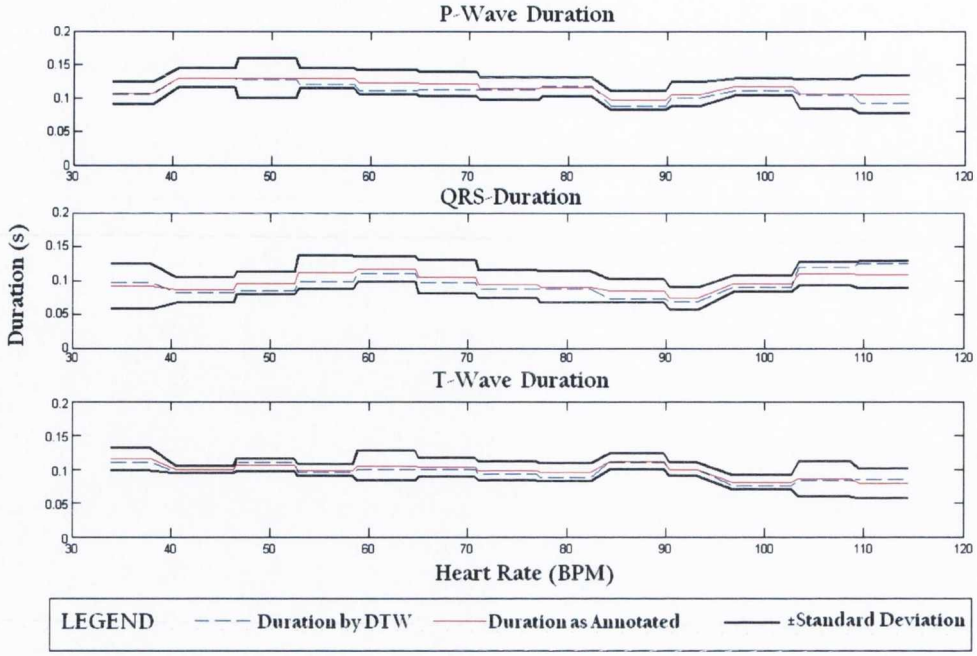

Figure 7.6: Arrhythmia constituent wave durations as detected by DTW

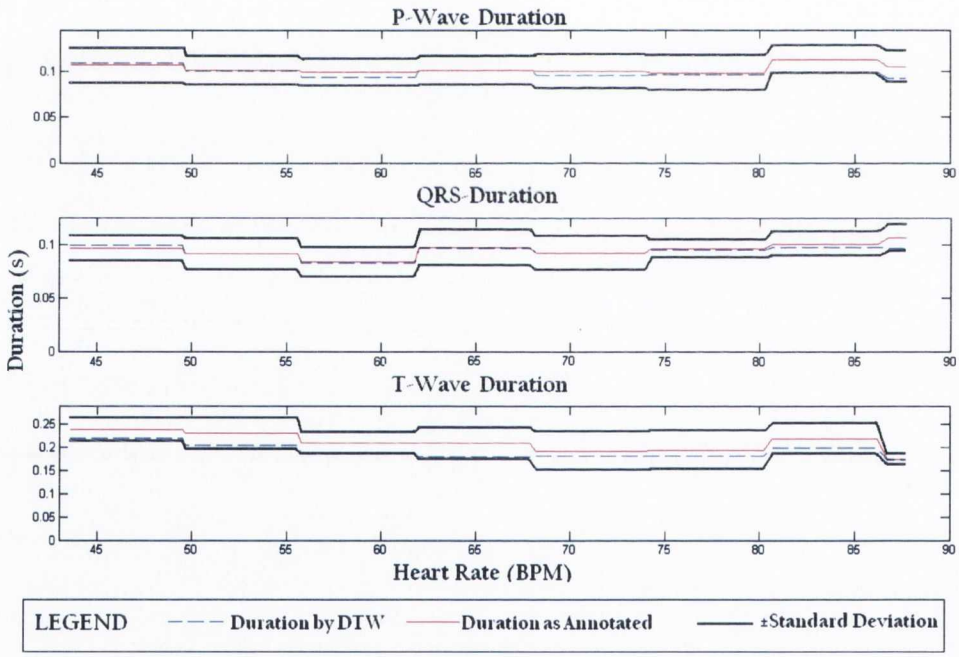

Figure 7.7: Normal Sinus Rhythm constituent wave durations as detected by DTW

mean durations as measured for each 6 bpm interval using the DTW process lie less than one standard deviation from the mean duration as measured by the experts.

7.4.5 Conclusions Regarding the DTW Process

The author has suggested a classifier that uses a time domain based combination of features including heart rate, degree of warping required and an amplitude difference

measurement. In doing so the DTW method is still used to warp and time align the two signal frames as accurately as possible, but the reference providing the best match is chosen using a number of features from the query and reference signal rather than just a single measurement.

The increased accuracy due to the addition of each feature in the classifier was demonstrated. The contribution of each feature to the classifier was optimized to achieve minimum error by weighting each feature's contribution using scalar coefficients. The performance of the DTW process was verified by comparison with expert identification of diagnostically significant information from signals within the reference database. It was shown in Table 7.5 that the component least accurately measured by comparison to acceptable deviations is the QRS complex. Based on this an alternative method of warping the QRS complexes is required.

7.5 An Alternative Approach to Warping the QRS Complex

The author suspects that the error in the case of the QRS fiducial points is due to the short duration, low amplitude characteristics that can effect the QRS complex morphology. The low amplitude Q and S waves which precede and follow the R peak of the complex in some recordings could be misaligned quite easily since the Euclidean distance between a QRS complex with and without them may be very small. They are also very short in duration so the classifier may also fail to detect an unintuitive alignment in the QRS onset and termination regions after warping for the same reason. To increase the accuracy of the process an alternative approach to warping the QRS complex is required.

7.5.1 QRS Morphology Classification

As discussed in Chapter 1 the QRS complex of a healthy subject's recording may or may not have Q or S waves which are minor deflections from the iso-electric baseline. Having viewed the ECG reference signals selected for this study and the recordings made by Nasor et al. it appears that in healthy subjects the QRS morphology remains consistent for the duration of a subjects recording. Classifying each QRS morphology shape pre-DTW and only warping similar shapes may increase the accuracy of the

process i.e. if a query signal has an RS morphology only reference signals with an RS morphology should be warped to the signal. The QRS complexes shall also be warped separately from the rest of the wave. Since the Q and S waves are comparatively low amplitude waves, DTW may misalign them if it results in a lower Euclidean difference between the much larger R-peak up and down slopes of the query and reference signals. So isolating the QRS waves before warping should limit the effects of the other features on the warping of the QRS.

The author decided to group the QRS complex shapes into four classes:

1. Class 0: Where the R peak has no clearly defined Q or S waves before or after it respectively.

2. Class 1: Where the R peak is preceded by a Q wave but not followed by an S wave.

3. Class 2: Where the R peak is followed by an S wave but not preceded by a Q wave.

4. Class 3: Where a full QRS complex is present i.e. including Q and S aves.

Classifying the signals visually is quite simple but an algorithm has been developed to aid in determining the QRS complex class and also the approximate location of the Q onset and S termination. These approximate values are used to window around the QRS complex wave so that they can be warped separately from the rest of the query and reference signals. The algorithm written in Matlab to classify the QRS shape is commented and included in Appendix A. The algorithm approximates the signal using the SAPA algorithm described in Chapter 6 to remove any spurious picks in the signal. The error threshold was fixed at 5 mV to accurately preserve the ECG morphology. The difference between each point and its adjacent one in the approximated signal is found to establish the trend of the data points i.e. up or down slopes. The QRS peak is found and an estimate for the beginning of the QRS up-slope and end of the down-slope locations are made based on the difference values found and the subsequent trends in the data. The thresholds for determining up and down slopes in the signal can be adjusted empirically by the user to ensure correct classification of the signals under test. Once the beginning of the QRS up-slope (or peak of the Q wave) has been determined the preceding 5 data points are searched for the maximum amplitude. The

same is repeated to find the end of the QRS down-slope (peak of the S wave) and the maximum amplitude within the 5 samples immediately following it. If the amplitude difference between the R up and down slopes and the maximum values surrounding these points exceeds 30 mV a Q or S wave is considered to be present. Again by analysing the trends in the difference values between points the onset of the Q and end of the S waves can approximately be found. An example of a Class 3 input signal and its difference values are shown in Figure 7.8.

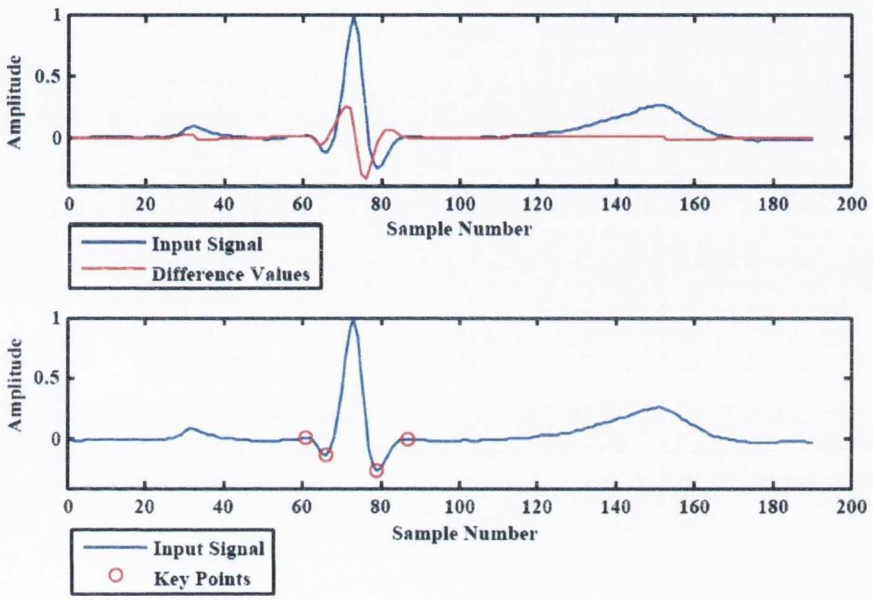

Figure 7.8: Example of QRS classification process

Shown in Figure 7.8 are the onset of the Q and termination R waves. Also shown is the beginning and end of the R wave up and down slopes, or extrema of the Q and S waves, as found by the algorithm.

The algorithm is limited in that it requires user intervention for significantly different morphologies. However, the author has tested the algorithm on the reference database and found that it can be used to classify accurately the four different QRS wave types and give approximate locations of the start and end of the QRS complex. When windowing around the QRS for DTW a tolerance of ± 3 samples is also added to the approximate onset and termination points to ensure the entire QRS complex is included in the analysis. An example of the four different morphology classes and the approximate onset and end points for the QRS complexes as found by the algorithm are shown in Figure 7.9. The onset and termination points at this stage are only for windowing purposes. The actual location of these fiducial points will still be found more accurately subsequently using DTW.

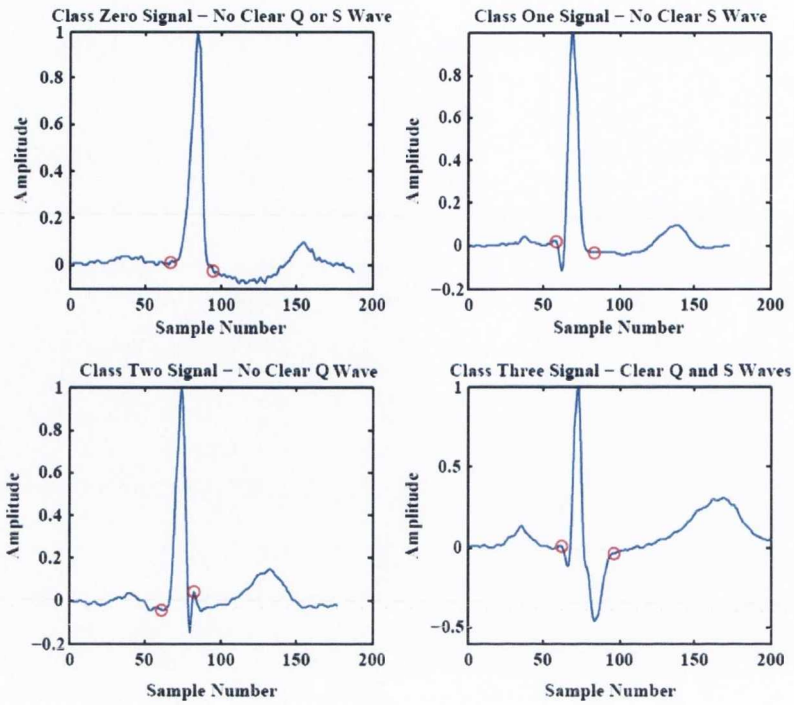

Figure 7.9: QRS classes and approximate onsets and terminations as found by the algorithm

Each query signal QRS morphology can now be classified and warped with reference signals of similar morphology.

7.5.2 A New QRS Warping Method

In an effort to increase accuracy the QRS complex is extracted from each query and reference ECG beat by windowing around the wave using the approximate points found during the morphological classification stage as shown in Figure 7.10 to allow it be examined separately.

Once the peak of the new QRS segment is determined, the up and down slopes can be split further into two different segments. The purpose of this is two-fold. Firstly the classifier can now be used to measure the accuracy of a query to reference warp for the up and down slopes separately. Secondly the offset at the beginning of the up slope and end of the down slope of the query and reference signals within the windows can be removed to ensure the onset and terminations points of each are aligned. The seperated up and down slopes of the same signals shown in Figure 7.10 are shown in Figure 7.11 before and after warping.

In theory the QRS complex should be warped more accurately now that the offsets have been removed and the up and down slope warps can be performed with the results

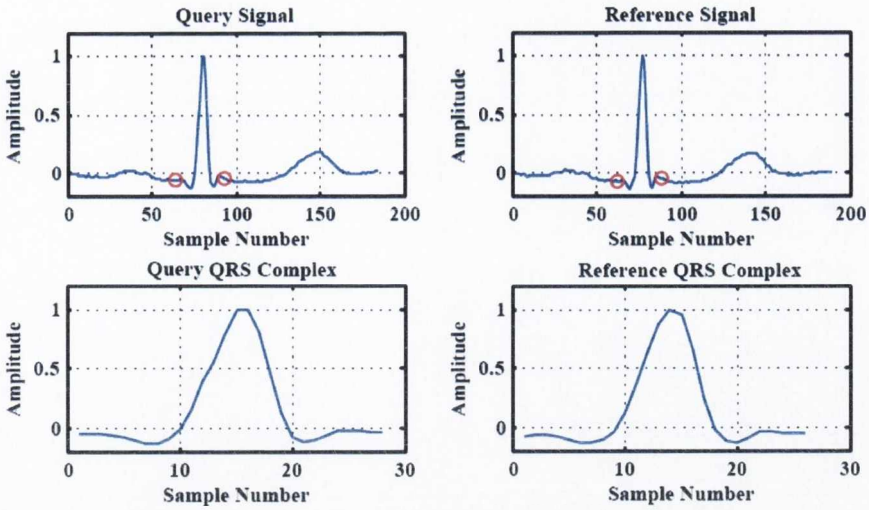

Figure 7.10: Each QRS complex is windowed from the Query and Reference signals

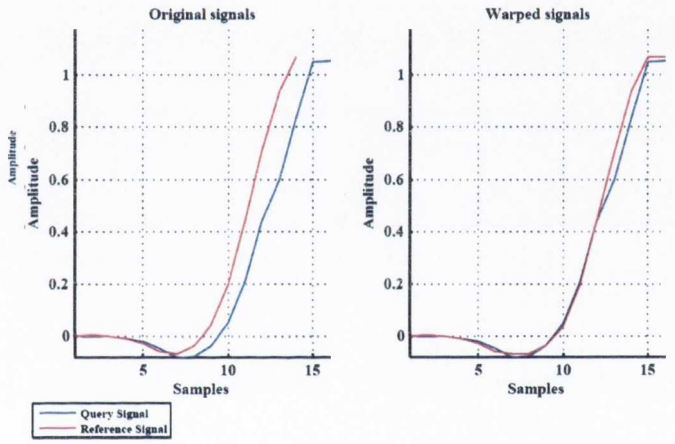

(a)

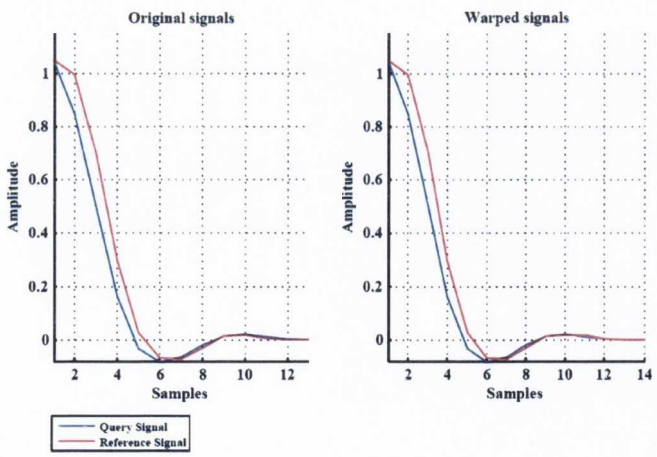

(b)

Figure 7.11: Figure 7.11a shows the up-slopes of the QRS before and after DTW. Figure 7.11b the down-slopes before and after DTW

classified separately. A point for the approximate beginning of the ST segment is now also known and could be used to remove offsets between the query and reference signal ST segments and T waves before composite normalisation and DTW is applied. This approach is not suitable for the P and T waves since it is not as easy to class the P and T waves into distinct groups nor find the approximate locations of the onset and termination of the waves.

7.5.3 Testing the Final Accuracy of the DTW Process

The DTW process as proposed by the author is now complete. In order to test the accuracy of the now complete DTW process a subset of signals from the reference database are examined. This subset of reference signals is also used in Chapter 8 in the characterisation of the constituent component durations. The purpose of this is to remove poor quality reference signals and reduce processing time. The reduction in the number of the reference signals should not reduce the accuracy of the process since the same variety of morphologies is present, only beats which are very similar to each other morphologically have been removed. Another benefit of using this subset of signals to test the algorithm is to establish how accurately the process can classify a larger database of query signals using a smaller set of reference signals. From the original 719 reference signals Table 7.6 shows the total number to be used as references for the remainder of this research:

Table 7.6: Selected Reference Signals

Component	Quantity of Reference Signals
P Wave	201
QRS Class 0	25
QRS Class 1	32
QRS Class 2	101
QRS Class 3	65
T Wave	140

So now instead of each query P wave being warped with 718 reference signals it is warped to 201 reference signals and the best match chosen, each Class 0 QRS query complex is warped to 25 reference signals etc. The accuracy of the entire process is still tested using each of the original 719 reference signals as queries, but comparing them with the smaller subset of reference signals as defined Table 7.6. The test results of

the final complete process are shown for the Normal Sinus Rhythm, Arrhythmia and both sets of signals combined in Table 7.7.

Table 7.7: Final testing of the algorithm

Fiducial Point	Expert (ms)	Normal-Sinus Rhythm (ms)	Arrhythmia (ms)	Combined (ms)
P-Onset	±10.2	2.21±12.21	3.08±15.85	2.68±14.01
P-Termination	±12.7	4.01±13.55	1.91±16.58	3.05±15.21
QRS-Onset	±6.5	2.76±8.01	-0.18±10.40	1.38±9.31
QRS-Termination	±11.6	3.17±8.48	-2.20±14.91	0.65±12.20
T-Onset	N/A	-13.09±24.02	-7.5±27.52	-10.48±25.78
T-Termination	±30.6	0.48±15.48	-1.20±20.91	-0.34±18.28

When compared with Table 7.5 it can be seen that for all except the QRS terminations point in the case of Arrythmia signals there has been a significant reduction in the standard deviation of error in determining the QRS fiducial points, while the mean error has remained at less than 4 ms (1 sample). Warping the QRS complex having first classified the morphology of the query signal and testing the QR and RS waves separately has reduced the error reported in Table 7.5. Note also that the P and T wave fiducial points have also been found with similar or better accuracy, using the smaller subset of references as defined in Table 7.6. In the case of the P wave, the overall reduction in the standard deviation of error is most likely to be due to the removal of poor quality signals from the reference database. In the case of the T wave fiducial points, the ability to approximate the location of the start of the ST segment allows the removal of offsets in this region in both the query and reference signals before composite normalisation, thus allowing a better alignment.

Importantly, the final figures for mean and standard deviation for all signals attainable by the modified DTW process are also shown in Table 7.7. The accuracy of the algorithm cannot be compared adequately to other DTW algorithms since many of the articles found in the literature have not included results for the determination of fiducial points in the ECG using a database of reference signals [78, 85, 90, 91]. Other algorithms are tested, depending on the intended application of the algorithm, using different databases such as the The Common Standards for Electrocardiography (CSE) database [119], and alternative subsets of the Physionet QT database e.g. sudden death and supraventricular arrhythmia recordings [92, 93]. Therefore, figures such as mean and standard deviation errors cannot be compared directly.

The intended application of DTW in this project is to find the time characteristics

of the constituent components of subjects having healthy ECG recordings and 719 test signals were chosen as they had been defined as showing normal sinus rhythm and are therefore the most appropriate. Finding the onset and termination or the fiducial points of the ECG components in a clinical setting may be assisted by automatic algorithms but the final analysis is performed by cardiologists. Therefore, the most suitable criteria to use to assess the accuracy of the algorithm is a comparison with expert deviations in annotations made by these experts as a benchmark. The figures shown throughout this Chapter for expert annotation of signals from the QT database have been provided by the creators of this database [80, 114] to provide that accuracy bench mark.

When compared with the standard deviation expected from multiple cardiologist annotations of the same signals it is clear the results of the DTW process are favourably comparable. In identifying all fiducial points the algorithm has either a lower standard deviation or a higher standard deviation of less than 4 ms greater than the expert deviations which in terms of the reference signal sampling rate (250 Hz) this is a difference of less than 1 sample. One must also consider that the expert deviations are differences in the annotation of the same beat, where as when testing the algorithm a different reference wave is used to annotate the query signal which will lead to an inherent deviation in the annotation of the fiducial points.

7.6 Conclusion

The concerns regarding the value-based DTW algorithm raised Chapter 6 have been addressed in this chapter. A composite method of normalising signals pre-DTW has been proposed and tested by the author. It has been shown to reduce the resulting errors associated with the use of value-based DTW, particularly when warping signals which have similar shape but different amplitudes.

Previously, the best match between a query and a reference signal has been found by choosing the one which results in the minimum difference between the two after warping. It was shown in Chapter 6 however, that often a dynamically optimised match can still result in unintuitive alignment of the signals. A time domain based classifier has been introduced by the author to measure the accuracy of a match between two signals after DTW. Rather than being based on a single feature e.g. a Euclidean difference, slope difference or residual amplitude the classifier is multi-featured. It has

been shown that each feature contributes to the accuracy of the classifier and that when combined with DTW it accurately determines the component durations of the ECG recordings in the test database.

Having combined value-based DTW with composite normalisation and the new classifier the author was still concerned with the resulting error deviation for the QRS fiducial points and the fact that it was significantly larger than found in expert deviation. A new method of classifying the QRS morphologies prior to DTW, and segmenting the signal to remove offsets to ensure the best query to reference warp was suggested. The classification of the QRS pre-DTW also allowed the removal of offsets from the ST segment to aid in ST segment and T wave warping.

A final subset of the original 719 test signals were chosen to remove poor recording quality reference signals and reduce processing time. A subset of reference signals was then used to find the fiducial points in all 719 signals. The entire process as described in this chapter was found to provide low mean and standard deviation of error which are similar to those obtained when experts annotate the same signal. This suggests that the process is suitable for an investigation of the constituent components of the excercise ECG database compiled by Nasor et al.

Chapter 8

Data Processing and Results

8.1 Introduction

In this chapter the ECG Lead II component durations are investigated. A database of ECG recordings that shall be used as the test data for the characterisation of these component durations is also described. Following the application of DTW and the extraction of each component from the ECG recordings, the component durations are calculated. Before attempting to characterise the variation of these components with respect to cardiac cycle time, it is important to pre-process the data by averaging the resulting component durations to ensure that the results reflect the characteristics of all subjects within the test database. Two different methods of averaging the data are investigated and the resulting effects on the final characterisation of the component durations using each method are compared. An appropriate method of pre-processing the data is decided upon and the variation of each ECG components duration with respect to cardiac cycle time is characterised using a second order equation. The resulting set of duration equations is compared to a similar study of these component durations and discussed in the context of larger clinical investigation.

8.2 The ECG Lead II Component Durations

As discussed in Chapter 1, the ECG signal is typically segmented into three distinct waves, two segments and two intervals, the duration and shape of which supply different diagnostically significant information. For clarity the ECG lead II signal and its constituent components are shown again in Figure 8.1. The duration, T, of each one

of these components are:

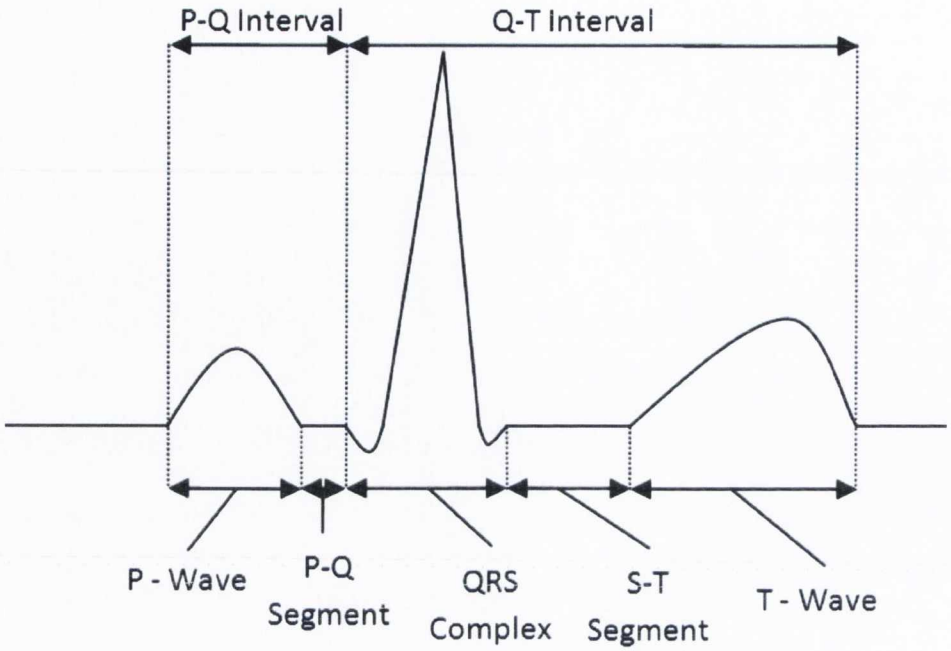

Figure 8.1: The ECG Lead II signal components to be characterised

1. The P Wave Duration - T_{PW}
2. The PQ Segment Duration - T_{PQ-Seg}
3. The PQ Interval Duration - T_{PQ-Int}
4. The QRS Complex Duration - T_{QRS}
5. The T Wave Duration - T_{TW}
6. The ST Segment Duration - T_{ST-Seg}
7. The QT Interval Duration - T_{QT-Int}

For each of the components an equation shall be established with respect to cardiac cycle time T_{RR}. The QT interval, as shall become apparent in this chapter, represents the most important of the seven ECG components due to its diagnostic significance. As such, it shall be used for illustration purposes throughout the chapter.

8.3 The Existing ECG Recording Test Database

Resting and exercise ECG's were recorded for 31 male and 19 female subjects by M. Nasor [26] and a resident cardiologist at the Stress Test Unit of St. James's Hospital,

Dublin during the period of 1995-1996. This process required approval by an ethics committee in the hospital and a significant amount of time in the stress test unit in St. James's Hospital. The recordings were verified as having been taken from healthy subjects, none having had any history of cardiovascular complications or showing any signs of pathological changes.

The recordings were made for 3 minute resting and 12 minute exercise intervals, although a number of older subjects could not complete the full 12 minute treadmill test. The recordings were made on a Marquette 12-Lead ECG recording machine which provided a Lead II signal that was fed through an anti-aliasing filter with a cut-off frequency of 200 Hz. The data was then sampled using a 12-bit analogue-to-digital converter that had a sampling frequency of 1.64 kHz [26].

For the purposes of preserving confidence in the accuracy of the results obtained, a subset of 10 male and 11 female subjects aged 13-65 years were chosen from the original pool of ECG recordings for analysis by M. Nasor. The subjects, recordings were chosen because it was verified that they were free from artefact and significant distortion. The resulting data set consisted of recordings with heart rates ranging from 46-184 beats per minute (bpm). This database offers an appropriate basis for an investigation of the Lead II ECG signal and for the purposes of comparison the author has used the same database for the analysis reported in this thesis.

In Chapter 5 the existing mathematical relationships for the duration of the constituent components of the ECG signal have been examined. It was decided that an equation of the form $A\sqrt{T_{RR}} + BT_{RR} + C$ would be fit to the resulting durations found in the analysis reported in this thesis in order characterise their variation with respect to T_{RR} since it has been shown by Burke & Nasor to characterise the variation of the QT interval duration most accurately.

8.4 Pre-Processing the ECG Recordings for DTW

All recordings from the test ECG signal database have been filtered and segmented in the same manner as during the creation of the reference signal database, reported in Chapter 6. However, some additional pre-processing of the test database is required.

At higher heart rates successive ECG beats begin to merge together. The database of reference signals used for DTW contains no reference signals which display such phenomena. Indeed if the P and T waves of successive beats are merged together the

determination of the onset and termination of these beats is at best estimated, since they are not visible in the recording, as shown in Figure 8.2. Given that there are no reference signals available for waves of this nature they cannot be classified using DTW and were therefore removed from the test recording database. After the removal of such beats from the database the remaining heart rates ranged from 46-160 bpm.

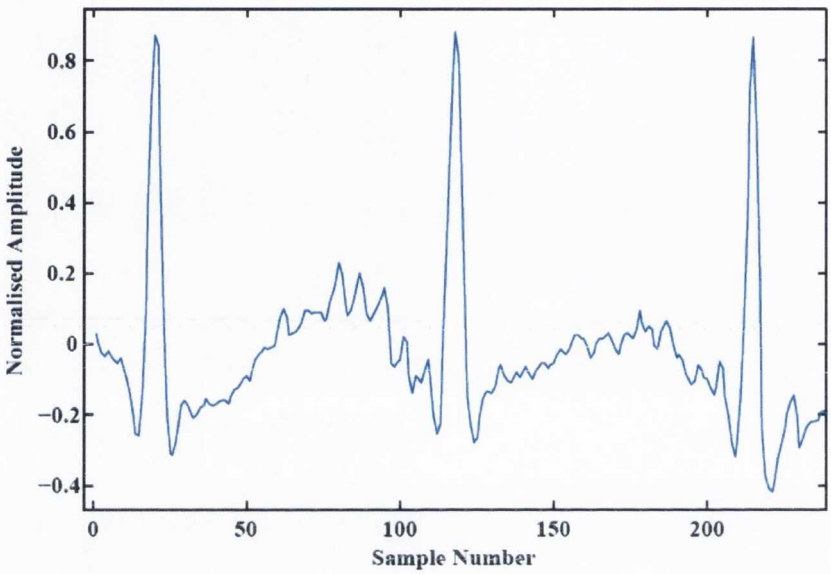

Figure 8.2: An ECG beat with a heart rate of 169 bpm showing the merging of the P and T waves.

The reference signals from the Physionet QT Database were recorded at a sampling frequency of 250 Hz. In order to allow an accurate comparison between the reference signals and the recordings in the database as described in Section 8.3 the test signals have been down-sampled to have a resulting sampling frequency of 273 Hz. The recordings in the database contain cases where there are low amplitude waves which are essentially within the recording noise level. This will result in an inaccurate designation of the onset and termination points of the waves such as those shown in Figure 8.3. It can be seen that no clearly distinguishable onset or termination point for the P-wave exists which yields a PQ interval duration in excess of 220 ms. To remove spurious errors from the DTW results, a PQ interval limit of 220 ms and a QT interval limit of 560 ms has been applied to the results of DTW. These limits are based on the healthy PQ and QT interval durations as defined clinically [2] and also allow a tolerance of 20 ms for each, results outside of these limits were disregarded. The tolerance allows for the fact that the interpretation of the specific onset and termination points of a wave, and therefore the duration of the component, differs between cardiologists as discussed in Chapter 6. The added tolerance accounts for this. Unfortunately, no clearly defined

limits for the other component durations exist in the literature as shall be discussed later.

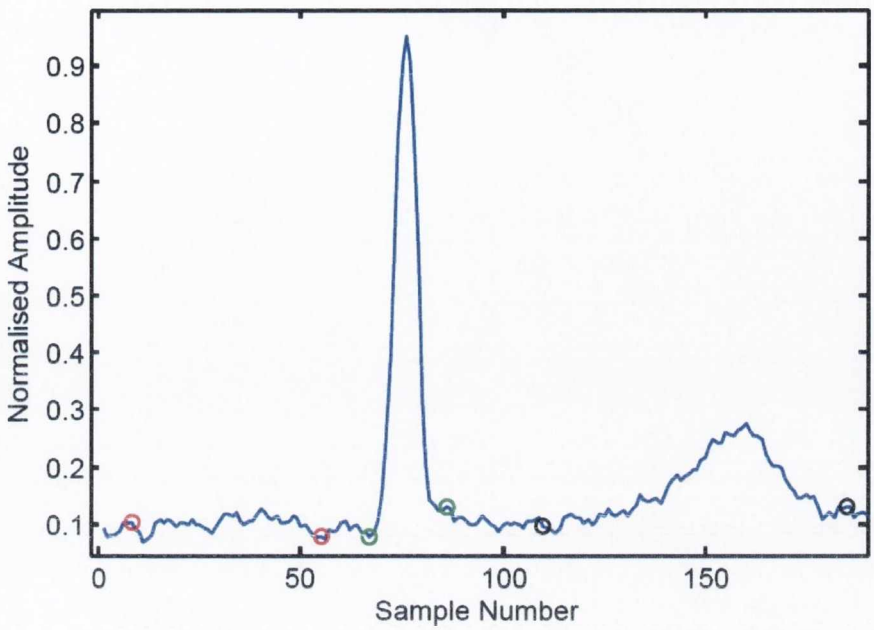

Figure 8.3: Low amplitude P wave resulting in excessively long P wave classification and hence PQ-interval duration

8.5 Processing the Results of DTW before Equation Fitting

Following the signal pre-processing, DTW and subsequent delineation of each beat in the test database of ECG recordings the onset and termination of each wave as defined in Figure 8.1 can be determined. Before an equation is fit to the data it is typically averaged into distinct beat per minute intervals. Previously the duration of components from different beats have been averaged into 1 bpm [26] or even 10 bpm [71] intervals before fitting a characterisation equation. Figure 8.4 is a plot of all QT interval durations for every individual beat from each subject, and illustrates why averaging is required.

There are 8755 QT interval durations from individual beats shown in Figure 8.4, and it is common procedure to average large data sets such as this to remove the effects of possible errors or outliers remaining within the data before attempting to characterise it. An investigation to establish what is the most appropriate method of averaging the data before attempting to fit an equation to characterise it is carried out.

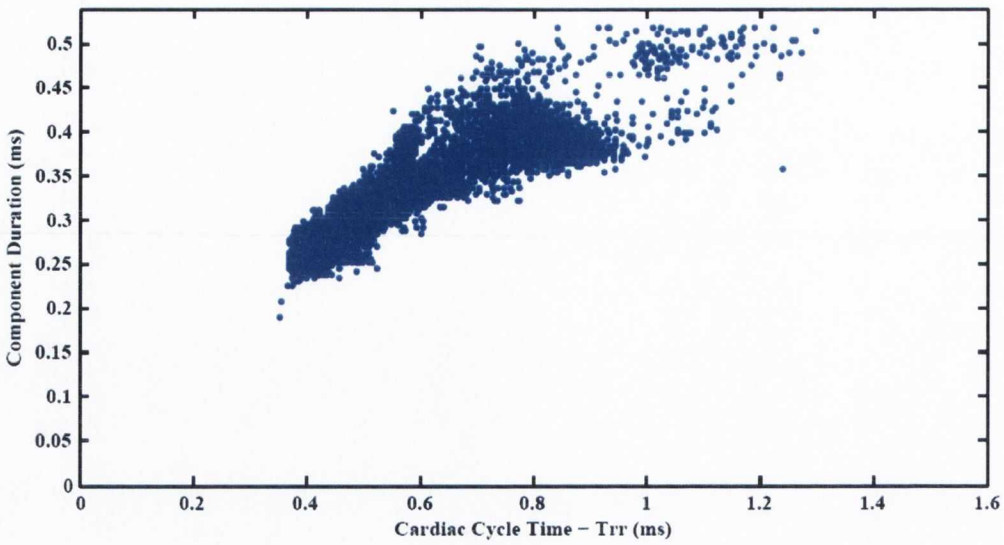

Figure 8.4: Authors QT interval durations of all beats without averaging

8.5.1 Methods of Averaging the Resulting Component Durations

There are two primary approaches to averaging the data. Previously all beats from all subjects have been placed into 1 bpm intervals and averaged. The problem with this method of averaging is that it assumes each subject contributes equally to each interval. If 1 of the 21 available subjects contributes a significantly higher number of beats to any given interval than the other subjects, then the mean value for the component duration within this heart rate interval is more reflective of this one subject than all of the subjects collectively. An alternative method of pre-processing is to average the component durations for each subject separately to 1 bpm intervals. After this they can be collated and the equation fit. Similarly, some 1 bpm intervals contain result contributions from more subjects than others so we would like to have one mean duration per interval rather than one mean duration per subject, per interval. Also to allow comparison to the other studies of the component durations one value per interval is necessary. To achieve this one can again average all subject means per interval. An analysis of the motivation for, and effects of, each type of averaging shall also be conducted.

8.5.2 Averaging all Beats into 1 bpm intervals

In the study previously carried out by M. Nasor [26] all beats from all subjects were collated and averaged into 1 beat per minute intervals. Unfortunately, this approach

to pre-processing the data allows one subject to dominate any given cardiac cycle time interval within the data set. Figure 8.5 shows the result of averaging all beats into 1-bpm intervals using the same method as Nasor on the DTW results of this study for the QT interval. The second order function proposed by Nasor is also fit, the fitting process and results shall be discussed in more depth in Section 8.6.

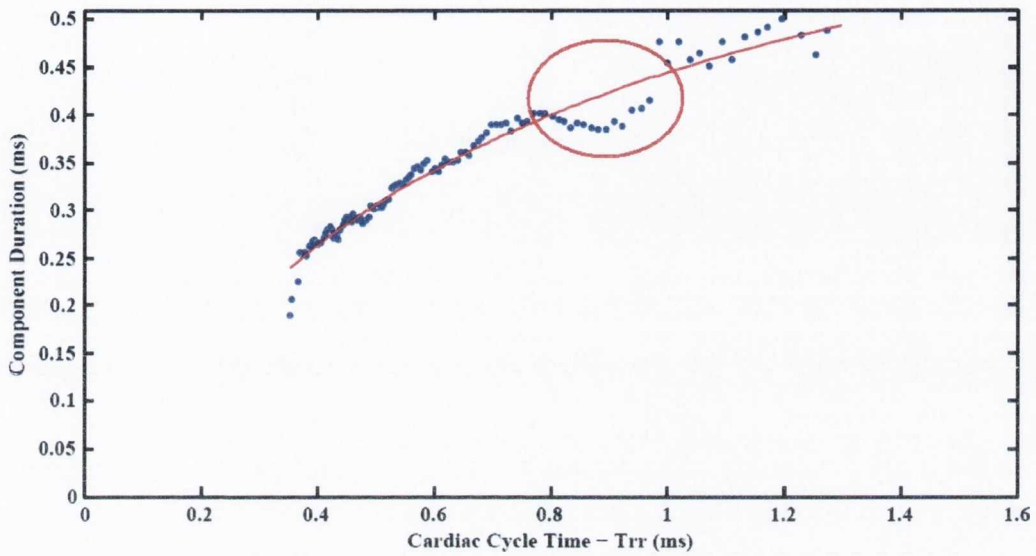

Figure 8.5: The result of averaging all beats into 1-bpm intervals

Note the apparent oscillatory nature of the data highlighted in Figure 8.5. Investigation of the data within the $0.8 \leq T_{RR} \leq 1.0$ range finds that two subjects have over 350 beats of the approximately 900 within this T_{RR} interval whilst other subjects contribute a significantly lower number of beats to the same interval. Consequently two of the subjects dominate the resulting mean QT interval durations within this range, reducing the mean in an inconsistent fashion for the interval shown. Extrapolation over the entire range of T_{RR} and the resulting mean durations for each component of the ECG will be more reflective of the subjects with the highest number of beats than all 21 subjects equally. An alternative method of averaging will overcome this limitation.

8.5.3 Averaging Each Subject Before Collating the Results

If one wishes to argue that they are characterising the duration of the constituent components of the ECG Lead II with respect to cardiac cycle time for all 21 test subjects then each subject should contribute equally to the mean result for any T_{RR} interval. Figure 8.6 shows the results of finding the mean QT interval duration for each subject separately, collating the results for each subject and fitting the second

order equation. At the extremes of heart rate the number of samples available are significantly lower. For example the three samples shown at the lowest cardiac cycle times in Figures 8.4 and 8.5 are the result of just 1 beat each from one subject. Rather than use such a small number of samples to characterise the duration in these regions, each incstance of this shall be removed from the analysis.

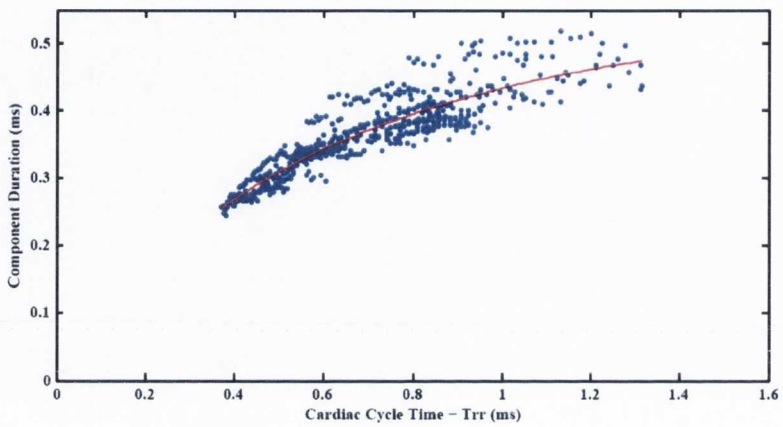

Figure 8.6: The result of averaging each subject at 1 bpm intervals and then collating the results

Figure 8.7 shows the results of a two step averaging process. The first step involves treating each subject individually as shown in Figure 8.6. It is difficult to make a comparison with Figure 8.5 due to the number of subjects in each interval. To overcome this a mean can be calculated for all subject means at each 1 bpm interval as shown in Figure 8.7. Note that the effects of the two dominant subjects as highlighted in Figure 8.5 has been greatly reduced because each subject now only contributes one value to each 1 bpm interval. Now the duration characteristics of each subject's ECG components are reflected evenly in the mean duration for any T_{RR} interval .

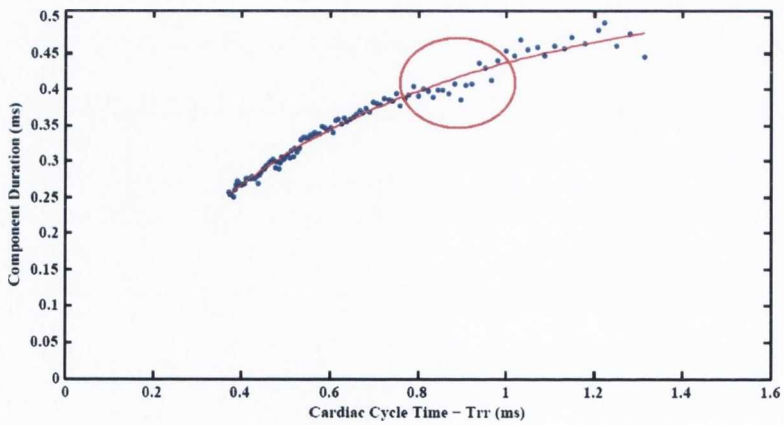

Figure 8.7: The result of collating the mean QT interval duration at 1 bpm intervals and then averaging.

Figure 8.8 shows how averaging all beat results of this study into 1 bpm intervals (like Nasor) or averaging in such a way as to allow each subject contribute one value to each 1 bpm interval (as proposed by author) has an effect on the final resulting fit and hence the characteristic equation for the QT interval. The maximum difference between the resulting QT duration is approximately 16 ms due to the effects of averaging.

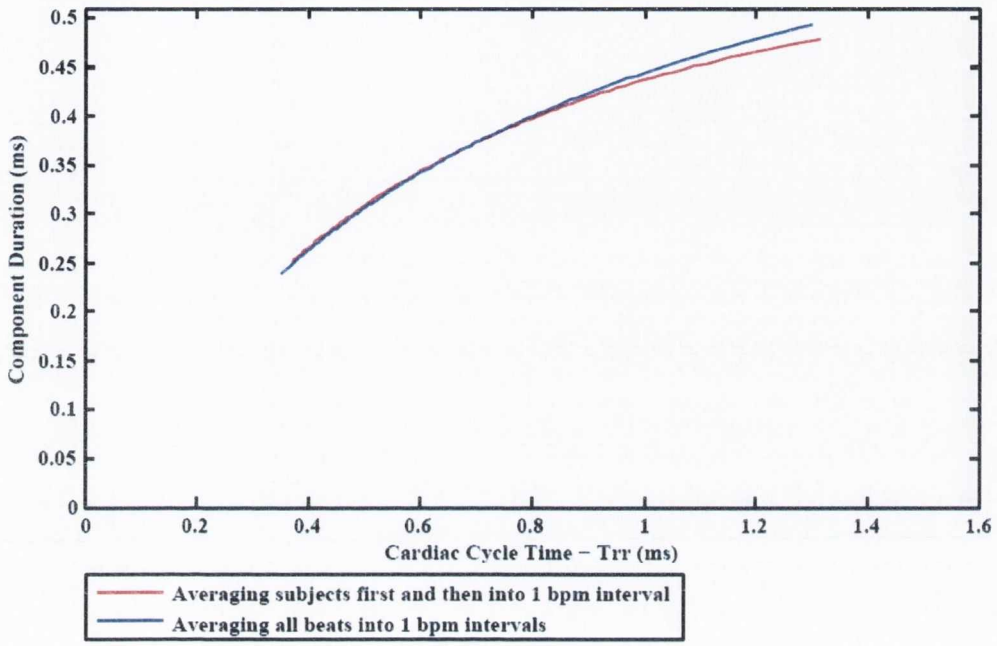

Figure 8.8: Comparing the effects of alternative averaging on the final characterisation of the QT interval duration

One concern with this process is what the effect of taking a mean for each subject individually and then a "mean of means" for all subject means collectively may be. It is possible that when fitting the proposed characteristic equation of the form $A\sqrt{T_{RR}} + BT_{RR} + C$ this two step averaging process may have a significant effect on the result. To investigate this Figure 8.9 shows the resulting equation fit when averaging only by subject and also the fit when finding the mean of all subject's means per interval. The results are shown for each ECG component separately. It can be seen in Figure 8.9 that finding the second mean of the two step averaging process has had very little effect on the resulting characteristic equation fit. The component showing the largest difference between each averaging method, the PQ segment, results in just a 5 ms difference in output duration at the point of greatest difference. To put this in context, at the sampling frequency used for the test data during DTW (273 Hz) this equates to approximately one output sample duration.

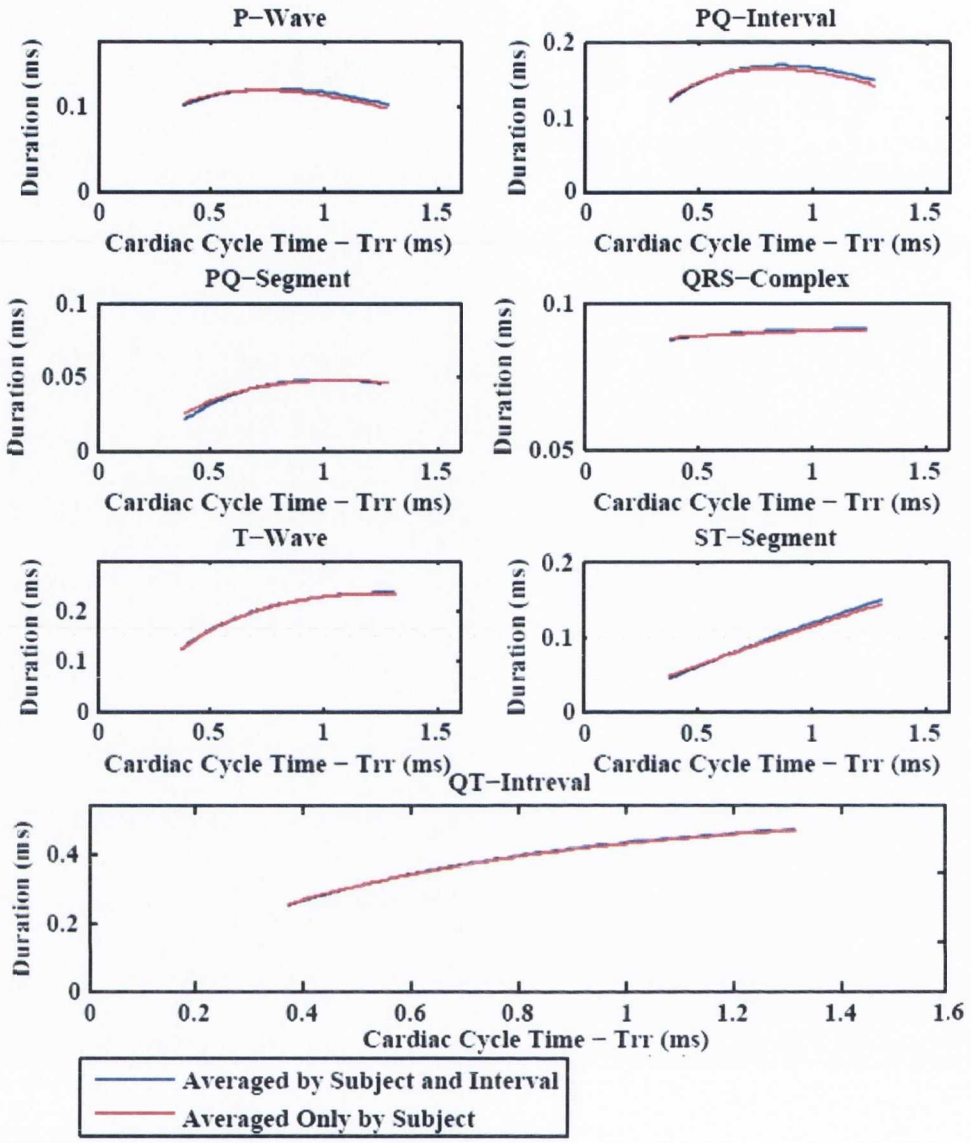

Figure 8.9: The resulting plots with and without averaging each subject in each interval

In summary these findings suggest that taking the average of all beats for all subjects in 1 bpm intervals as done by Nasor et al. does not correctly characterise the variation of the QT interval duration with respect to T_{RR} as it allows a small number of subjects to dominate if they happen to have significantly larger number of beats at a particular cardiac cycle time. To overcome this the mean of each subject's QT interval duration can be found and the results collated. With multiple subjects per 1 bpm interval it is still difficult to see trends in the data or compare the results with the overall averaging method demonstrated in Figure 8.5. It has been demonstrated that finding the mean of all of the individual subject's component means at each 1 bpm interval allows a direct comparison and that averaging at each interval has very little effect on the resulting function fit.

8.6 Mathematical Expressions for the ECG Components

One of the principal objectives of this research is to characterise the relationship between the duration of the constituent waves of a Lead II ECG signal recording with respect to cardiac cycle time or heart-rate. The data has been averaged as discussed in Section 8.5.2 and an equation of the form $A\sqrt{T_{RR}} + BT_{RR} + C$ fit using the least-mean-squares error method available in Matlab. The statistical data for these plots are available in Appendix B.

The following figures show the best fit curve using the second order equation for each of the seven ECG components as defined in Section 8.2. Also included are measures of accuracy for each fit i.e. the coefficient of determination, r^2 and mean squared error, MSE.

8.6.1 The P Wave Duration - T_{PW}

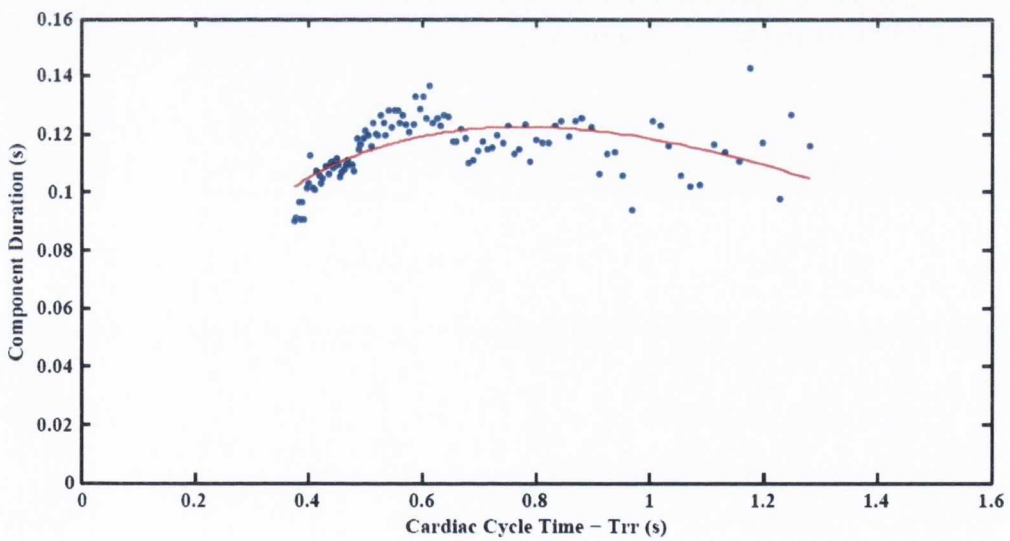

Figure 8.10: Data obtained for P wave duration with second order equation fitted

The equation fit for the P wave duration (s) in Figure 8.10 is:

$$T_{PW} = 0.509\sqrt{T_{RR}} - 0.289T_{RR} - 0.102 \tag{8.1}$$

with $r^2 = 0.359$; MSE = 6.86 x 10^{-5}

8.6.2 The PQ Segment Duration - T_{PQ-Seg}

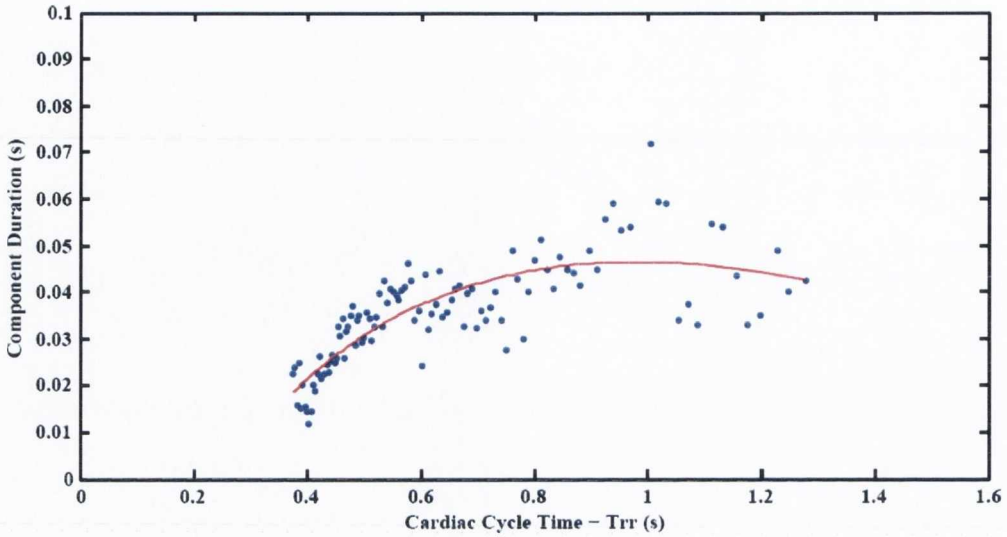

Figure 8.11: Data obtained for PQ segment duration with second order equation fitted

The equation fit for the PQ Segment duration (s) in Figure 8.11 is:

$$T_{PQ-Seg} = 0.390\sqrt{T_{RR}} - 0.197T_{RR} - 0.146 \tag{8.2}$$

with $r^2 = 0.637$; MSE = 4.33 x 10^{-5}

8.6.3 The PQ Interval Duration - T_{PQ-Int}

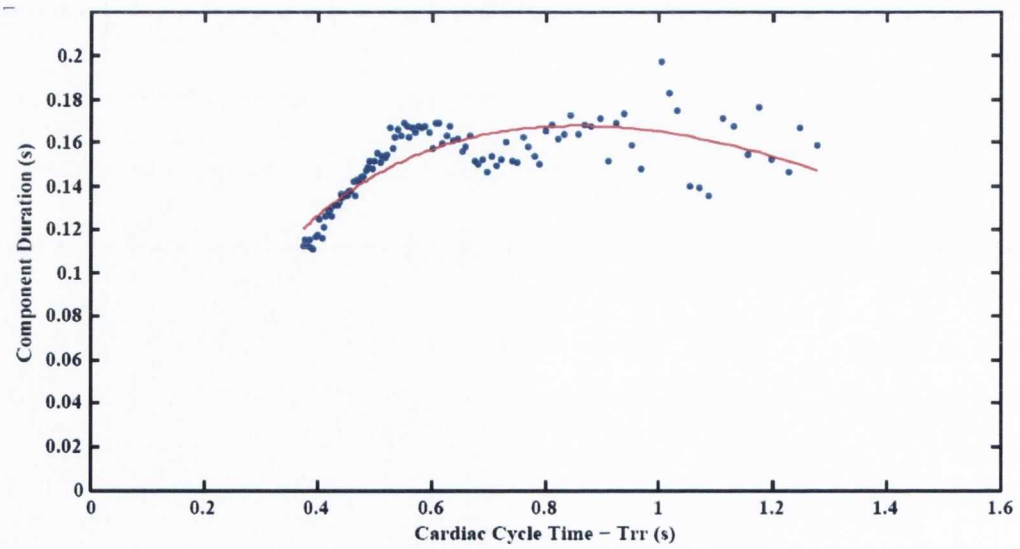

Figure 8.12: Data obtained for PQ interval duration with second order equation fitted

The equation fit for the PQ interval duration (s) in Figure 8.12 is:

$$T_{PQ-Int} = 0.899\sqrt{T_{RR}} - 0.486T_{RR} - 0.248 \tag{8.3}$$

with $r^2 = 0.647$; MSE = 1.09 x 10^{-4}

8.6.4 The QRS Complex Duration - T_{QRS}

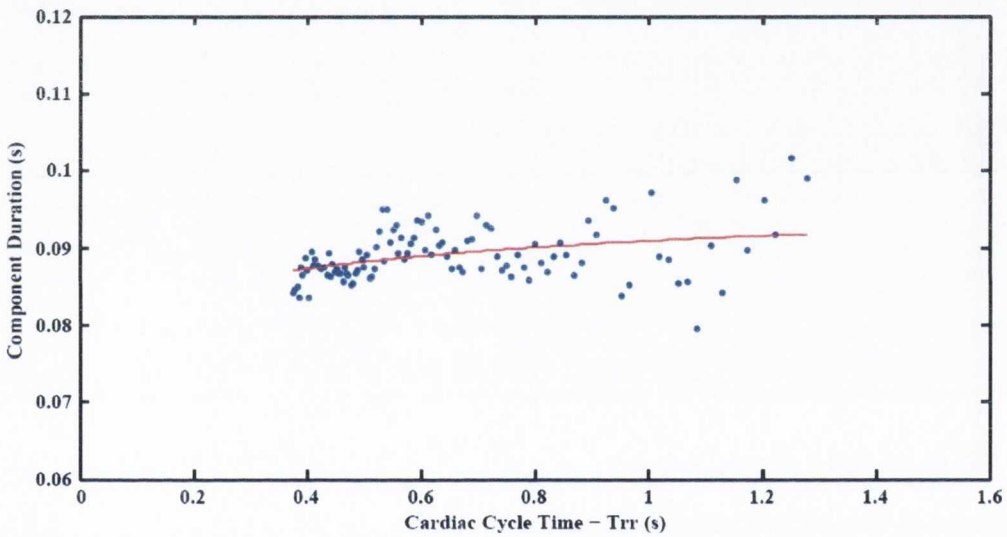

Figure 8.13: Data obtained for QRS complex duration with second order equation fitted

The equation fit for the QRS complex duration (s) in Figure 8.13 is:

$$T_{QRS} = 0.0213\sqrt{T_{RR}} - 0.0069T_{RR} + 0.0765 \tag{8.4}$$

with $r^2 = 0.146$; MSE = 1.08 x 10^{-5}

8.6.5 T wave Duration - T_{TW}

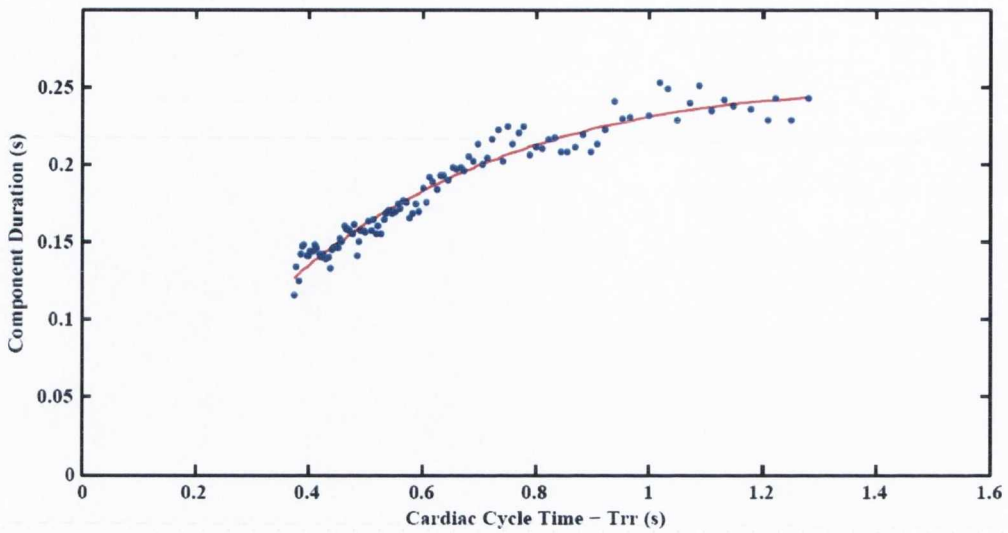

Figure 8.14: Data obtained for T wave duration with second order equation fitted

The equation fit for the T wave duration (s) in Figure 8.14 is:

$$T_{TW} = 0.818\sqrt{T_{RR}} - 0.340T_{RR} - 0.246 \tag{8.5}$$

with $r^2 = 0.949$; MSE = 6.37 x 10^{-5}

8.6.6 The ST Segment Duration - T_{ST-Seg}

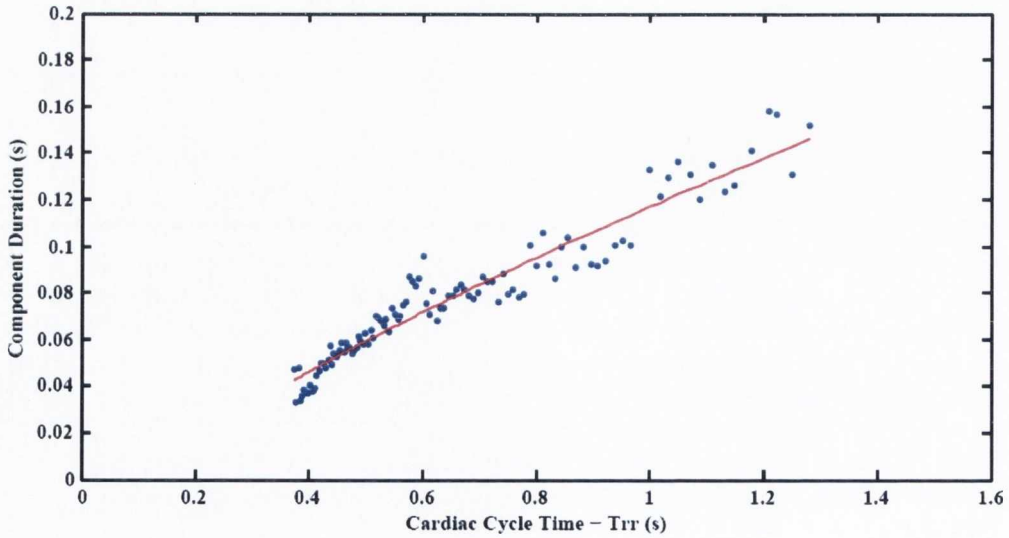

Figure 8.15: Data obtained for ST segment duration with second order equation fitted

The equation fit for the ST segment duration (s) in Figure 8.15 is:

$$T_{ST-Seg} = 0.108\sqrt{T_{RR}} + 0.053T_{RR} - 0.043 \tag{8.6}$$

$$\text{with } r^2 = 0.923 \text{ ; MSE} = 6.35 \text{ x } 10^{-5}$$

8.6.7 The QT Interval Duration - T_{QT-Int}

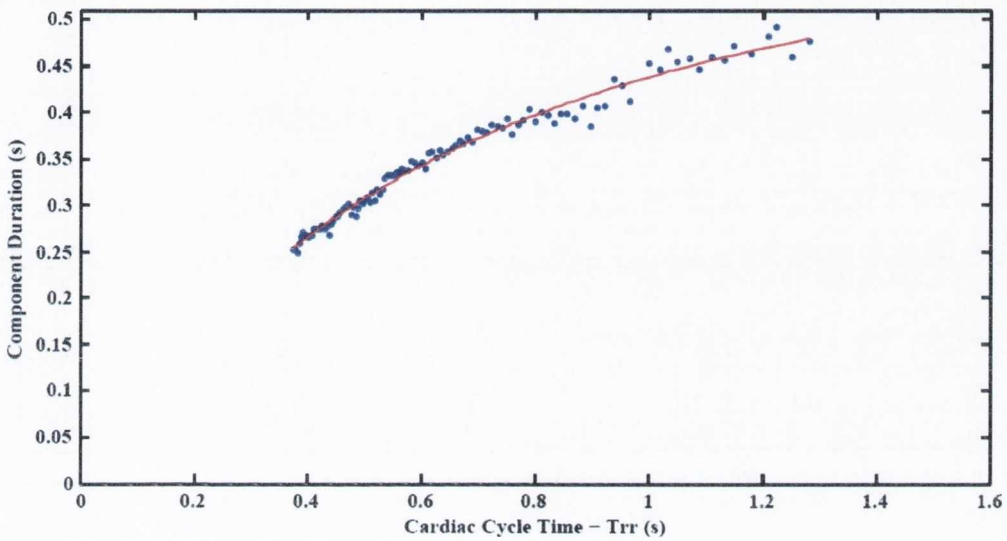

Figure 8.16: Data obtained for QT interval duration with second order equation fitted

The equation fit for the QT interval duration (s) in Figure 8.16 is:

$$T_{QT-Int} = 0.974\sqrt{T_{RR}} - 0.311T_{RR} - 0.225 \tag{8.7}$$

$$\text{with } r^2 = 0.982 \text{ ; MSE} = 7.11 \text{ x } 10^{-5}$$

8.7 Analysis of the Mathematical Expressions for the ECG Components

The accuracy of the derived relationships for the ECG components cannot be established by comparison with any given standard since no one standard or description of the normal durations for each component found in healthy subjects exists. We do, however, have the results of the most comprehensive investigation of these variations to date [10]. The suitability of some of the resulting equations can also be assessed in the context of large clinical studies of the components.

8.7.1 Comparing the Component Equations to the Nasor Study

Investigation of the literature since the latest publication of the finding's in 2004 [10] shows no case of contradiction that the second order equation of the form $A\sqrt{T_{RR}} + BT_{RR} + C$ is the most appropriate for characterising the QT interval duration. It has hence been used in the analysis here.

The resulting coefficients and hence durations for each component reported in Section 8.6 differ significantly than those reported by Burke & Nasor in Equations (5.8) - (5.14), for some of the components as shown in Figure 8.17.

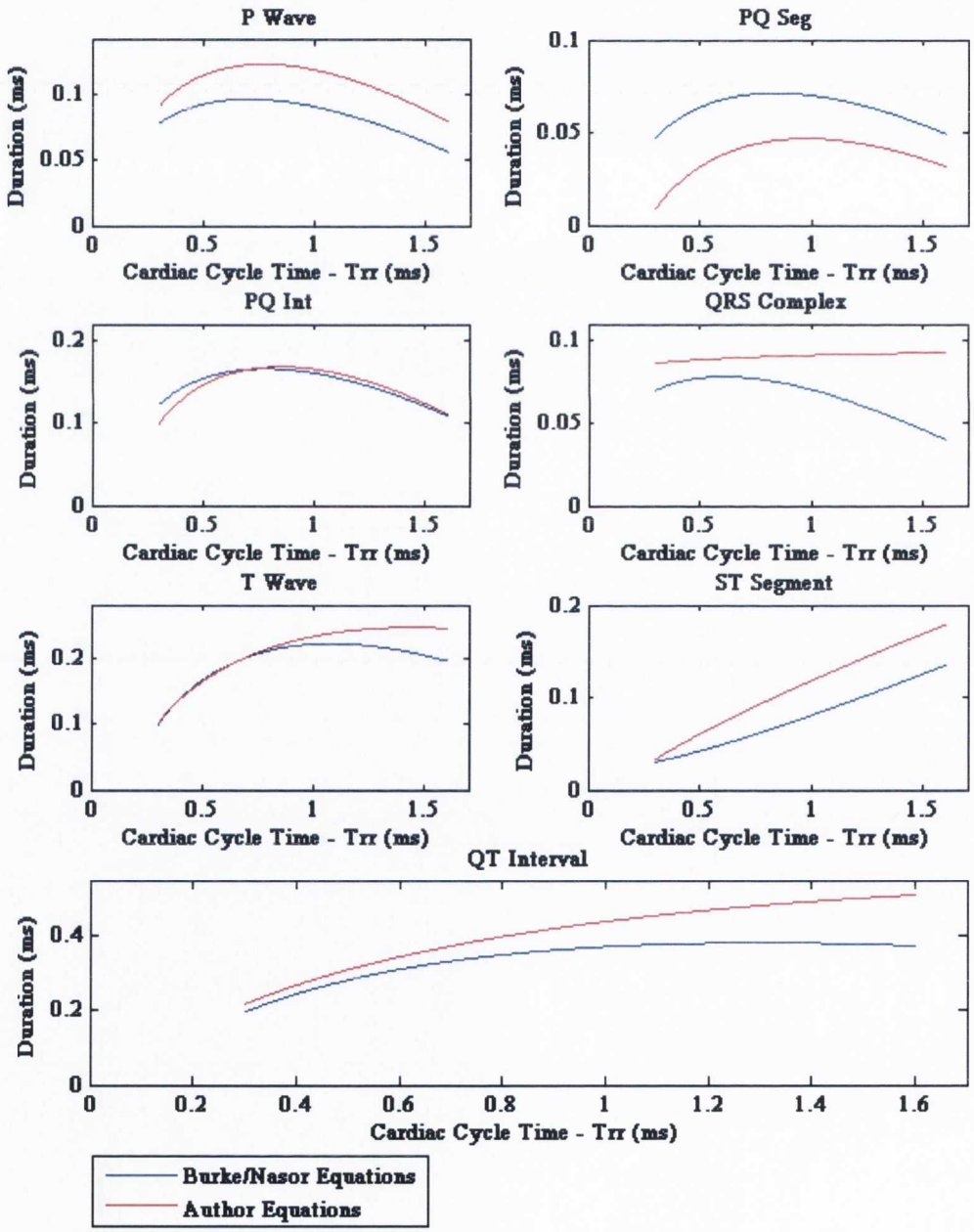

Figure 8.17: A plot of the Burke & Nasor Vs Author equations

As discussed in Chapter 5 the Burke & Nasor equations for both the QRS and QT interval durations do not agree with the results of larger studies. Note in Figure 8.17 how the ST segment equation derived by Burke & Nasor is unusual in that it results in a convex shape for the best fit curve which is the opposite of the other components. It is possible there may have been a systematic error which caused an inconsistency in the ST segment results. By comparison, all of the components result in the same concave type function during the derivation of the duration equations in Section 8.6.

Table 8.1: Fit accuracy measurements

ECG Component	Author r^2	Author MSE	Nasor r^2	Nasor MSE
P-Wave	0.359	6.86×10^{-5}	0.212	8.8×10^{-5}
PQ-Seg	0.637	4.33×10^{-5}	0.607	2.5×10^{-5}
PQ-Int	0.647	1.09×10^{-4}	0.645	6.3×10^{-5}
QRS Complex	0.146	1.08×10^{-5}	0.231	4.1×10^{-5}
T-Wave	0.949	6.37×10^{-5}	0.859	2.0×10^{-4}
ST-Seg	0.923	6.35×10^{-5}	0.649	2.0×10^{-4}
QT-Interval	0.982	7.11×10^{-5}	0.921	2.3×10^{-4}

It would appear from Table 8.1 that the second order equation has resulted in very similar accuracy in terms of the fit of the second order equation (r^2 and MSE) when comparing to the results of this study and those reported by Burke & Nasor. It is interesting, however, that the second order equation is better suited to characterising the QT interval (and the associated T and ST segment) results of this study than those of the wavelet based technique, given the second order equation was chosen based on its appropriateness in characterising the QT interval as discussed in Chapter 5. More significantly, the trend of the resulting equation for the QRS and QT interval with respect to heart rate, the two component equations derived by Burke & Nasor which are not in keeping with other studies of the components, are very different according to the authors equations. To actually measure the "correctness" of the newly derived equations as opposed to the existing ones the results of the mathematical expressions must be placed in a clinical context.

8.7.2 Comparison of Results with Clinical Research

8.7.2.1 The P Wave, PQ Segment and PQ Interval

A significant amount of research has been conducted in an effort to create "P Wave Indices" or a metric that can be used to measure the normal and abnormal durations of the P wave [120]. P wave dispersion or the difference between the maximum and minimum P wave durations observed in the same subject over a short period of time can be significant. The dispersion or variation in the duration of the P wave has been reported to be influenced by various phenomena including the season during which the recording was performed [121] and circadian body rhythm observed in a 24-hour cycle [122]. The mean P wave duration indices found in the literature are therefore varied and range from 96±11.0 ms [123] to over 120 ms [124]. The measurements and resulting P wave duration equation (8.1) reported in this study can therefore not be compared to any one metric but do not differ significantly from the results of the cited works.

The duration of the PQ segment is typically considered to have little clinical significance [2] and therefore indices for normal durations have not been found in the literature.

Due to the issues surrounding P wave duration and the PQ segment's lack of clinically significant information, the PQ interval is the characteristic most frequently used to assess the physiological state of the right atrium, atrial muscle fibres, atrioventricular node and the 'Bundle of His'. It is commonly accepted that a normal PQ interval duration ranges from 120-200 ms [17]. Observation of Figure 8.12 shows that the data and the fitted equation (8.3) for the PQ interval reflect the normal duration characteristics for the interval. Note that the limit of the maximum PQ interval imposed on the data in Section 8.4 was intentionally relaxed at 220 ms (as opposed to 200 ms which is the approximate maximum normal duration) in order to ensure that only significant and obvious errors were removed from the duration results. It can be seen in Figure 8.12 that the mean PQ interval duration never exceeds 200 ms which confirms that the majority of data remained within the clinically defined limits and significantly below the PQ interval limit.

Although its relationship to heart rate is not as clearly defined in the literature as the QT interval (it is not commonly considered to be as highly correlated), it is stated that shortening at higher heart rates i.e., stress testing > 80 bpm, can be expected

when compared with a rest state i.e. 60-80 bpm [125]. It can be observed in Figure 8.12 that the PQ interval duration as defined by equation (8.16) is shortest for higher heart rates of $>$ 80bpm.

8.7.2.2 The QRS Complex

The QRS Complex, which is the most readily observed component of the ECG signal is typically at its tallest in Leads I and II and is one of the reasons why Lead II is most commonly used in clinical diagnosis. There is a very wide range of normality for the QRS complex in terms of shape and duration. Its duration is highly variable due to the fact that the QRS complex may not actually posses a Q wave preceding the R peak nor any significant S wave following it depending on the individual subjects QRS complex type. It is typically expected that a normal QRS complex duration will not exceed 120 ms [17].

The relationship between heart rate or T_{RR} and QRS duration has been the focus of other researchers, such as a study of 150 males by Blackburn and Simonson [53], 42 subjects by Nakagawa et al. [54] and also in a comparison of healthy and unhealthy subjects by Ge et al. [52]. Each of these studies reports an inverse relationship with heart rate i.e. the lower the heart rate or higher the T_{RR} the longer the QRS duration among healthy subjects. In Chapter 5 it was demonstrated how Equation (5.11) did not provide QRS durations which coincide with the findings of these other studies. Figure 8.18 is a plot of the Burke & Nasor Vs Authors equation for QRS duration.

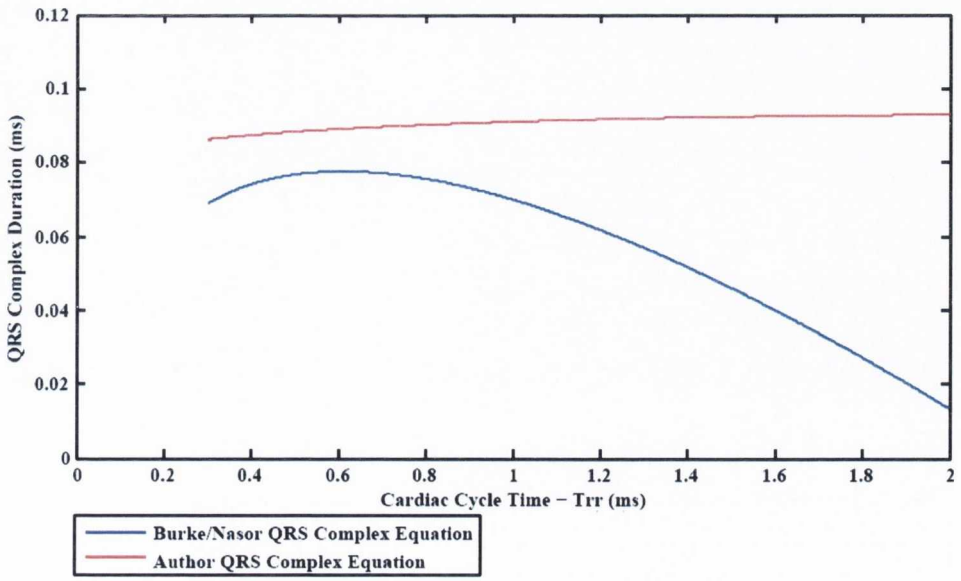

Figure 8.18: A plot of the Burke & Nasor Vs Author equation for QRS complex

Observation of Figure 8.18 and the author's derived equation (8.4) for T_{QRS} lies within the clinically defined bounds for QRS duration and its variation with respect to heart rate. The duration of the QRS complex increases with a decreased heart rate and does not exceed the expected duration of a healthy QRS complex waveform.

8.7.2.3 The T Wave, ST Segment and QT Interval

The QT interval duration which is essentially the sum of the QRS Complex, ST segment and T Wave duration is considered the ECG component of greatest diagnostic value. It is also the component which is most closely correlated with heart rate where the rule of thumb for the QT interval is "the faster the heart rate the shorter the QT interval" [2] (page 279). When used by a clinician the QT interval is typically corrected for heart rate using a correction equation, such as the most popular equation proposed by H.C. Bazett [17]:

$$QT_c = \frac{QT}{\sqrt{T_{RR}}} \tag{8.8}$$

It is widely accepted that the normal corrected QT interval duration ranges from 350-440 ms [2, 17, 51] which equates to an uncorrected QT interval of approximately 200-540 ms. Short QT intervals can indicate many illnesses such as Hypercalcaemia and Digitalis, while longer QT intervals can indicate acute myocardial infarction and cerebral injury.

One of the major limitations of the QT interval Equation (5.12) as proposed by M. Nasor is the apparent inconsistency of the equation when extrapolated outside the original 46-184 bpm range of data from which the equation was derived. Below a heart rate of 46 bpm or above a cardiac cycle time of 1.30 (s) the resulting QT interval duration begins to reduce as predicted by Equation (5.12). This is in contradiction to the clinical definition of the relationship that would suggest that Equation (5.12) does not characterise the QT interval duration adequately.

A valid comparison of the accuracy of the authors derived Equation (8.7) and the Burke & Nasor Equation (5.12) for the QT interval duration with a larger clinical definition can be performed using the study conducted by Goldenberg et al. [51] on 581 healthy subjects as introduced in Chapter 5. The plot shown in Figure 8.19 is based upon the figure provided by Goldenberg for estimating normal QT interval durations. Also sketched onto the figure is the approximate output duration using both the authors new equation (Shorten QT Interval Duration) and the Burke & Nasor equation

(Nasor QT Interval Duration). Note that the data for the figure originally created by Goldenberg is unavailable so the results for the Shorten and Nasor equations are manually sketched to the figure. The figure clearly shows the contradictory behaviour of Equation (5.12) when extrapolated for cardiac cycles times of greater than 1.30 seconds.

The figure also shows that Equation (8.7) provides a significantly better correlation with the study performed by Goldenberg over a much larger dataset. Equation (8.7) does slightly exceed the bounds of the "Normal" region at lower cardiac cycle times but the difference here is negligible when one considers the acceptable deviations in expert annotations as outlined in Chapter 6 and the fact that the equation has been derived on a dataset of 21 subjects as opposed to 581.

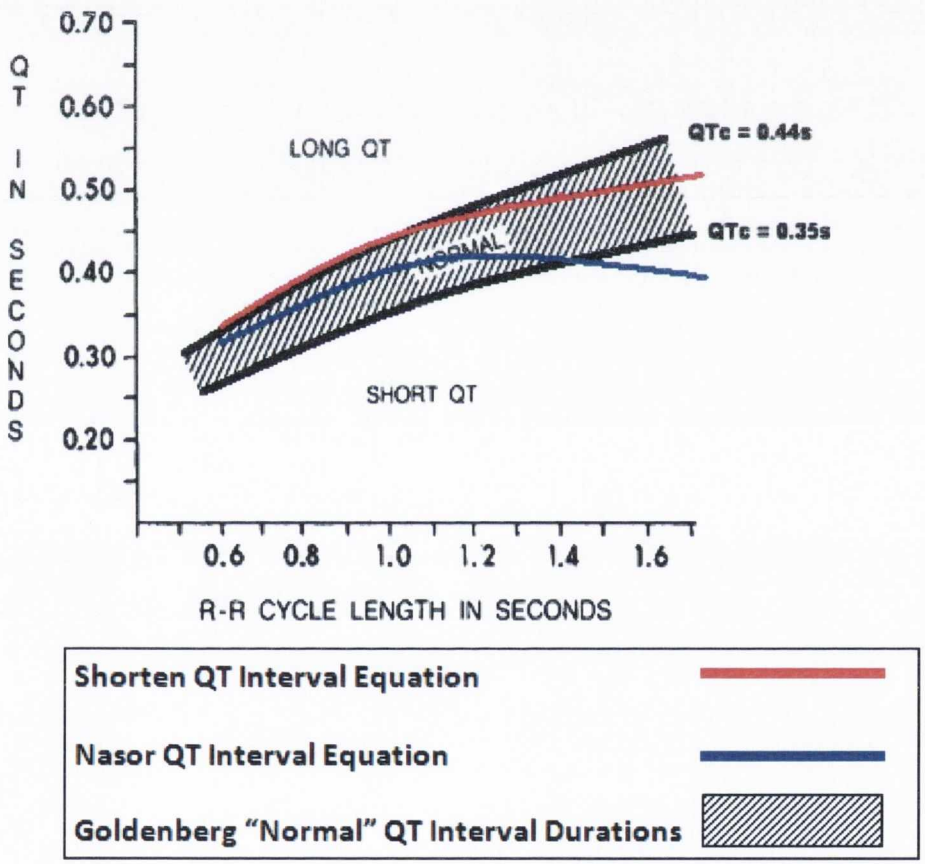

Figure 8.19: Comparing QT interval equations to the Goldengberg clinical Study

For further comparative purposes Figure 8.20 is a more accurate plot of the QT interval equation derived by Burke & Nasor Vs the authors equation for QT interval. The contradictory behaviour of the QT interval equation as derived by Burke & Nasor has been removed and a more consistent variation with respect to cardiac cycle time or

heart rate is observable using the authors equation. This figure also demonstrates the the difference between the two equations is due primarily to different duration results for the QT interval using DTW and those of the wavelet based method.

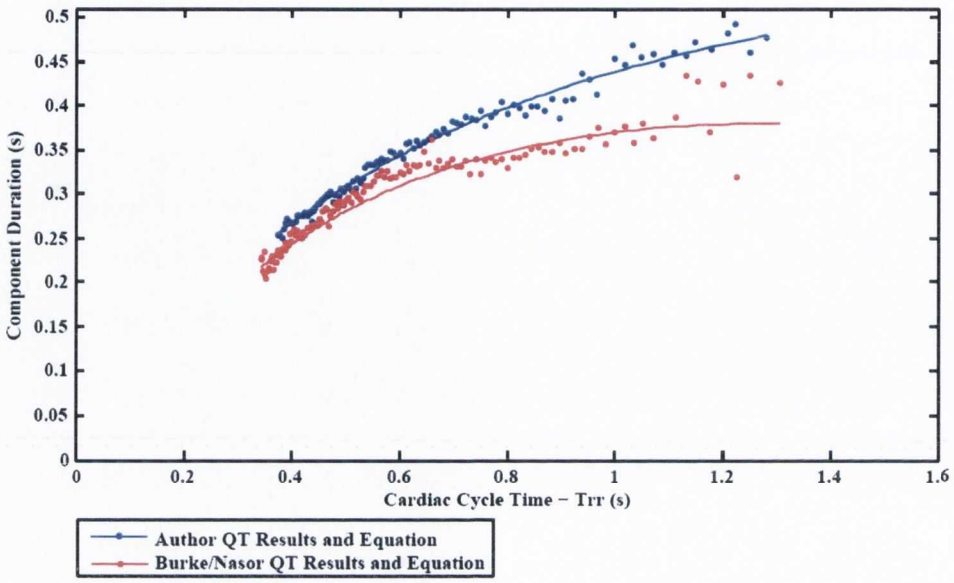

Figure 8.20: Burke & Nasor Vs Authors equation for QT interval duration

8.7.3 Conclusion

The resulting duration equations have been compared to those proposed by Burke & Nasor. The same form of equation has been used to characterise the timing characteristics of each ECG component with respect to heart rate in this study because it has been proven to represent QT interval duration more accurately than any other [10]. In terms of suitability of the function to adequately characterise the duration data i.e. r^2 and MSE the equations proposed in this study provide a better fit than in Nasor's study for the T wave, ST segment and QT interval, with similar results for the other components. This would imply that the measurements for the variation of each component's duration with respect to cardiac cycle time and heart rate found in this study are better characterised by the newly derived equations than those derived from the wavelet based study.

For the P wave, PQ segment and PQ interval durations the results of clinical literature have been examined and although no specific indices exist for the estimation of normal P and PQ segment duration the derived equations appear to be within the expected range. The definition of a normal PQ interval duration range, is more clearly defined in the clinical setting and the derived second order equation (8.3) characterises

this range appropriately.

The QRS complex equation (8.4) results in QRS durations which are within the clinically accepted bounds for normal QRS duration. The resulting QRS duration also varies with respect to T_{RR} in a fashion consistent with the findings of a number of larger epidemiological studies unlike the original equation derived by Burke & Nasor.

The duration of the QT interval is the single most diagnostically significant component of the ECG lead II signal. Comparison of the QT interval equation derived by Burke & Nasor with the clinically accepted correlation between QT interval and T_{RR} shows a significant error in the characterisation of the component. By contrast the newly derived equation shows a consistent relationship between heart rate and QT interval duration as defined by cardiology experts. The new equations should be used in conjunction with the signal generator to increase the accuracy and suitability of the instrument.

Chapter 9

Conclusion

The objectives of the research reported in this thesis can be summarised as follows:

- To create a fully tested and accurate programmable ECG signal generator.
- To select and improve a suitable ECG analysis technique to delineate the signal.
- To characterise the variation of the ECG constituent components adequately.

During the course of this research and as reported in this thesis the author believes that each of these objectives has been met to an acceptable standard, and as such represents a genuine contribution to this field of research.

9.1 The ECG Signal Generator

It is the author's belief that any ECG model to be used to generate a test signal is only as useful as the instrument which delivers it to the ECG machine. From the literature review of ECG signal generators over the last two decades the technical limitations and issues regarding the suitability of past and current instruments have been identified. The instrument presented by the author has addressed the technical limitations using an increased and consistent bit resolution and a novel architecture at the output stage of the device which attenuates the output signals after D/A conversion while also allowing complete variability of the constituent wave amplitudes. Moreover, not found previously in the literature, a comprehensive approach to rigorously testing the device has been taken. A comprehensive analytical model of voltage noise, offsets and temperature effects has been created and instrument performance verified by stringent electrical testing of the device. The result is a unit providing a true differential signal

with complete variation of the heart rate range in 1 bpm intervals and independent variation of P, QRS and T wave amplitudes. Beyond the purely technical improvements to the instrument significant thought has been given to the user of such a device. Rather than being a cumbersome device that requires effort to alter the output signal the instrument is fully controllable using a colour touch screen which can also be used to view a representation of the output test signal.

9.2 Characterisation of the Constituent Waves

It has been discussed in this research that one of the core characteristics used to form a diagnosis based on the ECG signal is through observation of constituent wave profiles and durations. As such any model or test ECG signal must reflect the variation of these durations as per *in vivo* signals. Significant research has been conducted in both the clinical and scientific setting to establish measures of normal and abnormal metrics for constituent component durations. It was found upon review of the literature that previous characterisation of the constituent component durations used as part of a synthetic test signal do not correlate correctly with the findings of larger clinical studies.

An alternative method of delineating the constituent components of the ECG signal via identification of the onset and termination points was sought. The author has shown that a suitable method was found in the Dynamic Time Warping (DTW) algorithm. Significant investigation of the various forms of the DTW algorithm has been performed and the value-based DTW algorithm chosen as the most suitable. The author has proposed and verified two improvements of the value-based approach to DTW by composite normalisation and using a multi-feature time domain based classifier to find the most accurate match between template reference signals and the query signal under investigation. The performance of the complete algorithm was verified in the most suitable fashion available, which is by comparison to standard deviations found within cardiologists annotation of ECG signals.

The complete process was used to establish the onset and termination points in a database of test signals previously used to characterise the component durations. In a comprehensive study of this same database previously by Burke & Nasor using a wavelet based method of characterisation the results have been shown to present some significant limitations when placed in the context of larger clinical studies. The author

has created a new set of duration equations of the same form as those used by Burke & Nasor but using the results of characterisation of the database by the DTW algorithm. The new duration equations show a significantly better correlation to the established metrics for component durations found in clinical literature. The ECG signal is the most commonly used form of Cardio-diagnosis in the world. Therefore, the author believes that increased accuracy both in terms of synthesis and delivery of an ECG test signal as reported in this thesis represents a genuine contribution to society.

9.3 Future Work

The author believes the research reported here provides a significant contribution to the field of biomedical instrumentation, ECG signal processing and ECG signal synthesis. However, time limitation prevented the author from further exciting research which could increase the usefulness of the results presented here.

Firstly, the ECG signal generator could be extended to generate all 12 test leads as opposed to the single Lead II ECG signal. To fully benefit from the addition of these test signals, however, time characterisation of the waves as observed in the other leads would be required. The same procedure using DTW could be applied if a large enough cohort of 12 lead signals could be sourced. The choice of the PIC24F chip and its associated architecture also allows the device to be easily connected to a wireless network via the PMP which could further improve its usefulness.

The time characterisation presented by the author has been aimed at realistic synthetic signal synthesis for test and calibration. If the cohort of adequate test signals available was larger than the one used, perhaps more clinically profound conclusions regarding component duration variation could be made. However, this kind of research would require a significant amount of time to be spent firstly in the acquisition of the signals and then in the analysis. The P wave duration for example is considered to have some clinical importance but at the same time no definitive metrics for its duration have been found in the literature, and definitions of normality and abnormality seem to vary significantly. The P wave amplitude and relatively short duration combined make it the component most susceptible to noise and its duration is thought to vary hourly and seasonally [121] within the same subject. The author has observed this variation and difficulty as reflected by the deviations found in the P wave duration reported in Appendix B. Calls have been made in the literature for a more comprehensive study

of P wave duration and the author would like to see what effects this may have on the resulting time characterisation.

Finally, it was found during the review of ECG modelling that research has been conducted into morphological modelling of the ECG signal. A versatile and fully controllable morphological model of the signal amplitude combined with the author's duration equations would be most useful. The core benefit of such a model is the ability to generate realistic ECG morphologies, without the noise associated with recording noise and artefacts. The spectral content of the synthetic signal is known precisely, hence after recording the test signal via the instrument under investigation, noise can be attributed to the recording instrument or environment. Ideally this allows the user to identify what stage in the recording process is distorting the signal and to investigate why. This type of analysis is not possible using rerecorded signals since they already contain a degree of unmeasurable distortion.

There are a number of existing models which use Gaussian pulses to mimic the shape of the P, QRS and T waves. Investigation of the models to date has left the author questioning whether or not the Gaussian pulse is the most suitable function to use or if another function may be better suited to certain components. The author suggests that other functions could be explored for each constituent wave such as the raised cosine for the P wave which would reflect the continuous shape at its onset and termination points, a set of hyperbolic functions e.g. $\frac{1}{2}[1 + tanh(t)]$ for the QRS complex or a function that can adequately reflect the asymmetrical shape of the T wave such as the exponential function shown in Figure 9.1.

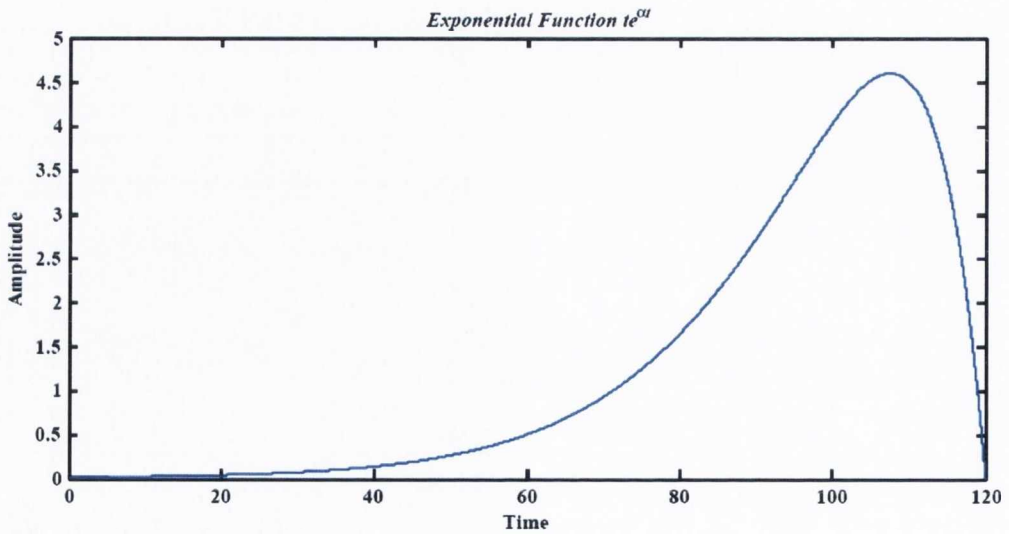

Figure 9.1: The asymmetric shape of this function is similar to that of a Lead II T wave

This is to name but a few alternative functions, the author suspects there are many different functions worth investigating and would propose this as an objective for another PhD research project. The author also proposes that very subtle differences between the ECG signal under analysis and the trigonometric template commonly being used for characterisation could be overcome using DTW to provide a better fit. The effects of this DTW on the resulting model could be analysed in the frequency domain to see if it has a profound effect on the known spectra of the template function. If not then the resulting model may be most useful.

9.4 Reference Test Signals

The author has used one of the largest and most frequently referenced database of signals as templates for the DTW process i.e. the PhysioNet QT database of ECG signals. However, there are a number of issues surrounding this database. Firstly, the sampling frequency used for the signals is just 250 Hz which is now in contravention of the required sampling rate as defined in the standards for diagnostic ECG recording which should be at least 500 Hz [126]. The author believes that the accuracy of the DTW process has been limited by this low sampling rate, given that an error in the location of a fiducial point of 1 sample equates to a 4 ms error. The quality of some of the signals which were annotated and used in the database were also quite poor and hence some of the original 719 signals used for test were removed and not used as reference signals in the characterisation of the Burke & Nasor database. Some annotations of the signals are also incomplete in that they do not contain a T wave onset annotation. A complete, accurate, and properly sampled database of test signals would be hugely beneficial to the field of ECG signal processing and analysis. Although this would be a massive undertaking and would require significant resources to achieve the author believes it would be a worthwhile exercise and indeed is a little surprised that it has not already been undertaken or made available.

Appendix A

QRS Classification Code

In this Appendix the Matlab code for the initial classification of the QRS complexes into their respective groups is provided. The code can be altered by the user empirically by changing the thresholds which determine the location of the up and down slopes of the QRS complex.

Classifying The QRS Morphology Mat Lab Code

```
[peak_val,peak_loc] = max(input_signal); %Find the peak in the beat
window_back = peak_loc-10;

      %These variables can be changed empirically by the user if the
      %algorithm is not working correctly;

s_distance = 20;
      %This is the maximum distance from the R peak one would expect
      %to find the     %end of the QRS down slope or start of the S
      %wave.

s_term_distance = 35;
      %Another variable that can be changed. It is a limit on how
      %far the end of an S wave can be from the R peak, some S waves
      %are longer than others.

      %Remove any extra points that might be at the end of a signal
      %as a result of how they are stored in the signal arrays.
pt=1;
flag=0;

while((pt<length(input_signal)-2) &&
      input_signal(pt)~=input_signal(pt+1) &&
      input_signal(pt+1)~=input_signal(pt+2))
      pt = pt+1;
end;

remove = input_signal(1:pt);
clear input_signal;
input_signal = remove;

if(window_back>20)

      % An error check to make sure a full beat has been passed to
      %the algorithm the input signal is approximated using the SAPA
      %approximation algorithm. This is intended to denoise the
      %signal as the purpose of this classification function is
      %to find trends in the  data.
      ansapprox = sapa(input_signal,0.005);
      approximation = ansapprox(1,:);

      %Find the difference between each adjacent sample in the
      %signal.
      derivative(2:length(approximation)) = diff(approximation);

      %These lines of code find max and min differences on the up
      %and down slope of the QRS complex.
      [max_up_val,max_up_loc] = max(derivative(1:peak_loc));
      [max_down_val,max_down_loc]
      =min(derivative(peak_loc:peak_loc+40));
      max_down_loc = peak_loc+max_down_loc-1;
```

```
%This loop finds a point at which the differences are reducing
%i.e. near to the beginning of the QRS upslope. The "flag"
%allows for glitches in the signal i.e. notches on the QRS
%which are not actual inflection points.
pt=max_up_loc;
flag=0;
counter=0;
while((derivative(pt-1)>(0.2*mean(derivative(pt:max_up_loc))))
||flag==0)
      pt = pt-1;
      if(derivative(pt-
      1)<(0.2*mean(derivative(pt:max_up_loc))))
            counter=counter+1;
            if(counter==1)
                  possible_end = pt;
            end;
      end;
      if(counter==2)
            flag=1;
      end;
end;

%The end_point_of_derivative represents a point at which the
%differences changed due to an inflection in the signal.
end_point_of_derivative = possible_end-1;

%We find the minimum amplitude value in this region and save
%it as a "tail_loc" or possible Q wave trough.
[tail_val,tail_loc] =
min(input_signal(end_point_of_derivative-
2:end_point_of_derivative+2));
tail_loc = find(input_signal==tail_val);

%Find the maximum amplitude point in this region, if a Q wave
%exists this will be the onset of it.
[max_val_front,max_val_front_loc] =
max(input_signal(tail_loc-    5:tail_loc));
max_val_front_loc = max_val_front_loc+tail_loc-5-1;
front_difference = input_signal(max_val_front_loc)-
input_signal(tail_loc);

%The possible onset and minimum inflection point of a Q wave
%have been found. Now the same must be found for any S wave
%that may exist in the signal.

%max_down_loc is the minimum derivative on the QRS down slope.
pt=max_down_loc;
flag=0;
counter=0;
possible_end=0;
over_flow=0;

%This loop searches for a point where the difference between
%two successive points may turn positive again i.e. as the S
%wave returns to near iso-electric zero. The other constraints
%on the loop are as follows:
%"flag": again allows for glitches in the signal i.e. notches
%on the QRS which are not actual inflection points.
```

```
%"over_flow": It is possible that there is no return to a
%after the QRS down slope reaches its minimum point i.e. no S
%wave. To account for this a limit of 10 samples (40ms if
%fs=250 Hz) allowed to search for an S wave.

while(((derivative(pt)<0) ||  flag==0)  && (over_flow<10))
      pt = pt+1;
      if(derivative(pt)>0)
            counter=counter+1;
      if(counter==1 || ((pt-possible_end)>2) )
          possible_end = pt;
      end;
      end;

      if(possible_end ~= 0)
            over_flow = over_flow+1;
      end;

      if(counter==2)
            flag=1;
      end;
end;

%A possible inflection point or end of the QRS downslope has
%been found.
      end_point_of_derivative = possible_end-1;
%Again the region is searched to find the actual minimum
%amplitude i.e. trough of the S wave.
[back_tail_val,back_tail_loc] =
min(input_signal(end_point_of_derivative-
2:end_point_of_derivative+2));
back_tail_loc = find(input_signal==back_tail_val);

%An error check to ensure the search of an S wave trough has
%not found a point so far from the R peak that it is not
%actually an S wave.
if((back_tail_loc-peak_loc)> s_distance)
      [back_tail_val,back_tail_loc] =
      min(input_signal(peak_loc:peak_loc+12));
      back_tail_loc = back_tail_loc + peak_loc -1;
end;

%With the minimum or trough of the S wave having been found
%the  region is searched for the end of the S wave i.e. a
%return to near isoelectric zero.
pt= back_tail_loc+1;
stop_flag = 0;
counter=0;
candidate_point = pt;
while(stop_flag==0)

      if(derivative(pt+1)<(0.25*
      mean(derivative(back_tail_loc+1:pt))))

          if(pt>candidate_point+2)
              counter=0;
          end;
```

```
            if(counter==0)
                candidate_point=pt;
            end;
            counter=counter+1;

            if(counter==2)
                stop_flag=1;
            end;
        end;
        pt=pt+1;
end;
pt= candidate_point;
back_peak_val = max(input_signal(pt-1:pt+1));
max_val_back_loc = find(input_signal==back_peak_val);

if((max_val_back_loc-peak_loc)>s_term_distance)
        [max_val_back,max_val_back_loc] =
        max(input_signal(back_tail_loc:back_tail_loc+5));
        max_val_back_loc = back_tail_loc+max_val_back_loc-1;
end;
back_difference = input_signal(max_val_back_loc) -
input_signal(back_tail_loc);

%If the difference between the trough and max value of the Q
%and S waves is <0.03 volts (R peaks have been normalized to
%1V before this process) then there is considered to be no Q
%or S wave respectively.
if(front_difference>0.03)
        front_tail_flag = 1; %There is a Q wave.
else
        front_tail_flag=0;  %There is no Q wave.
end;

if(back_difference>0.03)
        back_tail_flag = 1; %There is a S wave.
else
        back_tail_flag=0;   %There is no S wave.
end;

%Depending on the type of wave i.e. QRS , QR-no S e.t.c. a
%class type is assigned. The location of the Q wave onset or S
%wave termination is also saved as they can be used later to
%window around the QRS complex.

if(front_tail_flag==1 && back_tail_flag==0)
%Class 1 has a QR but no significant S wave.
        class_type=1;
        class_type(2,1) = max_val_front_loc;
        class_type(3,1) = back_tail_loc+3;
%Increased by +3 samples to ensure all of QRS is included if
%windowed later.

elseif(front_tail_flag==0 && back_tail_flag==1)
        %Class 2:Q but no S wave found
        class_type=2;
        class_type(2,1) = tail_loc-3;
        class_type(3,1) = max_val_back_loc;
```

```
        elseif(front_tail_flag==1 && back_tail_flag==1)
        %Class 3: Full QRS
                class_type=3;
                class_type(2,1) = max_val_front_loc;
                class_type(3,1) = max_val_back_loc;
        else
                class_type=0;%No Q or S waves apparent.
                class_type(2,1) = tail_loc-3;
                class_type(3,1) = back_tail_loc+3;
        end;

else
%An error catcher if the beat is not a complete one i.e. no p wave
%class type is -1
        class_type=-1;
        class_type(2,1) = 0;
        class_type(3,1) = 0;
end;
```

Appendix B

Statistical Data for Component Results

In this appendix the data for the subject means which are averaged and plot in Figures 8.10 to 8.16 are provided. The data shows the mean and standard deviation of each subjects mean sorted into 1-bpm intervals.

Mean of all Subject Component Durations When Averaged into 1-bpm Intervals

Trr (s)	HR(bpm)	$T_{PW\ (s)}$	$T_{PQ\text{-}Seg(s)}$	$T_{PQ\text{-}Int(s)}$	$T_{QRS(s)}$	$T_{TW(s)}$	$T_{ST\text{-}Seg(s)}$	$T_{QT\text{-}Int(s)}$
1.277	**47**	0.116	0.054	0.158	0.099	0.243	0.152	0.467
1.250	**48**	0.127	0.040	0.167	0.102	0.228	0.130	0.460
1.224	**49**	0.098	0.049	0.146	0.092	0.243	0.156	0.492
1.200	**50**	0.117	0.035	0.152	0.096	0.228	0.158	0.482
1.176	**51**	0.143	0.033	0.176	0.090	0.235	0.141	0.464
1.154	**52**	0.111	0.043	0.154	0.099	0.238	0.126	0.472
1.132	**53**	0.114	0.054	0.168	0.084	0.242	0.124	0.456
1.111	**54**	0.116	0.055	0.171	0.090	0.235	0.135	0.459
1.091	**55**	0.103	0.033	0.135	0.080	0.251	0.120	0.447
1.071	**56**	0.102	0.037	0.139	0.086	0.239	0.130	0.458
1.053	**57**	0.106	0.034	0.140	0.085	0.229	0.136	0.456
1.034	**58**	0.116	0.059	0.175	0.088	0.249	0.129	0.468
1.017	**59**	0.123	0.059	0.182	0.089	0.253	0.121	0.447
1.000	**60**	0.125	0.072	0.197	0.097	0.232	0.133	0.454
0.984	**61**	-	-	-	-	-	-	-
0.968	**62**	0.094	0.054	0.148	0.085	0.230	0.100	0.412
0.952	**63**	0.106	0.053	0.159	0.084	0.230	0.102	0.429
0.938	**64**	0.114	0.059	0.173	0.095	0.240	0.101	0.437
0.923	**65**	0.113	0.055	0.169	0.096	0.222	0.093	0.408
0.909	**66**	0.106	0.045	0.151	0.092	0.213	0.092	0.406
0.896	**67**	0.123	0.049	0.171	0.094	0.208	0.093	0.386
0.882	**68**	0.126	0.041	0.167	0.088	0.220	0.100	0.407
0.870	**69**	0.124	0.044	0.168	0.086	0.211	0.091	0.394
0.857	**70**	0.119	0.045	0.164	0.089	0.208	0.104	0.398
0.845	**71**	0.125	0.047	0.172	0.091	0.208	0.100	0.399
0.833	**72**	0.123	0.041	0.164	0.089	0.217	0.086	0.388
0.822	**73**	0.117	0.045	0.161	0.087	0.216	0.092	0.398
0.811	**74**	0.117	0.051	0.168	0.088	0.210	0.106	0.400
0.800	**75**	0.118	0.047	0.165	0.090	0.211	0.091	0.391
0.789	**76**	0.110	0.040	0.150	0.086	0.206	0.100	0.405
0.779	**77**	0.124	0.030	0.154	0.088	0.224	0.080	0.393
0.769	**78**	0.115	0.043	0.158	0.089	0.220	0.078	0.387
0.759	**79**	0.113	0.049	0.162	0.086	0.213	0.082	0.377
0.750	**80**	0.123	0.028	0.150	0.088	0.224	0.079	0.394
0.741	**81**	0.117	0.034	0.151	0.087	0.202	0.088	0.384
0.732	**82**	0.120	0.040	0.160	0.089	0.222	0.076	0.386
0.723	**83**	0.116	0.037	0.152	0.092	0.216	0.085	0.387
0.714	**84**	0.115	0.034	0.149	0.093	0.204	0.085	0.378
0.706	**85**	0.117	0.036	0.153	0.087	0.200	0.087	0.380
0.698	**86**	0.114	0.032	0.147	0.094	0.213	0.080	0.383
0.690	**87**	0.111	0.041	0.152	0.091	0.202	0.077	0.369
0.682	**88**	0.110	0.040	0.150	0.091	0.204	0.079	0.374
0.674	**89**	0.119	0.033	0.151	0.087	0.196	0.082	0.366
0.667	**90**	0.122	0.041	0.163	0.087	0.198	0.084	0.370
0.659	**91**	0.117	0.041	0.158	0.090	0.196	0.082	0.365
0.652	**92**	0.118	0.038	0.156	0.087	0.198	0.079	0.362
0.645	**93**	0.126	0.036	0.162	0.089	0.189	0.079	0.359
0.638	**94**	0.127	0.035	0.161	0.091	0.193	0.073	0.355
0.632	**95**	0.123	0.044	0.167	0.090	0.193	0.074	0.361
0.625	**96**	0.125	0.037	0.163	0.092	0.183	0.068	0.352
0.619	**97**	0.124	0.035	0.159	0.089	0.188	0.081	0.359
0.612	**98**	0.137	0.032	0.169	0.094	0.192	0.071	0.357
0.606	**99**	0.125	0.044	0.169	0.090	0.175	0.076	0.340

Mean of all Subject Component Durations When Averaged into 1-bpm Intervals

Trr (s)	HR(bpm)	$T_{PW\,(s)}$	$T_{PQ\text{-}Seg(s)}$	$T_{PQ\text{-}Int(s)}$	$T_{QRS(s)}$	$T_{TW(s)}$	$T_{ST\text{-}Seg(s)}$	$T_{QT\text{-}Int(s)}$
0.600	**100**	0.133	0.024	0.157	0.093	0.184	0.095	0.347
0.594	**101**	0.129	0.036	0.165	0.093	0.169	0.086	0.343
0.588	**102**	0.134	0.034	0.167	0.091	0.174	0.083	0.347
0.583	**103**	0.124	0.043	0.166	0.091	0.169	0.085	0.347
0.577	**104**	0.121	0.046	0.167	0.089	0.165	0.087	0.339
0.571	**105**	0.123	0.041	0.165	0.088	0.176	0.076	0.337
0.566	**106**	0.127	0.040	0.167	0.091	0.176	0.075	0.339
0.561	**107**	0.124	0.038	0.163	0.089	0.171	0.070	0.337
0.556	**108**	0.128	0.039	0.168	0.093	0.175	0.068	0.336
0.550	**109**	0.129	0.040	0.169	0.092	0.170	0.070	0.333
0.545	**110**	0.123	0.041	0.163	0.091	0.169	0.073	0.333
0.541	**111**	0.128	0.038	0.166	0.095	0.170	0.063	0.332
0.536	**112**	0.120	0.043	0.163	0.088	0.169	0.069	0.330
0.531	**113**	0.124	0.033	0.157	0.095	0.165	0.066	0.318
0.526	**114**	0.127	0.040	0.166	0.092	0.155	0.068	0.313
0.522	**115**	0.120	0.035	0.154	0.090	0.160	0.069	0.318
0.517	**116**	0.120	0.033	0.153	0.087	0.155	0.070	0.306
0.513	**117**	0.124	0.030	0.154	0.086	0.164	0.061	0.314
0.508	**118**	0.116	0.034	0.151	0.086	0.157	0.064	0.304
0.504	**119**	0.119	0.036	0.155	0.089	0.163	0.058	0.309
0.500	**120**	0.121	0.030	0.152	0.087	0.156	0.063	0.307
0.496	**121**	0.119	0.029	0.148	0.088	0.157	0.058	0.303
0.492	**122**	0.117	0.035	0.152	0.090	0.158	0.059	0.306
0.488	**123**	0.115	0.034	0.149	0.087	0.150	0.061	0.298
0.484	**124**	0.119	0.029	0.147	0.087	0.141	0.057	0.289
0.480	**125**	0.107	0.037	0.144	0.085	0.162	0.055	0.299
0.476	**126**	0.110	0.035	0.144	0.085	0.155	0.054	0.291
0.472	**127**	0.110	0.032	0.142	0.086	0.158	0.056	0.302
0.469	**128**	0.111	0.032	0.143	0.087	0.158	0.056	0.300
0.465	**129**	0.109	0.026	0.135	0.087	0.158	0.059	0.298
0.462	**130**	0.108	0.034	0.142	0.086	0.160	0.054	0.298
0.458	**131**	0.107	0.031	0.137	0.087	0.150	0.059	0.294
0.455	**132**	0.105	0.032	0.138	0.087	0.152	0.055	0.293
0.451	**133**	0.109	0.026	0.135	0.087	0.146	0.054	0.288
0.448	**134**	0.112	0.025	0.136	0.087	0.147	0.052	0.289
0.444	**135**	0.108	0.027	0.135	0.088	0.146	0.053	0.284
0.441	**136**	0.111	0.025	0.136	0.086	0.145	0.049	0.280
0.438	**137**	0.110	0.023	0.133	0.089	0.133	0.057	0.268
0.435	**138**	0.106	0.025	0.131	0.087	0.140	0.051	0.278
0.432	**139**	-	-	-	-	-	-	-
0.429	**140**	0.109	0.022	0.131	0.087	0.139	0.048	0.275
0.426	**141**	0.105	0.022	0.126	0.087	0.142	0.050	0.279
0.423	**142**	0.103	0.026	0.129	0.087	0.140	0.049	0.275
0.420	**143**	0.106	0.022	0.128	0.088	0.142	0.046	0.275
0.417	**144**	-	-	-	-	-	-	-
0.414	**145**	0.107	0.019	0.126	0.089	0.146	0.044	0.275
0.411	**146**	0.101	0.020	0.121	0.088	0.148	0.039	0.275
0.408	**147**	0.102	0.014	0.116	0.089	0.143	0.037	0.269
0.405	**148**	-	-	-	-	-	-	-

Mean of all Subject Component Durations When Averaged into 1-bpm Intervals

Trr (s)	HR(bpm)	$T_{PW\ (s)}$	$T_{PQ\text{-}Seg(s)}$	$T_{PQ\text{-}Int(s)}$	$T_{QRS(s)}$	$T_{TW(s)}$	$T_{ST\text{-}Seg(s)}$	$T_{QT\text{-}Int(s)}$
0.403	**149**	0.113	0.012	0.124	0.084	0.143	0.040	0.266
0.400	**150**	0.103	0.015	0.117	0.087	0.140	0.037	0.267
0.397	**151**	0.101	0.015	0.117	0.089	0.141	0.037	0.268
0.395	**152**	-	-	-	-	-	-	-
0.392	**153**	0.091	0.020	0.111	0.086	0.148	0.038	0.271
0.390	**154**	0.096	0.015	0.111	0.087	0.147	0.035	0.267
0.387	**155**	-	-	-	-	-	-	-
0.385	**156**	0.091	0.025	0.115	0.084	0.142	0.033	0.260
0.382	**157**	0.097	0.016	0.112	0.085	0.124	0.048	0.249
0.380	**158**	-	-	-	-	-	-	-
0.377	**159**	0.091	0.024	0.115	0.085	0.134	0.033	0.254
0.375	**160**	0.090	0.022	0.112	0.084	0.116	0.047	0.253

Standard Deviation of all Subject Component Durations When Averaged into 1-bpm Intervals

Trr (s)	HR(bpm)	$T_{PW\ (s)}$	$T_{PQ\text{-}Seg(s)}$	$T_{PQ\text{-}Int(s)}$	$T_{QRS(s)}$	$T_{TW(s)}$	$T_{ST\text{-}Seg(s)}$	$T_{QT\text{-}Int(s)}$
1.277	**47**	0.006	0.025	0.030	0.009	0.072	0.001	0.029
1.250	**48**	0.008	0.011	0.019	0.013	0.022	0.014	0.021
1.224	**49**	0.003	0.005	0.014	0.012	0.026	0.000	0.011
1.200	**50**	0.021	0.010	0.017	0.010	0.046	0.026	0.028
1.176	**51**	0.030	0.006	0.035	0.007	0.027	0.021	0.038
1.154	**52**	0.018	0.006	0.016	0.011	0.032	0.037	0.031
1.132	**53**	0.024	0.013	0.032	0.007	0.027	0.022	0.044
1.111	**54**	0.006	0.039	0.041	0.009	0.027	0.024	0.038
1.091	**55**	0.010	0.011	0.004	0.005	0.061	0.055	0.035
1.071	**56**	0.008	0.005	0.019	0.005	0.024	0.036	0.063
1.053	**57**	0.012	0.012	0.008	0.004	0.038	0.036	0.035
1.034	**58**	0.017	0.032	0.049	0.007	0.039	0.015	0.037
1.017	**59**	0.020	0.024	0.028	0.007	0.017	0.022	0.040
1.000	**60**	0.007	0.011	0.018	0.015	0.058	0.038	0.029
0.984	**61**	-	-	-	-	-	-	-
0.968	**62**	0.004	0.020	0.021	0.002	0.022	0.014	0.032
0.952	**63**	0.014	0.020	0.021	0.007	0.030	0.037	0.040
0.938	**64**	0.012	0.027	0.025	0.014	0.038	0.033	0.051
0.923	**65**	0.012	0.025	0.026	0.011	0.021	0.027	0.035
0.909	**66**	0.019	0.025	0.026	0.014	0.035	0.019	0.040
0.896	**67**	0.023	0.018	0.030	0.012	0.020	0.022	0.018
0.882	**68**	0.020	0.014	0.024	0.007	0.029	0.029	0.029
0.870	**69**	0.016	0.022	0.021	0.010	0.022	0.020	0.013
0.857	**70**	0.020	0.024	0.029	0.011	0.035	0.040	0.027
0.845	**71**	0.017	0.029	0.028	0.009	0.036	0.026	0.027
0.833	**72**	0.011	0.026	0.025	0.007	0.034	0.037	0.018
0.822	**73**	0.018	0.022	0.023	0.008	0.029	0.032	0.030
0.811	**74**	0.017	0.031	0.027	0.008	0.050	0.027	0.032
0.800	**75**	0.021	0.026	0.025	0.007	0.036	0.027	0.035
0.789	**76**	0.028	0.017	0.031	0.008	0.032	0.026	0.037
0.779	**77**	0.015	0.016	0.018	0.010	0.032	0.032	0.027
0.769	**78**	0.016	0.022	0.020	0.010	0.037	0.024	0.029
0.759	**79**	0.017	0.025	0.020	0.008	0.010	0.016	0.025
0.750	**80**	0.015	0.013	0.016	0.008	0.043	0.023	0.033
0.741	**81**	0.012	0.015	0.014	0.009	0.022	0.013	0.029
0.732	**82**	0.015	0.024	0.023	0.011	0.022	0.021	0.026
0.723	**83**	0.018	0.010	0.018	0.010	0.026	0.018	0.026
0.714	**84**	0.017	0.012	0.017	0.013	0.024	0.017	0.025
0.706	**85**	0.030	0.010	0.032	0.008	0.026	0.016	0.040
0.698	**86**	0.022	0.010	0.017	0.009	0.019	0.027	0.025
0.690	**87**	0.016	0.009	0.023	0.012	0.012	0.014	0.030
0.682	**88**	0.017	0.014	0.017	0.016	0.014	0.017	0.030
0.674	**89**	0.026	0.007	0.020	0.013	0.020	0.015	0.026
0.667	**90**	0.031	0.008	0.029	0.013	0.019	0.011	0.034
0.659	**91**	0.024	0.016	0.023	0.016	0.021	0.015	0.029
0.652	**92**	0.022	0.010	0.028	0.012	0.017	0.021	0.030
0.645	**93**	0.027	0.007	0.028	0.012	0.017	0.022	0.028
0.638	**94**	0.028	0.007	0.030	0.013	0.014	0.014	0.019
0.632	**95**	0.027	0.020	0.024	0.008	0.023	0.020	0.030
0.625	**96**	0.023	0.015	0.012	0.009	0.014	0.012	0.013
0.619	**97**	0.026	0.021	0.026	0.010	0.022	0.022	0.029
0.612	**98**	0.025	0.014	0.023	0.008	0.020	0.020	0.035
0.606	**99**	0.024	0.020	0.020	0.010	0.010	0.019	0.026

Standard Deviation of all Subject Component Durations When Averaged into 1-bpm Intervals

Trr (s)	HR(bpm)	$T_{PW\ (s)}$	$T_{PQ\text{-}Seg(s)}$	$T_{PQ\text{-}Int(s)}$	$T_{QRS(s)}$	$T_{TW(s)}$	$T_{ST\text{-}Seg(s)}$	$T_{QT\text{-}Int(s)}$
0.600	**100**	0.039	0.013	0.008	0.009	0.012	0.059	0.011
0.594	**101**	0.020	0.014	0.021	0.009	0.019	0.038	0.026
0.588	**102**	0.022	0.017	0.023	0.007	0.025	0.038	0.018
0.583	**103**	0.017	0.022	0.020	0.007	0.019	0.036	0.020
0.577	**104**	0.026	0.019	0.025	0.012	0.019	0.038	0.024
0.571	**105**	0.026	0.016	0.024	0.011	0.017	0.030	0.022
0.566	**106**	0.029	0.016	0.027	0.013	0.019	0.034	0.021
0.561	**107**	0.024	0.016	0.028	0.011	0.016	0.017	0.021
0.556	**108**	0.023	0.017	0.019	0.010	0.009	0.015	0.007
0.550	**109**	0.024	0.021	0.023	0.009	0.008	0.021	0.008
0.545	**110**	0.023	0.015	0.018	0.008	0.004	0.015	0.008
0.541	**111**	0.025	0.017	0.020	0.005	0.010	0.008	0.012
0.536	**112**	0.030	0.008	0.019	0.013	0.008	0.011	0.007
0.531	**113**	0.030	0.012	0.021	0.007	0.011	0.008	0.012
0.526	**114**	0.025	0.002	0.015	0.004	0.011	0.006	0.015
0.522	**115**	0.020	0.009	0.013	0.005	0.013	0.004	0.012
0.517	**116**	0.018	0.009	0.008	0.008	0.010	0.007	0.020
0.513	**117**	0.020	0.011	0.012	0.007	0.020	0.013	0.027
0.508	**118**	0.013	0.008	0.010	0.008	0.015	0.011	0.023
0.504	**119**	0.016	0.011	0.012	0.009	0.016	0.012	0.020
0.500	**120**	0.020	0.007	0.011	0.008	0.016	0.006	0.019
0.496	**121**	0.017	0.010	0.011	0.010	0.020	0.008	0.022
0.492	**122**	0.015	0.005	0.013	0.008	0.018	0.008	0.018
0.488	**123**	0.016	0.007	0.008	0.009	0.019	0.008	0.022
0.484	**124**	0.009	0.000	0.008	0.011	0.011	0.003	0.011
0.480	**125**	0.010	0.017	0.011	0.008	0.017	0.006	0.024
0.476	**126**	0.006	0.017	0.014	0.008	0.018	0.005	0.011
0.472	**127**	0.008	0.012	0.011	0.007	0.010	0.012	0.018
0.469	**128**	0.011	0.012	0.013	0.007	0.012	0.009	0.018
0.465	**129**	0.012	0.013	0.006	0.007	0.012	0.010	0.018
0.462	**130**	0.011	0.015	0.011	0.007	0.008	0.012	0.016
0.458	**131**	0.009	0.012	0.012	0.005	0.010	0.008	0.016
0.455	**132**	0.007	0.008	0.011	0.006	0.013	0.009	0.016
0.451	**133**	0.013	0.008	0.009	0.006	0.009	0.011	0.020
0.448	**134**	0.016	0.007	0.008	0.005	0.009	0.011	0.018
0.444	**135**	0.010	0.007	0.007	0.007	0.018	0.009	0.017
0.441	**136**	0.009	0.005	0.003	0.006	0.008	0.013	0.016
0.438	**137**	0.017	0.006	0.007	0.010	0.018	0.009	0.004
0.435	**138**	0.011	0.007	0.004	0.006	0.011	0.010	0.012
0.432	**139**	-	-	-	-	-	-	-
0.429	**140**	0.012	0.008	0.006	0.008	0.006	0.014	0.014
0.426	**141**	0.009	0.007	0.009	0.007	0.009	0.010	0.009
0.423	**142**	0.008	0.009	0.008	0.009	0.009	0.010	0.011
0.420	**143**	0.013	0.006	0.004	0.009	0.010	0.012	0.010
0.417	**144**	-	-	-	-	-	-	-
0.414	**145**	0.010	0.008	0.002	0.011	0.015	0.015	0.009
0.411	**146**	0.010	0.009	0.003	0.007	0.016	0.004	0.008
0.408	**147**	0.008	0.005	0.003	0.011	0.005	0.007	0.004
0.405	**148**	-	-	-	-	-	-	-

Standard Deviation of all Subject Component Durations When Averaged into 1-bpm Intervals

Trr (s)	HR(bpm)	$T_{PW\ (s)}$	$T_{PQ\text{-}Seg(s)}$	$T_{PQ\text{-}Int(s)}$	$T_{QRS(s)}$	$T_{TW(s)}$	$T_{ST\text{-}Seg(s)}$	$T_{QT\text{-}Int(s)}$
0.403	**149**	0.004	0.007	0.004	0.008	0.005	0.000	0.003
0.400	**150**	0.009	0.006	0.006	0.012	0.011	0.002	0.008
0.397	**151**	0.007	0.005	0.001	0.011	0.015	0.005	0.009
0.395	**152**	-	-	-	-	-	-	-
0.392	**153**	0.007	0.005	0.004	0.015	0.013	0.003	0.004
0.390	**154**	0.011	0.004	0.001	0.016	0.009	0.001	0.006
0.387	**155**	-	-	-	-	-	-	-
0.385	**156**	0.002	0.001	0.003	0.012	0.021	0.002	0.005
0.382	**157**	0.006	0.004	0.001	0.014	0.029	0.019	0.008
0.380	**158**	-	-	-	-	-	-	-
0.377	**159**	0.000	0.006	0.003	0.009	0.000	0.000	0.003
0.375	**160**	0.000	0.000	0.004	0.010	0.000	0.000	0.007

References

[1] W. Einthoven, "The string galvanometer and the human electrocardiogram.," in *Proceedings of the Section of Science of the Dutch Royal Society of Medicine*, vol. 4, pp. 107–115, 1904.

[2] J. R. Hampton, *The ECG in Practice*. Churchill Livingston, Edinburgh, 1997.

[3] J. J. Carr and J. M. Brown, *Introduction to Biomedical Equipment Technology*. Prentice Hall, 4th ed., 2001.

[4] M. Burke and M. Nasor, "An accurate programmable ECG simulator," *Journal of Medical Engineering and Technology*, vol. 25, pp. 97–102, 2001.

[5] J. Chang Chien, "Design of a programmable electrocardiogram generator using a microcontroller and the CPLD technology," in *33rd Annual Conference of the IEEE Industrial Electronics Society (IECON)*, 2007.

[6] H. Bazett, "An analysis of the time relations of the electrocardiogram," *Heart*, vol. 7, pp. 353–370, 1920.

[7] F. Itakura, "Minimum prediction residual principle applied to speech recognition," *IEEE Transactions on Acoustics, Speech and Signal Processing*, vol. 23, pp. 37–72, 1975.

[8] P. E. McSharry, G. D. Clifford, L. Tarassenko, and L. A. Smith, "A dynamical model for generating synthetic electrocardiogram signals," *IEEE Transactions on Biomedical Engineering*, vol. 50, pp. 289–294, 2003.

[9] G. D. Clifford and P. E. McSharry, "Method to filter ECG's and evaluate clinical parameter distortion using realistic ECG model parameter fitting," *IEEE Computers in Cardiology*, vol. 32, pp. 715–718, 2005.

[10] M. Burke and M. Nasor, "Wavelet based analysis and the characterization of the ECG signal," *Journal of Medical Engineering and Technology*, vol. 28, pp. 47–55, 2004.

[11] C. Lin, C. Mailhes, and J. Tourneret, "P- and T-wave delineation in ECG signals using a bayesian approach and a partially collapsed Gibbs sampler," *IEEE Transactions on Biomedical Engineering*, vol. 57, pp. 2840–2849, 2010.

[12] G. J. Tortora and M. T. Nielsen, *Principles of Human Anatomy.* John Wiley & Sons, 2009.

[13] G. F. Bastian, *An Illustrated Review of Basic Concepts of The Cardiovascular System.* Harper Collins, 1993.

[14] G. Ritchison. (2011).*The Cardiovascular System.* [Online] Available: http://people.eku.edu/ritchisong/301notes5.html.

[15] J. E. Hall and A. C. Guyton, *Guyton and Hall Textbook of Medical Physiology.* Suanders Elsevier, 2011.

[16] J. Malmivuo and R. Plonsey, *Bioelectromagnetism: principles and applications of bioelectric and biomagnetic fields.* Oxford University Press, 1995.

[17] J. R. Hampton, *The ECG Made Easy.* Churchill Livingston, Edinburgh, 1986.

[18] B. Robert. (2010).*An Introduction to Cardiac Conduction.* [Online] Available: http://byronroberts.wordpress.com.

[19] R. Dozio, "Phd thesis." This PhD shall be published in 2012.

[20] C. Assambo, *Amplifier front-end design in dry-electrode electrocardiography.* PhD thesis, Trinity College Dublin, 2011.

[21] J. Scherer and M. Kicklas, "Synthesis of the 12 lead electrocardiogram from a 3 lead semi-orthogonal subset using patient-specific linear transformation arrays," in *Computers in Cardiology*, 1989.

[22] J. Scherer and J. Willems, "Evaluation of 12-lead ECG synthesis using analysis measurements in 240 patients," in *Computers in Cardiology*, 1992.

[23] R. E. Klabunde. (2011).*Electrocardiogram Chest Leads (Unipolar).* [Online] Available: http://www.cvphysiology.com/Arrhythmias/A013c.html.

[24] D. Gleeson, "Low-power ECG amplifier and detector," Master's thesis, Trinity College Dublin, 1996.

[25] Y. Z. Ider and H. Koymen, "A new technique for line interference monitoring and reduction in biopotential amplifiers," *IEEE Transactions on Biomedical Engineering*, vol. 37, pp. 624–631, 1990.

[26] M. Nasor, *Wavelet Analysis and Microcontroller-Based Synthesis of the Human Electrocardiogram.* PhD thesis, Trinity College Dublin, 1998.

[27] B.S.I, *Particular Requirments for the safety, including performance, of electrocardiographic monitoring equipment.* British Standards Institute, 2006.

[28] E.C.E.S, *Medical electrical equipment, Part 2-51: Particular requirements for safety, including essential performance, of recording and analysing single channel and multichannel electrocardiographs.* European Committee for Electrotechnical Standardisation, 2003.

[29] L. Sornmo, "Time-varying filtering for removal of baseline wander in excercise ECG's," in *IEEE Computers in Cardiology*, 1991.

[30] N. Dabanloo, D. McLernon, A. Ayatollahi, and V. Johari, "A nonlinear signal processing approach to model heart rate variability," in *The fourth Symposium on Signal Processing and Information Technology*, 2004.

[31] E.C.R.I, *Healthcare Product Comparison System.* Emergency Care Research Institute, 2010.

[32] N. Kontodimopoulos, N. Pallikarakis, I. Christov, and I. Daskalov, "In-house development of test equipment for quality control and training. Case study: a prototype ECG simulator-tester," *Journal of Medical Engineering and Physics*, vol. 20, pp. 717–721, 1998.

[33] L. Shuqian and W. Tompkins, "Microcomputer-based simulator of the 12-lead electrocardiogram," in *The 10th Conference of the IEEE Engineering in Medicine and Biology Society*, 1988.

[34] R. J. Prineas, R. S. Crow, and H. Blackburn, *The Minnesota Code Manual of Electrocardiographic Findings: Standards and Procedures for Measurement and Classification.* J. Wright, 1982.

[35] I. Sadighi and M. Kejariwal, "A generalized ECG simulator: an educational tool," in *The 11th Conference of the IEEE Engineering in Medicine and Biology Society*, 1989.

[36] A. Josko and J. Rak, "Effective simulation of signlas for testing ECG analyzer," *IEEE Transactions on Instrumentation and Measurment*, vol. 54, pp. 1019–1024, 2005.

[37] D. Franchi, G. Palagi, and B. R, "A PC-based generator of surface ECG potentials for computer electrocardiograph testing," *Journal of Computers in Biomedical Research*, vol. 27, pp. 68–80, 1994.

[38] T. Mudrov, V. Krasteva, and I. Jekova, "Microcontroller-based ECG simulator prototype," in *The 13th International Scientific and Applied Science Conference Electronics*, 2004.

[39] A. Martnez, E. Rossi, L. Siri, and L. Nicola, "Microprocessor-based simulator of surface ECG signals," in *16th Argentine Bioengineering Congress and the 5th Conference of Clinical Engineering*, pp. 1–7, 2007.

[40] J. Chien Chang and C. Tai Chi, "Accurate programmable electrocardiogram generator using a dynamical model implemented on a microcontroller," *Review of Scientific Instruments*, vol. 77, pp. 0751041–0741045, 2006.

[41] C. Caner, M. Engin, and E. Zeki Engin, "The programmable ECG simulator," *Journal of Medical Systems*, vol. 32, pp. 355–359, 2008.

[42] G. P. Shorten and M. J. Burke, "A precision ECG signal generator providing full lead II QRS amplitude and an accuracte timing profile," in *The 31st Conference of the IEEE Engineering in Medicine and Biology Society*, 2009.

[43] G. P. Shorten and M. J. Burke, "A versatile temperature-stable ECG simulator," *Journal of Medical Engineering and Technology*, vol. 35, pp. 92–102, 2011.

[44] L. D. Jasio, *Programming 16-bit Microcontrollers in C.* Newnes, 2007.

[45] R. Mancini and B. Carter, *Op-Amps for Everyone.* Texas Instruments, 2002.

[46] A. Kay, *Analysis and Measurments of Intrinsic Noise in Op-Amp Circuits.* Texas Instruments Incorporated, 2007.

[47] A. Barna and D. Porat, *Operational Amplifiers.* Wiley-Interscience, 1971.

[48] M. J. Burke, *A Microcontroller Based Athletic Cardiotachometer.* PhD thesis, Trinity College Dublin, 1991.

[49] F. R. Connor, *Noise*. Edward Arnold, 1973.

[50] K. A. Stroud and B. J. Dexter, *Engineering in Mathematics*. Palgrave Mac Millan, 2007.

[51] I. Goldenberg, A. J. Moss, and W. Zareba, "QT Interval: How to measure it and what is "normal"," *Journal of Cardiovascular Electrophysiology*, vol. 17, pp. 333–336, 2006.

[52] J. Ge, A. Sun, V. Paajanen, S. Wang, C. Su, Z. Yang, Y. Li, S. Wang, J. Jia, K. Wang, Y. Zou, L. Gao, K. Wang, and Z. Fan, "Molecular and clinical characterization of a novel SCN5A mutation associated with atrioventricular block and dilated cardiomyopathy," *Circulation: Arrythmia and Electrophysiology*, vol. 2, pp. 83–92, 2008.

[53] H. W. Blackburn and E. Simonson, "The total QRS duration," *American Heart Journal*, vol. 53, pp. 699–710, 1957.

[54] M. Nakagawa, T. Iwao, S. Ishida, H. Yonemochi, T. Fujino, T. Saikawa, and M. Ito, "Circadian rhythm of the signal averaged electrocardiogram and its relation to heart rate variability in healthy subjects," *Heart*, vol. 79, pp. 493–496, 1998.

[55] O. Berenfeld and S. Abboud, "Simulation of cardiac activity and the ECG using a heart model with a reaction-diffusion action potential," *Medical Engineering & Physics*, vol. 18, pp. 615–625, 1996.

[56] R. Povinelli, M. Mneimneh, and M. Johnson, "Cardiac model based approach to QT estimation," *Computers in Cardiology*, vol. 33, pp. 333–336, 2006.

[57] A. Ghodrati, D. Brooks, G. Tadmor, and R. Macleod, "Wavefront-based models for inverse electrocardiography," *IEEE Transactions on Biomedical Engineering*, vol. 53, pp. 1821–1831, 2006.

[58] L. Sornmo, P. Borjesson, M. Nyhards, and O. Pahlm, "A method for evaluation of QRS shape features using a mathimatical model for the ECG," *IEEE Transactions on Bio-Medical Engineering*, vol. 10, pp. 713–717, 1981.

[59] C. Lamberti and G. Fanti, "ECG waveform synthesizer," in *The 33rd Conference of the IEEE Engineering in Medicine and Biology Society*, 1989.

[60] S. Murthy and M. Reddy, "ECG synthesis via discrete cosine transform," in *The 11th Conference of the IEEE Engineering in Medicine and Biology Society*, 1989.

[61] S. Suppappola, Y. Sun, and S. A.Chiaramida, "Gaussian pulse decomposition: An intuitive model of electrocardiogram waveforms," *Annals of Biomedical Engineering*, vol. 25, pp. 252–260, 1997.

[62] S. Paravaneh and M. Pashna, "Electrocardiogram synthesis using a gaussian combination model," *Computers in Cardiology*, vol. 34, pp. 621–624, 2007.

[63] G. D. Clifford and P. E. McSharry, "A realistic coupled nonlinear artifcial ECG, BP and respiratory signal generator for assessing noise performance of biomedical signal processing algorithms," tech. rep., Harvard-MIT and University of Oxford.

[64] R. Sameni, M. Shamsollahi, C. Jutten, and Babaie-Zadeh, "Filtering noisy ECG signals using the extended kalman filter based on a modified dynamic ECG model," in *Computers in Cardiology*, 2005.

[65] D. Kicmerova, "Modelling arrhythmics ECG signals with McSharry's model," in *17th International Conference Radioelektronika,*, 2007.

[66] M. Potter and W. Kinser, "Improved event interval reconstruction in synthetic electrocardiograms," *IEEE Transactions on Biomedical Engineering*, vol. 56, pp. 900–903, 2009.

[67] Z. Li and M. Ma, "ECG modeling with DFG," in *IEEE Engineering in Medicince and Biology 27th Annual Conference*, 2005.

[68] J. W. Wang and Z. Li, "An ECG segmentation model used for signal generator," in *The 2nd International Conference on Innovative Computing, Information and Control*, 2007.

[69] A. Nimunkar and W. Tompkins, "ECG synthesis based on morphing," in *IEEE Engineering in Medicince and Biology 26th Annual Conference*, pp. 879–881, 2004.

[70] E. Simonson, D. L. Cady, and M. Woodbury, "The normal Q-T Interval," *American Heart Journal*, vol. 63, pp. 747–753, 1962.

[71] R. Ashman and E. Hull, *Essentials of Electrocardiography for the Student and the Practitioner of Medicine.* New York:Macmillan, 1945.

[72] P. Davey, "A new physiological method for heart rate correction of the QT Interval," *Heart*, vol. 82, pp. 183–186, 1999.

[73] N. I. of Biomedical Imaging & Engineering, NBIB, N. I. of Health, and N. I. of General Medical Sceinces. (2011).*PhysioNet the research resource for complex physiologic signals.* [Online] Available: http://www.physionet.org.

[74] J. T. Wang, A. Sehmi, J. N.B., and D. de Bono, "A knowledge-based system for qualitative ECG simulation and ECG analysis," *Computers in Cardiology*, pp. 733–736, 1991.

[75] H. Sakoe and S. Chiba, "Dynamic programming algorithm optimization for spoken word recognition," *IEEE Transactions on Acoustics, Speech and Signal Processing*, vol. 26, pp. 43–49, 1978.

[76] T. Schmill, M .and Oates and P. Cohen, "Learned models for continuous planning," in *Seventh International Workshop on Artificial Anaylsis*, 1999.

[77] K. Gollmer and C. Posten, "Supervision of bioprocesses using a dynamic time warping algorithm," in *IFAC Workshop on on-line fault detection and supervision in the chemical process industries*, pp. 1287–1295, 1996.

[78] N. Venkatesh and S. Jayaraman, "Human electrocardiogram for biometrics using DTW and FLDA," in *The 20th International Conference on Pattern Recognition*, pp. 3838–3841, 2010.

[79] P. Tormene, T. Giorgino, S. Quaglini, and M. Stefanelli, "Matching incomplete time series with dynamic time warping: an algorithm and an application to post stroke rehabilitation," *Artificial Intelligence in Medicine*, vol. 45, pp. 11–34, 2009.

[80] P. Laguna, R. G. Mark, A. Godberger, and G. B.Moody, "A database for evaluation of algorithms for measurement of QT and other waveform intervals in the ECG," *Computers in Cardiology*, vol. 24, pp. 673–676, 1997.

[81] R. Longini, J. Giolma, C. Wall, and R. Quick, "Filtering without phase shift," *IEEE Transactions on Bio-Medical Engineering*, vol. 5, pp. 432–433, 1975.

[82] J. J. Carr and J. M. Brown, *Bioelectric Amplifiers.* No. Chapter 7, Prentice Hall, 2001.

[83] D. C. Hoaglin, F. Mosteller, and J. W. Tukey, *Understanding Robust and Exploratory Data Analysis.* John Wiley & Sons, 1983.

[84] S. Theodoridis and K. Koutroumbas, *Pattern Recognition.* San Diego CA: Academic Press, 2006.

[85] B. Huang and K. W, "ECG frame classification using dynamic time warping," in *IEEE Canadian Conference on Electrical & Computer Engineering*, vol. 2, pp. 1105–1110, 2002.

[86] V. Tuzcu and S. Nas, "Dynamic time warping as a novel tool in pattern recognition of ECG changes in heart rhythm," in *IEEE International Conference on Systems, Man and Cybernetics*, vol. 5, pp. 182–186, 2005.

[87] M. Kotas, "Application of dynamic time warping to ECG processing," in *XI Conference in Medical Informatics & Technologies*, pp. 169–175, 2006.

[88] T. Felty, "Dynamic time warping." Matlab Central File Exchange, December 2005.

[89] R. E. Bellman, *Dynamic Programming.* Princeton University Press, 1957.

[90] E. J. Keogh and M. J. Pazzani, "Derivative dynamic time warping," in *First SIAM International Conference on Data Mining*, 2001.

[91] Y. Xie and B. Wiltgent, "Adaptive feature based dynamic time warping," *International Journal of Computer Science and Security*, vol. 10, pp. 264–273, 2010.

[92] H. Vullings, M. Verhaegen, and H. Verbruggen, "Automated ECG segmentation with dynamic time warping," in *The 20th Conference of the IEEE Engineering in Medicine and Biology Society*, 1998.

[93] A. Zifan, S. Saberi, M. H. Moradi, and F. Towhidkhah, "Automated ECG segmentation using piecewise derivative dynamic time warping," *International Journal of Biological and Life Sciences*, vol. 1, pp. 181–185, 2005.

[94] H. Vullings, M. Verhaegen, and H. Verbruggen, "ECG segmentation using time-warping," in *Advances in Intelligent Data Analysis, Proceedings of the Second International Symposium IDA-97*, pp. 275–285, 1997.

[95] G. Shorten and M. Burke, "A novel approach in testing the accuracy of ECG compression using partial percentage RMS difference and dynamic time warping," in *The 10th World Scientific and Engineering Academy and Society International Conference on Signal Processing, Robotics and Automation*, 2011.

[96] G. Shorten and M. Burke, "The application of dynamic time warping to measure the accuracy of ECG compression," *International Journal of Circuits, Systems and Signal Processing*, vol. 5, pp. 305–313, 2011.

[97] B. Furht and A. Perez, "An adaptive real-time ECG compression algorithm with variable threshold," *IEEE Transactions on Biomedical Engineering*, vol. 35, pp. 489–494, 1988.

[98] V. Kumar, S. Saxena, V. Giri, and D. Singh, "Improved modified AZTEC technique for ECG data compression: Effect of length of parabolic filter on reconstructed signal," *Computers and Electrical Engineering*, vol. 31, pp. 334–344, 2005.

[99] M. Ishijima, S.-B. Shin, G. H. Hostetter, and J. Sklansky, "Scan-along polygonal approximation for data compression of electrocardiograms," *IEEE Transactions on Biomedical Engineering*, vol. 11, pp. 928–938, 1983.

[100] V. Kumar, S. Saxena, and V. Giri, "Direct data compression of ECG signal for telemedicine," *International Journal of Systems Science*, vol. 37, pp. 45–63, 2006.

[101] A. Koski and M. Juhola, "Segmentation of digital signals based on estimated compression ratio," *IEEE Transactions on Biomedical Engineering*, vol. 43, pp. 928–938, 1996.

[102] A. Hamadan, S. Karimifard, H. Sadoughi, and M. Abdoli, "An efficient piecewise modeling of ECG signals based on hermitian basis functions," in *The 29 th Conference of the IEEE Engineering in Medicine and Biology Society*, pp. 3180–3183, 2007.

[103] M. Lascu and D. Lascu, "Electrocardiogram compression and optimal filtering algorithm," in *The 7th WSEAS International Conference on Signal, Speech and Image Processing*, pp. 26–30, 2007.

[104] A. Ramakrishnan and S. Saha, "ECG coding by wavelet based linear prediction," *IEEE Transactions on Biomedical Engineering*, vol. 44, pp. 1253–1261, 1997.

[105] M. Moazami-Goudarzi, A. Taheri, and M. Pooyan, "Efficient method for ECG compression using two dimensional multiwavelet transform," *International Journal of Information Technology*, vol. 2, pp. 257–263, 2005.

[106] B. Reddy and S. Murthy, "ECG data compression using fourier descriptor," *IEEE Transactions on Biomedical Engineering*, vol. 33, pp. 428–434, 1968.

[107] E. Skordalakis and G. Barlas, "A novel family of compression algorithms for ECG and other semiperiodical , one-dimensional, biomedical signals," *IEEE Transactions on Biomedical Engineering*, vol. 43, pp. 820–828, 1996.

[108] B. Yarman, H. Gurkan, U. Guz, and B. Aygun, "A novel method to represent ECG signals via predefined personalized signature and envelope functions," in *The 23rd Conference of the IEEE Engineering in Medicine and Biology Society*, 2001.

[109] S. M. Jalleddine, C. Hutchens, R. D. Strattan, and W. A. Coberly, "ECG data compression techniques-a unified approach," *IEEE Transactions on Biomedical Engineering*, vol. 37, pp. 329–343, 1990.

[110] Y. Zigel, A. Cohen, A. Abu-Ful, A. Wagshal, and A. Katz, "Analysis by synthesis ECG signal compression," in *Computers in Cardiology*, 1997.

[111] C. Monica Fira and L. Goras, "An ECG signals compression method and its validation using NN's," *IEEE Transactions on Biomedical Engineering*, vol. 44, pp. 1319–1326, 2008.

[112] P. Rossi, A. Casaleggio, M. Chiappalone, M. Morando, G. Corbucci, M. Reggiani, G. Sartori, and S. Chierchia, "Computationally inexpensive methods for intracardiac atrial bipolar electrogram compression," *Eurospace*, vol. 4, pp. 295–302, 2002.

[113] W. J. Tompkins, *Biomedical Digital Signal Processing.* Prentice Hall, 1993.

[114] R. Jane, J. Garcia, and P. Laguna, "Evaluation of an automatic threshold based detector of waveform limits in holter ECG with the QT Database," *Computers in Cardiology*, vol. 24, pp. 295–298, 1997.

[115] T. yeda Mahmood, D. Beymer, and F. Wang, "Shape-based matching of ECG recordings," in *The 29th Conference of the IEEE Engineering in Medicine and Biology Society*, 2007.

[116] G. P. Shorten and M. J. Burke, "Pre-processing for value based dynamic time warping of the ECG signal," in *The 22nd Irish Signals and Systems Conference*, (Trinity College Dublin), pp. 201–206, IET, 2011.

[117] S. Olmos, M. Millan, J. Garica, and P. Laguna, "ECG data compression with the Karhunen-Loeve Transform," *Computers in Cardiology*, pp. 253–256, 1996.

[118] G. P. Shorten and M. J. Burke, "A time domain based classifier for ECG pattern recognition," in *The 33rd Conference of the IEEE Engineering in Medicine and Biology Society*, pp. 4980–1983, 2011.

[119] P. Laguna, R. JanB, and P. Caminal, "Automatic detection of wave boundaries in multilead ECG signals: validation on the CSE database.," *Computers in Biomedical Research*, vol. 27, pp. 45–60, 1994.

[120] J. W. Magnani, M. A. Williamson, P. T. Ellinor, K. M. Monahan, and E. J. Benjamin, "P wave indices current status and future directions in epidemiology, clinical and research applications," *Journal of The American Heart Association*, vol. 2, pp. 72–79, 2009.

[121] S. Kose, K. Aytemir, I. Can, A. Iyisoy, A. Kilic, B. Amasyali, H. Kursaklioglu, E. Isik, A. Oto, and E. Demirtas, "Seasonal variation of P-wave dispersion in healthy subjects," *Journal of Electrocardiography*, vol. 35, pp. 307–311, 2002.

[122] P. E. Dilaveris, P. Frbom, V. Batchvarov, A. Ghuran, and M. Malik, "Circadian behavior of P-wave duration, P-wave area, and PR interval in healthy subjects," *Annals of Noninvasive Electrocardiology*, vol. 6, pp. 92–97, 2001.

[123] E. Gialafos, P. Dilaveris, A. Synetos, G. Tsolakidis, T. Papaioannou, G. Andrikopoulos, D. Richter, F. Triposkiadis, and G. JE., "P wave analysis indices in

young healthy men: data from the digital electrocardiographic study in Hellenic Air Force Servicemen (DEHAS)," *Pacing and Clinical Electrophysiology*, vol. 26, pp. 367–372, 2003.

[124] C. A. Caceres and G. A. Kelser Jr., "Duration of the normal P wave," *American Journal of Cardiology*, vol. 3, pp. 449–452, 1959.

[125] C. Blakemore and S. Jennett, *The Oxford Companion to The Body.* Oxford University Press, 2001.

[126] J. Bailey, A. Berson, A. Garson, L. Horan, P. Macfarlane, D. Mortara, and C. Zywietz, "Recommendations for standardization and specifications in automated electrocardiography: Bandwidth and digital signal processing," *Circulation*, vol. 2, pp. 730–739, 1990.